USC
UNIVERSIDADE DE SANTIAGO DE COMPOSTELA

INTERNATIONAL DOCTORAL SCHOOL OF THE USC

Catarina Helena
da Silveira Miranda Guedes Pimentel

PhD Thesis

REMOVAL OF POLLUTANTS FROM LIQUID AND GASEOUS EFFLUENTS BY ADSORBENTS PREPARED FROM WASTE BIOMASS

Santiago de Compostela, 2023

Doctoral Programme in Chemical and Environmental Engineering

ESCOLA DE DOUTORAMENTO
INTERNACIONAL DA USC

DOCTORAL THESIS

REMOVAL OF POLLUTANTS FROM LIQUID AND GASEOUS EFFLUENTS BY ADSORBENTS PREPARED FROM WASTE BIOMASS

Author

Catarina Helena da Silveira Miranda Guedes Pimentel

Supervisor/s: Julia González Álvarez and María Sonia Freire Leira

Tutor: Julia González Álvarez

PHD PROGRAMME IN CHEMICAL AND ENVIRONMENTAL ENGINEERING

SANTIAGO DE COMPOSTELA

To my mother and my grandfather.

Acknowledgments

Three intense years of victories and challenges, a complete journey that would undoubtedly not have been possible without the presence of several people who were fundamental to the development of this project.

Words cannot express my gratitude to my supervisors Prof. Julia González Álvarez and Prof. María Sonia Freire Leira who always encouraged me, with their advice, guidance and support. Thank you for welcoming me into your research group and always being present with your good disposition. I would like to extend my gratitude to Prof. Diego Gómez Díaz, who generously provides his knowledge and expertise, always being present helping me overcome each challenge of this project with a cheerful disposition. Without you, none of this would be possible. Being part of the process intensification for a sustainable development group was one of the greatest privileges I have ever had.

I would like to thank all my laboratory partners, Adela, Adrián Ferreiro, Adrián Rial, Ainoha, Clara, Emilio, Federica, Lídia Díaz, Lídia Domínguez, Rubén and Vahid who made all the hours spent here much better and fun. Also, for sharing knowledge and great conversations. Thank you for each and every moment that will always remain in my heart. I am also thankful to Alba, Alexandra, Andrea, Carlos, Cristina, Leticia and Mauro for being with me from the beginning and for the indispensable company on coffee breaks that made every day so much better. Thank you everyone for always supporting me.

My appreciation also goes to my friends Ana, Isabel, Poliane, Sandra Martins and Sandra Rodrigues who, despite the distance, were always following my progress and never stopped giving a word of support and comfort. Thank you for all the moments we shared together. I also appreciate the support of Jemima, Margarita, Sam, Rocío and Zoraida for their motivation and strength.

I would be lacking if I didn't mention my family, I would like to thank my father and especially my brother for never stopping believing in me and always giving me reasons to smile. Thanks should also go to my brothers-in-law for everything they contributed to this journey, especially Gabriel. Also to my in-laws for always being available in the easiest moments and also in the most difficult ones.

Lastly, I would like to acknowledge and give my warmest thanks to the pillar of my life, my husband, who makes every day worth it, and never stopped believing in me.

I would like to acknowledge the financial supported provided by Consellería de Educación, Universidade e Formación Profesional, Xunta de Galicia, grant number ED431B 2020/039 and by MCIN/AEI/10.13039/501100011033 / FEDER, UE (PID2021-122923NB-I00).

Abstract

The intense industrial activity developed in recent decades has led to excessive CO_2 emissions into the atmosphere, which is the primary cause of global warming and to a discharge of a significant amount of wastewater containing various toxic compounds. The challenge is to develop effective separation processes to avoid or reduce the emission of the pollutants in gas and liquid streams. Adsorption with newly adsorbents as an alternative to the commercial ones is proposed to separate CO_2 from gas streams and wood dyes from aqueous solutions. Pine sawdust, a cheap waste product from the wood industry, one biochar and five chemically activated carbons produced from sawdust under different conditions were characterized and used as adsorbents. Pine sawdust was an efficient adsorbent to remove wood dyes from aqueous solutions in batch mode. Anyway, adsorption efficiency improved significantly using sawdust-based biochar and activated carbons due to the increased surface area. The carbon activated with KOH at a ratio 1:4 (w/w) and 850 °C led to the best results for dyes removal, while for CO_2 capture, activation at a lower temperature (600 °C) improved separation selectivity. To plan the scale-up of the process wood dye adsorption was also studied in continuous mode using the carbon selected with the best adsorption performance for all dyes from batch experiments. The research done constitutes a significant contribution to the development and application of new biomass-based materials for CO_2 capture and dye-contaminated wastewater remediation.

Resumen

La intensa actividad industrial desarrollada en las últimas décadas ha provocado excesivas emisiones de CO_2 a la atmósfera, que es el principal causante del calentamiento global, y a la descarga de una importante cantidad de aguas residuales que contienen diversos compuestos tóxicos. El desafío consiste en desarrollar procesos de separación efectivos para evitar o reducir la emisión de contaminantes en corrientes gaseosas y liquidas. En esta Tesis se propone la adsorción empleando nuevos adsorbentes como alternativa a los comerciales para separar el CO_2 de corrientes gaseosas y colorantes para madera de disoluciones acuosas. Así, el serrín de pino, un residuo de la industria de la madera de bajo coste, el serrín carbonizado y cinco carbones activados químicamente producidos a partir del serrín en distintas condiciones fueron caracterizados y utilizados como adsorbentes. El serrín de pino se mostró como un adsorbente eficaz para eliminar colorantes de madera de soluciones acuosas en modo discontinuo. No obstante, la eficiencia de adsorción mejoró significativamente con el uso del material carbonizado y de los carbones activados debido al aumento del área superficial. El carbón activado con KOH en una proporción de 1:4 (p/p) y 850 °C alcanzó los mejores resultados para la eliminación de colorantes, mientras que para la captura de CO_2, la activación a temperatura más baja (600 °C) mejoró la selectividad de la separación. Para planificar la aplicación del proceso a mayor escala, también se estudió la adsorción de colorantes para madera en modo continuo utilizando el carbón activado con el mejor rendimiento de adsorción para todos los colorantes en discontinuo. La investigación realizada constituye una contribución significativa al desarrollo y aplicación de nuevos materiales basados en biomasa para la captura de CO_2 y el tratamiento de aguas residuales contaminadas con colorantes.

Resumo

A intensa actividade industrial desenvolvida nas últimas décadas provocou a liberación de excesivas emisións de CO_2 á atmosfera, que é a principal causa do quecemento global, e a vertedura dunha importante cantidade de augas residuais que conteñen diversos compostos tóxicos. O reto consiste en desenvolver procesos de separación eficaces para evitar ou reducir a emisión de contaminantes en correntes gasosas e líquidas. Proponse a adsorción empregando novos adsorbentes como alternativa aos comerciais para separar o CO_2 das correntes gasosas e colorantes da madeira de solucións acuosas. Caracterizáronse e utilizáronse como adsorbentes serraduras de piñeiro, un residuo da industria da madeira de baixo custe, dito residuo carbonizado e cinco carbóns activados quimicamente producidos a partir das serraduras en diferentes condicións. As serraduras de piñeiro amosáronse coma un material eficaz no proceso de adsorción para eliminar colorantes de madeira de solucións acuosas en modo descontinuo. Con todo, a eficiencia da adsorción mellorou significativamente co uso do material carbonizado e dos carbóns activados debido ao aumento da área superficial. O carbón activado con KOH nunha proporción de 1:4 (p/p) e 850 °C atinxiu os mellores resultados para a eliminación de colorantes, mentres que para a captura de CO_2, a activación a menor temperatura (600 °C) mellorou a selectividade da separación. Para planificar o emprego do proceso a maior escala, tamén se estudou a adsorción de colorantes de madeira en modo continuo utilizando o carbón activado seleccionado con mellor rendemento de adsorción para todos os colorantes en modo descontinuo. A investigación realizada constitúe unha importante achega ao desenvolvemento e aplicación de novos materiais baseados na biomasa para a captura de CO_2 e o tratamento de augas residuais contaminadas con colorantes.

Contents

1. OBJECTIVES

Objectives

The pollution levels are increasing as a result of the use of coal, oil and manufacturing processes based on fossil fuels, causing a serious threat to the environment and to public health. The release of greenhouse gases, with carbon dioxide (CO_2) being the one that contributes the most, continues to grow and affects climate change and global warming. Additionally, due to a rapid growth in industrialization, water contamination is also one of the most significant environmental issues, being dyes one of the most discharged contaminants in wastewater that present a high level of toxicity for the aquatic environment, which can reach the food chain. In this Thesis, acid wood dyes were used since they are widely used in the wood industry to color their products and were provided by a local industry in Galicia. Therefore, it is mandatory to address the reduction of CO_2 and dye emissions to atmosphere and water bodies, respectively.

One of the most commonly used methods for the removal of a wide range of pollutants from gas and liquid streams is the adsorption onto activated carbons. The production and use of these carbons has increased significantly, however, the commercial ones besides coming from non-renewable sources, are expensive and difficult to regenerate. So, it is essential to find alternative precursors for the production of activated carbons, among which biomass and particularly waste biomass stands out. Using biomass wastes to produce activated carbon represents a sustainable waste disposal alternative to the conventional practice of burning it. Otherwise, carbon physical properties and effectiveness in removing contaminants depend not only on the precursor used but also on the carbonization and activation conditions, therefore, with a wise selection of these conditions, biomass derived activated carbons could show high adsorption performance compared to the commercial ones.

Based on these considerations, the general objective of the present Thesis was the use of an abundant and inexpensive biomass waste from our local wood industry, *Pinus radiata* sawdust, as adsorbent for the removal of wood dyes and CO_2 from liquid and gas streams, respectively, without any pretreatment or after converting it into biochar or chemically-activated carbons. To accomplish this general objective, some specific objectives were proposed.

The first specific objective was to evaluate the adsorption capacity of raw pine sawdust for the removal of wood dyes and CO_2 from aqueous solutions and gaseous streams, respectively. This objective was addressed in the paper "*Pimentel, C.H., Freire, M.S., Gómez-Díaz, D., González-Álvarez, J. Removal of wood dyes from aqueous solutions by sorption on untreated pine (Pinus radiata) sawdust. Cellulose 30, 4587–4608 (2023).* https://doi.org/10.1007/s10570-023-05145-4" and the following sub-objectives were proposed:

- To characterize the pine sawdust structure and morphology before and after adsorption experiments using BET surface area and pore size distribution determined from N_2 and CO_2 adsorption isotherms, scanning electron microscopy coupled with energy dispersive X-ray analysis and point of zero charge determination.

Objectives

- To evaluate the adsorption capacity of pine sawdust for dye removal through batch experiments analyzing the influence of different variables (adsorbent dose, pH, initial dye concentration agitation rate and contact time) on adsorption performance.
- To study the kinetics and equilibrium of the adsorption process in order to investigate the mechanisms responsible for adsorption.
- To study adsorbent regeneration performing adsorption/desorption cycles after selecting a suitable desorbent agent.

In order to investigate if sawdust adsorption performance could be improved a second specific objective was proposed, namely, the preparation of biochar and chemically-activated carbons from sawdust as precursor and their use for wood dye removal. This objective was addressed in the papers *"Pimentel, C.H., Freire, M.S., Gómez-Díaz, D., González-Álvarez, J. Preparation of activated carbon from pine (Pinus radiata) sawdust by chemical activation with zinc chloride for wood dye adsorption. Biomass Conv. Bioref. (2023).* https://doi.org/10.1007/s13399-023-04138-4" and "*Pimentel, C.H., Castro-Agra, R., Freire, M.S., Gómez-Díaz, D., González-Álvarez, J. Removal of wood dyes from aqueous solutions using KOH chemically activated carbons from pine (Pinus radiata) sawdust, submitted for publication"* and the following sub-objectives were proposed:

- The characterization of the materials prepared before and after adsorption following the methods previously described for pine sawdust and also by Transmission Electron microscopy, X-ray diffraction, CHNS elemental analysis, X-ray photoelectron spectroscopy and Fourier transform infrared spectroscopy, analysing the influence of the variables involved in the biochar and activated carbons preparation such as carbonization and activation temperature, type and concentration of the chemical agent and activation method on carbon characteristics and adsorption performance
- To evaluate the adsorption performance of biochar and activated carbons for dye removal in batch mode analysing the influence of the variables mentioned above for pine sawdust.
- To study the kinetics and equilibrium of the adsorption process in order to investigate the mechanisms responsible for adsorption.
- To study adsorbent regeneration performing adsorption/desorption cycles after selecting a suitable desorption agent.

Typically, batch investigation is used to assess the adsorbate removal capacity of adsorbents under various operational conditions and serve as a standard for establishing how efficient they are for removing a particular adsorbate. However, dye contaminated wastewaters must be treated in continuous mode, being fixed-bed adsorption the most commonly used alternative. Thus, the third specific objective was the study of dye adsorption in fixed-bed using the carbon that led to the best results in the previous stage. This objective was addressed in the paper "*Pimentel, C.H., Freire, M.S., Gómez-Díaz, D., González-Álvarez, J. Continuous adsorption of acid*

wood dyes onto an activated carbon prepared from pine sawdust, in preparation*"* and the following sub-objectives were proposed:

- To evaluate the adsorption performance of the selected activated carbon for dye removal in continuous mode analyzing the influence of influent flow rate, initial dye concentration and bed height.
- To model the fixed-bed column using different dynamic models for establishing the adsorption performance.
- To study carbon regeneration in fixed-bed performing adsorption/desorption cycles after selection a suitable desorption agent.

As previously mentioned, there is great interest in reducing CO_2 emissions that are the major cause of global warming and this is where the last specific objective arises, the use of sawdust, biochar and activated carbons for the separation of CO_2 from post combustion streams. This objective was addressed in the paper *"Pimentel, C.H., Díaz-Fernández, Lidia, Freire, M.S., Gómez-Díaz, D., González-Álvarez, J. Separation of CO_2 using biochar and KOH and $ZnCl_2$ activated carbons derived from pine sawdust, Journal of Environmental Chemical Engineering (2023). https://doi.org/10.1016/j.jece.2023.111378"* and the following sub-objectives were proposed:

- To evaluate the adsorption performance of pine sawdust, biochar and activated carbons for CO_2 separation analyzing the influence of temperature and pressure.
- To analyze adsorption equilibrium for CO_2 and N_2 using different isotherm models at different temperatures.
- To analyze the selectivity for the separation of CO_2 from CO_2/N_2 gas streams.

2. INTRODUCTION

Environmental contamination, including water pollution and the greenhouse effect, has caused considerable issues to human health as a result of rapid industrial expansion and over-exploitation of natural resources, therefore, it is crucial to solve these environmental problems [1]. Over the last years it has been increasingly recognized that global warming, causing harmful effects on the world's population is among the main causes of climate change, being carbon dioxide one of the compounds that contributes more to atmospheric pollution. In addition, another major factor that contributes to the pollution of water and habitats is the discharge wastewater containing dyes. These compounds are widely used in various industries, such as textiles, cosmetics, clothing, and wood, and their discharge without pretreatment has caused serious problems with aquatic contamination. These compounds have complex and stable aromatic structures, which are often toxic and present considerable difficulties in their degradation, creating a risk not only for aquatic contamination, but also for human health [2]. Thus, there is a growing interest in solving these environmental issues and several techniques have been developed based on physical, chemical and biological methods and in oxy-fuel combustion, pre-combustion and post-combustion processes for dyes and CO_2 removal for fuel-burning processes such as those in power plants, respectively [3,4]. Among them, adsorption stands out as one of the most promising techniques not only for capturing CO_2 but also for removing dyes from contaminated water, because it has many advantages over the other methods [5]. Thus, the development of materials as adsorbents to tackle environmental contamination is crucial and has become a research focus. As a result, from a sustainable point of view, it would be essential to produce multifunctional materials that can be used for wastewater treatment and for CO_2 capture. Therefore, in recent years the research on these types of materials has increased significantly. Some of the most used adsorbents are graphene, nanosilica, clays, polymeric materials, activated carbons, metal-organic frameworks, zeolite based materials, metal oxides, silicon-based molecular sieve materials, etc. [2,6].

2.1 Wastewater treatment

As mentioned before, water pollution is increasingly one of the biggest problems worldwide due not only to population and economic growth, but also to the urbanization and industrialization of the largest cities. Inevitably, these factors increase the use of chemical compounds and as a result, the volume of wastewater, which represents a high risk for existing water sources as well as for human health since it can trigger many diseases, neurological problems and cancer. Pure water is a precious commodity and exists in limited amounts, for this reason it becomes imperative to treat wastewater. Nowadays, three out of every ten people suffer from water scarcity according to a report produced by the United Nations [7]. It also reveals that only 3% of water is present in pure form, suitable for consumption and domestic use. Moreover, there are more than 663 million people without access to clean water and 2.2 million people die each year due to diarrhea caused by the consumption of untreated water. In this way, the demand for water increases by 1% annually, while the population increases [8, 9]. The presence of contaminants, such as pesticides, fertilizers, heavy metals, dyes and medicines in wastewater has been rising every year making them more toxic and causing a negative effect on living organisms when released into the environment [10]. Furthermore, the dye-laden

effluents will inevitably affect the aesthetics of water bodies. If this serious problem is not resolved, it is estimated that more than half of the population will live in regions without access to drinking water [7].

In particular, within the diversity of wastewaters, water contaminated by dyes requires special attention due to the huge volumes of dyes released into water bodies by the printing and dyeing industries over the last century. In various industries such as paper, plastic, printing, wood, rubber and leather, these chemical components are widely used for the final aesthetic effect they have on their products [11]. Consequently, there are more than 100,000 dyes or pigments used by different industries, which result in around $7x10^5$ tons of dyes synthesized globally each year [12]. In addition to the effects already mentioned, dyes also prevent sunlight transmission due to their accumulation, which will negatively influence aquatic life. Furthermore, they are known to contain hazardous compounds such as heavy metals (like lead and chromium) and aromatic compounds that are very harmful to human life [11]. In general, the classification of dyes can be carried out based on their chemical structure, including azo, indigoid, nitro or nitroso, anthraquinone and triarylmethane; or based on their solubility in water, in water insoluble such as azoic, vat, sulfur and dispersive dyes and in highly soluble such as acid, direct, basic and reactive. Although today they are essential in modern life, synthetic dyes present the limitation that even exposed to high temperatures, oxidizing agents or strong light, have very high chemical stability and tend to resist degradation [12]. For the above reasons, an efficient treatment of dye-contaminated wastewater is essential.

2.2 Gaseous effluents treatment

In the context of global warming, greenhouse gas emissions represent one of the biggest environmental concerns that many countries try to counterbalance [13]. Human activities and industrial production lead to the excessive release of CO_2 resulting from the burning of fossil fuels, which have contributed to a serious environmental problem and have caused the greenhouse effect. As a consequence, a gradual increase in the surface temperature of the earth is occurring which can lead to sea-level rise, abrupt weather shifts, and more frequent natural disasters [5]. Carbon dioxide, as the primary component of globally emitted greenhouse gases, accounts for approximately 75% of total emissions [13]. Fossil fuels account for 86.4% of world energy expenditure. The release of CO_2 has been problematic, but the use of fossil fuels has also increased other carbon emissions such as CO and CH_4, creating several challenges to mitigate environmental pollution issues. The high increase in CO_2 levels in the atmosphere, around 21.3 billion tons per year, of which only half are absorbed by natural processes has created some alarm as represents a net increase of around 10.65 billion tons per year. As a consequence, currently the level of CO_2 in the atmosphere has reached more than 400 ppm, which represents an increase of 40% compared to 1750, and continues to increase at 2 ppm/year causing an increase in temperature worldwide [14].

CO_2 is commonly found in oil and gas production plants, in water treatment plants, emissions from the combustion of fossil fuels, biogas, etc. It can cause corrosion problems, and the gas emission problem represents a safety risk. Confusion, headaches and shortness of breath are some of the

symptoms caused by CO_2 overload [1]. Thus, the development of CO_2 utilization and storage techniques is required. CO_2, being an acidic gas, might be eliminated via absorption utilizing monoethanolamine and diethylamine as solvents. High energetic requirements for regeneration, high corrosivity of the amine solutions and the large absorber capacity represent some of the main limitations of this procedure [15]. Hence, CO_2 capture and storage (CCS) technologies, including adsorption, have been identified as a significant alternative for reducing CO_2 emissions. According to literature, the deployment of CCS techniques can decrease future CO_2 emissions by about 20% [13], therefore, it is highly desirable to explore these separation techniques that can lead to high-efficiency CO_2 uptake.

2.3 Technologies for dye removal and CO_2 capture

2.3.1 Dye removal methods

Water and soil contamination has increased in recent years due to the continued use of organic products such as dyes. In this way, a long-term sustainable and at the same time effective solution must be developed for the treatment of effluent containing dyes. In the past, importance was not given to this problem, and only in the last 30 years it has received the necessary attention due to the emergence of several health problems. Thus, solutions were promptly presented both by the governments and by the dye manufacturers. In recent years, the government environmental agencies set a law that forced companies to ensure that wastewater discharged from their facilities complies with The International Dye Industry Wastewater Discharge Quality Standards, which were adopted from the Zero Discharge of Hazardous Chemicals Programme (ZDHC) [16]. The international standard for dye effluents discharge is shown in Table 1.

Table 1. International standard for the discharge of dye effluents into the environment.

Pollutant factor	Amount permissible to be release
Biological oxygen demand	Below 30 mg/L
Chemical oxygen demand	Below 50 mg/L
pH	Between 6-9
Colour	Below 1 ppm
Suspended solids	Below 20 mg/L
Temperature	Below 42 °C
Toxic pollutants	Not allowed

Therefore, to meet these discharge criteria, application of current dye removal treatments to wastewater which can be classified in biological, chemical and physical, is mandatory.

- Biological treatments

These treatments are widely used in several countries. Generally, numerous microorganisms are used under aerobic or anaerobic or a combination of both conditions prior to the release of dye-laden effluents into the environment. Besides the conventional method (aerobic-anaerobic combination), other techniques include adsorption by microbial biomass, breakdown by algae and enzymes, fungal and microbial cultures, as well as pure and mixed cultures [16,17]. These procedures are not

expensive and can be carried out easily, however, this treatment alone is not sufficient to remove dangerous dye residues from wastewater. Moreover, its efficiency is frequently unsatisfactory due to the formation of extra sludge, and it takes a long time.

- Chemical treatments

Another efficient alternative to removing dyes from wastewater is chemical treatment. However, this is more expensive due to the high consumption of chemical reagents and electrical energy as it requires specific equipment. In addition, this approach may be ineffective as interactions may occur between chemical reagents and wastewater contaminants, and at a large-scale, the use of chemical reagents in huge volume is another disadvantage of this type of treatment. Furthermore, secondary contamination can occur because of harmful chemicals that are also released. Ultraviolet irradiation, ozonation, photochemical, oxidation, Fenton reaction dye removal and electrochemical coagulation are some of the most commonly used chemical dye removal methods. For all the reasons mentioned, excluding electrochemical degradation, and compared to physical or biological treatments, most of these methods are expensive and commercially unappealing [16,17].

- Physical treatments

Adsorption, membrane filtration, irradiation, reverse osmosis, ion exchange and coagulation and flocculation represent the most common techniques among physical methods. Compared to the other methods, the physical ones are the most used due to their effectiveness and simplicity. Moreover, these techniques require fewer chemicals and do not include living organisms. Particularly, the adsorption technology has proven to be very useful and very effective in treating wastewater as it can remove pollutants and discolour water sources, which is why it has been one of the most broadly used techniques [16,17].

2.3.2 CO_2 capture methods

As previously mentioned, carbon capture, utilization and storage (CCUS) methods and technologies are among the main strategies to reduce CO_2 emissions. The objective of these methods is to capture CO_2 from industries and store it or convert it into value-added products [18]. The Copenhagen accord requires that global temperature rise be limited to 2 °C above pre-industrial temperature levels by 2100, and International Energy Agency (IEA) stated that CCUS technology is required to reach the ± 2 °C goal with a contribution of 19% in 2050 [19]. Additionally, the European Commission mentioned the importance of using CCUS technologies and they are officially mentioned in documents such as the European Green Deal.

The CO_2 capture and storage techniques consist, as the name suggests, firstly in capturing CO_2 from major industrial sources (such as the flue gas from fossil-fuel power plants) and its subsequent storage in underground structures or convert it into useful products. These technologies incorporate pre-combustion carbon capture, post-combustion carbon capture and oxy-combustion carbon capture [18]. Afterwards, the CO_2 that is captured can have multiple uses such as in the food, pulp and paper, petroleum, cement, ammonia and iron and steel industries [20].

- Pre-combustion process

In this case, CO_2 from fossil fuels is eliminated before the complete combustion process, through fuel gasification with oxygen (e.g. Integrated Gasification Combined Cycle (IGCC) coal gasification technology) or with steam obtaining finally high concentrated CO_2 stream, facilitating its following separation. It is an extremely efficient process from an energy point of view. Moreover, pure H_2 is obtained after complete separation and storage of CO_2. As a result, it is cost effective, has a low water consumption, low regeneration cost, and the H_2 gas obtained can be used as a fuel [18,20,21].

- Post-combustion process

This process is useful to capture CO_2 from a flue gas or even a mixture of gases produced (CO_2, nitrogen and some oxygenated compounds like SO_2, NO_2 and O_2) by burning of carbonaceous materials. Some technologies that can be applied in this procedure are chemical absorption, physical adsorption, membrane separation, cryogenic separation, process with microalgae, or the use of a chemical loop. Chemical absorption with an alkanolamine-based solvent is currently well established on the market and can now be used and installed in coal-fired based thermal power plants. The amine can selectively absorb CO_2 allowing nitrogen and oxygen go to the atmosphere. The amine-CO_2 is then stripped using steam, obtaining at the end a concentrated CO_2 stream, and the absorbent could be reused. However, it presents some disadvantages, such as requiring a high volume of gas for treatment due to low CO_2 pressure, the high cost of the amine solvent, the cost of energy regeneration (80% of the entire process), the large size of the equipment, and the capital investment [18,20].

- Oxy-combustion process

The oxy-combustion procedure is applied after the combustion process in an atmosphere that contains only oxygen by utilizing, for instance, an oxygen gas turbine to separate the CO_2 produced during the oxy-combustion process. The stream contains mainly CO_2 and water vapor, and the separation of CO_2 is performed by condensation. This process does not require an excessively expensive CO_2 capture system and appears as an alternative to the post combustion process. Despite the attention given to this process due to the purity of CO_2 that it is possible to obtain (approximately 100%) and economical operation, it has several disadvantages, such as the extremely high process temperatures (around 3500 °C), the high volume of oxygen required, the risk of the operation, and high cost, which is why it is not yet commercialized [18,20].

Consequently, solid adsorption is the suggested to overcome the drawbacks of conventional separations and procedures commonly used in the abovementioned processes [19].

2.3.3 Dye and CO_2 separation by adsorption

The adsorption technique is based on the ability of a given solid (adsorbent) to retain specific substances (adsorbates) from liquid or gaseous streams on its surface [22,23]. In general, adsorption is a multi-step process. Firstly, as the fluid flows through the particles, the adsorbate (contaminant) diffuses from the bulk fluid to the external surface of the adsorbent, then within the pore to the surface where it is adsorbed [24]. However, increasing the porosity of the adsorbent will

automatically increase the area available for adsorption to take place, since adsorption is a surface phenomenon. Adsorption is an excellent pollutant elimination procedure since it does not require special equipment and is simple to use. Aside from that, before adsorption begins, it is not necessary a pre-treatment. To ensure efficient contaminants removal, porous materials are ideal for carrying out the adsorption process.

Given the diversity of existing adsorbents and the growing interest in green technology and biotechnology, there are numerous applications for the adsorption process. Some adsorption applications are listed below [23].

- For liquid-phase adsorption
    a. Decolourizing, drying, or degumming petroleum products.
    b. Eliminating dissolved organic species from drinking water sources.
    c. Eliminating flavour, colour, and odour from water sources.
    d. Industrial and domestic wastewater advanced treatment.
    e. Vegetable oils and crude sugar syrup are decoloured.
    f. Protein, pharmaceutical, and bio-compound recovery and concentration from diluted solutions.
    g. Isoparaffin and paraffin bulk separation.

- For gas-phase adsorption
    a. Recovering vaporized organic solvent.
    b. Gases' dehydration.
    c. Eliminating noxious substances and odours for personal safety.
    d. Air separation.
    e. Distinguishing isoparaffin aromatics from regular paraffins.
    f. Using CO_2 capture to combat climate change.

Adsorption can be divided into chemical adsorption or chemisorption and physical adsorption or physisorption. Chemical adsorption implies the occurrence of strong chemical interactions between molecules through electron exchange, which is why it is often irreversible. On the other hand, physical adsorption involves weak Van der Waals forces, hydrogen bonds, dipole-dipole π-π interactions, etc., between adsorbent and adsorbate and thus it is reversible in most cases [17,22]. In general, the main differences can be summarized as follows [25]:

- The degree of specificity of the physisorption phenomenon is quite low when compared with chemical adsorption.
- In general, in chemical adsorption, monolayer formation occurs when molecules are linked to active centres of the surface. Physisorption often occurs in multilayer adsorption at high relative pressures.
- The identity of a molecule is lost, due to the chemical interactions either by reaction or dissociation, when chemically adsorbed and is not recovered through desorption. This does

not happen in the case of physical adsorption, in which the molecule maintains its identity even after dissociating.

- The enthalpy of chemisorption is comparable to the that of a chemical reaction. Physical adsorption is exothermic, but the energy involved in the process is usually not higher than the energy of condensation. However, a large increase in the adsorptive energy occurs when physical adsorption takes place in very narrow pores.
- In chemical adsorption, sometimes the system does not have enough energy to reach thermodynamic equilibrium at low temperatures since the adsorption rate is low. Physical adsorption usually reaches equilibrium quite quickly if the limiting stage is not the transport process.

The adsorption technique alone represents an appealing alternative for the treatment of wastewater and polluted gas streams. However, it is even more advantageous than the other techniques when using economical adsorbents that do not need pre-treatment. This technique has been presented as an excellent alternative in terms of design, flexibility, starting cost, simplicity, sensitivity to hazardous contaminants and easy to put into practice. Furthermore, this technique does not generate hazardous chemicals, such as oxidizing agents (ozone) or free radicals. Some of the most studied factors that can affect the adsorption efficiency are adsorbate-adsorbent interaction, adsorbent surface area, adsorbent to adsorbate ratio, adsorbent particle size, temperature, pH and contact time, among others [22].

2.3.3.1 Dye removal

Due to the stability of synthetic dyes, their removal using conventional methods previously mentioned is very difficult, which makes adsorption an appealing process for their removal. Moreover, effluents treated by adsorption show a much higher quality than those treated by conventional methods. However, the main drawback of this process is the high cost of the adsorbent. This can be overcome by the appearance of inexpensive adsorbents that are equally efficient and present high adsorption capacities. Therefore, this technique stands out not only for its cost but also for its efficiency.

When doing lab-scale tests, it is important to study the influence of the aforementioned variables in order to guarantee that the target rate of removal is achieved. Furthermore, they can help in the development and implementation of industrial-scale dye removal methods [16,26].

In general, during dye adsorption, various mechanisms between the dye and the adsorbent could be involved (Figure 1), such as electrostatic interactions, the formation of hydrogen bonds, π-π interactions, proton migration, and chemical precipitation or hydrophobic interactions. Apart from that, adsorption is dependent on pore and adsorbate size and contact time.

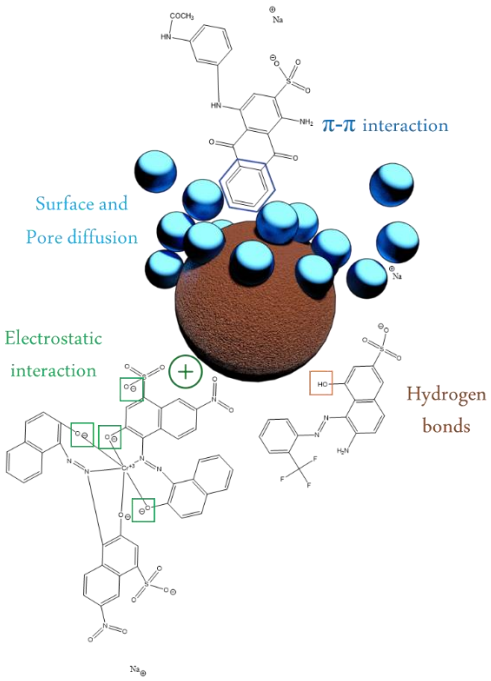

Figure 1. Illustration of adsorption process and some mechanisms for dye removal from wastewater.

- **Electrostatic interaction:** this mechanism may include both electrostatic attraction and repulsion. When the surface of the adsorbent has an opposite charge to the dye, cation or anion exchange can occur. On the other hand, electrostatic repulsion occurs when both adsorbent surface and adsorbate present the same charge. Furthermore, depending on the pH of the solution, the surface charge of the adsorbent can be altered, thus allowing selective adsorption of both cationic and anionic dyes with the same adsorbent [27].
- **Formation of hydrogen bonds:** The electronegative atoms such as fluorine, nitrogen, and oxygen form hydrogen bonds with electropositive hydrogen atoms. The probability of formation of these bonds increases when some functional groups (such as amines, alcohols or carboxylic acids) are present both on the surface of the adsorbent and in the dye structure [27].
- **π-π interaction:** Dyes are normally aromatic compounds, and aromatic structures can also be found in many adsorbents such as MOFs, carbon-based materials and polymer-based materials. Therefore, electron donor-acceptor (EDA) or π- interactions can occur during the dye adsorption process [27].
- **Proton migration:** protonated dyes are cationic dyes that have positive charges due to bonded hydrogen ions (H^+). In this case, it is interesting to employ adsorbents with high H^+ affinity [27].
- **Chemical precipitation and hydrophobic interactions:** Due to the increase in ionic strength, when there is no electrostatic interaction, the adsorption process may be due to the increase of hydrophobicity interactions (nonpolar molecules) [28]. Otherwise, mainly at high dye concentrations, in some cases, chemical precipitation of the dye is the main mechanism forming conglomerates and floccules [29].

- **Size-dependent adsorption:** size-dependent selective adsorption can be a viable option, being the smallest dye the one that will be adsorbed in greater quantities into the pores of the adsorbent. However, it may be necessary to analyse the factors that can affect each particular case [27].
- **Time-dependent adsorption:** adsorption process comprises distinct stages, including external mass transport of dye from the bulk phase to the solid-liquid interface, internal diffusion (intraparticle mass transfer) and intrinsic kinetics (physisorption or chemisorption) which are time dependent and can control the adsorption process. Therefore, the analysis of this time dependence must be performed to understand the adsorption process [27,30].

All this evidence the complexity of the adsorption phenomena, especially due to the wide range of dyes, types of adsorbent, and operational conditions involved.

2.3.3.2 CO_2 recovery

As mentioned previously, adsorption appears to be the best option for CO_2 capture compared to other techniques such as aqueous amine absorption [19].

In brief, CO_2 molecules that are contained in a gaseous stream are attracted and retained as a result of either physical or chemical interaction on the available active sites on the adsorbent surface. Afterwards, when equilibrium is attained, the CO_2 molecules can be recovered in their pure form by desorption varying pressure or temperature, and subsequently the adsorbent can be reused. Mostly activated carbons or molecular sieves are employed for CO_2 adsorption. Some factors that can most influence the adsorption process are surface characteristics of the adsorbent, temperature, pore volume or size, CO_2 concentration, CO_2 partial pressure, among others.

In physical adsorption, no chemical reaction occurs with the adsorbent, instead, Van der Waals or electrostatic forces interact with the CO_2 molecules and the adsorbent surface. This type of adsorption can be reversible through changes in temperature or pressure. When the adsorption process takes place at room temperature, physical adsorption is favoured and is directly connected with the surface structure of the adsorbent. Some of the advantages of this process are that it is preferred for high-pressure operations, the adsorbent's regeneration is straightforward, and requiring less energy demand. On the other hand, some drawbacks are the low CO_2 adsorption at low pressure, the low CO_2 selectivity, the limited adsorption capacity in presence of moisture, and the decrease in CO_2 adsorption of with increasing temperature [20].

The main limitation of physical adsorption is the poor CO_2 selectivity. In the chemical adsorption the selectivity is improved preparing the adsorbent with chemical coating (applying a coat on the pore surface) or grafting procedure (by add functional groups to the porous surface). Coating is performed by the addition of some primary compounds (mainly amine) having basic groups in its structure that will improve the capture of acidic CO_2 molecules. Furthermore, the addition of Lewis bases improves the material affinity for CO_2, since this molecule behaves as a weak Lewis acid. The main types of

chemical adsorbents prepared in this way are carbonates, alkali metal oxides and amine-functionalized porous materials. In the chemical adsorption process the adsorbent present high CO_2 capture capacity even in the presence of moisture or at low CO_2 partial pressures. However, this method has some disadvantages related to adsorbent regeneration as a high energetic requirements, a poor cyclic capacity due to amine degradation, corrosion of equipment, and a high cost of operation [20].

Physical adsorbents' capacities are mainly determined by surface area and affinity for CO_2, whereas the chemical adsorbents characteristics can vary greatly depending on how they interact with CO_2 molecules [31].

An appropriate adsorbent for CO_2 capture should fulfil the following requirements: (a) low-cost of the precursor raw material, (b) low heat capacity, (c) rapid kinetics, (d) high CO_2 adsorption capacity, (e) high CO_2 selectivity and (f) thermal, chemical and mechanical stability under frequent cycling [19]. Table 2 resumes the criteria that a good CO_2 adsorbent should satisfy.

Table 2. Values of different parameters for selecting an effective CO_2 adsorbent [32].

Parameter	Requisite
CO_2 adsorption capacity	3-4 mmol/g
Regeneration	>1000 cycles
CO_2 gas selectivity	>100
Adsorption/desorption kinetics	>1 mmol/g.min
Cost of the adsorbent	$5-15/kg sorbent

Depending on the adsorbent's structure, different processes may take place for CO_2 adsorption, and either compete or work together, such as molecular or bulk diffusion in the macropores and surface diffusion where the adsorbate can migrate contributing to intraparticle diffusion due to the formation of multilayers. However the rate of diffusion can be restricted if the adsorbate have a similar size of the micropore [31].

2.4. Adsorbents used in water and gas treatment

As previously described, adsorption is the most promising technique for both water and gas purification. The main element in the adsorption process is the adsorbent, which is characterized by being commonly a porous and insoluble material that can easily be recovered and whose cost generally affects the cost of the process. Thus, various commercial materials as activated carbons are widely used in diverse industries for liquid and gaseous effluent treatment. However, the cost-effectiveness and difficulty of their regeneration justify the search for alternative adsorbents. In general, an adsorbent can be considered low-cost when no treatment is required, it is abundant in nature, or it is an industrial waste that no longer presents economic value or is considered as a by-product. Apart from being inexpensive, the material should be easily accessible and non-hazardous in nature. Moreover, from the point of view of its performance, the four critical factors that define a good adsorbent are: (1) a good adsorption capacity; (2) a high surface area which increases with

increasing porosity; (3) a high adsorption capacity in a short adsorption time; and (4) versatility in removing different contaminants in different conditions [16,22].

With this goal, numerous adsorbents have been employed for dye removal [16,22].

- **Agricultural wastes:** They are environmentally friendly, inexpensive, efficient, and capable of replacing commercial activated carbons commonly utilized. Tree barks or wood sawdust are examples of waste materials often used as adsorbents with good potential due to their physicochemical properties.
- **Biomass-based activated carbon derived from solid wastes:** Activated carbon is a carbonaceous material available in powder, granular, extrudate, spherical, fiber, bead, or cloth forms and exhibits an amorphous structure with an elevated level of porosity, physicochemical stability, mechanical strength and degree of surface reactivity. The most typical sources used to produce activated carbon on a large scale are wood, anthracite and bituminous charcoal, peat shells, lignite and coconut. It has pores that are cylindrical, rectangular, or irregularly shaped with pore widths lower than 2 nm for micropores, between 2 and 50 nm for mesopores and higher than 50 nm for macropores. Additionally, any inexpensive carbonaceous material with a high carbon content, minimal ash content, and a substantial volatile matter content can be used to create activated carbon. Based on the type of precursor used for its production, activated carbon can be categorized in fossil resources, graphene, synthetic resin, synthetic polymer, biopolymer and biomass derived activated carbon [32–34]. Activated carbon has been frequently linked to the presence of heteroatoms such as oxygen, sulphur, hydrogen, nitrogen, halogen, and other elements in the form of functional groups or atoms that were chemically bonded to the structure. Functional groups such as carboxyl, carbonyl, phenol, lactone, and others containing oxygen were discovered to be the essential functional groups present in its structure. The type and number of oxygen surface groups found in activated carbon are influenced by both the precursor and the activation procedure. Activated carbon from agricultural wastes has the great advantage of being a low-cost material that often replaces granular activated carbon derived from non-renewable coal. Additionally, it has an adsorption efficiency comparable and sometimes higher than the other. Due to their abundance, agricultural by-products are useful raw materials for the manufacturing of activated carbons. Besides, the initial precursor and the type of material used for the production of activated carbon will directly influence its quality, characteristics and features.
- **Industrial by-products:** fly ash, red mud, biosolids, metal hydroxide sludge, and waste slurry are inexpensive and easily accessible materials that can be also used as adsorbents for dye removal.
- **Inorganic materials:** materials like clay minerals, siliceous materials, and zeolites are effective adsorbents. Clays can be combinations of fine-grained clay minerals and clay-sized crystals of other minerals such quartz, carbonate, and metal oxides. Natural siliceous adsorbents are frequently utilized for wastewater treatment as they have a very high

adsorption capacity, availability, chemical reactivity and hydrophilic surface. Silica is a mesoporous material with a substantial surface area (700-1500 m^2/g) and a mesoporous channel that is regularly shaped (cylindrical) with pores size range between 2 and 30 nm. Sol-gel processes, template-assisted procedures, microwave-assisted techniques, and chemical etching methods can be used to produce them. However, they contain several surface groups that strongly and frequently irreversibly promote non-specific adsorption. Zeolites are extremely porous, have a three-dimensional structure with homogeneous pore diameters between 0.5 and 1.2 nm that is made up of interconnecting channels and are negatively charged. Moreover, as they are inexpensive, usually have a high surface area (between 400 and 925 $m^2\ g^{-1}$) and ion-exchange capacity, they become attractive adsorbents. Silica, aluminum, inorganic and/or organic structure directing agent molecules are the sources used in a basic aqueous medium to synthesize crystalline zeolites via hydrothermal method.

- **Microbial biomass:** To remove colour from solutions, biological components such as chitin, chitosan, peat, yeasts, fungi, or bacterial biomass are utilized as sorbents. These are frequently more selective than commercial activated carbons and traditional ion-exchange resins. Diverse functional groups, such as amino, carboxyl, sulphate or hydroxyl groups presented on the sorbent promote the binding mechanism. However, their use is limited as they have low mechanical stability and elasticity, low regeneration rate and sorbent swelling or clogging [22,35].

Although several inexpensive adsorbents have been investigated, the studies performed show that the main limitation is the low surface area, which results in low adsorption capacity [36]. Consequently, efforts to found substitute low-cost materials are currently ongoing.

A diversity of adsorbents for CO_2 capture have been discovered and synthesized including physical adsorbents such as silica materials, activated carbons, alkali-metal/metal oxides based materials, covalent organic framework (COF), ordered porous carbon, zeolites, activated carbon fiber (ACF), carbon molecular sieves (CMS), graphene and metal organic framework (MOF); and chemical adsorbents such as composite adsorbents made through impregnation with K_2CO_3, binary eutectic mixture (KNO_3 and $LiNO_3$), $NaNO_3$, Al_2O_3, TiO_2, MnO_2, ZnO, ionic liquid (IL) and aqueous amine into the support matrix. The most frequently adsorbents used in research studies are described below.

- **Zeolites:** They can be used to adsorb CO_2 due to the exchangeable alkaline or alkaline-earth cations in the zeolite framework's channel.
- **Silica:** Due to its excellent chemical and thermal stability, tuneable pore width, substantial specific surface area, simple functionalization, and mesoporous character it can be employed for CO_2 adsorption.
- **Metal organic framework (MOF):** exhibit three-dimensional crystallographic structure and a high surface area of 1000-10000 m^2/g. MOFs have pores up to 150 nm in size and are made up of metal ions, metal clusters, and organic ligands. Hydrothermal, electrochemical, mechanochemical, microwave assisted, ultrasound assisted, spray-drying and flow

chemistry are the ways available for their synthesis. These structures are used not only for CO_2 adsorption but also for hydrogen (H_2), methane/ethane (CH_4/C_2H_6) and hydrocarbons adsorption and catalysis owing to their high surface areas, surface functionality within the frameworks and exceptional chemical adjustable pore geometry.

- **Activated carbon:** Advantages of using this type of material for CO_2 capture include the capability of maintaining thermal stability under inert atmospheres and at high temperatures, a high adsorption capacity at ambient pressure, low acid-base reactivity, large porous surface area with well-developed porous structure, changeable surface chemistry and pore structure, elevated hydrophobicity, and suitability to be used at moderate temperature and atmospheric pressure [34]. Due to the vast abundance and well-distributed worldwide biomass, its conversion into porous activated carbon has been adopted as a common practice.

2.4.1 Wood sawdust and derived activated carbon

Sawdust is an inexpensive lignocellulosic material that is widely accessible (over 24.25 million m^3 per year produced worldwide). It is a waste from both agricultural and industrial activities and is therefore widely distributed, generating disposal problems. As a waste product, sawdust is generated when the wood is cut, edged, sawed, trimmed and smoothed. The major sources of sawdust are woodwork and wood-processing industries being incineration. However, recently, there has been a lot of interest in its management and research studies have been conducted to convert it into different substances for particular applications [37,38]. Sawdust mostly contains cellulose (45-50%), lignin (23-30%), hemicelluloses (20-30%) and numerous extractives (acids, soluble sugar, resins, waxes, oil, etc.) (1.5-5%) (Figure 2). Therefore, it may be appropriate for adsorbing a wide range of contaminants since it has several functional groups, including carboxyl, amide, phenolic, and hydroxyl groups in its structure. Some of its remarkable characteristics include its rough surface, elevated porosity, carbon content and reasonable surface area, strong liquid holding capacity, low specific gravity, good mechanical stability, and ease of biodegradation and modification [37].

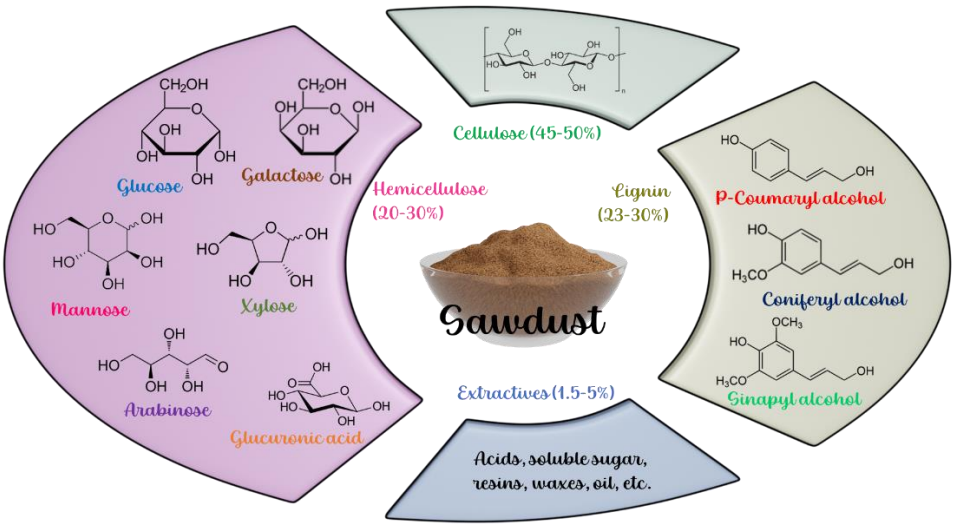

Figure 2. Sawdust and its structure adapted from [37].

Sawdust, as a lignocellulosic material, can be also utilized as a sustainable precursor to generate activated carbon. A crucial factor in the development of pores, pore volume, and surface area of the activated carbons is the chemical composition of precursor [12].

As mentioned before, generally there are two main sources to produce activated carbon: (1) coal and (2) agricultural by-products or lignocellulosic materials. As the carbon content of the latter is lower than those of anthracite, coal or peat, the yield of the activated carbon is expected to be lower [39]. Usually, two different techniques can be used for activated carbon production: physical and chemical activated methods. In order to improve the surface area and adsorption properties of activated carbons, agents such as strong acids, alkalis or salts can be applied in chemical activation, while carbon dioxide, water steam or gas mixtures can be applied in physical activation [37]. Both methods include the carbonization process with the purpose of eliminating the volatile matter from the raw material at low temperature (400-700°C) and then produce activated carbon from the char that was previously produced and presenting an elevated content of fixed carbon. During the thermal decomposition of the precursor carried out through carbonization or pyrolysis, volatiles and non-carbon species such as hydrogen, oxygen and nitrogen are removed, and the percentage of carbon in the biochar increases. A thorough selection of the carbonization conditions is crucial since they have a major impact on the process and the quality of the biochar produced. Some factors to consider are carbonization temperature, the rate at which reactions heat up, the flow rate of inert gas, and the carbonization residence time, also known as the holding period. Additionally high temperature reduces the charcoal yield [8].

The physical activation method comprises two steps: (1) biomass carbonization in an inert atmosphere (nitrogen or helium); and (2) activation of the carbonized material at elevated temperatures (between 800 and 1100 °C) under an atmosphere of air, oxygen, carbon dioxide, steam, or mixed. This method generates an activated carbon with a porous structure. It is inexpensive and it is considered as a green approach since chemical agents are not used. However, requires a long

activation time and high energy expenditure and usually the activated carbon presented a low adsorption capacity [40].

Chemical activation method can involve one or two stages. Except for the carbonization stage, both processes are identical. In the single-stage process, the material is not carbonized, and the dry material is directly activated through interaction with dehydrating chemical agents like sodium hydroxide (NaOH), potassium hydroxide (KOH), zinc chloride ($ZnCl_2$), or phosphoric acid (H_3PO_4). In the two-step method, first the raw material goes through the carbonization process in order to generate biochar at a temperature generally between 400 and 600 °C, followed by activation. The activation can occur via impregnation (wet method) of the raw material or by mixing the obtained char with dehydrating chemical agents (dry method) [8,41]. By degrading, dehydrating, and complexing with organic carbon present in the precursor, the use of chemical agents accelerates the pore development in the activated carbon. Contrasting with physical activation, low temperatures without the need for an oxidizing atmosphere can be applied to this process; however, it is necessary to wash the material to remove products that have not reacted and chemical subproducts.

A scheme with the possible ways to obtain the activated carbon is presented in Figure 3. Usually, both techniques have been employed by researchers in order to achieve the good performance activated carbon from precursors [12].

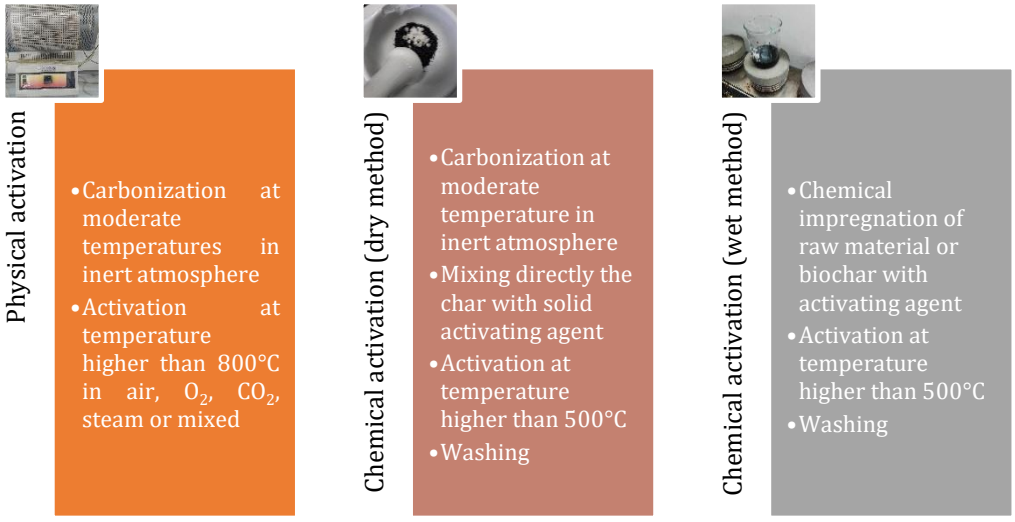

Figure 3. A scheme of the activation process of sawdust-derived activated carbon.

Chemical activation agents are dehydrating substances that have an impact on pyrolytic decomposition increasing the yield of activated carbon and developing the porous structure. These activating chemicals that deeply penetrate the carbon structure led to the creation of smaller pores, which consequently increase the surface area. The main chemicals employed as potential activating agents and the different reactions with the precursor are described below.

- **Activation with phosphoric acid:** for lignocellulosic materials, due to cellulose's resistance to acid hydrolysis, the first reaction occurs with lignin and hemicelluloses.

Depolymerisation, dehydration and relocation of biopolymers in the lignocellulosic materials are the principal processes of activation with H_3PO_4. Also, due to the reaction with this activating agent, volatile substances and products in the form of particles are generated, which lead to pore creation or the increase in the number of pores. Moreover, this agent leads to the expansion of micropores and mesopores, so the resulting carbon is very porous. The surface hydrophilic properties are enhanced by the addition of more acid groups. The two main functions of H_3PO_4 are the improve of the pyrolytic decomposition and the creation of a grid-like structure. This requires a low activation temperature.

- **Activation with zinc chloride:** $ZnCl_2$ acts as a dampening agent during activation. Volatile compounds move through the pores that are saturated with zinc chloride and are released from the activated carbon surface through the activation process. This agent causes swelling in the cellulose molecular structure, an electrolytic action. The cellulose molecules decompose due to the swelling, increasing the number of cavities and increasing the surface area. In the activation process, as the lignocellulosic material turns into charcoal, the hydrogen, oxygen, carbon monoxide and dioxide, methane and aldehydes are released. Moreover, $ZnCl_2$ prevents the bitumen formation and other substances that may obstruct the carbon's surface. With this agent the yield increases due to polymerisation and the production of some larger ring aromatic compounds. It acts as a Lewis acid, improving the condensed aromatic reactions by promoting the formation of molecular hydrogen derived from hydro-aromatic structures originating from precursors. As a result, polymerization reactions occur and are influenced by the activating agent because some of the active sites from the nearby molecules are excluded. Increasing the amount of $ZnCl_2$ can lead to a decrease in productivity due to the micropores break down forming mesopores.
- **Activation with potassium carbonate:** Upon activation with K_2CO_3, porosity develops due to its reduction under inert condition to form K, K_2O, CO_2 and CO. The char matrix interior structure is penetrated by the potassium composite created in the activation process, which also causes new pores to emerge. Additionally, pores or cavities may form on the surface of the coal due to the evaporation of the activating agent that previously occupied these locations. This can lead to the development of micro and mesopores. In carbons activated with this agent, phenolic groups are more specific than the other groups. By raising the activating agent dosage, the dehydration effect decreases and result in mesopores degradation, reducing the adsorption efficiency. On the other hand, the increase of the activating temperature increases the microporosity.
- **Activation with sodium hydroxide:** alkaline materials usually lead to the production of large amounts of micropores. The interaction between NaOH and the carbon led to the occurrence of some chemical reactions with the formation of Na_2CO_3, Na and H_2. This results in micropores formation due to the release of CO, CO_2 and H_2 gases produced by Na_2CO_3 decomposition at elevated temperatures and hydroxyl reduction, and also the carbon structure intercalation of an alkali metal. The evaporation of NaOH creates a rough surface with various pore diameters. The pores enlarge due to sodium hydroxide separation and

disintegration of the graphite layers during the oxidation-reduction process. The increase of the NaOH-char ratio has a significant influence on the creation of pores, which consequently increases the surface area and pore volume. However, excess of NaOH may lead to a strong gasification that will reduce the surface area by destroying the walls between the pores.

- **Activation with potassium hydroxide:** this activating agent has been widely used due to its ability to produce activated carbon with high specific surface area, minimal environmental contamination, reduced corrosiveness, cost-effectiveness, and generation of a good pore size distribution. KOH promotes the pore formation because of its evaporation from sites previous occupied by it during the activation. KOH activation promotes a high surface area and pore volume, but normally has a lower yield (10-40%). The formation of alkali metals and carbonates during the activation process with alkali substances confers stability to the activated carbon and enlargement of the gaps between the carbon-atom layers in the carbon matrix, as well as effectiveness and adsorption capacity. Activation occurs through oxidation in an alkaline environment with a high oxygen content. The surface area increases with pore formation that are generated when activation occurs with a high KOH content, which leads to the removal of carbon atoms from the internal structure. When gasification takes place, potassium metal is assumed to be inserted into the carbon matrix internal structure, causing pores to expand and form new ones. As a result, increasing the potassium hydroxide concentration is crucial for porosity development. Activating with KOH requires high temperature, usually above 650 °C. When activation is carried out with alkaline agents such as KOH, this agent acts as an electron donor promoting a rise in the positive charge of the material, which is desired to adsorb anionic contaminants.

In general, chemical activation is cheaper and still has some advantages over physical activation such as the requirement for lower activation temperature, less processing time and a higher carbon effectiveness. Additionally, compared to physical activation, the structure of activated carbon produced through chemical activation is more porous. A porous structure is created when activated chemical compounds interact with carbon matrices and release gas products [40].

3. METHODOLOGY

Acid wood dyes (Blue for wood AGN-270%, Red for wood GRA-200%, and Black Hispalan M-RN-140%) were supplied by a wood company (A Coruña, Spain). Their elemental composition was evaluated through energy dispersive X-ray analysis (EDX) (ZEISS EVO LS 15 microscope). The stability was evaluated through the analysis of the visible absorption spectra of the dyes recorded by UV/Vis spectroscopy (V-630, Jasco) analyzing the influence of pH and time. The dissociation constant (pK_a) was determined using two different methods. For the red dye that presents a color shift with pH changes, pK_a was determined using UV/VIS spectroscopy (V-630, Jasco) by measuring the absorption wavelength at different pH values. For the blue and black dyes, pK_a values were determined by potentiometric titration with NaOH (Chapter 3, paper 1).

Pine (*Pinus radiata*) sawdust was supplied by a regional sawmill (Lugo, Spain). It was air-dried and used without pretreatment. It was sieved using a RoTap type electrical sieve shaker (FTL-0200), and the fraction between 0.5 and 1 mm was selected for the adsorption experiments and stored in plastic containers. Before these experiments and to assure that the sawdust does not release colored components that could interfere with the adsorption measurements, the sawdust was kept in water for 24 h in an Unitronic orbital C shaker (Selecta) at different pH values (2, natural (5.1) and 12). Based on the results obtained of water coloration pH = 12 was excluded for adsorption experiments (Chapter 3, paper 1).

Pine sawdust was characterized through the determination of the specific surface area and pore volume by the adsorption/desorption of N_2 at -196 °C and CO_2 at 0 °C using an ASAP 2020 surface area analyzer (Micromeritics). Barrett-Joyner-Halenda (BJH) desorption isotherm was used to determine the pore volume and pore size distribution. The material was also analyzed by scanning electron microscopy (SEM) coupled with EDX (ZEISS EVO LS 15 microscope) to evaluate its morphological properties and determine its elemental composition. The pH of the point of zero charge (pH_{PZC}) was determined by putting in contact the corresponding amount of pine sawdust with distinct NaCl solutions at a pH range between 2 and 12 for 48 h, and then measuring the final pH values (pHmeter, HANNA instruments Edge) (Chapter 3, paper 1). Additionally, to analyze the stability of pine sawdust during the thermal treatment to produce activated carbons, a thermogravimetric analysis (TGA Q5000 IR thermal analyzer) was carried out from 50 to 1000 °C under N_2 atmosphere at 25 mL min^{-1} (Chapter 3, paper 2).

To produce the biochar and activated carbons, pine sawdust was first carbonized at 600 °C for 1 h under N_2 atmosphere. Then, in the dry activation method, the biochar was mixed by milling with the activating agent (KOH or $ZnCl_2$) at the corresponding weight ratio (1:4 or 1:2 w/w) and then activated in the furnace at 600 °C or 850 °C for 2 h under N_2 atmosphere (Carbolite, Sheffield at small scale and Nabertherm GmbH-Germany at large scale). After activation, the material was washed with HCl 0.1 M under stirring and then with distilled water. Finally, it was dried overnight at 105 °C (Chapter 3, paper 2). Regarding the wet method, after carbonization, a 25% $ZnCl_2$ solution was mixed with the biochar for 22 h and then dried for 2 hours at 105 °C. Then it was activated followed by washing as described previously (Chapter 3, paper 3).

The morphology of the carbons was characterized by SEM (ZEISS EVO LS 15 microscope) and transmission electron microscopy (TEM) (JEOL JEM 2010 transmission electron microscope). Furthermore, the specific surface area, pore volume and pore size distributions of the carbons were determined using the methods previously described for the sawdust. X-ray diffraction (XRD) (BRUKER D8 ADVANCE type X-ray diffractometer equipped with a sealed X-ray tube (CuKα1, λ = 1.5406 Å), and a LYNXEYE XE-T type detector) was employed to analyze the crystalline structure of the carbons. Besides, the carbons were analyzed for carbon, nitrogen, hydrogen, sulphur, and oxygen (by difference) content by elemental analysis (Flash Smart CHNS Elemental Analyzer (Thermo Scientific)). The surface elemental composition and surface functional groups were also determined by X-ray photoelectron spectroscopy (XPS) technique (Thermo Scientific NEXSA (XPS) instrument equipped with aluminium Kα monochromatized radiation) (Chapter 3, paper 3). The pH_{PZC} was determined for the carbons as previously described for pine sawdust. Fourier transform infrared (FTIR) (VARIAN FTIR 670 spectrometer) spectra of activated carbons were recorded for KBr pellet method before and after dye adsorption (Chapter 3, paper 2 and chapter 4, paper 1).

Regarding dye adsorption, batch experiments were carried out for sawdust, biochar and activated carbons. The influence of some variables such as pH, agitation rate, adsorbent dose, and initial dye concentration on adsorption performance was studied. Experiments were performed at 25 °C in an Unitronic orbital C shaker (Selecta) for 100 rpm and in a shaking water bath (H20 SOW-LAUDA) for 210 rpm. The material was put in contact with the dye solution in an Erlenmeyer flask at the conditions selected and samples were collected at predefined times and centrifuged (Unitronic P Selecta) for 15 minutes at 4000 rpm. Dye initial and residual concentrations were determined by measuring the absorbance of the supernatant at the maximum dye wavelength using a UV/Vis spectrophotometer (V-630, Jasco) (Chapter 3, papers 1 and 2 and Chapter 4, paper 1). The adsorption equilibrium was studied using the best operation conditions resulted from previous experiments by mixed the adsorbent with the dye solution at different initial concentrations during the equilibrium time. Equilibrium data were analyzed using Langmuir, Freundlich, Dubinin-Radushkevich or Temkin isotherm models and kinetic data using the pseudo-first order, pseudo-second order, and intraparticle diffusion models. Desorption batch experiments were conducted employing several desorption agents such as hydrochloric acid or sodium hydroxide 0.1 M by putting in contact the loaded adsorbent with the desorption agent solution and agitated on the orbital shaker VWR (Cienythec) for 4 hours. The residual dye concentration was measured as indicated before. Desorption experiments were performed with sawdust and with the activated carbon which showed the best performance in batch experiments, and for the latter, also in continuous mode (Chapter 3, paper 1 and Chapter 4, paper 1 and 2).

Adsorption experiments in continuous mode were carried out for the carbon which led to the best results in batch mode, the activated carbon at 850 °C with KOH ratio 1:4 (w/w). Experiments were performed in a fixed-bed column at ambient temperature (approximately 20 °C) using a cylindrical tube (internal diameter 1.86 cm; height 12.5 cm) made from Pyrex glass. Glass-wool was placed at the top and bottom of the column to prevent the displacement of the adsorbent. Dye solution was

pumped by a peristaltic pump (Heidolph PD5201) at distinct flow rates in an up-flow configuration. The influence of initial dye concentration, flow rate, and bed height on adsorption efficiency was analyzed. The breakthrough curves were modelized and Thomas, Yoon-Nelson, and Bohart-Adams empirical models were used to fit experimental data (Chapter 4, paper 2).

In the works where statistical analysis was performed, the experiments were done in triplicate, and one-way analysis of variance (ANOVA) was applied using IBM SPSS Statistics 25 software (Chapter 3, paper 2 and Chapter 4, paper 1).

Finally, the static CO_2 and N_2 adsorption were evaluated using the adsorption isotherms obtained by the volumetric system Micromeritics ASAP 2020 analyzer at different temperatures (0 °C, 25 °C and 50 °C) and a pressure range between 0 and 760 mmHg. Prior to experiments, the samples were degassed at 300 °C for 2 h under vacuum to eliminate moisture and impurities. To maintain the targeted temperature, an ice bath in a Dewar was used for experiments at 0 °C and a temperature-controlled vessel using a Selecta Sensoterm sensor for other temperatures. These experimental data were fitted to Langmuir, Freundlich, and Toth models. On the other hand, the experimental data corresponding to the adsorption isotherms of each gas were employed to calculate the CO_2 over N_2 apparent and IAST selectivity values. The last one was estimated using GraphIAST software package based on Python module pyIAST (Chapter 3, paper 3).

Further details about the methodology employed in this Thesis are presented in each corresponding publication.

4. PUBLICATIONS

Cellulose
https://doi.org/10.1007/s10570-023-05145-4

ORIGINAL RESEARCH

Removal of wood dyes from aqueous solutions by sorption on untreated pine *(Pinus radiata)* sawdust

Catarina H. Pimentel · M. Sonia Freire · Diego Gómez-Díaz · Julia González-Álvarez

Received: 26 October 2022 / Accepted: 10 March 2023

Abstract In this work, the possibility of using untreated pine (*Pinus radiata*) sawdust as biosorbent for the removal of three wood dyes (blue, red and black) from aqueous solutions was investigated. The BET surface area of the material was 1.55 ± 0.81 m^2 g^{-1} using N_2 at -196 °C and 17.83 ± 0.032 m^2 g^{-1} using CO_2 at 0 °C. The point of zero charge was 4.8. In addition, the material was characterized before and after adsorption by surface analytical techniques. Assays were performed to analize the stability of wood dyes with time and pH and also to estimate the pKa values. Batch adsorption experiments were performed and the influence of experimental parameters such as contact time (up to equilibrium), stirring rate (100 and 210 rpm), adsorbent dose (2–10 g L^{-1}), pH (2–9) and initial dye concentration (5 and 300 mg L^{-1}) were studied. The optimum conditions were pH 2 and adsorbent dose of 6 g L^{-1} and the highest adsorption percentages achieved at 5 mg L^{-1} were: 100.0% for the blue, 99.7% for the black and 92.4% for the red. For 300 mg L^{-1} adsorption efficiency decreased to 85.6, 57.0 and 63.8% for the blue, black and red ones, respectively. Kinetic data were best fitted to the pseudo-second order model, suggesting a chemisorption process. Freundlich and Dubidin-Radushkevich were the best isotherm models. Regeneration study showed that un-treated pine sawdust could be reused efficiently for red dye removal at least in up to four repeated adsorption–desorption cycles using NaOH as desorption agent.

Keywords Biomass · Pine sawdust · Wood dyes · Biosorption · Wastewaters · Chemisorption

Introduction

Synthetic dyes are essential resources used in industries like wood, paper, cosmetic, textile, etc. to color their products. It is estimated that there are more than 100,000 commercial dyes and about 350,000 tons are wasted every year (Şentürk and Yildiz 2020). The discharge of these dyes in wastewaters without treatment is of great concern for the environment and human health since it prevents photosynthesis by reducing light transmission and compromises the food chain transfer. In addition, the complex and stable chemical structure of the dyes tends to resist degradation when in contact with water, oxidizing agents, light, among others. On the other hand, dyes can cause functional disorders in the human body and their accumulation in some aquatic organisms carries the risk of toxic

Supplementary Information The online version contains supplementary material available at https://doi.org/10.1007/s10570-023-05145-4.

C. H. Pimentel · M. S. Freire · D. Gómez-Díaz · J. González-Álvarez (✉)
Department of Chemical Engineering, School of Engineering, Universidade de Santiago de Compostela, Rúa Lope Gómez de Marzoa s/n, 15782 Santiago de Compostela, Spain
e-mail: julia.gonzalez@usc.es

Published online: 20 March 2023

and carcinogenic products (Gemici et al. 2021; Chikri et al. 2020). Furthermore, water is an essential component for life and the earth's ecosystem and its protection and prevention of contamination are crucial.

There are a variety of techniques that have been studied for the removal of dyes from wastewaters, such as chemical oxidation, ion exchange, photocatalysis, biodegradation, chemical coagulation, electrolysis, precipitation, membrane separation, and flotation. However, most of these techniques involve disadvantages such as the high cost, the generation of huge amounts of concentration sludge, a reduced efficiency, and sensitive operating conditions (Can 2015; Al-Kadhi 2020; Chandarana et al. 2021). An efficient technique to remove dyes from wastewaters should be able to eliminate large amounts of dye in a short period of time without causing secondary pollution (Mashabi et al. 2022).

The adsorption technique being cost-efficient and with a simple design and operation has been revealed as one of the most effective processes for dye removal (Kumar et al. 2018; Elwakeel et al. 2017). A wide range of adsorbents have been used for dye removal from aqueous solutions. Activated carbons have been the most applied ones mainly due to their high surface area and porosity, however, their high cost and their regeneration difficulty have promoted the research on low-cost adsorbents (Ighalo et al 2022; Philippou et al. 2021). Numerous biowastes such as grapefruit peel, canola hull, pine cone, pine sawdust, peanut husk and rice hull have been pointed out as promising biosorbents due to the lack of hazardous by-product formation, eco-friendliness, cost-effectiveness, flexibility regarding operating conditions and good surface characteristics (Aragaw and Bogale 2021).

Pine trees of various species are present in huge amounts around the world. They are among the most commercially important trees highly valued by industry (Özdemir 2019). In northwest Spain, monterrey pine (*Pinus radiata*) and maritime pine (*Pinus pinaster*) are important natural resources and together with eucalyptus the most used in productive stands (Ogana et al. 2020). Pine sawdust is available as a residue from the wood industry and inherent activities and by using it as an adsorbent, wood waste which are improperly disposed on the environment could be reduced (Bortoluz et al. 2020). Previous studies revealed that the functional groups present in this material like carboxyl, phenolic or hydroxyl enhance the adsorption process through mechanisms such as complexation, hydrogen bonding, ion exchange, etc. (Aragaw and Bogale 2021; Şentürk and Yildiz 2020). Further, pine sawdust from species like *Pinus duragensis*, *Pinus resinosa*, and *Pinus tabulaeformis* have been previously investigated for dyes removal such as acid yellow and methylene blue and revealed promising results (Can 2015; Salazar-Rabago et al. 2017; Sahmoune and Yeddou 2016). However, it has been found that the wood species affects significantly the adsorption capacity (Salazar-Rabago et al. 2017). Additionally, some studies have reported the need for an acid or base pretreatment or an extensive washing to improve the adsorption efficiency (Şentürk and Yildiz 2020; Bortoluz et al. 2020; Islam et al. 2018) while others obtained a positive outcome without any previous treatment which is a simpler and more profitable alternative (Al-Kadhi 2020; Akhouairi et al. 2019). The conversion of biomass into products of high added value is a significant contribution to the circular economy and to the concept of green chemistry. Therefore, at present, the search for biosorbents for dyes removal is attracting attention which highlights the importance of the present study (Philippou et al. 2021; Aragaw and Bogale 2021).

To the best of authors' knowledge, no studies have been conducted on the removal of wood dyes from aqueous solutions by pine (*Pinus radiata*) sawdust. Therefore, in the present study, pine (*Pinus radiata*) sawdust, received from a sawmill without any pretreatment, was directly used as an alternative, cost-effective and environmentally friendly adsorbent for the removal of three industrial acid wood dyes (blue, red and black) from aqueous solutions. Batch experiments were performed to evaluate the influence of various operational conditions such as stirring rate, adsorbent dose, pH, contact time and initial dye concentration. The kinetics of the adsorption process using pseudo-first, -second and intraparticle diffusion models was studied and the Langmuir, Freundlich, Temkin and Dubidin-Radushkevich isotherms were used to fit the equilibrium data.

Materials and methods

Adsorbent preparation

Pine (*Pinus radiata*) sawdust (PS) was provided by a regional sawmill (Lugo, Spain). It was air-dried

till equilibrium and the corresponding moisture content (11.61 wt%, on wet basis) was determined using an Infrared moisture determination balance (Sartorius MA30). Then, PS was sieved using a Ro-Tap type electrical sieve shaker (FTL-0200). The fraction between 0.5 and 1 mm was selected, stored in a plastic container, and used directly for adsorption experiments. Before adsorption experiments and to assure that PS does not release colored components that could interfere adsorption measurements, PS was kept in water (5 g L^{-1}) for 24 h in an Unitronic orbital C shaker (Selecta) at 100 rpm, 25 °C and pH 2, natural (5.1) and 12. Color release was observed at pH 12 whereby this pH was excluded for adsorption experiments.

Adsorbent characterization

The surface area, pore volume and structural properties of PS were determined by adsorption/desorption of N_2 at − 196 °C using an ASAP 2020 surface area analyzer (Micromeritics). This characterization was completed by adsorption experiments with CO_2 at 0 °C with the same equipment in order to analyze the ultramicroporosity of the material. Previously, the samples were dried under vacuum at 50 °C for 72 h and then degassed under vacuum at 300 °C for 1 h. Brunauer-Emmet-Teller (BET) equation was used to determine surface areas and Barrett-Joyner-Halenda (BJH) desorption isotherm to determine the pore volume and pore size distribution. A relative pressure of 0.99 was used to determine the total pore volume and to estimate micropore volume based on mesopores volume (from the BJH equation). PS was analyzed by scanning electron microscope coupled with EDX (ZEISS EVO LS 15 microscope) to study its morphological features and to determine its elemental composition before adsorption. For SEM analysis, PS samples were covered with a thin layer of iridium. The pH of the point of zero charge (pH_{PZC}) for PS was evaluated according to the method described in Şentürk and Yildiz (2020), although slightly modified. Thus, 0.2 g of PS were put in contact with 50 mL of a 0.01 M NaCl solution at 200 rpm for 48 h to assure equilibrium (Nordine et al. 2016).

Dye characterizations

Acid wood dyes were used: Blue for wood AGN-270%, Red for wood GRA-200%, and Black Hispalan M-RN-140%. Dye solutions were prepared by dilution of a stock aqueous solution of 500 mg L^{-1} with distilled water. The elemental composition of the dyes was determined by EDX. To study dye stability, 50 mL of dye solution (25 mg L^{-1}) at natural pH (5.1, 6.0 and 6.2 for blue, black and red dyes, respectively) and at pH 2 were placed in a hydro shaking water bath (H20 SOW-LAUDA) at 210 rpm and 25 °C. For predefined times (from 30 min to 96 h), the visible absorption spectra of the samples were recorded by UV/VIS spectroscopy (V-630, Jasco).

The determination of the dissociation constant (pKa) was performed using two different techniques. Regarding the red dye that presents a color shift with pH changes, pKa was determined using the UV/VIS spectroscopy method by measuring the absorption wavelength (V-630, Jasco) of a 10 mg L^{-1} solution at pH values from 1.5 to 12.5 following the method proposed by De Meyer et al. (2014). For the blue and black dyes, pKa values were determined by potentiometric titration. An aqueous solution of each dye (10 mg L^{-1}) was titrated potentiometrically at 25 °C under continuous stirring by adding small aliquots (0.05 mL) of 0.05 M NaOH up to pH 11. For weak acids, the pH could be calculated as follows:

$$\mathrm{pH} = pKa + \log[A^-]/[HA] \quad (1)$$

where $[A^-]$ is the conjugate base and [HA] the weak acid. The half-neutralization point occurs when $[A^-]$ is equal to [HA] that corresponds to pH = pKa (Zafar et al. 2014; Kantar et al. 2015).

Adsorption experiments

In a first stage, experiments were performed at 100 rpm in an Unitronic orbital C shaker (Selecta). For this, PS was mixed with a 5 mg L^{-1} dye aqueous solution at adsorbent doses of 5 or 10 g L^{-1}, natural pH (5.1, 6.0 and 6.2 for blue, black and red dyes, respectively) and 25 °C. In a second stage, to evaluate the effect of the agitation speed on adsorption efficiency experiments were performed at 210 rpm and adsorbent dose of 10 g L^{-1} at the same previous

conditions. Finally, the influence of other variables was also studied at 210 rpm: initial pH (2–9), adsorbent dose (2, 6 and 10 g L^{-1}) and initial dye concentration (5 and 300 mg L^{-1}). At predefined times, samples were removed and centrifuged for 15 min at 4000 rpm. Dye concentration was determined by measuring the absorbance of the supernatant at the maximum dye wavelength, λ_{max}, using an UV/VIS spectrophotometer (V-630, Jasco). Dye removal efficiency was calculated as the percentage of dye adsorbed (Eq. 2). The adsorption capacity was calculated as the amount of dye adsorbed per mass unit of PS (Eq. 3).

$$\text{Adsorption}\ (\%) = (C_0 - C)/C_0 \times 100 \tag{2}$$

$$q\left(\text{mg g}^{-1}\right) = (C_0 - C)V/m \tag{3}$$

where C_0 and C are the initial and residual dye concentrations (mg L^{-1}), q is the adsorption capacity (mg g^{-1}), V is the volume of the dye solution (L) and m is the dry mass of adsorbent used (g).

SEM-EDX was conducted to characterize the PS samples after the adsorption process as explained above.

Kinetic models were applied to explain the dye adsorption process and examine the mechanism of the interactions:

- Pseudo-First Order

$$\log\left(q_e - q_t\right) = \log q_e - k_1 t/2.303 \tag{4}$$

where q_t and q_e are the amounts of dye adsorbed (mg g^{-1}) at time t (min) and at equilibrium, respectively, and k_1 represents the first-order rate constant (min^{-1}).

- Pseudo-Second Order

$$t/q_t = (1/k_2 q_e^2) + t/q_e \tag{5}$$

where k_2 (g mg^{-1} min^{-1}) is the pseudo-second-order rate constant (Ho and McKay 1999).

- Intra-particle Diffusion

$$q_t = k_{id} t^{1/2} + I \tag{6}$$

where I is the intercept and k_{id} is the rate constant of intra-particle diffusion (mg g^{-1} $min^{-1/2}$) (Weber et al. 1963).

The adsorption equilibrium was studied using the operational conditions selected in the previous studies. PS (6 g L^{-1}) was mixed with a dye aqueous solution (initial concentrations varied between 5 and 300 mg L^{-1}) at pH 2 and 25 °C for 4 days for blue and red to assure the equilibrium and 12 h for black also to guarantee the stability. The equilibrium data were analyzed by the Freundlich (Eq. 7), Langmuir (Eq. 8), Temkin (Eq. 9) and Dubidin-Radushkevich (D-R) (Eq. 10) isotherm models:

$$q_e = k_F C_e^{1/n} \tag{7}$$

$$q_e = \frac{q_{max} k_L C_e}{1 + k_L C_e} \tag{8}$$

$$q_e = B\left(\ln K_T C_e\right) \tag{9}$$

$$q_e = q_{m,D} \exp\left(-K_{DR}\varepsilon^2\right) \tag{10}$$

where q_e and q_{max} are the amount of dye adsorbed at equilibrium and the maximum adsorption capacity (mg g^{-1}); k_F [mg g^{-1} (L $mg^{-1})^{-1/n}$] and k_L (L mg^{-1}) are the Freundlich and Langmuir constants; C_e is the equilibrium dye concentration (mg L^{-1}); n represents the intensity of the adsorption (Langmuir 1918; Freundlich 1907); K_T is the equilibrium binding constant (L mg^{-1}); B is related to the adsorption heat (J mol^{-1}) (Chandarana et al. 2020); ε is equal to $RT\ln(1 + 1/C_e)$; $q_{m,D}$ is the theoretical monolayer saturation capacity (mol g^{-1}); and K_{DR} is the constant of the adsorption energy (mol^2 kJ^{-2}) which is related to the mean adsorption energy, E, equal to $1/\sqrt{2K_{DR}}$ (kJ $mol.^{-1}$) (Collins et al. 2019; Özdemir 2019) Langmuir model can also be characterized by another parameter, the adsorption rate (R_L), that can be determined using Eq. (11). R_L indicates if the adsorption process is irreversible, linear or favorable according to the R_L value, $R_L = 0$, $R_L = 1$ and $0 < R_L < 1$, respectively (Al-Kadhi 2020, Şentürk and Yildiz 2020)

$$R_L = \frac{1}{1 + k_L C_0} \tag{11}$$

Desorption and regeneration of the adsorbent

Batch desorption experiments were conducted to evaluate the possibility of reusing *Pinus radiata* sawdust after performing an adsorption experiment using an adsorbent dose of 10 g L^{-1}, pH 2, a dye concentration of 300 mg L^{-1} and a contact time of 4 days for the blue and red dyes and 12 h for the black dye. Then, the loaded adsorbent was filtered and dried at 105 °C for 24 h. Two desorption agents were selected, namely, hydrochloric acid 0.1 M and sodium hydroxide 0.1 M (Bortoluz et al. 2020; Mashkoor et al. 2018). In this way, 0.5 g of loaded PS were put in contact with 10 mL of the selected desorption agent and agitated at 350 rpm on the orbital shaker VWR (Cienythec) at 25 °C for 4 h. Then the suspension was filtered and the solid washed with distilled water until neutral pH. Before filtration, the residual dye concentration in the solution was measured as indicated before, and the desorption percentage (%Desorption) was calculated by Eq. 12:

$$\%Desorption = m_{des}/m_{rem} \times 100 \quad (12)$$

$$m_{rem} = m_{retained} + m_{adscycle} \quad (13)$$

where, m_{des} is the amount of dye desorbed (mg), m_{rem} is the mass of dye that remained adsorbed on the PS after each adsorption/desorption cycle (mg), $m_{retained}$ is the mass retained after the previous desorption cycle (mg) and $m_{ads\ cycle}$ is the amount of dye adsorbed in each adsorption cycle (mg). The reusability of PS was studied by carrying out four repeated adsorption–desorption cycles and each cycle was evaluated by the percentages of dye adsorption and desorption.

Results and discussion

Adsorbent characterization

In this study gas sorption isotherms were performed for N_2 at − 196 °C and CO_2 at 0 °C to examine the surface area and pore structure of PS. The nitrogen adsorption–desorption plot is shown in Fig. 1.

The N_2 isotherm is mainly type II which is typical of macroporous materials with heterogeneous surface

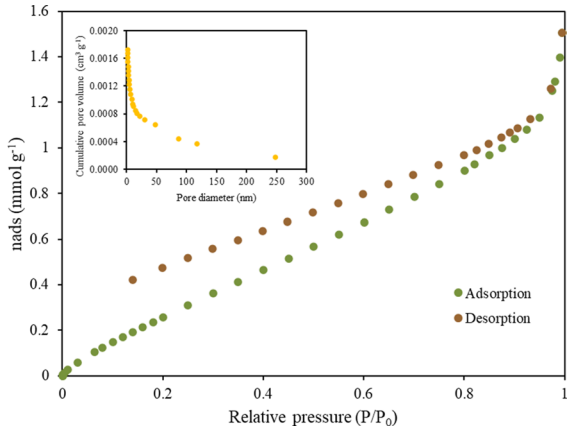

Fig. 1 Nitrogen adsorption–desorption cycle at − 196 °C on PS and BJH pore size distribution

according to the IUPAC classification (Rouquerol et al. 2014). Physical adsorption on macroporous adsorbents leads to unrestricted monolayer-multilayer adsorption. However, the initial behavior of N_2 adsorption capacity at low pressure corresponds to a type III isotherm, suggesting that the material also contains micro and mesopores that will lead to the formation of multiple layers with increasing relative pressure. The hysteresis between the adsorption and desorption curves at high relative pressures could be associated with the filling and emptying of mesopores by capillary condensation. The asymptotic behavior which occurs at relative pressures approaching one, suggests a significant amount of macropores (Lorenz et al. 2019). A similar behavior has been reported by Jaouadi (2021) for pinewood sawdust. The PS BET surface area, total pore volume and mean pore diameter for N_2 were, respectively, 1.55 ± 0.81 m^2 g^{-1}, 1.94×10^{-3} cm^3 g^{-1} and 5.15 nm. According to the pore size distribution (Fig. 1) that indicates that the major pore size is in the range between 2 and 50 nm, PS can be categorized as a mesoporous material since the average pore diameter was between 2 and 50 nm according to the pore's IUPAC classification (Rouquerol et al. 2014). Similar values have been reported for pine and durian (*Durio zibethinus*) wood sawdust (Chowdhury et al. 2016; Jaouadi 2021). Previous studies demonstrated that N_2 adsorption–desorption isotherm could have some limitations for ultra-microporous materials as N_2 cannot access into the micropores (Kim et al. 2016). To obtain a greater insight into the porosity of PS, and due to the

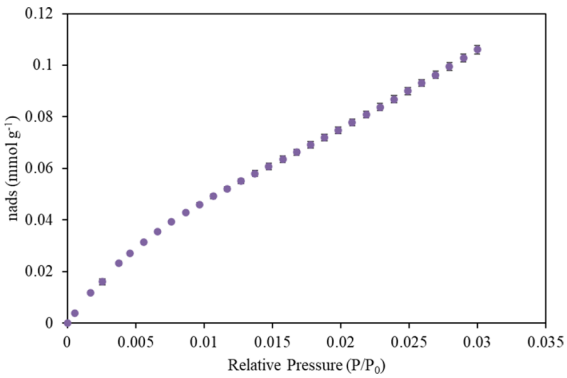

Fig. 2 CO_2 adsorption isotherm at 0 °C on PS

hysteresis cycle, which suggests microporosity, CO_2 adsorption isotherm was studied. Figure 2 shows the CO_2 adsorption isotherm recorded up to a relative pressure of 0.03 at 0 °C.

By the results obtained, PS revealed a higher BET surface area with CO_2 adsorption of 17.83 ± 0.032 m^2 g^{-1} suggesting that microporosity could play an important role in adsorbate accessibility.

The morphology of the PS surface was analyzed by SEM. The images of the biosorbent before the adsorption process are shown in Fig. 3.

As can be seen in Fig. 3a with 500 magnifications, PS presented a multi-layer surface with a tubular structure (Semerjian 2018). Figure 3b and c with 1000 and 5000 magnifications respectively, revealed a heterogeneous and fibrillar structure with pores which can favor the adsorption process. Similar characteristics were found in previous studies for *Pinus elliottii*, *Tectona grandis* and *Pinus halepensis* sawdust (Akhouairi et al. 2019; Semerjian 2018; Mashkoor et al. 2018).

The elemental composition of PS is shown in Table 1. The results indicated that carbon and oxygen are the main components due to the organic nature of the material and presented traces of Al that could result from the material used to cut in the sawmill. In addition, pine sawdust contained only a small amount of Cu, K, Ca and Mg which indicates that the content of metals on the surface were negligible.

The relationship between pH and pH_{PZC} plays a key role in understanding the adsorption process since pH affects the surface charge of the adsorbent, the degree of ionization, and in turn, the binding specificity of the adsorbate. The point of zero charge of PS is 4.8 (Fig. S1), indicating that when the pH is lower than pH_{PZC} the PS surface is positively charged and negatively charged when it is higher than pH_{PZC}. When pH is less than pH_{PZC} the sawdust will adsorb anionic dyes and when pH is higher than pH_{PZC} the adsorbent will adsorb cationic dyes (Ratnamala et al. 2016). Acid wood dyes are negatively charged, so it is probable that a positively charged PS surface leads to increased adsorption of acid dye anions.

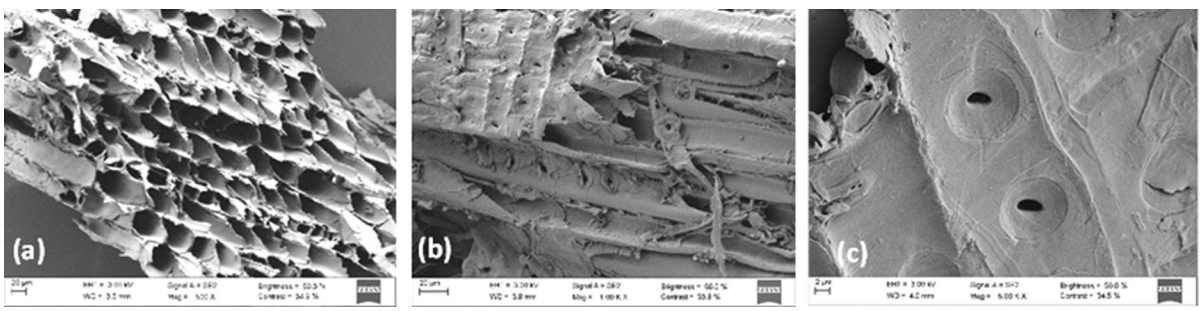

Fig. 3 SEM images of pine sawdust before adsorption **a** 500, **b** 1000 and **c** 5000 magnifications

Table 1 Elemental composition of pine sawdust

	wt%						
PS	C	O	Al	Cu	K	Ca	Mg
	58.6 ± 0.1	38.8 ± 0.1	2.0 ± 0.0	0.3 ± 0.0	0.1 ± 0.0	0.1 ± 0.0	0.1 ± 0.0

Dyes characterization

The elemental composition of the dyes was analyzed by EDX and is shown in Table 2. The results indicated that the main component is carbon together with a considerable oxygen percentage, especially for the red dye. For the black dye, the presence of chromium and the high sulfur content stand out. Thus, considerable differences were found among dyes both in terms of the components present and their percentage contribution.

Dye stability as a function of pH at 25 mg L^{-1} was studied (Figs. S2a-f). From the spectral scans, the maximum wavelength in the visible region to consider for the stability study were 602 nm, 506 nm and 572 nm for the blue, red and black dyes, respectively. For the blue and red dyes, either for natural (Figs. S2a, S2c) or acid pH (Figs. S2b, S2d), there were no significant changes in the absorbance values for 4 days, which demonstrates their stability. For the black dye, the stability was also verified at natural pH (Fig. S2e). Otherwise, at acid pH a decrease on dye absorbance of about 10% occurred up to 12 h being more evident (30%) at 4 days. Simultaneously, there was a shift of the maximum wavelength with the consequent loss of stability after 12 h (Fig. S2f). Thus, for the black dye, further experiments were only performed up to 12 h assuring the stability region.

Acid dissociation constant (pKa) is an important parameter to better understand the behavior of chemical substances. Changing the availability of protons or the acidity of the medium the equilibrium changes which provides the possibility of measuring the capacity of protons release or dissociation of a site. The pKa could be described as the pH at which the protonated and deprotonated forms are equal. Thus, the site will be more deprotonated or protonated as the pH is higher or lower than pKa, respectively (Zafar et al. 2014).

Firstly, the visible spectrum of the red dye at different pH values was obtained from UV/VIS spectroscopy (Fig. S3). It can be observed that the color changes from red to orange at pH higher than 10 which corresponds with a shift of λ_{max} from 506 to 483 nm (Fig. S3a). A change in acidity that leads to color changes is usually due to the presence of a chromophore close to the ionization site of the molecule (Reijenga et al. 2013). The pKa was estimated from the crossing point in Fig. S3b as 10.6, through the measure of the absorbance at the two maximum wavelengths previously determined at each pH value.

To estimate the pKa values of the blue and black dyes in aqueous solution, direct micro-potentiometry titration was performed with NaOH as a strong base as commented before. The pH variation for these dyes with the addition of NaOH is shown in Fig. S4. It can be observed that from 0 to 60 µL the pH significantly increases from 6 to 10 and then it stabilizes forming a buffer zone used to calculate the pKa as the pH of the half neutralization point. It was found to be 10.4 for the blue dye and 10.3 for the black one.

It can be seen that there are no significant differences among the pKa values of the red, blue and black dyes which would be related with their molecular structures and functional groups, and since the lower the pKa the stronger the acidity, the dyes used in this study could be classified as weak acids (Zafar et al. 2014; Kantar et al. 2015; Schaffer and Licha 2014).

Adsorption experiments

Effect of adsorbent dose and agitation speed at natural pH

Adsorption experiments were started at the natural pH of the dyes solutions and Fig. 4a shows the results obtained for the adsorption efficiency versus time for the blue, red, and black dyes at two adsorbent doses (5

Table 2 Elemental composition of wood dyes

Dye	wt%										
	C	O	N	S	Na	Cl	Br	Cu	P	Cr	Mg
Blue	62.1 ± 0.1	18.4 ± 0.1	7.2 ± 0.1	6.7 ± 0.0	4.8 ± 0.0	0.4 ± 0.0	0.2 ± 0.0	0.1 ± 0.0	–	–	–
Red	49.7 ± 0.1	28.3 ± 0.1	3.4 ± 0.1	7.1 ± 0.0	10.1 ± 0.0	0.9 ± 0.0	–	0.1 ± 0.0	0.4 ± 0.0	–	–
Black	27.5 ± 0.2	18.4 ± 0.1	–	21.3 ± 0.1	11.1 ± 0.1	–	–	1.6 ± 0.1	–	20.0 ± 0.1	0.1 ± 0.0

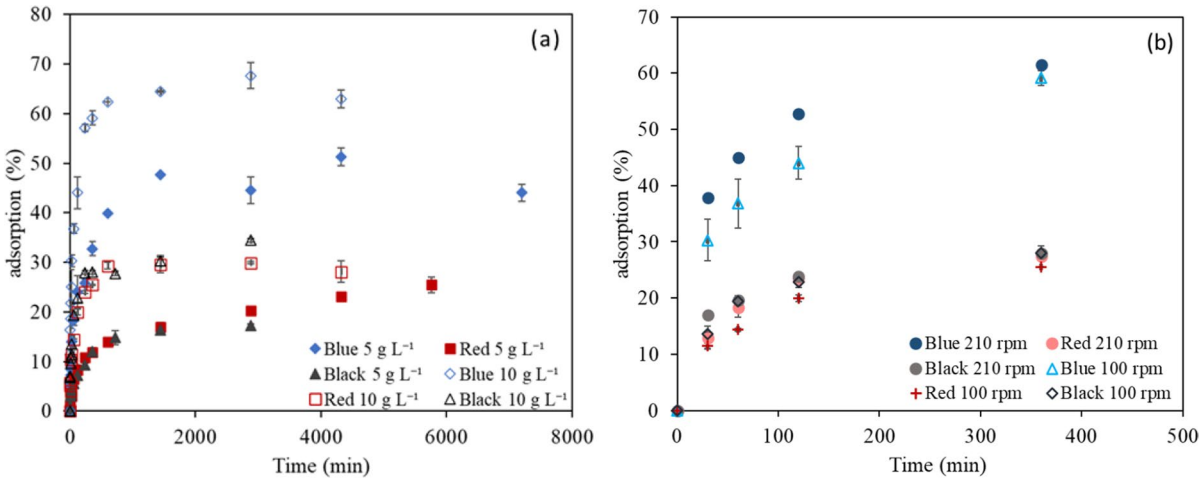

Fig. 4 Adsorption efficiency versus time for blue, red and black dyes at the natural pH **a** adsorbent dose 5 or 10 g L^{-1}, initial dye concentration 5 mg L^{-1}, temperature 25 °C, agitation speed 100 rpm, **b** agitation speed 100 or 210 rpm, adsorbent dose 10 g L^{-1}, initial dye concentration 5 mg L^{-1}, temperature 25 °C

Table 3 Equilibrium removal efficiency and adsorption capacity for blue, red and black wood dyes onto pine sawdust

Adsorbent dose	Blue	Red	Black
(g L^{-1})	*Equilibrium dye adsorption efficiency (%)*		
5	51.30 ± 1.83	25.47 ± 1.54	17.25 ± 0.37
10	67.67 ± 2.46	29.93 ± 0.27	34.46 ± 0.34
	Equilibrium adsorption capacity (mg g^{-1})		
5	0.51 ± 0.02	0.28 ± 0.02	0.18 ± 0.00
10	0.37 ± 0.03	0.16 ± 0.00	0.18 ± 0.00

and 10 g L^{-1}), initial dye concentration of 5 mg L^{-1}, 100 rpm and 25 °C. As can be seen, the adsorption proceeds in two stages. A fast first stage is followed by a slower one until equilibrium is reached. At the initial phase, the sawdust presents a more available and porous surface, with the presence of mesopores, which favors the rapid adsorption of the dye. As the adsorption progresses the surface becomes progressively saturated with the consequent decrease in the number of sorption sites on the PS and the adsorption becomes slower (Al-Kadhi 2020).

The time necessary to reach equilibrium was 72 h at 5 g L^{-1} and 48 h at 10 g L^{-1} for the blue dye, 96 h at 5 g L^{-1} and 48 h at 10 g L^{-1} for the red one, and 48 h for the black one at both adsorbent doses. The maximum adsorption efficiency was attained for the blue dye at both adsorbent doses (Table 3) which can be related to the lower natural pH of this dye (5.1) in comparison with those of the black (6.0) and the red (6.2) ones. At pH far above the pH_{PZC} the surface might be more negatively charged, and this could lead to electrostatic repulsion and, consequently, to a lower amount of dye adsorbed. Previous studies with pine sawdust also demonstrated that for acid dyes, adsorption improved at lower pH (Can 2015; Akhouairi et al. 2019; Özacar and Şengil 2005).

Table 3 shows the influence of the adsorbent dose on the equilibrium adsorption efficiency and capacity. The adsorption efficiency increased when increasing the adsorbent dose from 5 to 10 g L^{-1}, but more remarkably for the blue and black dyes. This can be explained by the increase in the number of available adsorption sites and enhanced surface area due to larger adsorbent dose. Regarding the equilibrium adsorption capacity (q_{max}), it decreased with increasing the adsorbent dose, except for the black dye which does not change.

To investigate the effect of the agitation speed, kinetic experiments were conducted at 210 rpm. Figure 4b shows that the first stage gets faster when agitation speed is increased even though equilibrium conditions do not change significantly. Consequently, all other experiments were carried out at 210 rpm.

Effect of pH on dye adsorption

The pH is a significant parameter that influences the interaction between adsorbate and adsorbent depending on the ionization degree and surface characteristics (Şentürk and Yildiz 2020). Adsorption experiments were performed at different contact times assuring the stability of the dyes (Fig. S2), for an adsorbent dose of 10 g L^{-1} and initial dye concentration of 5 mg L^{-1}, at different pH values ranging from 2 to 9 and the results obtained are shown in Fig. 5. From these results it can be concluded, as mentioned previously, that pH has a significant effect on dye removal efficiency.

The maximum dye removal efficiency was obtained at pH 2 and it was 100.0% for the blue dye, 95.1% for the red dye and 85.5% for the black one. When pH increased from 2 to 9, adsorption efficiency rapidly decreased to 50.5%, 34.2% and 27.7% for the blue, red and black dyes, respectively. It is possible to explain the nature of possible charge-driven interactions based on the pH_{PZC} of the adsorbent and the pKa of the adsorbate (Kah et al. 2017). Depending on the dye molecular structure and according to the estimated values of the pKa (10.6, 10.4 and 10.3 for the red, blue and black dyes, respectively), at acid pH below the pKa, the adsorbate could be protonated to the neutral form which can lead to interactions between the functional groups (Lewis acid–base, π–π bond, hydrophobic effect and H-bond). Moreover, since the PS surface is positively charged when the pH is below the pH_{PZC} (4.8) with a high concentration of H^+ in solution, acid dye anions are expected to interact electrostatically and to increase the adsorption capacity (Can 2015; Kah et al. 2017; Konicki et al. 2013). Other studies also reported that the optimum pH is usually around 2–4 since as pH decreases, the protonation of amine groups increases (Elwakeel 2010). These results demonstrated that for all dyes a better removal efficiency is attained at pH 2 instead of natural pH and subsequent experiments were conducted at acid pH.

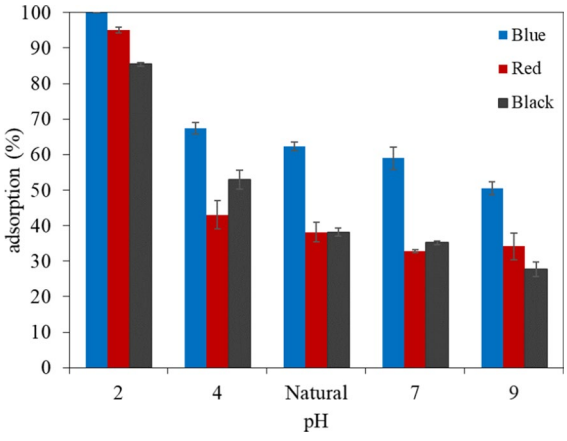

Fig. 5 Effect of pH on adsorption of blue, red and black wood dyes by PS (natural pH 5.1, 6.2 and 5.8 for blue, red and black, respectively; initial dye concentration 5 mg L^{-1}; adsorbent dose 10 g L^{-1}; contact time 24 h for blue, 48 h for red and 12 h for black; temperature 25 °C; agitation speed 210 rpm)

Adsorption experiments at acid pH

Dye adsorption on PS at the pH selected (pH = 2) was analyzed depending on contact time and adsorbent dose to determine the equilibrium time and the optimal adsorbent dose. The results are shown in Fig. 6.

The behavior of the adsorption process did not differ from the aforementioned for natural pH. The total removal of the blue dye was achieved at all adsorbent doses, however the equilibrium time increased from 30 min to 6 and 48 h when the PS dose decreased from 10 to 6 and 2 g L^{-1}, respectively. Regarding the red dye from 10 to 6 g L^{-1} there was no change in the equilibrium time (18 h) but a slight difference on removal efficiency from 98.3% to 92.4% occurred. Conversely, for 2 g L^{-1} there was a significant increase in the equilibrium time to 48 h and also a decrease in the removal efficiency (86.2%). In the case of black dye, to guarantee the stability, the study was performed for 12 h, and from 10 to 6 g L^{-1} both equilibrium time (2 h) and removal efficiency (99%) were maintained but the adsorption efficiency decreased to approximately 80% and the equilibrium time increased to 12 h when the adsorbent dose was reduced to 2 g L^{-1}. Consequently, it can be concluded that for all dyes at pH 2 and low concentration the optimum adsorbent dose is 6 g L^{-1}. This improvement on the adsorption process compared to the previous results could be described by the effect of ionic interaction due to the low pH value (Chikri et al. 2020; Özacar and Şengil 2005).

To overcome the diffusive mass transfer resistance in the adsorption process between the aqueous and solid phases, initial dye concentration is an important variable to be assessed which provides an important

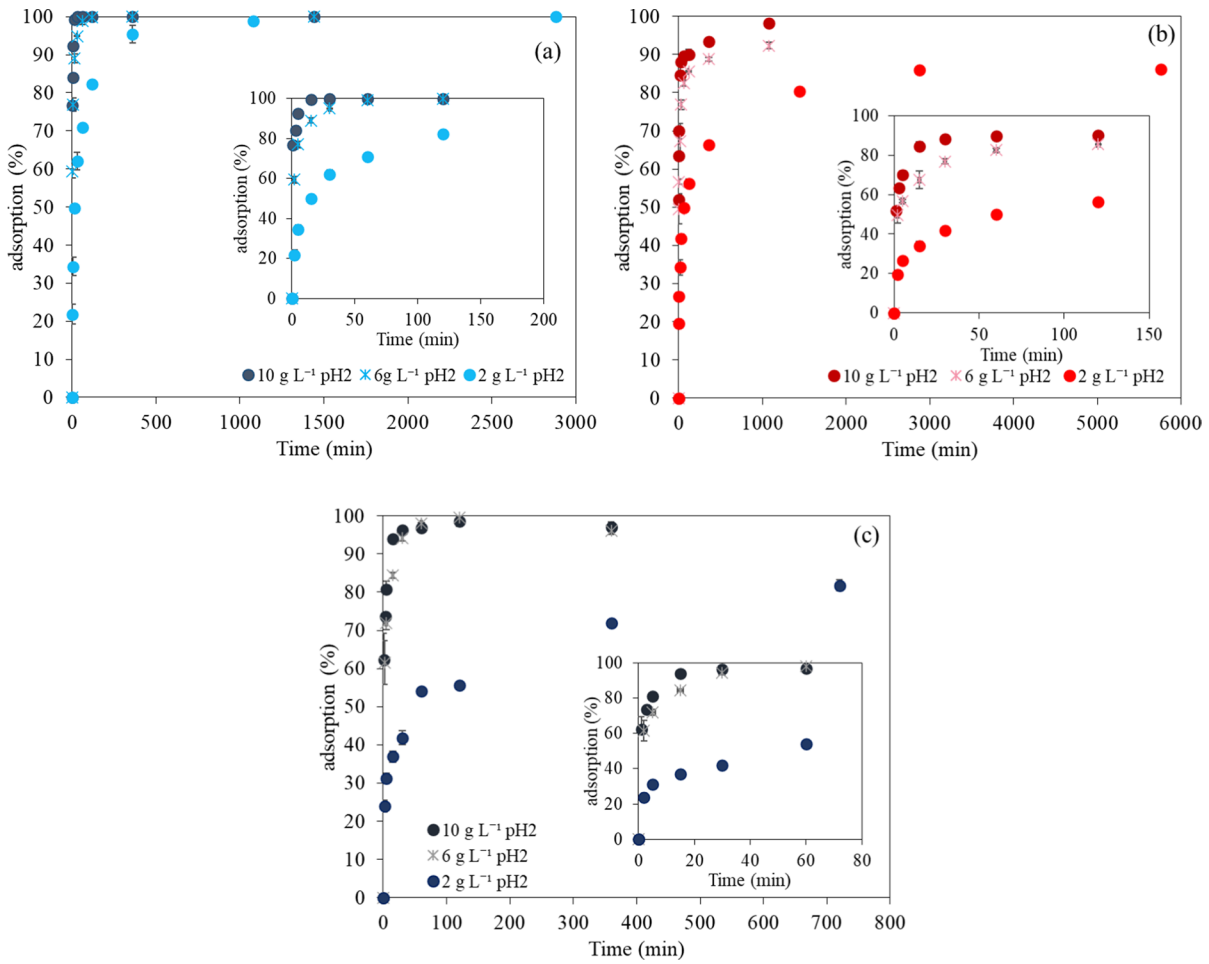

Fig. 6 Effect of adsorbent dosage on the adsorption efficiency of blue **a**, red **b** and black **c** dyes using PS (initial dye concentration 5 mg L^{-1}; pH 2; adsorbent dose 2, 6 and 10 g L^{-1}; temperature 25 °C and agitation speed 210 rpm)

driving force (Esmaeili and Foroutan 2019; Khataee et al. 2013). Then, to investigate the efficiency of PS at the optimal pH to remove high dye concentrations, initial dye concentration was increased from 5 to 300 mg L^{-1}. Due to this increase, firstly the highest adsorbent dose (10 g L^{-1}) was used to determine if total dyes removal was achieved. The results obtained are shown in Fig. 7.

It is observed that at 300 mg L^{-1} the dye removal percentage decreased with respect to that obtained for 5 mg L^{-1} which demonstrates the influence of initial concentration. The adsorption efficiency of PS decreased from 100.0, 98.3 and 98.6% to 85.6, 63.8 and 57.0% for the blue, red and black dyes, respectively, at equilibrium (48 h), for blue and red and for a contact time of 12 h for the black dye due to the aforementioned stability problems. This reduction could be explained since the increase of initial dye concentration causes a saturation in the total number of active binding sites which increases the repulsion by the electrostatic force between the adsorbed and non-adsorbed dye molecules (Bortoluz et al. 2020; Esmaeili and Foroutan 2019). Moreover, perhaps the surface area generated by ultra-micropores could not be available for the dyes due to size-exclusion. Although increasing the initial dye concentration from 5 to 300 mg L^{-1} reduced the removal efficiency, an increase of the maximum adsorption capacity occurred from 0.50 to 27.47 mg g^{-1} for the blue dye, from 0.48 to 18.55 mg g^{-1} for the red dye and from 0.40 to 16.62 mg g^{-1} for the black one. The increase in the initial dye concentration caused

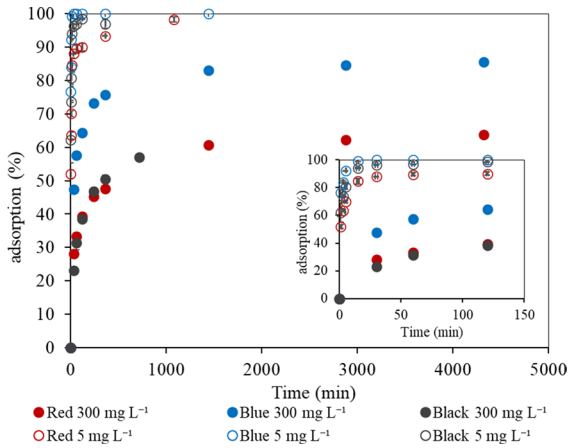

Fig. 7 Effect of initial dye concentration on dyes removal (initial dye concentration 5 and 300 mg L^{-1}; adsorbent dose 10 g L^{-1}; pH 2; temperature 25 °C; agitation speed 210 rpm)

a strong interaction between the adsorbent and the dye molecules that resulted from the increase in the driving force of the concentration gradient (Şentürk and Yildiz 2020). Thus, for 300 mg L^{-1} the maximum adsorption capacity increased and for the blue dye, the adsorption capacity was very close to the theoretical maximum value (30 mg g^{-1}). This could be due to differences in the dyes functional groups that lead to different interactions between the sorbent and the sorbate.

Finally, Fig. 8 shows the SEM analysis results for PS after dye adsorption at a 5000× magnification. It can be observed that after the adsorption process the PS surface is covered by the dyes. Moreover, the presence of new elements that belong to the dyes could be confirmed by EDX analysis (Table 4).

Adsorption kinetics

Kinetic behavior and the controlling mechanisms involved in the adsorption process as diffusion control, mass transfer or chemical reaction could be predicted using some kinetic models (Şentürk and Yildiz 2020). Therefore, to explain the kinetics of dye removal using un-treated pine sawdust, the experimental data was fitted to the pseudo-first order (Eq. 4), pseudo-second order (Eq. 5), and intraparticle

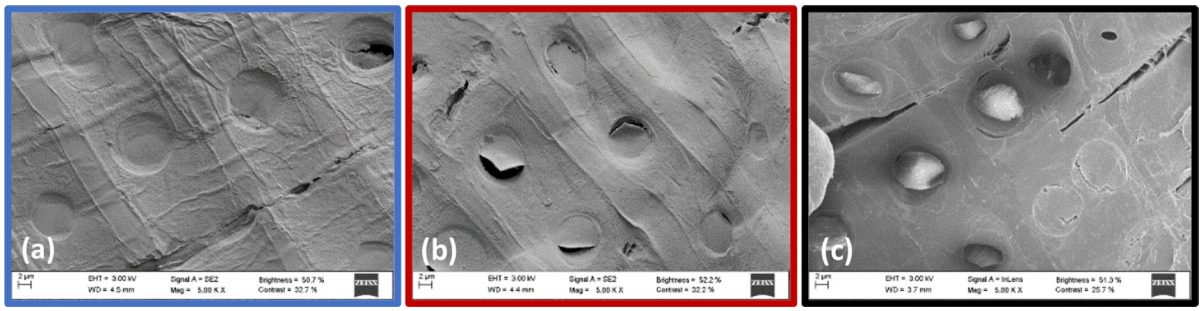

Fig. 8 SEM images of pine sawdust after adsorption of blue **a**, red **b** and black **c** wood dyes (initial dye concentration 300 mg L^{-1}; pH 2; adsorbent dose 10 g L^{-1}; temperature 25 °C; equilibrium time for blue and red dyes and maximum adsorption time for the black one; agitation speed 210 rpm)

Table 4 EDX of PS before and after dye adsorption (pH 2; initial dye concentration 300 mg L^{-1} for blue and red and 5 mg L^{-1} for black; equilibrium time)

Material	wt%										
	C	O	Al	Cu	K	Ca	Mg	S	N	Cl	Cr
PS	58.6 ± 0.1	38.8 ± 0.1	2.0 ± 0.1	0.3 ± 0.0	0.1 ± 0.0	0.1 ± 0.0	0.1 ± 0.0	–	–	–	–
PS + Blue	57.6 ± 0.1	42.3 ± 0.1	–	–	–	–	–	0.1 ± 0.0	–	–	–
PS + Red	58.0 ± 0.3	34.9 ± 0.3	0.1 ± 0.1	1.3 ± 0.1	–	–	–	0.2 ± 0.0	5.0 ± 0.4	0.5 ± 0.0	–
PS + Black	66.6 ± 1.0	28.0 ± 1.0	–	–	–	–	–	1.5 ± 0.2	–	1.4 ± 0.2	2.5 ± 0.4

diffusion (Eq. 6) kinetic models. The kinetic parameters obtained are listed in Table 5. Kinetic constants and correlation coefficients were obtained by plotting log (q_e-q_t) versus t for the pseudo-first order model, t/q_t against t for the pseudo-second order model and q_t versus $t^{1/2}$ for the intraparticle diffusion model.

In view of the results, the predicted adsorption capacities ($q_{e,\ calc}$) for the pseudo-first order model were found to be much lower than the experimental ones ($q_{e,\ exp}$) as consequence of the low correlation coefficients obtained in most cases. This demonstrates that this model is not suitable to describe the adsorption process. However, the second order model is the one that best fits the experimental data with correlation coefficients higher than 0.975 and lower sum of square error (SSR) values for all dyes and conditions essayed and a good agreement between the experimental $q_{e,}$ and that predicted by the model ($q_{e,\ calc}$) was obtained. Regarding the intraparticle diffusion kinetic model, the kinetics of the adsorption process was divided into two linear regions (1) lower contact times and rapid uptake and (2) higher contact times and slow uptake until reaching equilibrium. In most of the experiments, high correlation coefficients (> 0.9) were obtained for the first region corroborated by a low SSR, which suggests the possibility of intraparticle diffusion of the dye from the outer surface into the pores of the sawdust at the initial phase of the adsorption process. However, the low correlation coefficients for the second region indicate a change in the adsorption mechanism.

In summary, the pseudo-second order kinetic model can describe the whole adsorption process through a chemical sorption mechanism involving valence forces due to the interchange of electrons. Simultaneously, the intraparticle diffusion kinetic model also explains the adsorption process at the initial stage with the transfer of the dye from the outer surface into the pores of the material (Şentürk and Yildiz 2020; Semerjian 2018).

Adsorption equilibrium

To better understand the mechanism of adsorption, the equilibrium data for the blue, red and black dyes on PS were obtained and fitted to the Langmuir, Freundlich, Temkin and Dubidin-Radushkevich models (Fig. 9). The study was performed considering the optimal adsorbent dose selected for low concentrations (6 g L^{-1}) and from the results obtained it was possible to establish the limit initial dye concentration to achieve dyes removal equal to or greater than 90% (50 mg L^{-1}, 25 mg L^{-1} and 12.5 mg L^{-1} for blue, red and black dyes, respectively). Langmuir model assumes the presence of a homogeneous surface with a limited number of adsorption sites without transmigration of the adsorbate molecules onto the surface, with equal energies of adsorption, leading to monolayer adsorption. Freundlich model describes adsorption as a multilayer process with different energies levels due to the heterogeneous surface (Şentürk and Yildiz 2020; Esmaeili and Foroutan 2019). Temkin model considers that the adsorption heat of the molecules reduces in a linear way with the increase in coverage of the adsorbent surface. That adsorption is distinguished by a uniform distribution of binding energies up to a maximum. Dubidin-Radushkevich (D-R) isotherm represents a mechanism of adsorption with a Gaussian energy spreading on a heterogeneous surface. Thus, this model suggests at first a pore-filling mechanism followed by adsorption and allows to distinguish if it is going to occur a chemical or a physical adsorption through the isotherm parameters regarding sorption energy (Chandarana et al. 2020; Şentürk and Yildiz 2020).

From Fig. 9, the isotherm models that best fitted the experimental data for all cases were the Freundlich and the D-R models which do not tend to a saturation condition when adsorbate concentration in solution increases and consider that the adsorbent surface is heterogeneous (Deniz and Dogan 2022; Şentürk and Yildiz 2020). The parameters for each model are presented in Table 6.

As can be seen, both Freundlich and D-R isotherms presented the best fits with high correlation coefficients (> 0.98) and generally with the lower SSR. Freundlich isotherm with n values higher than 1 suggests a favorable adsorption and implies the presence of a heterogeneous surface with reversible adsorption and multilayer formation). The adsorbate concentration in the adsorbent increases with increasing the adsorbate concentration in solution which leads to a non-saturation behavior as shown in Fig. 9 (Bortoluz et al. 2020; Şentürk and Yildiz 2020). The adsorption equilibrium data were also satisfactorily fitted to the D-R isotherm model which considers that a pore-filling mechanism is also involved in a heterogeneous surface and is very useful for predicting the type of

Table 5 Pseudo-first, pseudo-second order and intraparticle diffusion kinetic model parameters

Pseudo-first order						Pseudo-second order						Intraparticle diffusion					
Dye (g L^{-1})	$q_{e,exp}$ (mg g^{-1})	k_1 (min^{-1})	$q_{e,calc}$ (mg g^{-1})	R^2	SSR	k_2 (g mg^{-1} min^{-1})	$q_{e\,calc}$ (mg g^{-1})	R^2	SSR	$k_{i,1}$ (mg g^{-1} $min^{1/2}$)	$k_{i,2}$ (mg g^{-1} $min^{1/2}$)	C_1 (mg g^{-1})	C_2 (mg g^{-1})	R_1^2	R_2^2	SSR_1	SSR_2
Natural pH, 5 mg L^{-1}																	
Blue 5 g L^{-1}	0.51±0.02	9.21×10^{-4}	0.34	0.644	0.40	4.15×10^{-2}	0.46	0.995	0.037	1.69×10^{-2}	2.00×10^{-4}	0.024	0.450	0.963	0.030	4.02×10^{-3}	4.14×10^{-3}
Blue 10 g L^{-1}	0.37±0.03	2.07×10^{-3}	0.22	0.783	0.34	1.41×10^{-1}	0.35	0.998	0.014	2.14×10^{-2}	7.00×10^{-4}	0.031	0.317	0.951	0.448	2.09×10^{-3}	1.21×10^{-3}
Red 5 g L^{-1}	0.28±0.02	4.61×10^{-4}	0.22	0.920	0.47	1.53×10^{-2}	0.26	0.975	0.0091	7.20×10^{-3}	2.60×10^{-3}	0.002	0.074	0.965	0.989	1.32×10^{-2}	2.42×10^{-1}
Red 10 g L^{-1}	0.16±0.00	2.99×10^{-3}	0.11	0.955	0.035	3.24×10^{-1}	0.15	0.995	0.0043	7.80×10^{-3}	3.00×10^{-4}	0.013	0.137	0.931	0.149	1.93×10^{-3}	4.10×10^{-4}
Black 5 g L^{-1}	0.18±0.00	3.22×10^{-3}	0.15	0.969	0.0072	6.64×10^{-2}	0.17	0.994	0.0031	6.00×10^{-3}	4.00×10^{-4}	0.006	0.144	0.970	0.289	4.03×10^{-4}	4.48×10^{-4}
Black 10 g L^{-1}	0.18±0.00	1.15×10^{-3}	0.11	0.578	0.083	1.67×10^{-1}	0.17	0.995	0.0022	9.10×10^{-3}	6.00×10^{-4}	0.018	0.132	0.957	0.510	7.39×10^{-4}	5.71×10^{-4}
pH 2, 5 mg L^{-1}																	
Blue 10 g L^{-1}	0.50±0.00	3.12×10^{-1}	0.24	0.943	0.65	8.59	0.50	1.000	0.0029	2.02×10^{-1}	7.00×10^{-5}	0.065	0.498	0.848	0.286	2.07×10^{-2}	9.89×10^{-6}
Blue 6 g L^{-1}	0.70±0.00	4.31×10^{-2}	0.23	0.869	1.81	1.23	0.70	1.000	0.0027	1.58×10^{-1}	7.00×10^{-4}	0.097	0.678	0.854	0.355	3.35×10^{-2}	6.56×10^{-4}
Blue 2 g L^{-1}	1.99±0.00	3.68×10^{-3}	1.04	0.906	8.59	2.90×10^{-2}	2.00	1.000	0.16	1.79×10^{-1}	8.30×10^{-3}	0.165	1.610	0.943	0.710	7.81×10^{-2}	2.94×10^{-2}
Red 10 g L^{-1}	0.48±0.00	5.99×10^{-3}	0.13	0.488	1.17	4.82×10^{-1}	0.48	1.000	0.050	1.54×10^{-1}	2.00×10^{-3}	0.038	0.421	0.906	0.929	6.99×10^{-3}	1.92×10^{-4}
Red 6 g L^{-1}	0.75±0.01	6.91×10^{-3}	0.25	0.655	2.11	2.34×10^{-1}	0.75	1.000	0.057	1.35×10^{-1}	4.00×10^{-3}	0.099	0.632	0.815	0.824	3.26×10^{-2}	1.65×10^{-3}
Red 2 g L^{-1}	2.06±0.01	1.61×10^{-3}	1.24	0.864	7.53	1.11×10^{-2}	2.07	1.000	0.54	1.42×10^{-1}	1.13×10^{-2}	0.191	1.341	0.916	0.833	7.42×10^{-2}	7.06×10^{-2}

Table 5 (continued)

	Pseudo-first order					Pseudo-second order						Intraparticle diffusion					
Dye (g L^{-1})	$q_{e,exp}$ (mg g^{-1})	k_1 (min^{-1})	$q_{e,calc}$ (mg g^{-1})	R^2	SSR	k_2 (g mg^{-1} min^{-1})	$q_{e\,calc}$ (mg g^{-1})	R^2	SSR	$k_{i,1}$ (mg g^{-1} $min^{1/2}$)	$k_{i,2}$ (mg g^{-1} $min^{1/2}$)	C_1 (mg g^{-1})	C_2 (mg g^{-1})	R_1^2	R_2^2	SSR_1	SSR_2
Black 10 g L^{-1}	0.40 ± 0.00	6.22×10^{-2}	0.12	0.752	0.63	6.95	0.40	1.000	0.0061	1.46×10^{-1}	7.00×10^{-4}	0.039	0.388	0.889	0.322	7.52×10^{-3}	1.29×10^{-4}
Black 6 g L^{-1}	0.72 ± 0.00	6.08×10^{-2}	0.35	0.922	1.03	4.05	0.70	1.000	0.046	1.52×10^{-1}	3.00×10^{-4}	0.108	0.698	0.823	0.011	3.89×10^{-2}	9.25×10^{-4}
Black 2 g L^{-1}	1.45 ± 0.01	1.01×10^{-2}	0.96	0.799	2.11	4.72×10^{-2}	1.47	0.989	0.24	1.91×10^{-1}	4.27×10^{-2}	0.109	0.651	0.871	0.987	4.21×10^{-2}	2.60×10^{-3}
pH 2, 300 mg L^{-1}																	
Blue 10 g L^{-1}	27.47 ± 0.20	2.53×10^{-3}	11.02	0.866	2333.17	1.11×10^{-3}	27.93	1.000	7.14	1.97	7.79×10^{-2}	1.867	23.181	0.924	0.890	20.29	1.42
Red 10 g L^{-1}	18.55 ± 0.30	2.32×10^{-3}	10.83	0.950	544.71	7.52×10^{-4}	19.19	0.999	13.38	1.09	1.13×10^{-1}	0.906	12.336	0.943	0.887	4.63	3.06
Black 10 g L^{-1}	16.62 ± 0.04	4.84×10^{-3}	11.93	0.863	173.35	1.15×10^{-3}	17.09	0.976	14.68	1.25	4.04×10^{-1}	0.355	6.040	0.955	0.904	2.33	2.33

*1: first stage of ID; 2: second stage of ID; SSR: Sum of square error; R: correlation coefficient

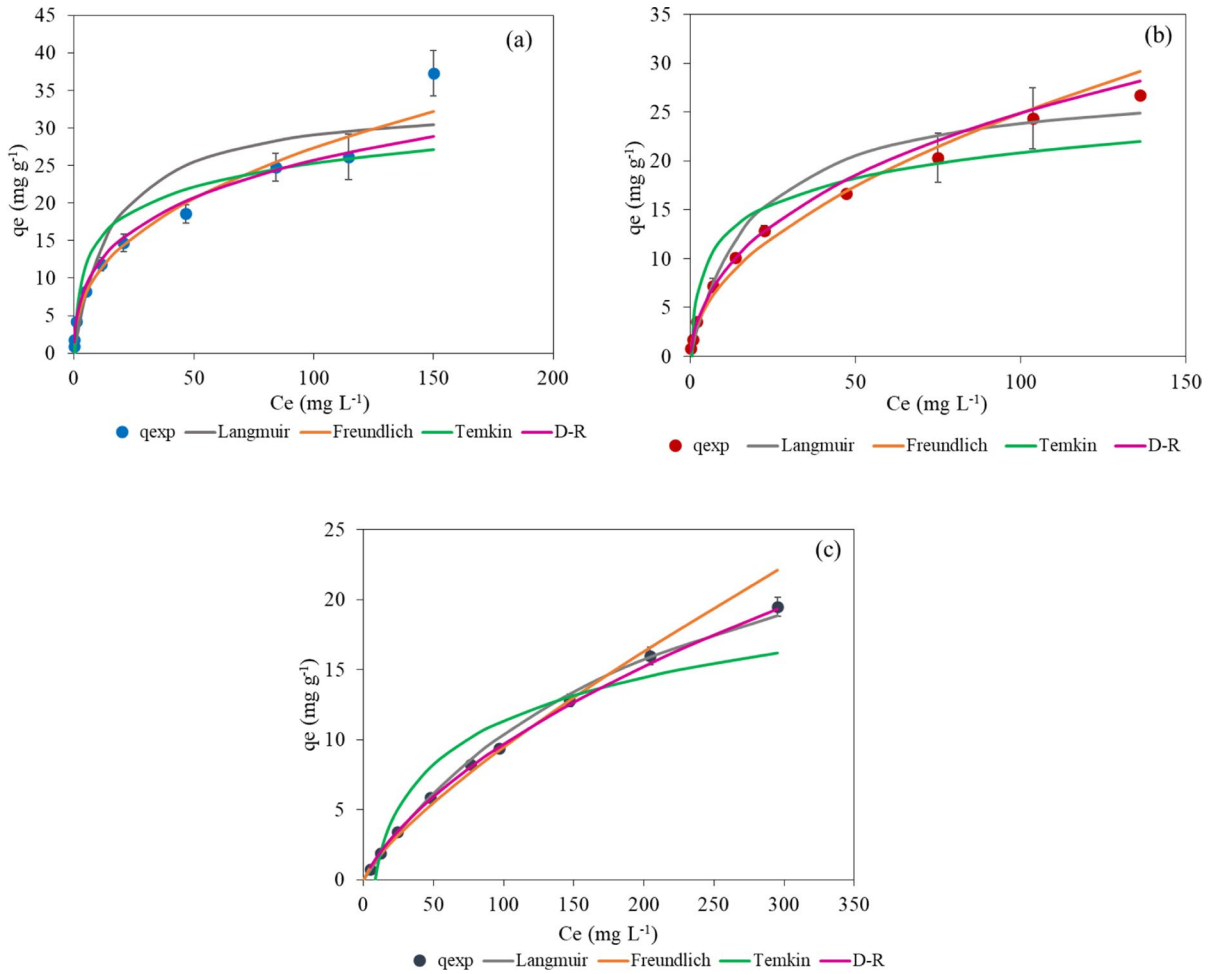

Fig. 9 Adsorption isotherms of blue **a**, red **b** and black **c** dyes by pine sawdust (initial dye concentration 5–300 mg L^{-1}; adsorbent dose 6 g L^{-1}; pH 2; time 4 days for blue and red and 12 h for black; temperature 25 °C; agitation speed 210 rpm)

adsorption through the mean adsorption energy (E) parameter. If E is lower than 8 kJ mol^{-1} a physisorption process occurs with van der Waals interactions. However, if $8 < E < 16$ kJ mol^{-1} adsorption is a chemical process with high adsorption enthalpy because of the ion-exchange mechanism (Deniz and Dogan 2022; Şentürk and Yildiz 2020). Moreover, the values of the monolayer saturation capacity, $q_{m,D,}$ in D-R equation are significantly higher than those for the maximum adsorption capacity,q_m, in the Langmuir one since $q_{m,D}$ represents the total specific meso and macropore volume of the biosorbent. Considering this, PS could be considered a porous biosorbent in agreement with the above-mentioned characterization (Horciu et al. 2020). The adsorption mechanism is very important to understand the basis of the adsorption process. Based on the most common functional groups present on pine sawdust (Orozco et al. 2023) and similar to those described in literature, such as carboxyl, phenolic or hydroxyl (Bortoluz et al. 2020; Salazar-Rabago et al. 2017; Şentürk and Yildiz 2020) and also on the results from the adsorption kinetic and equilibrium studies an adsorption mechanism was proposed (Fig. 10).

The maximum adsorption capacities (q_m) calculated by the Langmuir model (33.78 mg g^{-1} for blue and 28.41 mg g^{-1} for red) are close to the experimental q_{max} obtained (37.30 mg g^{-1} for blue and 26.78 mg g^{-1} for red), except for black dye (q_m calculated: 32.47 mg g^{-1} and q_{max} obtained: 19.47 mg g^{-1})

Table 6 Parameters of isotherm models for the adsorption of the blue, red and black dyes on pine sawdust

Isotherms	Parameters	Blue dye	Red dye	Black dye
Langmuir	q_m (mg g^{-1})	33.78	28.41	32.47
	K_L (L mg^{-1})	0.062	0.052	0.0047
	R_L (5–300 mg L^{-1})	0.764–0.051	0.796–0.060	0.977–0.415
	R^2	0.912	0.963	0.980
	SSR	142.93	30.79	32.04
Freundlich	n	2.47	1.95	1.28
	K_F (mg g^{-1} (L $mg^{-1})^{-1/n}$)	4.22	2.34	0.26
	R^2	0.994	0.991	0.993
	SSR	37.36	12.43	53.02
Temkin	B (J mol^{-1})	4.52	3.77	4.48
	K_T (L mg^{-1})	2.67	2.51	0.13
	R^2	0.829	0.868	0.904
	SSR	287.63	104.39	35.65
Dubidin-Radushkevich	$q_{m,D}$ (mg g^{-1})	91.47	137.61	217.41
	K_{DR} (mol^2 kJ^{-2})	2.82×10^{-9}	3.97×10^{-9}	6.05×10^{-9}
	E (kJ mol^{-1})	13.32	11.22	9.09
	R^2	0.984	0.996	0.997
	SSR	139.70	8.14	0.51

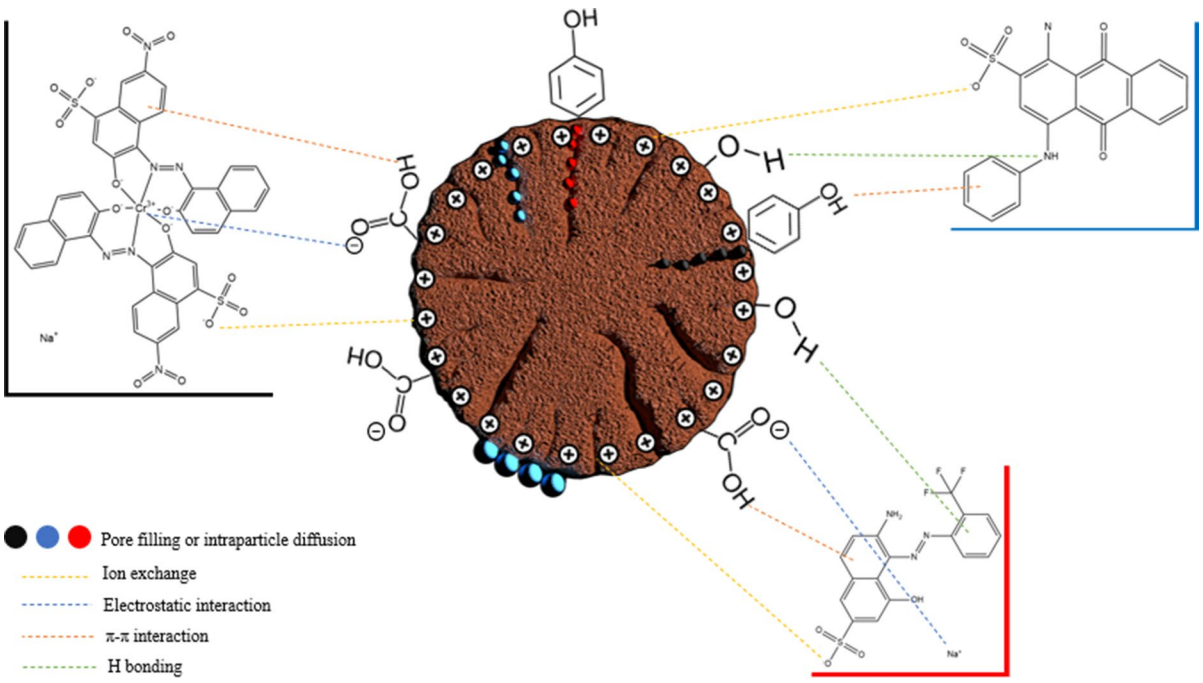

Fig. 10 Proposed mechanism for blue, red and black dye adsorption by un-treated PS

which could be due to and insufficient contact time for high concentrations. R_L values obtained for the three dyes between 0 and 1 indicate favorable adsorption, although it is more favorable at low concentrations since R_L is closer to 1 (Al-Khadi 2020; Şentürk and Yildiz 2020). Regarding the Temkin isotherm, which

Table 7 Application of various bioadsorbents for dyes removal

Material	Treatment	Dye	Conditions*	q_m (mg g^{-1})	References
Pinus radiata sawdust	–	Blue for wood	Dose: 2-10 g L^{-1}; C: 5–300 mg L^{-1}; pH: 2–9; T: 25 °C	27.5	In this study
Pinus radiata sawdust	–	Red for wood	Dose: 2-10 g L^{-1}; C: 5–300 mg L^{-1}; pH 2–9; T: 25 °C	18.6	In this study
Pinus radiata sawdust	–	Black for wood	Dose: 2-10 g L^{-1}; C: 5–300 mg L^{-1}; pH 2–9; T: 25 °C	16.6	In this study
Pinus pinaster bark	Washed	Congo red	pH: 2–9; dose: 1–10 g L^{-1}; T: 25–60 °C; C: 5 mg L^{-1}	0.3–1.6	Litefti et al. (2019)
Pinecone	Washed	Methylene blue	Dose: 2 g L^{-1}; C: 50–250 mg L^{-1}; T: 25–50 °C	125	Özdemir (2019)
Pine sawdust	Pre-treated	Maxilon Red GRL	pH: 6; T: 25 °C; C: 250 mg L^{-1}; dose: 8 g L^{-1}	312.5	Şentürk and Yildiz (2020)
Casuarina equisetifolia pines	Washed	Methylene blue	Dose: 0.5 g L^{-1}; C: 100 mg L^{-1}; pH: 7	41.4	Chandarana et al. (2021)
Aleppo Pine cones	Washed	Methylene blue	C: 100 mg L^{-1}; dose: 0.5 g L^{-1}; pH 10	93.6	Elmoubarki et al. (2016)
White Pine (*Pinus durangensis*) sawdust	Washed	Methylene blue	T: 15–35 °C; pH: 3–10; C: 300 mg L^{-1}; dose: 2 g L^{-1}	70.0	Salazar-Rabago et al. (2017)
Cedar sawdust	–	Methylene blue	pH: 2–12; C: 50–2000 mg L^{-1}; T: 25–60 °C; dose: 5 g L^{-1}	100	Fayoud et al. (2015)
Pine sawdust	–	Methylene blue	pH: 2–12; C: 50–2000 mg L^{-1}; T: 25–60 °C; dose: 10 g L^{-1}	71.4	Fayoud et al. (2015)
Wheat straw	–	Methylene blue	pH: 2–12; C: 50–2000 mg L^{-1}; T: 25–60 °C; dose: 5 g L^{-1}	143	Fayoud et al. (2015)
Provence cane Arundo donax	–	Methylene blue	pH: 2–12; C: 50–2000 mg L^{-1}; T: 25–60 °C; dose: 5 g L^{-1}	91	Fayoud et al. (2015)
Turkish red pine sawdust	Pre-treated	Acid blue 256	pH: 2; C: 200 mg L^{-1}; dose 1 g L^{-1}; T: 25 °C	54.2	Can (2015)
Pine Cone	Washed	Acid black 26	C: 50 mg L^{-1}; pH: 2; dose: 1 g L^{-1}; T:25–65 °C;	57.5	Mahmoodi et al. (2011)
Pine Cone	Washed	Acid blue 7	C: 50 mg L^{-1}; pH: 2; dose: 2 g L^{-1}; T:25–65 °C;	31.6	Mahmoodi et al. (2011)
Oak leaves	Washed	Methylene blue	C: 50 mg L^{-1}; dose: 0.1 g L^{-1}; pH: 7; T: 25 °C	33.5	Sulyman and Gierak (2020)
Pine tree cones (*P. radiata)*	Washed	Congo Red	pH: 3.55; C: 20 mg L^{-1}; T: 30 °C; dose: 0.4 g L^{-1}	32.7	Dawood and Sen (2012)
Pine tree cones (*P. radiata*)	Pre-treated	Congo Red	pH: 3.55; C: 20 mg L^{-1}; T: 30 °C; dose: 0.4 g L^{-1}	40.2	Dawood and Sen (2012)

*Dose: adsorbent dose; C: Initial dye concentration; T: Temperature

Table 8 Desorption percentage of dyes from dye loaded PS using NaOH 0.1 M and HCl 0.1 M

Dye	%Desorption (HCl)	%Desorption (NaOH)
Blue	0.38 ± 0.03	16.26 ± 0.56
Red	0.70 ± 0.01	90.86 ± 0.52
Black	0.91 ± 0.02	24.75 ± 0.02

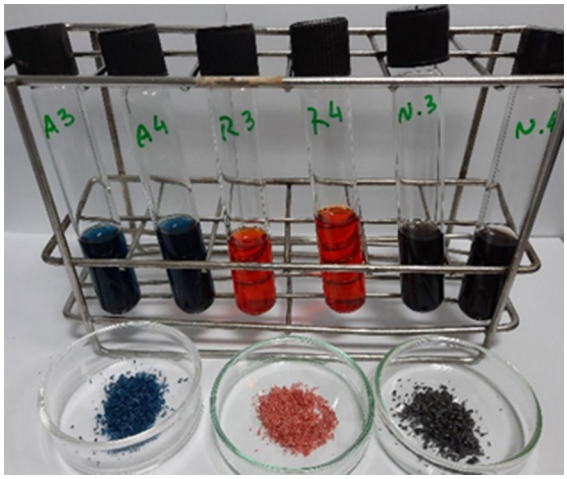

Fig. 11 Dye color intensity in replicated samples after the last desorption stage from dye loaded PS using NaOH 0.1 M and PS material after desorption (Adsorption stage: pH = 2, dye concentration 300 mg L^{-1}; adsorbent dose 10 g L^{-1}; contact time 4 days for blue and red and 12 h for black; temperature 25 °C; agitation speed 210 rpm; desorption stage: adsorbent dose 50 g $L.^{-1}$; contact time 4 h; temperature 25 °C; agitation speed 350 rpm)

implies adsorbent interactions between the adsorbent and the adsorbate, model fitting was worse than with the other models. The positive values of B_T suggest that the adsorption reaction is endothermic (Collins et al. 2019).Fig. 9 shows that the experimental data do not tend to saturation as the Langmuir or Temkin models predict and correlation coefficients were lower than for Freundlich and D-R models.

Bortoluz et al. (2020) and Esmaeili and Foroutan (2019) showed that the Freundlich model was also the one that better described the adsorption of methylene blue by *Pinus elliotti* sawdust and by sawdust of palm trees, eucalyptus and sour lemon, respectively. Moreover, Blaga et al. (2022) and Deniz and Dogan (2022) also reported a great fit to the D-R isotherm model for dye adsorption by biosorbents based on waste biomass.

Table 7 summarizes the adsorption capacity of different bioadsorbents, mostly from pine species, for the adsorption of blue, red and black dyes under different experimental conditions.

Desorption and regeneration of the adsorbent

The adsorption process can be considered more operative and economical if the material used can be regenerated and reused in several adsorption/desorption cycles (El Messaoudi et al. 2021; Kamran et al. 2022). Furthermore, dye loaded material can cause a waste disposal problem, so the study of the desorption process acquires a significant role (Mirza and Ahmad 2020). Ion exchange mechanisms can be involved on dye desorption using relatively economical acids, salts, organic acids and bases (Mashkoor et al. 2018). In this work the maximum dye adsorption capacity was achieved at acid pH, so to validate if desorption efficiency is improved in basic medium desorption experiments were carried out comparing HCl 0.1 M and NaOH 0.1 M as desorption agents and the results are shown in Table 8.

Sodium hydroxide led to significantly higher desorption efficiencies than hydrochloric acid for all dyes, mainly for the red one with a high desorption percentage above 90%, although the solid

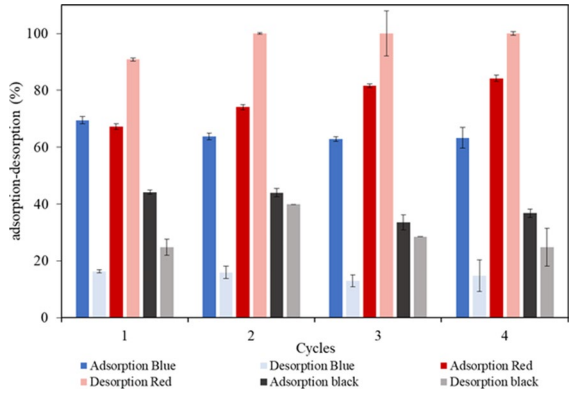

Fig. 12 Adsorption and desorption cycles of blue, red and black dyes onto PS (Adsorption stage: pH = 2, dye concentration 300 mg L^{-1}; adsorbent dose 10 g L^{-1}; contact time 4 days for blue and red and 12 h for black; temperature 25 °C; agitation speed 210 rpm; desorption stage: adsorbent dose 50 g L^{-1}; contact time 4 h; temperature 25 °C; agitation speed 350 rpm)

material preserves some color. As well, as illustrated by Fig. 11, although the adsorption percentages for the blue and black dyes are not greater than 25%, it is possible to observe the high color intensity in these experiments proving the effectiveness of NaOH as desorption agent. This behavior can be explained considering that at basic pH the number of negative charges on the adsorbent surface significantly increases and leads to electrostatic repulsion between the dye components and the adsorbent and, therefore, the dye desorbs from the adsorbent surface. Additionally, alkali components break the connection between the adsorbate and the adsorbent through a chemical reaction (Hu et al. 2020). By the contrary, the lower dye desorption from PS for blue and black dyes indicates a stronger interaction between the adsorbent and the adsorbate, usually by chemisorption which is irreversible contrary to electrostatic interactions (Salazar-Rabago et al. 2017). High desorption efficiencies in alkaline medium as for red dye were also obtained by Kamran et al. (2022) and El Messaoudi et al. (2021) for the desorption of acid red 1 from chemically modified sugarcane bagasse and congo red from date stones and jujube shells, respectively.

The reusability of PS for dye adsorption was investigated by repeating the adsorption–desorption process up to four times using a 0.1 M NaOH solution for desorption. The results are presented in Fig. 12.

High desorption percentages between 91 and 100% were achieved for the red dye and the adsorption percentage increased from 67 to 84% in subsequent cycles. An improvement occurs from the first to the fourth adsorption stage with a decrease on the red color intensity. This could be explained considering that NaOH is one of the most common chemical activating agents used to enhance the adsorbent surface and increase its adsorption efficiency (Şentürk and Yildiz 2020; Azzaz et al. 2016). Desorption efficiency of red dye can be increased by electrostatic repulsion between negatively charged sites on the PS and anionic dye molecules. In addition, the abundance of OH^- ions in the basic solution and its exchange with dye ions on PS could increase the desorption efficiency depending on the dye structure (Daneshvar et al. 2017). These results confirm that, in the case of the red dye, PS offers the potential to be used at least four times with an increase of about 17% in the removal efficiency.

The regeneration input revealed that a slight decrease, about 7–11% in the adsorption percentage, occurs as the PS is reused for blue and black dyes which can be explained by the progressive accumulation of dye molecules on the PS surface owed to the lower desorption percentages that promotes adsorbent exhaustion. Nevertheless, PS can be reused at least four times without significant loss on the adsorption percentage. Similar results, with the slight decrease in the adsorption percentage at each cycle for congo red and crystal violet dyes were observed by El Messaoudi et al. (2021) and Mashkoor et al. (2018) respectively.

Conclusions

Pine sawdust was used as an adsorbent for the removal of wood dyes for wastewater treatment. The effect of some parameters on the adsorption efficiency was studied and the results obtained showed that the highest removal efficiency occurred at pH 2 and increased with increasing contact time till equilibrium was reached and adsorbent dose, except for blue wood dye that reached 100% in all cases. Based on contact time and removal percentage the optimum adsorbent dose for dyes removal was 6 g L^{-1}. On the other hand, removal efficiency decreased with increasing initial dye concentration.

The kinetics of dye adsorption was better explained by the pseudo-second order kinetic model characteristic of a chemical adsorption mechanism. Also, the first stage of the adsorption process could be described by the intraparticle diffusion model with dye transfer into the pores of the material.

The adsorption equilibrium study revealed that the models that better represented the adsorption process for the blue, red and black dyes was the Freundlich and D-R isotherms that describes a heterogeneous surface and a multilayer process.

Sodium hydroxide, showing desorption efficiencies of 16.3%, 90.9% and 24.8% for the blue, red and black dyes, respectively, in the first adsorption/desorption cycle, was selected as desorption agent. It was demonstrated that the sorbent can be reused at least in four consecutive adsorption/desorption cycles for the red dye desorption with improved removal efficiencies.

Regarding the blue and black dyes, the desorption efficiency achieved lower values but did not lead to a significant decrease in the adsorption percentage and could be applied if considering combining adsorption–desorption with an additional post-treatment stage to improve the regeneration of adsorbent or including, so as not to add another stage, testing the desorbing agents under different conditions.

The obtained results showed that pine sawdust is an efficient adsorbent to remove wood dyes from aqueous solutions and factors such as pH, contact time and initial dye concentration influence dye sorption and removal efficiency. Due to the great potential of the studied adsorbent, further studies should be performed with real textile wastewater to better understand the effect of coexisting contaminants.

Author contribution CHP: Investigation, Validation, Visualization, Writing–original draft (catypimentelster@gmail.com). MSF: Conceptualization, Methodology, Supervision, Funding acquisition, Writing—review & editing (mariasonia.freire@usc.es). DG-D: Conceptualization, Methodology, Supervision, Funding acquisition, Writing—review & editing (diego.gomez@usc.es). JG-Á: Conceptualization, Methodology, Supervision, Funding acquisition, Writing—review & editing (julia.gonzalez@usc.es).

Funding Open Access funding provided thanks to the CRUE-CSIC agreement with Springer Nature. This work was financial supported by Xunta de Galicia (ED431B 2020/039).

Data availability All data generated or analyzed during this study are included in this article.

Declarations

Conflict of interest The authors declare no competing interests.

References

Akhouairi S, Ouachtak H, Addi AA, Jada A, Douch J (2019) Natural sawdust as adsorbent for the eriochrome black T dye removal from aqueous solution. Water Air Soil Poll 230(8):1–15. https://doi.org/10.1007/s11270-019-4234-6

Al-Kadhi NS (2020) Removal of fluorescein dye from aqueous solutions using natural and chemically treated pine sawdust. Int J Anal Chem 2020:1–9. https://doi.org/10.1155/2020/8824368

Aragaw TA, Bogale FM (2021) Biomass-based adsorbents for removal of dyes from wastewater: a review. Front Environ Sci 9:558. https://doi.org/10.3389/fenvs.2021.764958

Azzaz AA, Jellali S, Assadi AA, Bousselmi L (2016) Chemical treatment of orange tree sawdust for a cationic dye enhancement removal from aqueous solutions: kinetic, equilibrium and thermodynamic studies. Desanilation Water Treat 57(46):22107–22119. https://doi.org/10.1080/19443994.2015.1103313

Blaga AC, Tanasă AM, Cimpoesu R, Tataru-Farmus RE, Suteu D (2022) Biosorbents based on biopolymers from natural sources and food waste to retain the methylene blue dye from the aqueous medium. Polymers 14(13):1–14. https://doi.org/10.3390/polym14132728

Bortoluz J, Ferrarini F, Bonetto LR, da Silva CJ, Giovanela M (2020) Use of low-cost natural waste from the furniture industry for the removal of methylene blue by adsorption: isotherms, kinetics and thermodynamics. Cellulose 27(11):6445–6466. https://doi.org/10.1007/s10570-020-03254-y

Can M (2015) Equilibrium, kinetics and process design of acid yellow 132 adsorption onto red pine sawdust. Water Sci Technol 71(12):1901–1911. https://doi.org/10.2166/wst.2015.164

Chandarana H, Suganya S, Madhava AK (2020) Surface functionalized Casuarina equisetifolia pine powder for the removal of hetero-polyaromatic dye: characteristics and adsorption. Int J Environ Anal Chem 102(17):5457–5471. https://doi.org/10.1080/03067319.2020.1798418

Chandarana H, Senthil Kumar P, Seenuvasan M, Anil Kumar M (2021) Kinetics, equilibrium and thermodynamic investigations of methylene blue dye removal using Casuarina equisetifolia pines. Chemosphere 285:131480. https://doi.org/10.1016/j.chemosphere.2021.131480

Chikri R, Elhadiri N, Benchanaa M, El maguana Y (2020) Efficiency of sawdust as low-cost adsorbent for dyes removal. J Chem 2020:17. https://doi.org/10.1155/2020/8813420

Chowdhury ZZ, Ziaul Karim M, Ashraf MA, Khalid K (2016) Influence of carbonization temperature on physicochemical properties of biochar derived from slow pyrolysis of durian wood (Durio zibethinus) sawdust. Bioresources 11(2):3356–3372. https://doi.org/10.15376/biores.11.2.3356-3372

Collins ON, Elijah OC, Okechukwu OD (2019) Adsorption of a dye (Crystal Violet) on an acid modified non-conventional adsorbent. J Chem Technol Metall 54(1):95–110

Daneshvar E, Vazirzadeh A, Niazi A, Kousha M, Naushad M, Bhatnagar A (2017) Desorption of Methylene blue dye from brown macroalga: effects of operating parameters, isotherm study and kinetic modeling. J Clean Prod

152:443–453. https://doi.org/10.1016/J.JCLEPRO.2017.03.119

Dawood S, Sen TK (2012) Removal of anionic dye Congo red from aqueous solution by raw pine and acid-treated pine cone powder as adsorbent: equilibrium, thermodynamic, kinetics, mechanism and process design. Water Res 46(6):1933–1946. https://doi.org/10.1016/j.watres.2012.01.009

De Meyer T, Hemelsoet K, Van Speybroeck V, De Clerck K (2014) Substituent effects on absorption spectra of pH indicators: an experimental and computational study of sulfonphthaleine dyes. Dyes Pigm 102:241–250. https://doi.org/10.1016/j.dyepig.2013.10.048

Deniz F, Dogan F (2022) Effective cleaning of a hazardous synthetic triarylmethane-type dye from aquatic environment with a multifunctional waste biomass–based biosorbent. Biomass Convers Biorefinery. https://doi.org/10.1007/s13399-021-01995-9

Elmoubarki R, Moufti A, Tounsadi H, Mahjoubi FZ, Farnane M, Machrouhi A, Elhalil A, Abdennouri M, Zouhri A, Barka N (2016) Kinetics and thermodynamics study of methylene blue adsorption onto Aleppo pine cones. J Mater Environ Sci 7(8):2869–2879

Elwakeel KZ (2010) Environmental application of chitosan resins for the treatment of water and wastewater: a review. J Dispersion Sci Technol 31(3):273–288. https://doi.org/10.1080/01932690903167178

Elwakeel KZ, El-Bindary AA, Ismail A, Morshidy AM (2017) Magnetic chitosan grafted with polymerized thiourea for remazol brilliant blue R recovery: effects of uptake conditions. J Dispersion Sci Technol 38(7):943–952. https://doi.org/10.1080/01932691.2016.1216436

Esmaeili H, Foroutan R (2019) Adsorptive behavior of methylene blue onto sawdust of sour lemon, date palm, and eucalyptus as agricultural wastes. J Dispers Sci Technol 40(7):990–999. https://doi.org/10.1080/01932691.2018.1489828

Fayoud N, Tahiri S, Alami Younssi S, Albizane A, Gallart-Mateu D, Cervera ML, de la Guardia M (2015) Kinetic, isotherm and thermodynamic studies of the adsorption of methylene blue dye onto agro-based cellulosic materials. New Pub: Balaban 57(35):16611–16625. https://doi.org/10.1080/19443994.2015.1079249

Freundlich H (1907) Über die adsorption in lösungen. Z Phy Chem 57(1):385–470

Gemici BT, Ozel HU, Ozel HB (2021) Removal of methylene blue onto forest wastes: adsorption isotherms, kinetics and thermodynamic analysis. Environ Technol Innov 22:101501. https://doi.org/10.1016/j.eti.2021.101501

Ho YS, McKay G (1999) Pseudo-second order model for sorption processes. Process Biochem 34(5):451–465

Horciu IL, Blaga AC, Rusu L, Zaharia C, Suteu D (2020) Biosorption of reactive dyes from aqueous media using the *Bacillus* sp. Residual biomass. Desalin Water Treat 195:353–360. https://doi.org/10.5004/dwt.2020.25901

Hu L, Guang C, Liu Y, Su Z, Gong S, Yao Y, Wang Y (2020) Adsorption behavior of dyes from an aqueous solution onto composite magnetic lignin adsorbent. Chemosphere 246:125757. https://doi.org/10.1016/J.CHEMOSPHERE.2019.125757

Ighalo JO, Zhou Y, Zhou Y, Igwegbe CA, Anastopoulos I, Raji MA, Iwuozor KO (2022) A review of pine-based adsorbents for the adsorption of dyes. Biomass Deriv Mater Environ Appl. https://doi.org/10.1016/B978-0-323-91914-2.00013-1

Islam MT, Saenz-Arana R, Hernandez C, Guinto T, Ahsan MA, Kim H, Lin Y, Alvarado-Tenorio B, Noveron JC (2018) Adsorption of methylene blue and tetracycline onto biomass-based material prepared by sulfuric acid reflux. RSC Adv 8(57):32545–32557. https://doi.org/10.1039/C8RA05395B

Jaouadi M (2021) Characterization of activated carbon, wood sawdust and their application for boron adsorption from water. Int Wood Prod J 12(1):22–33. https://doi.org/10.1080/20426445.2020.1785605

Kah M, Sigmund G, Xiao F, Hofmann T (2017) Sorption of ionizable and ionic organic compounds to biochar, activated carbon and other carbonaceous materials. Water Res 124:673–692. https://doi.org/10.1016/j.watres.2017.07.070

Kamran U, Bhatti HN, Noreen S, Tahir MA, Park SJ (2022) Chemically modified sugarcane bagasse-based biocomposites for efficient removal of acid red 1 dye: kinetics, isotherms, thermodynamics, and desorption studies. Chemosphere 291(P2):132796. https://doi.org/10.1016/j.chemosphere.2021.132796

Kantar C, Akal H, Kaya B, Islamoğlu F, Türk M, Şaşmaz S (2015) Novel phthalocyanines containing resorcinol azo dyes; Synthesis, determination of pKa values, antioxidant, antibacterial and anticancer activity. J Organomet Chem 783:28–39. https://doi.org/10.1016/j.jorganchem.2014.12.042

Khataee AR, Vafaei F, Jannatkhah M (2013) Biosorption of three textile dyes from contaminated water by filamentous green algal *Spirogyra* sp.: kinetic, isotherm and thermodynamic studies. Int Biodeterior Biodegrad 83:33–40. https://doi.org/10.1016/J.IBIOD.2013.04.004

Kim KC, Yoon TU, Bae YS (2016) Applicability of using CO_2 adsorption isotherms to determine BET surface areas of microporous materials. Microporous Mesoporous Mater 224:294–301. https://doi.org/10.1016/j.micromeso.2016.01.003

Konicki W, Cendrowski K, Chen X, Mijowska E (2013) Application of hollow mesoporous carbon nanospheres as an high effective adsorbent for the fast removal of acid dyes from aqueous solutions. Chem Eng J 228:824–833. https://doi.org/10.1016/j.cej.2013.05.067

Kumar NS, Asif M, Al-Hazzaa MI (2018) Adsorptive removal of phenolic compounds from aqueous solutions using pine cone biomass: kinetics and equilibrium studies. Environ Sci Pollut Res 25:21949–21960. https://doi.org/10.1007/s11356-018-2315-5

Langmuir I (1918) The adsorption of gases on plane surfaces of glass, mica and platinum. J Am Chem Soc 40(9):1361–1403

Litefti K, Freire MS, Stitou M, González-Álvarez J (2019) Adsorption of an anionic dye (congo red) from aqueous solutions by pine bark. Sci Rep 9(1):1–11. https://doi.org/10.1038/s41598-019-53046-z

Lorenz M, Paganini C, Storti G, Morbidelli M (2019) Macroporous polymer-protein hybrid materials for

antibody purification by combination of reactive gelation and click-chemistry. Materials 12(10):1580. https://doi.org/10.3390/ma12101580

Mahmoodi NM, Hayati B, Arami M, Lan C (2011) Adsorption of textile dyes on Pine Cone from colored wastewater: kinetic, equilibrium and thermodynamic studies. Desalination 268(1–3):117–125. https://doi.org/10.1016/j.desal.2010.10.007

Mashabi RA, Khan ZA, Elwakeel KZ (2022) Chitosan or glycidyl methacrylate-based adsorbents for dyes removal from the aqueous solutions: a brief review. Mater Adv 3(14):5645–5671. https://doi.org/10.1039/d2ma00320a

Mashkoor F, Nasar A, Asiri AM (2018) Exploring the reusability of synthetically contaminated wastewater containing crystal violet dye using tectona grandis sawdust as a very low-cost adsorbent. Sci Rep 8(1):1–16. https://doi.org/10.1038/s41598-018-26655-3

El Messaoudi N, El Khomri M, Chlif N, Chegini ZG, Dbik A, Bentahar S, Lacherai A (2021) Desorption of Congo red from dye-loaded Phoenix dactylifera date stones and Ziziphus lotus jujube shells. Groundw Sustain Dev 12:100552. https://doi.org/10.1016/j.gsd.2021.100552

Mirza A, Ahmad R (2020) An efficient sequestration of toxic crystal violet dye from aqueous solution by Alginate/Pectin nanocomposite: a novel and ecofriendly adsorbent. Groundw Sustain Dev 11:200373. https://doi.org/10.1016/J.GSD.2020.100373

Nordine N, El Bahri Z, Sehil H, Fertout RI, Rais Z, Bengharez Z (2016) Lead removal kinetics from synthetic effluents using Algerian pine, beech and fir sawdust's: optimization and adsorption mechanism. App Water Sci 6(4):349–358. https://doi.org/10.1007/s13201-014-0233-3

Ogana FN, Corral-Rivas S, Gorgoso-Varela JJ (2020) Non-linear mixed-effect height-diameter model for Pinus pinaster ait. and Pinus radiata d. don. Cerne 26(1):150–161. https://doi.org/10.1590/01047760202026012695

Orozco CI, Freire MS, Gómez-Díaz D, González-Álvarez J (2023) Removal of copper from aqueous solutions by biosorption onto pine sawdust. Sustain Chem Pharm 32:101016. https://doi.org/10.1016/j.scp.2023.101016

Özacar M, Şengil IA (2005) Adsorption of metal complex dyes from aqueous solutions by pine sawdust. Bioresour Technol 96(7):791–795. https://doi.org/10.1016/j.biortech.2004.07.011

Özdemir ÇS (2019) Equilibrium, kinetic, diffusion and thermodynamic applications for dye adsorption with pine cone. Sep Sci Technol 54(18):3046–3054. https://doi.org/10.1080/01496395.2019.1565769

Philippou K, Anastopoulos I, Pashalidis I, Hosseini-Bandegharaei A, Usman M, Kornaros M, Omirou M, Kalderis D, Milojković JV, Lopičić ZR, Abatal M (2021) Chapter 6 - The application of pine-based adsorbents to remove potentially toxic elements from aqueous solutions. In: Núñez-Delgado A (ed) Sorbents materials for controlling environmental pollution. Elsevier, pp 113–133

Ratnamala GM, Deshannavar UB, Munyal S, Tashildar K, Patil S, Shinde A (2016) Adsorption of reactive blue dye from aqueous solutions using sawdust as adsorbent: optimization, kinetic, and equilibrium studies. Arab J Sci Eng 41(2):333–344. https://doi.org/10.1007/s13369-015-1666-1

Reijenga J, van Hoof A, van Loon A, Teunissen B (2013) Development of methods for the determination of pKa values. Anal Chem Insights 8(1):53–71. https://doi.org/10.4137/ACI.S12304

Rouquerol J, Rouquerol F, Sing KSW, Llewellyn P, Maurin G (2014) Adsorption by powders and porous solids: principles, methodology and applications. Academic Press, London

Sahmoune MN, Yeddou AR (2016) Potential of sawdust materials for the removal of dyes and heavy metals: examination of isotherms and kinetics. Desalin Water Treat 57(50):24019–24034. https://doi.org/10.1080/19443994.2015.1135824

Salazar-Rabago JJ, Leyva-Ramos R, Rivera-Utrilla J, Ocampo-Perez R, Cerino-Cordova FJ (2017) Biosorption mechanism of Methylene Blue from aqueous solution onto White Pine (*Pinus durangensis*) sawdust: effect of operating conditions. Sustain Environ Res 27(1):32–40. https://doi.org/10.1016/j.serj.2016.11.009

Schaffer M, Licha T (2014) A guideline for the identification of environmentally relevant, ionizable organic molecule species. Chemosphere 103:12–25. https://doi.org/10.1016/j.chemosphere.2013.12.009

Semerjian L (2018) Removal of heavy metals (Cu, Pb) from aqueous solutions using pine (*Pinus halepensis*) sawdust: equilibrium, kinetic, and thermodynamic studies. Environ Technol Innov 12:91–103. https://doi.org/10.1016/j.eti.2018.08.005

Şentürk I, Yıldız MR (2020) Highly efficient removal from aqueous solution by adsorption of Maxilon Red GRL dye using activated pine sawdust. Korean J Chem Eng 37(6):985–999. https://doi.org/10.1007/s11814-020-0526-1

Sulyman M, Gierak A (2020) Green environmental approach for adsorption of hazardous dye from water using tree and sea plant leaves (Dead L.). Acta Sci Agric 4(2):1–10

Weber WJ Jr, Morris JC (1963) Kinetics of adsorption on carbon from solution. J Sanit Eng Div 89(2):31–59

Zafar S, Akhtar S, Tariq T, Mushtaq N, Akram A, Ahmed A, Arif M, Naeem S, Anwar S (2014) Determination of pKa values of new phenacyl-piperidine derivatives by potentiometric titration method in aqueous medium at room temperature (25±0.5°C). Pak J Pharm Sci 27:925–929

Biomass Conversion and Biorefinery
https://doi.org/10.1007/s13399-023-04138-4

ORIGINAL ARTICLE

Preparation of activated carbon from pine (*Pinus radiata*) sawdust by chemical activation with zinc chloride for wood dye adsorption

Catarina H. Pimentel[1] · M. Sonia Freire[1] · Diego Gómez-Díaz[1] · Julia González-Álvarez[1]

Received: 29 December 2022 / Revised: 14 March 2023 / Accepted: 24 March 2023

Abstract
Wastewater containing dyes are released into water bodies generating serious problems in human health and marine life. To contribute to the solution of this problem, a novel activated carbon was prepared from untreated pine (*Pinus radiata*) sawdust by dry chemical activation with $ZnCl_2$ and was used for wood dye adsorption. The carbon was characterized by point of zero charge, N_2 and CO_2 adsorption isotherms, SEM-EDX, and FTIR. N_2 and CO_2 surface areas were 471.4 and 319.5 $m^2\ g^{-1}$, respectively, with 91% of micropores. Wood dye adsorption was studied in function of pH (2–12), adsorbent dose (0.1–4 g L^{-1}), time (up to 48 h for blue and red and 12 h for black), and initial concentration (5–500 mg L^{-1}). The equilibrium data for the blue and black dyes were satisfactorily fitted to the Freundlich model while those for the red dye to the Langmuir model. Kinetic data were explained by the pseudo-second order (chemisorption process) and intraparticle diffusion models. At 5 mg L^{-1}, a 100% removal efficiency was achieved at all pH for the blue dye, whereas for the red and black, natural pH (5.1) and pH = 2, respectively, led to the best removal efficiencies, 96 and 56%. Increasing concentration above 25 mg L^{-1} significantly reduced adsorption efficiency for blue and red dyes. For the black dye increasing the dose to 1 g L^{-1}, the adsorption efficiency reached 82% at 25 mg L^{-1}. High removal efficiencies were achieved for all dyes at 25 mg L^{-1} and 4 g L^{-1}.

Keywords Activated carbon · Chemical activation · Zinc chloride · Adsorption · Pine sawdust · Wood dyes

1 Introduction

A problem that has persisted over the years and has attracted the attention of many researchers is water pollution. With the huge expansion of industrialization (such as textile, wood, rubber, and dye industries), the volume of untreated wastewaters that are discharged into streams and water bodies also increased. Among the wastewater contaminants, particularly dyes can generate serious problems in human health due to their toxicity, mutagenicity, and carcinogenicity even at low concentrations. Moreover, they are highly resistant to light, aerobic digestion, and oxidizing agents due to their chemical stability [1–3]. Therefore, wastewater treatment is essential and various technologies have been employed for dye removal such as electrocoagulation; photocatalytic, oxidative, and biochemical degradation; and adsorption. Adsorption has received special attention due to its simplicity, high efficiency, including the treatment of concentrated dye effluents, low cost, and the possibility of reusing the adsorbent through its recovery and regeneration [4, 5].

Adsorption on activated carbons (AC) has been widely used for dye removal due to their high porosity, surface area, physicochemical stability, mechanical strength, and surface reactivity. However, due to their high cost and regeneration difficulty, numerous investigations have focused on their production from natural, abundant, safe, and low-cost precursors [6–8]. Activated carbons can be prepared by physical (in which steam, nitrogen, or carbon dioxide can be used for moderate reduction of the carbonaceous matter) or chemical activation (a chemical dehydrating agent is employed to activate the biomass or char) by one- or two-step processes. Usually, activated carbon prepared by chemical activation presents higher surface area, smaller pore size, and has wider use in many applications [9, 10]. Agarwal et al. [4] reported the two-step process as the most effective due to the high porosity developed: (1) carbonization of the material under an inert atmosphere which enables the removal of moisture, volatile compounds, and other aromatic and then resulting

✉ Julia González-Álvarez
julia.gonzalez@usc.es

[1] Department of Chemical Engineering, School of Engineering, Universidade de Santiago de Compostela, 15782 Santiago de Compostela, Spain

Published online: 31 March 2023

in a char with high carbon content; and (2) activation at elevated temperature to degrade the cellulosic materials in the precursor and to attain specific characteristics which will depend on the process conditions used. Carbonization depends on several factors such as the existence of an inert atmosphere, the heating rate, the carbonization temperature, and time [5, 10]. The resulting char can be activated through chemical activation that could be performed by impregnation (wet oxidation) or by mixing the char with the solid activating agent (dry oxidation) [11–13]. Regarding the activating agents, they act as dehydrating agents which influence the decomposition by pyrolysis and inhibit the formation of tar. Additionally, the activation agent will strongly influence the properties of the activated carbon. Among the most used activating chemical agents such as $ZnCl_2$, KOH, H_3PO_4, and K_2CO_3, which present an enhanced effect on carbon surface area and porosity, $ZnCl_2$ stands out as an excellent activating agent [4]. The activation process using $ZnCl_2$ increases the yield due to polymerization and operates as a Lewis acid favoring the creation of certain large-ring aromatic compounds, produces a template effect inducing the formation of uniform micropores and could be more selective [3, 11, 14, 15]. Moreover, the carbon activated with this agent usually presents outstanding properties such as large pore volume with smaller pore size, higher surface area, and abundant reactive groups for contaminant uptake. Additionally, it has been reported that activated carbons prepared using $ZnCl_2$ as activating agent showed good results particularly for dye removal [16, 17]. Activated carbon, as general adsorbent, has a long history of manufacture and application, although there are still various production aspects that could be considerably improved [18].

Waste biomass from agricultural or forest byproducts has arisen as the best alternative since these raw materials can be used as adsorbents without treatment, or by carbonization and activation, improving their adsorption capacity. Besides, unwanted and abundant wastes can be converted into useful and valuable adsorbents [19]. There has been demand for cost-effective precursors for the production of activated carbon and recent research have reported the preparation of AC from materials such as grape stalk, semi-coke, coconut shell, slash pinewood, and *Sterculia alata* nutshell [5, 9, 14, 19, 20]. This type of carbon-based materials demonstrates characteristics such as high surface area, stability, range of functional groups, and a porous structure [5]. Nevertheless, depending on the nature of the biomass and the pyrolysis/activation conditions, biochar with a porous structure and different carbon content having a high surface area can be produced [21]. Both chemical structure and surface chemistry depend not only on the type of biomass but also on the parts of the biomass. Cellulosic biomass usually consists of cellulose, hemicelluloses, and lignin but the proportions change depending on the material which will influence the characteristics of activated carbons [22, 23]. Furthermore, in most of the studies [5, 14, 19, 20], the raw material is washed or pre-treated which increases the use of chemicals in the production of activated carbon. Different waste biomass has been converted into activated carbon and has been successfully used to remove acid dyes from wastewaters: *Paulownia tomentosa* wood to remove acid red 4 [24], apple wood to remove acid red 337 and acid blue 349 [25], walnut and poplar woods to remove acid red 18 [26], pine-cone to remove acid black 1 and acid blue 113 [27].

Pine trees of different species are present in large amounts around the world and are among the most commercially valuable tree species for timber or wood pulp [28]. Pine sawdust, a byproduct from the wood industry, is a lignocellulosic material containing hemicellulose, cellulose, lignin, and some functional groups (e.g., carboxyl, phenolic, hydroxyl) which makes it a good precursor to produce activated carbons [6]. Pine sawdust from *Pinus radiata*, an abundant species in the northwest of Spain, could be an exceptional choice from an economic and environmental viewpoint due to its availability and low cost. To the best of our knowledge, pine sawdust from *Pinus radiata* has never been applied as raw material for the production of activated carbon for dye adsorption [28, 29].

Due to the great concern with the discharge of wastewater containing dyes into water bodies that pose a diversity of hazards for humans and marine life, the present study was focused on the production and characterization of a novel activated carbon based on untreated pine (*Pinus radiata*) sawdust (PS). The carbon was activated by direct mixing with $ZnCl_2$ and used for the removal of acid wood dyes from aqueous solutions. Thus, a double objective is achieved, to replace expensive commercial activated carbons and at the same time reduce the costs of biomass waste management, in addition to proposing an alternative for solving the challenge of dye wastewater pollution. Batch adsorption experiments were performed to evaluate the influence of various operating conditions such as pH, adsorbent dose, and initial dye concentration on the removal efficiency. The carbon was characterized for its structural and surface properties, by the point of zero charge (pH_{PZC}), BET surface area obtained from nitrogen (N_2) and carbon dioxide (CO_2) sorption isotherms, and pore volume. Also, Fourier transform infrared spectroscopy (FTIR) and scanning electron microscopy coupled with energy dispersive X-ray analysis (SEM-EDX) were performed before and after adsorption. Kinetic and equilibrium studies were carried out under selected conditions in order to analyze the adsorption mechanism.

2 Experimental section

2.1 Materials

Pine (*Pinus radiata*) sawdust (PS) was provided by a regional sawmill (Lugo, Spain). After air-drying to

equilibrium moisture content (11.61 wt%), PS was sieved and the fraction between 0.5 and 1 mm was selected, stored in a plastic container, and used directly for the AC production.

Acid wood dyes were used: Blue for wood AGN-270%, Red for wood GRA-200%, and Black Hispalan M-RN-140%. Dye solutions were prepared by dilution of a stock aqueous solution of 1000 mg L^{-1} with distilled water. Natural pH was determined for each dye at 5, 25, and 500 mg L^{-1} using a digital pH meter (Hanna edge).

Zinc chloride ($ZnCl_2$, 98%, Scharlau), sodium chloride (NaCl, 99.5%, Probus), sodium hydroxide (NaOH, 98%, Sigma-Aldrich), and hydrochloric acid (HCl, 37%, Sigma-Aldrich) were used.

2.2 Production of activated carbon

To analyze the transformations of pine sawdust during the thermal treatment, thermogravimetric analysis was performed from 50 to 1000°C under N_2 atmosphere at 25 mL min^{-1}. According to the results (Fig. S1), 600°C was selected as carbonization temperature since cellulose, hemicelluloses, and lignin decomposition usually takes place below this temperature [15, 30] and no weight loss occurred at higher temperatures.

PS was carbonized at 600°C for 1 h under a N_2 atmosphere (10 mL min^{-1}) in a horizontal tubular furnace (Carbolite, Sheffield) applying a ramp of 5°C min^{-1} up to 600°C. Afterward, it was cooled down to room temperature. Thereafter, the biochar produced after carbonization was mixed by milling with $ZnCl_2$ at a weight ratio of 1:4 (w/w) and activated in the furnace at 850°C for 2 h under a constant N_2 flow rate (10 mL min^{-1}) using a heating rate of 5°C min^{-1} ($AC_{ZnCl2\text{-}850}$). After activation, the obtained material was washed with HCl 0.1 M under stirring, and later with distilled water under vacuum filtration up to neutral pH. Finally, the washed sample was dried overnight at 105°C [12].

2.3 Activated carbon characterization

The point of zero charge (pH_{PZC}) was evaluated according to the method described by Carabineiro et al. [31]. Briefly, 20 mg of $AC_{ZnCl2\text{-}850}$ was put in contact with 20 mL of a 0.01 M NaCl solution at 200 rpm for 48 h to assure equilibrium. The pH of solutions was adjusted between 2 and 12 by adding HCl or NaOH with concentrations between 0.5 and 2 M.

The pore volume, surface area, and structural properties of $AC_{ZnCl2\text{-}850}$ were characterized by N_2 and CO_2 adsorption isotherms using an ASAP 2020 sorption analyzer (Micromeritics). N_2 and CO_2 adsorption isotherms were recorded at −196°C and 0°C, respectively. Before measurements, a degassing procedure was carried out under vacuum at 300°C for 1 h. N_2 and CO_2 surface areas were determined using the Brunauer-Emmet-Teller (BET) equation and the mesopore volume and pore size distribution were determined by Barrett-Joyner-Halenda desorption isotherm. Total pore volume was determined at a relative pressure of 0.99 and this value was used to calculate micropore volume on the basis of mesopore volume neglecting the macropore volume (from the BJH equation) [19].

$AC_{ZnCl2\text{-}850}$ was analyzed by a scanning electron microscope coupled with EDX (ZEISS EVO LS 15 microscope) to study its morphological features and to determine its elemental composition before and after adsorption. Additionally, Fourier transform infrared (FTIR) spectra of $AC_{ZnCl2\text{-}850,}$ before and after adsorption were recorded with a VARIAN FTIR 670 spectrometer to characterize the fundamental sample functional groups.

2.4 Adsorption kinetic experiments

To optimize the adsorption process, batch experiments were performed at different pH (2, natural pH, 7, 9, and 12), initial dye concentration (5, 25, and 500 mg L^{-1}), and adsorbent dose (0.1–4.0 g L^{-1}) to study the removal of acid blue, red, and black industrial wood dyes by the $AC_{ZnCl2\text{-}850}$ prepared. An agitation speed of 210 rpm and a temperature of 25°C were ensured by a shaking water bath (H20 SOW-LAUDA). Samples were withdrawn at predefined times and centrifuged (Centronic, P Selecta) for 15 min at 4000 rpm. Dye concentration was determined by measuring the absorbance of the supernatant at the maximum dye wavelength, λ_{max}, using a UV/VIS spectrophotometer (V-630, Jasco), namely 602 nm and 572 nm for blue and black dyes, respectively, and for the red one at 506 nm from pH 2 to 7, 499 nm at pH 9 except at 500 mg L^{-1} which maintains at 506 nm and 483 nm at pH 12.

The sorption efficiency was calculated using Eq. (1) as the percentage of dye adsorbed. The amount of dye adsorbed in mg g^{-1} was calculated following Eq. (2).

$$\%\ \text{Adsorption} = \left(C_0 - C\right)/C_0 \times 100 \tag{1}$$

$$q = \left(C_0 - C\right)V/m \tag{2}$$

where C_0 and C are the initial and residual dye concentrations (mg L^{-1}), q is the adsorption capacity (mg g^{-1}), V is the volume of the dye solution (L), and m is the dry mass of adsorbent used (g).

The kinetic models applied for the study of the adsorption process and the interaction mechanisms were the pseudo-first-order and pseudo-second-order kinetic models and the intraparticular diffusion model.

The pseudo-first-order kinetic model is related with the solid capacity and solution concentration and is applicable only during the initial stage of the adsorption process. It is given by:

$$\log\left(q_e - q_t\right) = \log\ q_e - k_1 t/2.303 \tag{3}$$

where q_t and q_e are the amounts of dye adsorbed (mg g^{-1}) at time t (min) and at equilibrium, respectively, and k_1 represents the first-order rate constant (min^{-1}) [32].

The pseudo-second-order kinetic model can predict the behavior over the whole range of the adsorption process, and it is based on a solid phase sorption, usually related with chemisorption mechanism [32, 33]. The linearized form of the model is:

$$t/q_t = \left(1/k_2 q_e^2\right) + t/q_e \tag{4}$$

where k_2 (g mg^{-1} min^{-1}) is the pseudo-second-order rate constant.

The intraparticle diffusion model distinguishes different diffusion mechanisms and usually four steps are described to control the rate of adsorption process. These include (1) molecular diffusion from the solution to a film layer encircling the adsorbent; (2) diffusion occurring from the film to particle surface; (3) migration inside the adsorbent particle by "surface diffusion" or "pore diffusion"; and (4) adsorption uptake by many interaction mechanisms such as chemisorption, physisorption, complexation, or ion exchange. The intraparticle diffusion equation is as follows:

$$q_t = k_{id} t^{1/2} + C \tag{5}$$

where C (mg g^{-1}) is the intercept and k_{id} is the rate constant of intraparticle diffusion (mg g^{-1} $min^{-1/2}$) [4, 34].

2.5 Adsorption equilibrium experiments

Equilibrium data were obtained through batch experiments in which 2 g L^{-1} of $AC_{ZnCl2\text{-}850}$ for black and 4 g L^{-1} of $AC_{ZnCl2\text{-}850}$ for blue and red dyes were added to 25–500 mg L^{-1} of dye solution at pH = 2 and 25°C for the equilibrium time (48 h) for blue and red dyes and 12 h for black dye to assure stability.

Langmuir and Freundlich isotherm models were employed to analyze the experimental data since they are the most commonly used for the study of equilibrium data [35]. According to the Langmuir's isotherm model, the uptake of adsorbate molecules takes place on a homogeneous surface with a limited number of adsorption sites giving rise to the formation of a monolayer and not including the interaction between adsorbed molecules. The linearized isotherm equation is represented by Eq. (6).

$$C_e/q_e = C_e/q_m + 1/q_m K_L \tag{6}$$

where C_e (mg L^{-1}) is the equilibrium dye concentration, q_e (mg g^{-1}) is the amount of dye at equilibrium, q_m (mg g^{-1}), and K_L (L mg^{-1}) are the Langmuir constants related to adsorption capacity and adsorption energy, respectively.

Dimensionless constant separation factor or equilibrium parameter, one of the essential characteristics of this model, can be expressed by the following equation:

$$R_L = 1/\left(1 + K_L C_0\right) \tag{7}$$

where C_0 is the initial dye concentration (mg L^{-1}). R_L indicates if the adsorption process is irreversible, linear, or favorable accordingly with the R_L value, $R_L = 0$, $R_L = 1$, and $0 < R_L < 1$, respectively.

The Freundlich isotherm model assumes that multilayer adsorption occurs in a non-uniform way with different values of heat of adsorption and with variable affinity to heterogeneous surface. The linear form of Freundlich isotherm model is described as follows:

$$\ln q_e = \ln K_F + 1/n\left(\ln C_e\right) \tag{8}$$

where K_F (L mg^{-1}) indicates the adsorption capacity and $1/n$ the adsorption intensity. If $1 < n < 10$ indicates that adsorption is favorable, if $n < 1$ is irreversible and $n > 10$ is unfavorable [4, 5].

2.6 Statistical analysis

All the experiments were done in triplicate and the values averaged. The existence of significant differences among the results for adsorption efficiency of $AC_{ZnCl2\text{-}850}$ for all dyes was analyzed. In this regard, the one-way analysis of variance (ANOVA) was used, followed by Tukey or T3 Dunnet test according to the significant level. All statistical tests were performed at a 5% significance level using IBM SPSS Statistics 25 software.

3 Results and discussion

3.1 Effect of concentration on the natural pH of dye solutions

Natural pH was determined for each dye at concentrations of 5, 25, and 500 mg L^{-1} and changes were noticed with increasing concentration, but more remarkably for the red dye (Table 1).

pH is an important parameter that could influence the adsorption process and the pH effect on the adsorption will be evaluated

Table 1 Natural pH for blue, black, and red dyes at different concentrations

Natural pH			
	5 mg L^{-1}	25 mg L^{-1}	500 mg L^{-1}
Blue	6.0	5.1	6.6
Black	4.8	5.7	6.7
Red	5.1	6.7	9.0

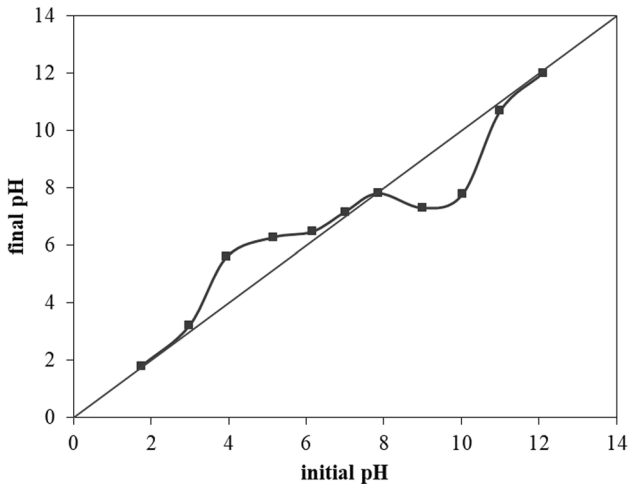

Fig. 1 Determination of pH_{PZC} for $AC_{ZnCl2\text{-}850}$

3.2 Activated carbon characterization before adsorption

The yield of $AC_{ZnCl2\text{-}850}$ was calculated after activation and washing and it was 19.3±1.3% (based on pine sawdust on dry basis).

pH_{PZC} is the pH value at which the final pH is equal to the initial pH and represents when the net surface charge of the adsorbent is zero. Particularly, the pH_{PZC} reflects the acid or basic character of the adsorbent surface since the surface charge below the pH_{PZC} is positive and above this value is negative. Thus, pH_{PZC} is an important parameter to understand the interfacial properties and interactions during adsorption studies, indicating the ability of the activated carbon for the removal of anionic, cationic, or molecular pollutants since pH_{PZC} indicates the presence of acidic or basic surface functional groups [14, 15, 36]. Figure 1 shows the pH_{PZC} of the $AC_{ZnCl2\text{-}850}$ to be 7.8.

This value falls in the basic region and the value of $pH_{PZC} > 7$ demonstrates the prevalence of basic groups over acidic groups. Acid wood dyes are negatively charged which implies that when the pH is lower than pH_{PZC}, the $AC_{ZnCl2\text{-}850}$ could have more affinity with dyes.

BET surface areas were calculated from N_2 and CO_2 adsorption isotherms presented in Fig. 2, and with total and mesopore (2–50 nm) volumes and average pore diameter calculated from N_2 adsorption-desorption isotherm of the $AC_{ZnCl2\text{-}850}$ are shown in Table 2.

Nitrogen adsorption-desorption isotherms of $AC_{ZnCl2\text{-}850}$ show a reversible type I isotherm according to the IUPAC classification, suggesting that the carbon is particularly microporous since the significant uptake of N_2 at lower

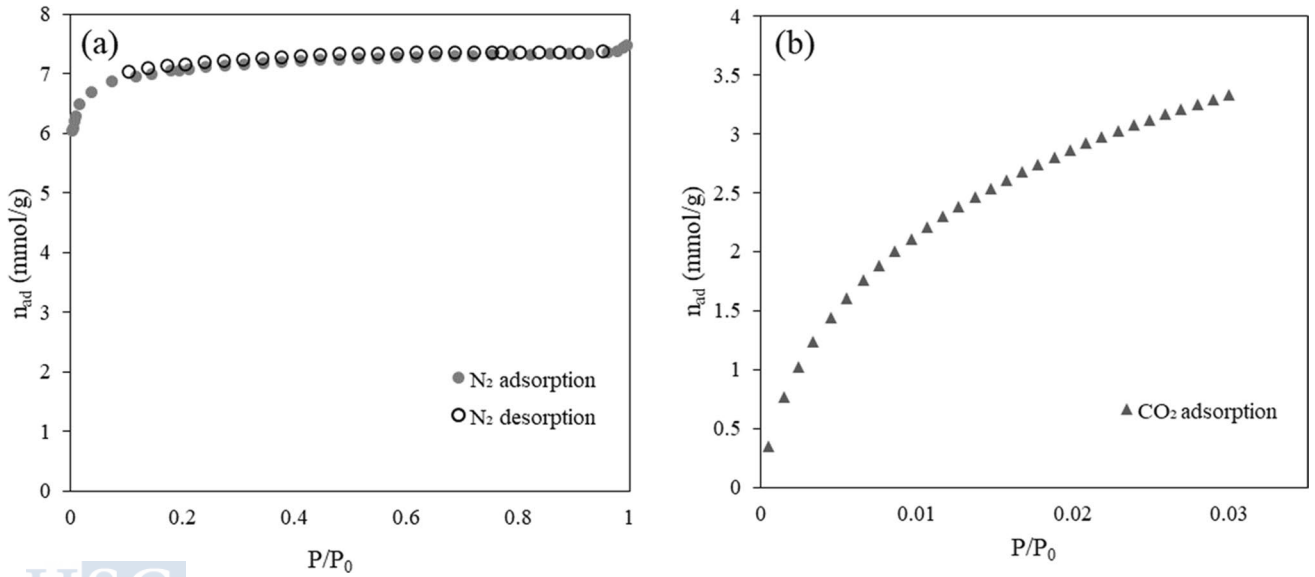

Fig. 2 Adsorption isotherms of (**a**) nitrogen and (**b**) carbon dioxide by $AC_{ZnCl2\text{-}850}$

Table 2 Surface characterization of the activated carbon prepared

Parameters	$AC_{ZnCl2\text{-}850}$
BET surface area N_2 ($m^2\ g^{-1}$)	471.4
BET surface area CO_2 ($m^2\ g^{-1}$)	319.5
Total pore volume ($cm^3\ g^{-1}$)	0.26
Mesopore volume ($cm^3\ g^{-1}$)	0.03
Micropore volume ($cm^3\ g^{-1}$)	0.23
Average pore diameter (nm)	2.26

pressures is characteristic for the adsorption in micropores [37]. The initial sharp uptake could be also related with the presence of small mesopores [16]. Type I isotherms can be further subdivided into two types, I(a) and I(b), and from the analysis of Fig. 2a, it can be concluded that, in this case, it corresponds to a type I(a) isotherm which is characteristic of materials with pore size smaller than 1 nm [37, 38]. Additionally, the low amount of nitrogen adsorbed on the surface in the range of partial pressures used for BET area determination is related to the existence of a low surface area (Table 2). Previous studies have shown similar or higher surface area values in activated carbons produced from wood-based biomass [10]. Furthermore, the surface analysis has been completed by performing CO_2 adsorption (Fig. 2b) since the N_2 adsorption-desorption isotherms analysis can be limited due to micropore presence and low diffusivity [39]. The high CO_2 adsorption capacity, in comparison with similar fabricated carbons [9, 40], can be attributed to the activated carbon microporous nature. In addition, the low value of the surface area determined by nitrogen adsorption in comparison with the corresponding CO_2 surface area indicates an important presence of ultramicroporosity (pore diameter lower than 0.7 nm), together with a significant presence of micropores (with pore diameters higher than 0.7 nm) and low amount of mesopores. This pore size distribution agrees with the average pore size of the carbon [41–43].

The high microporosity percentage (91%) combined with the high BET surface area calculated with CO_2 reveals the important role of microporosity on gas adsorption. This percentage also indicates that the chemical activation process generates a high-quality carbonaceous material in which micropores are predominant [25].

The type of starting material and carbonization and activation conditions are the most important factors that influence the features of activated carbon porosity [7]. The total surface area of $AC_{ZnCl2\text{-}850}$ is 471.4 $m^2\ g^{-1}$ of which 91% corresponds to micropores (< 2 nm) due to the effect of $ZnCl_2$ on micropore formation that inhibits the development of tar and favors the release of volatiles [35, 36]. Moreover, as seen the activated carbon prepared with $ZnCl_2$ as chemical activator has a well-developed microporosity. A preceding study on the preparation of activated carbon from *Eucalyptus camaldulensis* wood showed that the type of activation agent and its concentration influence the surface area and pore volume and the BET surface area and porosity increased in the subsequent order: KOH > H_3PO_4 > $ZnCl_2$. $ZnCl_2$ and its hydrates mainly cause the formation of small and uniform size micropores due to its minuscule particle size [10, 16]. Previous studies using agricultural wastes with the same activation agent reported similar values for surface area [5, 19] and microporosity [14, 44].

SEM micrographs of $AC_{ZnCl2\text{-}850}$ are presented in Fig. 3. The development of pores was observed in the activated carbon prepared, suggesting a high surface area and supporting the information provided by the surface area and porosity analysis. As mentioned before, the pores on the surface of the carbon were probably due to the $ZnCl_2$ evaporation during the activation process and to the catalytic effect of the $ZnCl_2$ on the pyrolytic decomposition [15]. Moreover, the SEM image at 1000× magnification (Fig. 3a) shows a prominent honeycomb structure originated from the cell wall of the raw sawdust [5, 12].

The elemental composition of $AC_{ZnCl2\text{-}850}$ is shown in Table 3. High carbon content is observed that may be due to the decomposition of cellulose and hemicelluloses (between 200 and 400°C) and lignin (between 150 and 750°C) [10, 15]. Oxygen, one of the main components of sawdust, showed the opposite behavior. The presence of zinc and chloride atoms indicates that during the activation process, $ZnCl_2$ reacted with PS revealing the activation efficiency [14, 45].

Up to now, various papers can be found in literature on $ZnCl_2$-activated carbons from biomass feedstocks, but apparently none of them prepared through a dry activation process by milling, but through impregnation with a $ZnCl_2$ dissolution [7, 11]. Therefore, it can be concluded that the dry activation technique is also efficient, faster, and with no formation of aqueous chemical residues. EDX results after adsorption will be discussed in Section 3.3.5.

To obtain a greater insight into the functional groups on the surface of the material before and after adsorption, the FTIR spectra were collected. The FTIR spectra of $AC_{ZnCl2\text{-}850}$ before and after dye adsorption are shown in Fig. 4.

The occurrence of a strong and broad peak around 3400 cm^{-1} which is ascribed to a stretching vibration of hydrogen-bonded (O-H) hydroxyl groups from carboxyl, phenols, alcohols, or surface bonded water is observed. The adsorption small bands between 2919 and 2852 cm^{-1} correspond to asymmetric and symmetric C-H stretching vibrations of alkyl side chains. The two small peaks around 2300 cm^{-1} could be attributed to the alkyne group

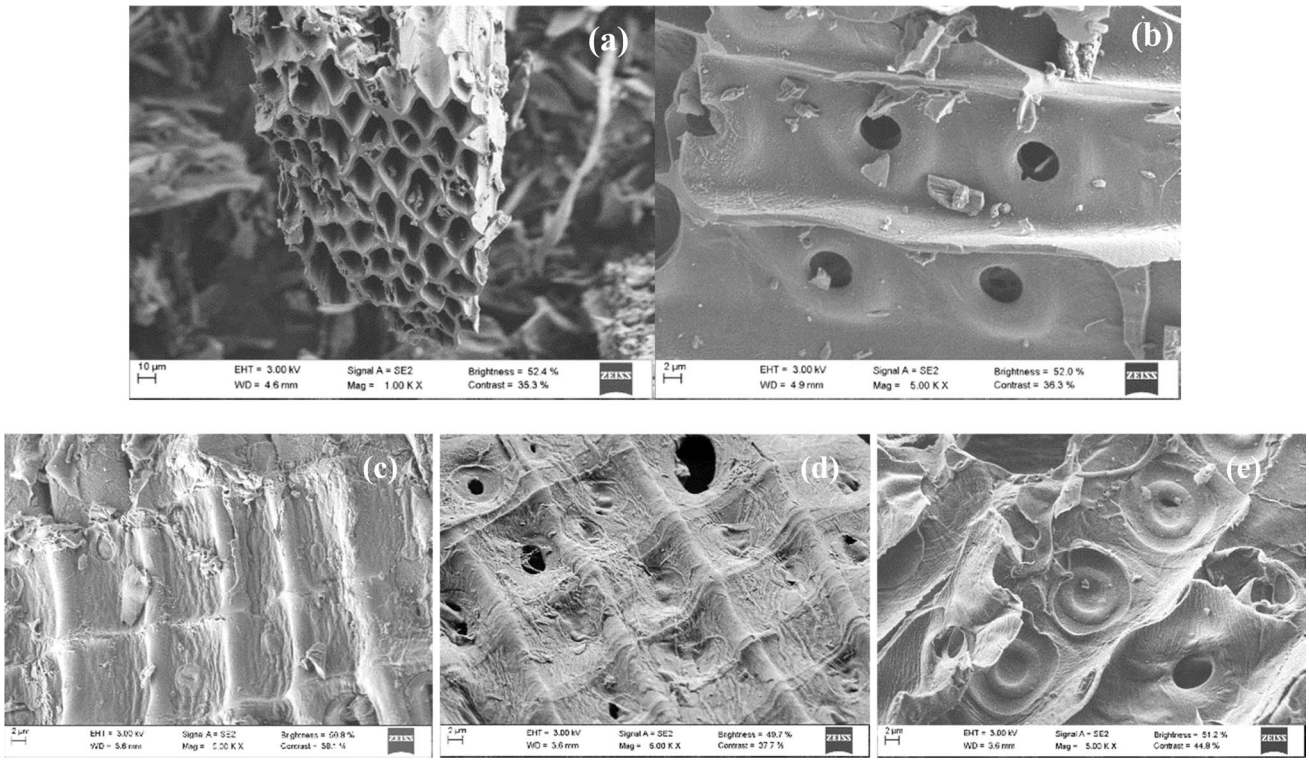

Fig. 3 SEM images of $AC_{ZnCl2-850}$ at (**a**) 1000 and (**b**) 5000× magnifications before adsorption and after adsorption with (**c**) blue, (**d**) red, and (**e**) black wood dyes (500 mg L^{-1}; pH = 2; adsorbent dose: 0.4 g L^{-1} for blue, 0.5 g L^{-1} for red, and 1 g L^{-1} for black dyes; contact time: 48 h for blue and red dyes and 12 h for black dye; temperature: 25 °C; agitation speed: 210 rpm) at 5000×

Table 3 Elemental composition of dyes and $AC_{ZnCl2-850}$ before and after adsorption (500 mg L^{-1}; pH = 2; adsorbent dose: 0.4 g L^{-1} for blue, 0.5 g L^{-1} for red, and 1 g L^{-1} for black; contact time: 48 h for blue and red dyes and 12 h for black dye; temperature: 25 °C; agitation speed: 210 rpm)

wt%	$AC_{ZnCl2-850}$	Blue dye	Black dye	Red dye	$AC_{ZnCl2-850}$ +blue dye	$AC_{ZnCl2-850}$ +black dye	$AC_{ZnCl2-850}$ +red dye
C	90.4	62.1	27.5	49.7	90.7	92.7	93.3
O	2.6	18.4	18.4	28.3	7.2	5.2	4.1
Zn	2.3	-	-	-	0.6	-	-
S	2.1	6.7	21.3	7.1	1.8	0.1	0.2
F	1.6	-	-	-	-	-	-
Cl	0.6	0.4	-	0.9	0.9	1.8	2.3
Si	0.1	-	-	-	0.1	0.03	0.03
Ca	0.1	-	-	-	0.3	0.1	0.1
N	-	7.2	-	3.4	-	-	-
Na	-	4.8	11.1	10.1	-	-	-
Br	-	0.2	-	-	-	-	-
Cu	-	0.1	1.6	0.1	0.1	0.2	0.3
P	-	-	-	0.4	-	-	-
Cr	-	-	20.0	-	-	0.1	-
Mg	-	-	0.1	-	-	-	-

(C≡C). The spectral bands at 1650 and 1540 cm^{-1} correspond to the C=C aromatic ring. Likewise, the small band at 1380 cm^{-1} is associated to C=C stretching aromatic rings polarized by oxygen atoms bound near of the carbon atoms [16, 37]. Finally, a broad band at 1047 cm^{-1} is assigned to C-O stretching alcohols.

3.3 Adsorption experiments

3.3.1 Effect of pH

Initial pH plays an essential role in the adsorption process, affecting not only the chemistry of dye molecules but also

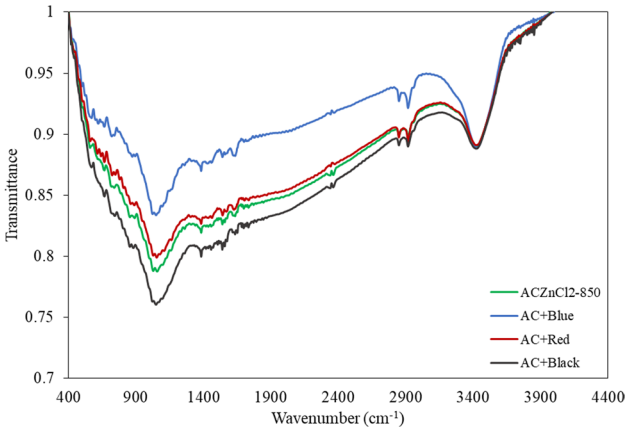

Fig. 4 FTIR spectra of $AC_{ZnCl2\text{-}850}$ before and after adsorption with blue, red, and black dyes (500 mg L^{-1}; pH = 2; adsorbent dose: 0.4 g L^{-1} for blue, 0.5 g L^{-1} for red, and 1 g L^{-1} for black dyes; contact time: 48 h for blue and red dyes and 12 h for black dye; temperature: 25°C; agitation speed: 210 rpm)

the carbon surface binding sites [4, 33]. The pH effect was evaluated (Fig. 5) at an initial dye concentration of 5 mg L^{-1}, an adsorbent dose of 0.5 g L^{-1}, and a contact time of 48 h to assure equilibrium, except for the black dye that was not stable for times greater than 12 h as determined in a previous work (accepted for publication).

Figure 5 shows that the total removal of the blue dye was achieved at all pH values essayed. For the red dye, the highest removal was obtained at pH = 2 (96.8%) and natural pH (96.0%) but decreased when pH was increased from 7 to 12. Regarding the black dye, the removal percentages were much lower than those for the red and blue ones. The greatest elimination was achieved at pH = 2 (55.6%) and progressively fell by increasing pH from 2 to 12. Possibly, the increase of dye adsorption at pH lower than pH_{PZC} is because the activated carbon surface is positively charged and becomes highly protonated; hence, acid dye anion adsorption increases through electrostatic attraction and hydrogen bonding [4, 5]. Therefore, according to these results, the influence of the adsorbent dose was analyzed at the most favorable pH, natural pH for blue and red dyes, and pH = 2 for the black one.

In a previous study (accepted for publication), the removal of wood dyes by pine (*Pinus radiata*) sawdust was evaluated as function of pH. It was found that at an initial dye concentration of 5 mg L^{-1} and the optimum conditions (pH = 2 and an adsorbent dose of 6 g L^{-1}), adsorption capacities of 0.70, 0.75, and 0.72 mg g^{-1} and removal percentages of 100, 92.4, and 99% were obtained for the blue, red, and black dyes, respectively. It is important to point out that the values of adsorption performance depend on the conditions used and it is not possible to compare them directly. In addition, the removal of the three dyes by pine sawdust biochar at the same conditions than for $AC_{ZnCl2\text{-}850}$ (5 mg L^{-1}, pH = 2, adsorbent dose of 0.5 g L^{-1}) was analyzed and maximum adsorption capacities of 2.13, 2.55, and 1.94 mg g^{-1} and removal percentages of 19.7, 25.1, and 23.2% for blue, red, and black dyes, respectively, were achieved. These results confirm the efficacy of the activation process, since the adsorption capacities for PS and biochar were lower than for $AC_{ZnCl2\text{-}850}$ (10.15, 9.36, and 5.52 mg g^{-1} for blue, red, and black, respectively).

3.3.2 Effect of adsorbent dose

The effect of adsorbent dose on dye adsorption was studied and the results are presented in Fig. 6. For the blue and red dyes that showed high removal efficiencies at natural pH

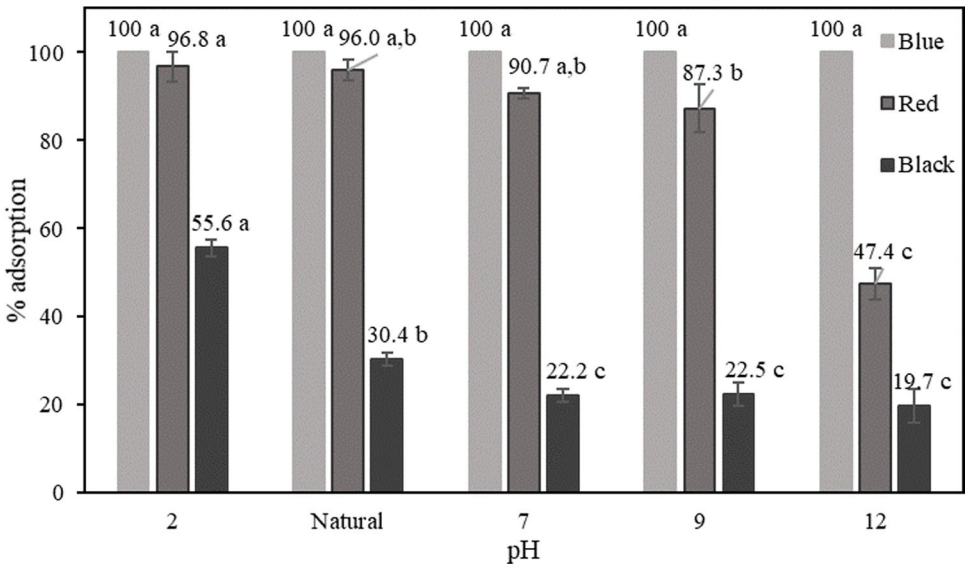

Fig. 5 Effect of pH on adsorption of blue, red, and black wood dyes onto $AC_{ZnCl2\text{-}850}$ (natural pH: 6.0, 5.1, and 4.8 for blue, red, and black dyes, respectively; dye initial concentration: 5 mg L^{-1}; adsorbent dose: 0.5 g L^{-1}; contact time: 48 h for blue and red dyes and 6 h for black dye; temperature: 25°C; agitation speed: 210 rpm). For each dye, different letters indicate significant differences ($p \leq 0.05$) between samples

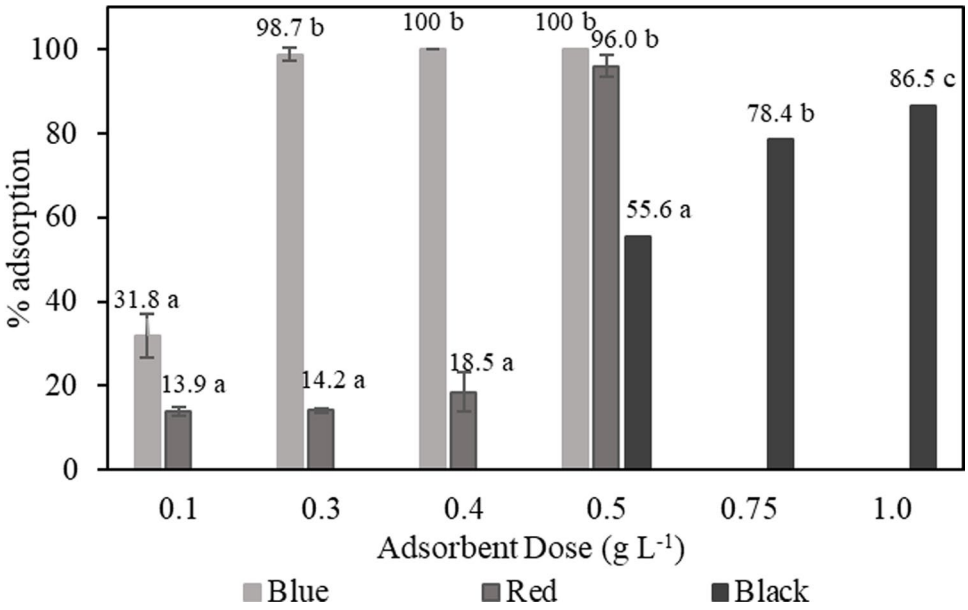

Fig. 6 Effect of adsorbent dose on adsorption of blue, red, and black wood dyes onto $AC_{ZnCl2\text{-}850}$ (pH: 6.0 and 5.1 for blue and red dyes respectively and pH = 2 for black dye; dye initial concentration: 5 mg L^{-1}; contact time: 48 h for blue and red dyes and 6 h for black dye; temperature: 25°C; agitation speed: 210 rpm). For each dye, different letters indicate significant differences ($p \leq 0.05$) between samples

and 5 mg L^{-1}, the adsorbent dose was reduced to 0.1 g L^{-1}. For the black dye, given the poor results at 0.5 g L^{-1}, the adsorbent dose was increased up to 1.0 g L^{-1}.

For the blue colorant, a 100% removal percentage was maintained by reducing the dose from 0.5 to 0.4 g L^{-1}, but there was a significant decrease to 31.8% when the adsorbent dose was lowered to 0.1 g L^{-1}. Regarding the red colorant, it was not possible to reduce the adsorbent dose ensuring the total removal of dye since the percentage decreased to 18.5% and 14.0% at 0.4 g L^{-1} and 0.1 g L^{-1}, respectively. Finally, for the black dye, an increase in the adsorbent dose from 0.5 to 0.75 and 1.0 g L^{-1} increased the dye removal percentage from 55.6 to 78.4% and 86.5%, respectively. In general, this behavior can be explained by the increase of the adsorption sites available with increasing the adsorbent dose, and by a high ratio of dye molecules to empty sites [4, 33]. Regarding the equilibrium adsorption capacity (q_{max}), it decreased from 17.2 to 10.2 mg g^{-1} for the blue and from 9.3 to 6.8 mg g^{-1} for the red with increasing the adsorbent dose from 0.1 to 0.5 g L^{-1}. For the black dye, q_{max} decreased from 5.5 to 4.2 mg g^{-1} with increasing the adsorbent dose from 0.5 to 1 g L^{-1}.

3.3.3 Effect of initial dye concentration

The influence of the initial dye concentration (25 and 500 mg L^{-1}) on dye removal at different pH was studied at the adsorbent doses selected from the previous experiments (0.5 g L^{-1} for the blue and the red dyes and 1 g L^{-1} for the black one) and the obtained results are presented in Fig. 7. Adsorption percentage decreased with increasing initial dye concentration due to the saturation of the adsorbent surface while adsorption capacity increased due to the higher concentration gradient which acts as a driving force to overcome resistances to dye mass transfer between the aqueous phase and the solid phase [46].

With respect to the blue wood dye, the highest adsorption percentages were obtained at pH = 2 at both initial dye concentrations and the maximum adsorption capacity was 6.27 and 97.56 mg g^{-1} for 25 and 500 mg L^{-1}, respectively. Regarding the red dye, the natural pH increased significantly with increasing the initial dye concentration (Table 1). Therefore, the higher removal percentage occurred at different pH depending on initial dye concentration and decreased with increasing dye concentration. It was 30% at pH = 9 for 25 mg L^{-1} with an adsorption capacity of 16.46 mg g^{-1} and 9.1% at pH = 2 for 500 mg L^{-1} with an adsorption capacity of 86.61 mg g^{-1}. As mentioned above, usually when the pH is less than pH_{PZC}, there will be more H^+ ions and will balance the charge of anionic groups in the adsorbent surface favoring anionic adsorption due to an electrostatic interaction and hydrogen bonding. At 25 mg L^{-1}, this behavior was not verified which suggests that the adsorption process is probably ascribed to other mechanisms [20]. In previous work above mentioned, it was found that the pKa for these dyes is around 10 which means that pH = 9 is above the pH_{PZC} and below the pKa, then, the molecules are protonated and Lewis acid-base, π-π bond, or hydrophobic effects could also occur [47]. For the black dye, at 25 mg L^{-1}, the maximum removal (82.4%) was obtained at pH = 2 with an adsorption capacity of 19.71 mg g^{-1}, following the same trend with the pH increase as for the low concentration. Then, the initial concentration was increased to 500 mg L^{-1} at pH = 2 and the removal percentage decreased to 13.9% with an adsorption capacity of 62.73 mg g^{-1}. Similar results in which the removal percentage decreased with

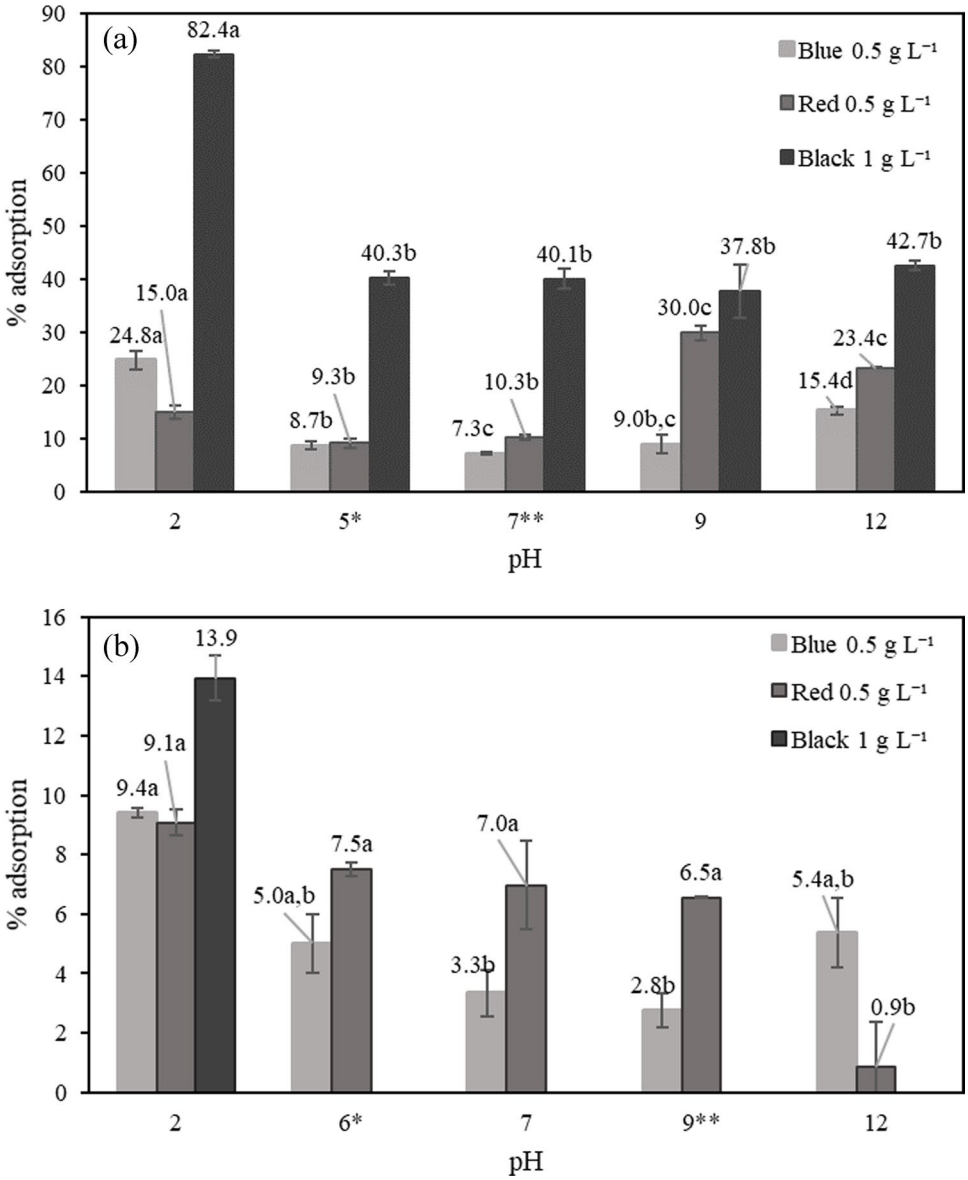

Fig. 7 Effect of initial dye concentration at different pH values on adsorption of blue, red, and black wood dyes onto $AC_{ZnCl2\text{-}850}$ at (**a**) 25 mg L^{-1} and (**b**) 500 mg L^{-1} (natural pH at 25 mg L^{-1}: *5.1, **6.7, and *5.7; natural pH at 500 mg L^{-1}: *6.6 and **9.0 for blue and red dyes, respectively; contact time: 48 h for blue and red dyes and 12 h for black dye; temperature: 25°C; agitation speed: 210 rpm). For each dye, different letters indicate significant differences ($p \leq 0.05$) between samples

increasing the initial dye concentration have been reported in literature for dyes removal by activated carbons [4, 44].

In view of the good results obtained for the blue and red dyes with 5 mg L^{-1} and pH = 2 at an adsorbent dose at 0.5 g L^{-1} (Fig. 5), the initial concentration was increased maintaining the dose and a considerable decrease in the adsorption efficiency was obtained as seen in Fig. 7. Then, the effect of the adsorbent dose (0.5, 1, 2, and 4 g L^{-1}) was analyzed for an intermediate concentration of 25 mg L^{-1}. For both dyes, the removal percentage increased to around 55% using 1 g L^{-1}, and to 91 and 95% for blue and red dyes, respectively, with 2 g L^{-1}, and the complete removal was achieved for 4 g L^{-1}, as observed in Fig. 8.

For the black dye, in an attempt to achieve the total dye removal for an intermediate concentration of 25 mg L^{-1} and pH = 2, the adsorbent dose was increased to 2 g L^{-1}. This increase in the adsorbent dose was effective since it increased the dye removal percentage from 82.4 to 98.1% with complete color removal (Fig. 8). As mentioned before, the increase on the adsorption percentage can be related with the surface area and the availability of more adsorption sites.

Additionally, in order to check the existence of size exclusion affecting dye adsorption, the highest distance between two extreme atoms of each dye molecule was measured through ChemDraw 21.0.0 software. These values, shown in Fig. 9, were 1.37, 1.28, and 1.53 nm for blue, red, and black dyes, respectively, which are lower than carbon average pore diameter, 2.26 nm (Table 2), although the important presence of microporosity (91%) should be considered. In addition, the value of surface area determined with CO_2 at 0°C (319.5 m^2 g^{-1}) indicates

Fig. 8 Effect on color intensity with the maximum dose of adsorbent on dye removal (pH = 2; initial dye concentration: 25 mg L^{-1}; adsorbent dose: 4 g L^{-1} for blue and red dyes and 2 g L^{-1} for black; contact time: 48 h for blue and red dyes and 12 h for black dye; temperature: 25°C; agitation speed: 210 rpm)

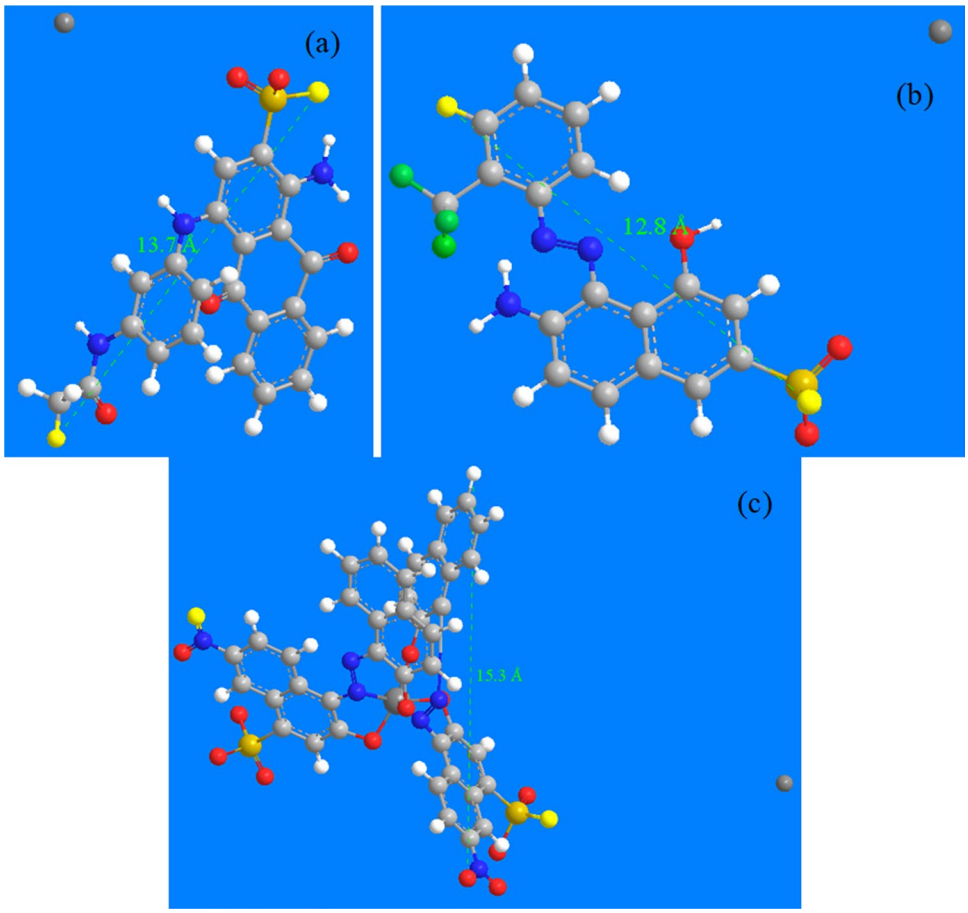

Fig. 9 Chemical structures with distance between two extreme atom measurements of (**a**) blue dye, (**b**) red dye, and (**c**) black dye (H = white, C = grey, N = blue, S = yellow, O = red, F = green, Na = dark grey)

the high presence of pores in the ultramicroporosity range (lower than 0.7 nm) which hinders the access of the dye molecules. Therefore, considering the results found in this work, where for given conditions the adsorption performance depended on the dye essayed, it cannot be concluded that only limitation by sizes exists but distinct interactions between the carbon and the different dye molecules.

3.3.4 Adsorption kinetics

The pseudo-first-order, pseudo-second-order, and intraparticle diffusion models were employed at the conditions selected to elucidate the mechanisms of the adsorption process. The fitting results of the experimental data of adsorption of blue, black, and red dyes onto $AC_{ZnCl2\text{-}850}$ adsorbent using pseudo-first-order, pseudo-second-order, and intraparticle diffusion models are shown in Fig. 10. The obtained results for kinetic parameters and correlation coefficient (R^2) are shown in Table 4.

The R^2 values for the pseudo-second-order kinetics model were higher than 0.999 and the calculated adsorption capacities ($q_{e,calc}$) were close to the experimental ones ($q_{e,exp}$) which revealed that kinetic data were best fitted to this model, an indication of a chemisorption mechanism.

Regarding the intraparticle diffusion model, in which the adsorption of soluble species from a solution involves their transfer to the surface of an adsorbent, as evident from Fig. 10c, the linear plots presented multilinearity, indicating that the adsorption occurs in two steps and that the intraparticle diffusion was not the only process that controlled the adsorption [33]. Usually, the first corresponds to the molecular diffusion of adsorbate through the bulk solution to the external surface of the adsorbent originating a film layer. The second one implies the migration by intraparticle diffusion into the adsorbent pores until the final equilibrium stage [4, 6, 26, 44]. Based on the R^2 values (> 0.9) presented in Table 4, for the first stage dye adsorption, the experimental data are well fitted to the intraparticle diffusion model. Moreover, C value is proportional to the extent of the boundary layer thickness and in this case, as it is higher than 0 means that intraparticle diffusion is not the only rate-controlling step and implies a certain controlling degree of film diffusion and rapid adsorption [46].

The adsorption capacity of distinct adsorbents varies according to the primary source of the adsorbent, the process conditions of adsorption, adsorption modification, and the type of contaminant [48]. Nowadays is very important to find adsorbents with good adsorption capacity and low cost. Extensive research has been done and the adsorption capacity of activated carbons derived from wood for

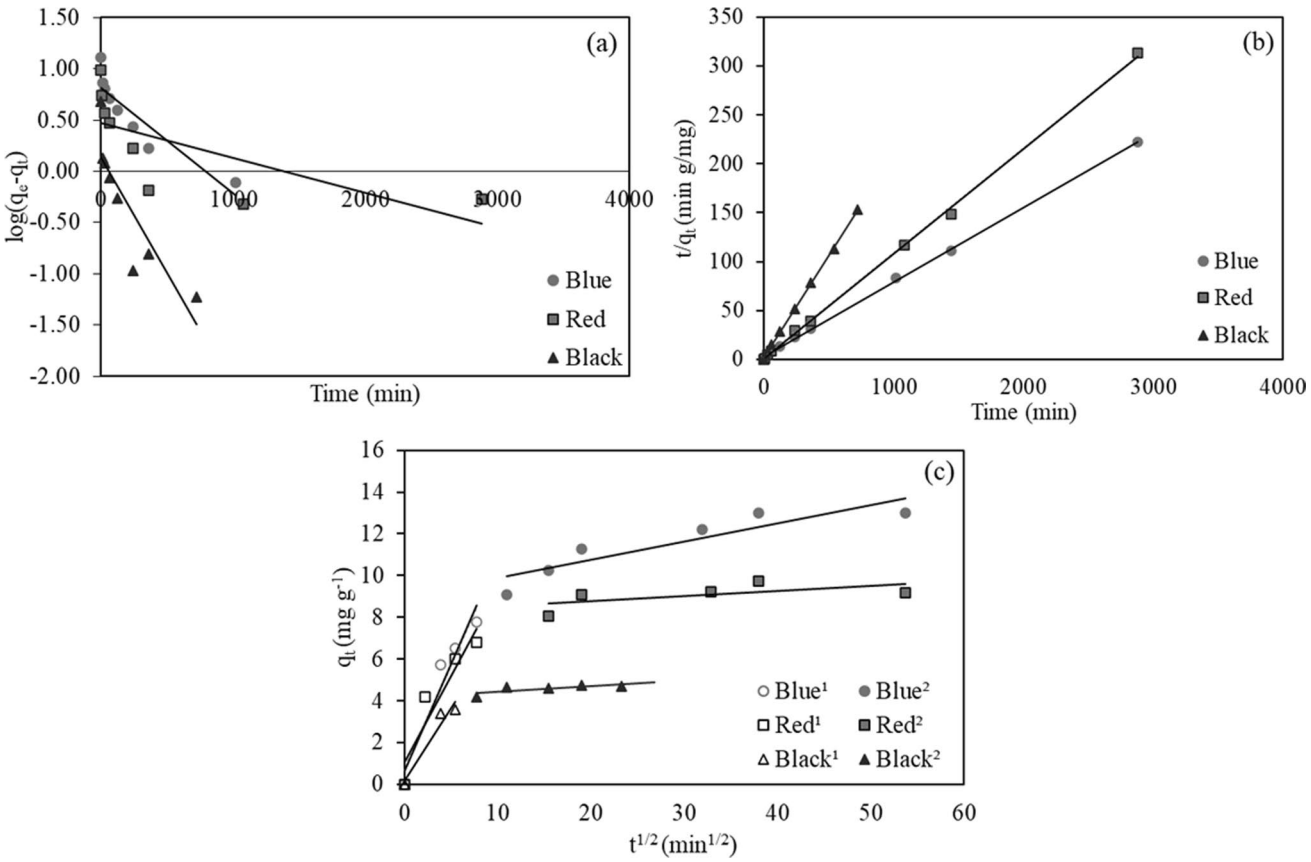

Fig. 10 (**a**) Pseudo-first-order, (**b**) pseudo-second-order, and (**c**) intraparticle diffusion (1: first stage and 2: second stage) kinetic plots (natural pH: 6.0 and 5.1 for blue and red dyes, respectively; pH = 2 for black dye; dye concentration: 5 mg L^{-1}; adsorbent dose: 0.4 g L^{-1} for blue, 0.5 g L^{-1} for red, and 1 g L^{-1} for black dyes; contact time: 48 h for blue and red dyes and 12 h for black dye; temperature: 25°C; agitation speed: 210 rpm)

Table 4 Pseudo-first-order, pseudo-second-order, and intraparticle diffusion kinetic model parameters

Model	Parameter	Adsorption conditions		
		Blue 0.4 g L^{-1} natural pH	Red 0.5 g L^{-1} natural pH	Black 1.0 g L^{-1} pH = 2
Pseudo-first-order	$q_{e,exp}$ (mg g^{-1})	12.98	9.73	4.76
	$q_{e,calc}$ (mg g^{-1})	6.57	4.14	1.36
	k_1 (min^{-1})	$2.30 \cdot 10^{-3}$	$2.30 \cdot 10^{-3}$	$5.30 \cdot 10^{-3}$
	R^2	0.825	0.704	0.754
Pseudo-second-order	$q_{e,calc}$ (mg g^{-1})	13.12	9.33	4.77
	k_2 (g mg^{-1} min^{-1})	$1.92 \cdot 10^{-3}$	$1.17 \cdot 10^{-2}$	$2.44 \cdot 10^{-2}$
	R^2	0.999	0.999	1.000
Intraparticle diffusion	$k_{id,1}$ (mg g^{-1} $min^{-1/2}$)	1.02	0.83	0.69
	C_1 (mg g^{-1})	0.65	1.05	0.17
	R^2	0.934	0.876	0.937
	$k_{id,2}$ (mg g^{-1} $min^{-1/2}$)	$8.78 \cdot 10^{-2}$	$2.43 \cdot 10^{-2}$	$2.70 \cdot 10^{-2}$
	C_2 (mg g^{-1})	8.99	8.29	4.18
	R^2	0.812	0.381	0.584

Table 5 Comparison of the adsorption capacities of activated carbons prepared from various wood-based biomass for dye removal

Precursor	Adsorbate	Adsorption capacity (mg g^{-1})	Reference
Pine sawdust	Blue for wood	12.98	Present work
Pine sawdust	Red for wood	9.73	Present work
Pine sawdust	Black for wood	4.76	Present work
Ailanthus altissima wood	Acid blue 1	0.453	[49]
Outer rind of wood apple	Crystal violet	19.8	[50]
Outer rind of wood apple	Methylene blue	40.1	[50]
Poplar wood	Acid red 18	3.91	[51]
Wood apple outer shell	Methylene blue	35.1	[52]
Acacia mangium wood	Methyl orange	7.54	[53]
Oak wood	Malachite green	4.34	[54]
Peanut sticks wood	Methylene blue	2.57	[55]
Poplar wood	Acid red 18	3.91	[26]
Citrus limon wood	Crystal violet	23.6	[48]

dye adsorption is compared in Table 5 with those of the present work. Otherwise, Table 6 compares the kinetic modeling of dye adsorption onto $ZnCl_2$-activated carbons from biomass.

3.3.5 Activated carbon characterization after adsorption

SEM-EDX technique was employed after adsorption to compare the surface physical morphology and elemental analysis of the materials with the original one. Figure 3 also shows the SEM photographs of the $AC_{ZnCl2\text{-}850}$ after adsorption with blue, red, and black dyes, respectively, at pH = 2 and the highest dye initial concentration essayed.

The SEM images showed that the surface of the carbon was changed due to the binding of dye molecules. It is observed that the pores were occupied by dyes that formed a slight cover over the entire surface, which was confirmed by comparing EDX analysis before and after adsorption. The EDX results shown in Table 3 reflect that after adsorption, in all cases, the amounts of C and O increased with respect to the original activated carbon. In addition, Cu and Cr atoms present in dye composition appear in $AC_{ZnCl2\text{-}850}$, evidencing the adsorption of dye molecules to the activated carbon surface.

The FTIR spectrum of the activated carbon before and after dye adsorption is pretty similar but modifications in the intensity of several peaks appeared (for instance between 2919 and 2852 and at around 2300, 1650, 1540, and 1047 cm^{-1}), demonstrating that the activated carbon functional groups such as carboxyl, phenols, alcohols, or alkynes participated in the adsorption mechanism. Previous studies demonstrated that functional groups containing oxygen of carboxylic and carbonyl species enhance the adsorption of methylene blue dye molecules due to electrostatic interaction [8].

3.3.6 Adsorption equilibrium

To analyze the adsorption equilibrium, the Langmuir and Freundlich models were applied (Fig. 11) and the calculated parameters are listed in Table 7.

Table 6 Various kinetic and isotherm studies for dye adsorption onto $ZnCl_2$-activated carbon from biomass

Raw material	Dye	Kinetic model	Isotherm model	Reference
Pine sawdust	Blue for wood; Black for wood	Pseudo-second-order and intraparticle diffusion	Freundlich	Present work
Pine sawdust	Red for wood	Pseudo-second-order and intraparticle diffusion	Langmuir	Present work
Paulownia tomentosa wood	Acid red 4; methylene blue	Pseudo-second-order	Langmuir	[24]
Mixture of orange peel and watermelon rind	Crystal violet; methylene blue	Pseudo-second-order	Freundlich	[16]
Mixture of carrot juice pulp and pomegranate peel	Crystal violet	Pseudo-second-order	Freundlich	[17]
Coconut shell	Malachite green	Intraparticle diffusion	Freundlich	[5]
Tomato processing	Methylene blue; metanil yellow	-	Langmuir	[35]
Pine sawdust	Malachite green	Pseudo-second-order and intraparticle diffusion	Langmuir	[44]
Enteromorpha prolifera	Reactive red 23; reactive blue 171; reactive blue 4	Pseudo-second-order	Freundlich	[57]
Cashew nut shells	Methylene blue	-	Langmuir	[37]
Shaddock peel	Methylene blue	Pseudo-second-order	Langmuir	[59]
Glycerine pitch distillate	Methylene blue	Pseudo-second-order	Langmuir and Redlich-Peterson	[46]

For the blue and black dyes, the Freundlich isotherm offered the better adjustment with values of the coefficient of determination (R^2) of 0.981 and 0.839, respectively (Table 7). The Freundlich model suggests the heterogeneity of the carbon surface with multilayer adsorption of dyes. Moreover, the values of n between 1 and 10 suggest a favorable adsorption. The removal of malachite green using $ZnCl_2$-activated carbon from coconut shell was also well described by the Freundlich model [5]. Regarding the Langmuir model, R_L values lower than 1 also indicated that dye adsorption was favorable.

Regarding the red dye, the equilibrium adsorption capacity was 12.89 mg g^{-1} at 100 mg L^{-1} and decreased with increasing dye initial concentration. Thus, the experimental equilibrium data in the range essayed were not suitable for isotherm modeling. This behavior can be related to observed pH changes with dye concentration, as pH affects the carbon's surface and, therefore, the adsorption capacity [56]. Even though, for dye concentrations below 100 mg L^{-1}, the isotherm models were tested (Fig. 11) and the calculated parameters are presented in Table 7. From these results, it can be clearly concluded that Langmuir model offers the best adjustment to the experimental data. Thus, red dye adsorption equilibrium differs from the other dyes, and, probably, monolayer adsorption occurs which can explain the maximum capacity reached at 100 mg L^{-1} due to nearly complete coverage of the active sites [57]. Besides, the value of the dimensionless separation factor (R_L) between 0 and 1 indicates that the red dye adsorption onto this carbon is favorable. The Langmuir isotherm also explained the adsorption equilibrium of Congo red dye onto *Bombax Buonopozense* bark-activated carbon [58]. Table 6 compares equilibrium modeling of dye adsorption onto $ZnCl_2$-activated carbon from biomass.

3.3.7 Adsorption mechanism of wood dyes onto activated carbon

The adsorption mechanism not only depends on the contaminant's properties but also on the surface chemistry of the adsorbent [3]. The key interactions found in literature for dye removal include electrostatic interaction, pore-filling, π-π interaction, and hydrogen bonding [16]. Some of these interactions may be involved in the adsorption process of blue, red, and black wood dyes by $AC_{ZnCl2\text{-}850}$ as shown in Fig. 12.

The positively charged surface of $AC_{ZnCl2\text{-}850}$ when pH is below the pH_{PZC} may promote the electrostatic interaction between activated carbon and dye anions. In addition, the interaction of nitrogen atoms of the adsorbate with free hydrogen atoms of the adsorbent creates H-bonding interactions which contribute to dye adsorption. In the case of the red dye, the different behaviors at 25 mg L^{-1} as previously mentioned in section 3.3.3 suggest that Lewis acid-base, π-π bond, or hydrophobic effects could also occur. Moreover, the kinetic analysis showed an adsorption process by chemisorption and intraparticle diffusion into the adsorbent pores. This is corroborated by BET and SEM analysis which confirmed the porous structure of the activated carbon that according to the size of the dye molecules may potentially be occupied by them.

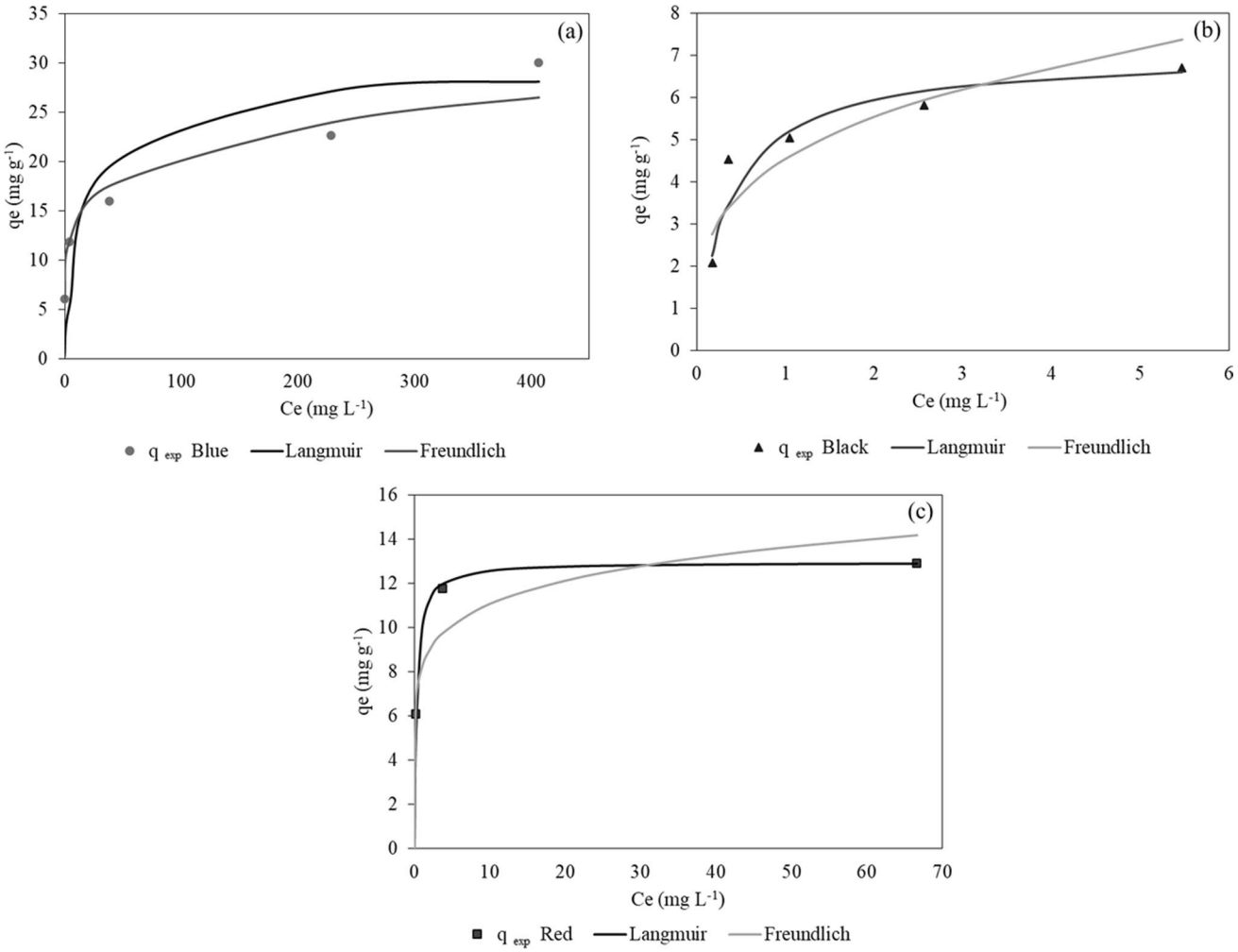

Fig. 11 Experimental and calculated adsorption isotherms of (**a**) blue, (**b**) black, and (**c**) red dyes onto $AC_{ZnCl2\text{-}850}$ (25–500 mg L^{-1} for blue and black dyes, 25–100 mg L^{-1} for red dye; pH = 2; adsorbent dose: 4 g L^{-1} for blue and red and 2 g L^{-1} for black; contact time: 48 h for blue and red and 12 h for black dye; temperature: 25°C; agitation speed: 210 rpm)

Table 7 Parameters of the isotherm models for the adsorption of the blue, black, and red dyes on $AC_{ZnCl2\text{-}850}$

Isotherms	Parameters	Blue dye	Black dye	Red dye
Langmuir	q_m (mg g^{-1})	29.4	68.5	13.0
	K_L (L mg^{-1})	0.051	0.0134	3.271
	R_L	0.441–0.038	0.749–0.130	0.012–0.0006
	R^2	0.970	0.799	1.000
Freundlich	n	5.71	3.83	7.68
	K_F (mg g^{-1} (L $mg^{-1})^{-1/n}$)	9.25	9.85	8.20
	R^2	0.981	0.839	0.839

4 Conclusions

This study has demonstrated that a newly activated carbon with a reasonably good surface area can be prepared by carbonization and chemical activation of pine (*Pinus radiata*) sawdust with $ZnCl_2$ as activating agent.

Adsorption of blue, red, and black wood dyes onto activated carbon has been carried out and the adsorption efficiency was remarkably influenced by the variables studied such as adsorbent dose, pH, and initial dye concentration. The results showed that activated carbon had a great adsorption capacity at low dye initial concentration; however, limitations appeared as the concentration increased. Hence, according to the results obtained, $AC_{ZnCl2\text{-}850}$ showed the greatest efficiency of 100% and 96.0% for the blue and red dyes, respectively, at an initial dye concentration of 5 mg L^{-1}, an adsorbent dose of 0.5 g L^{-1} and natural pH, and only of 55.6% for the black dye at pH = 2 in this case. The complete dye removal was attained at 25 mg L^{-1} and pH = 2 by increasing the adsorbent dose to 4 g L^{-1} for blue and red dyes and 2 g L^{-1} for the black one.

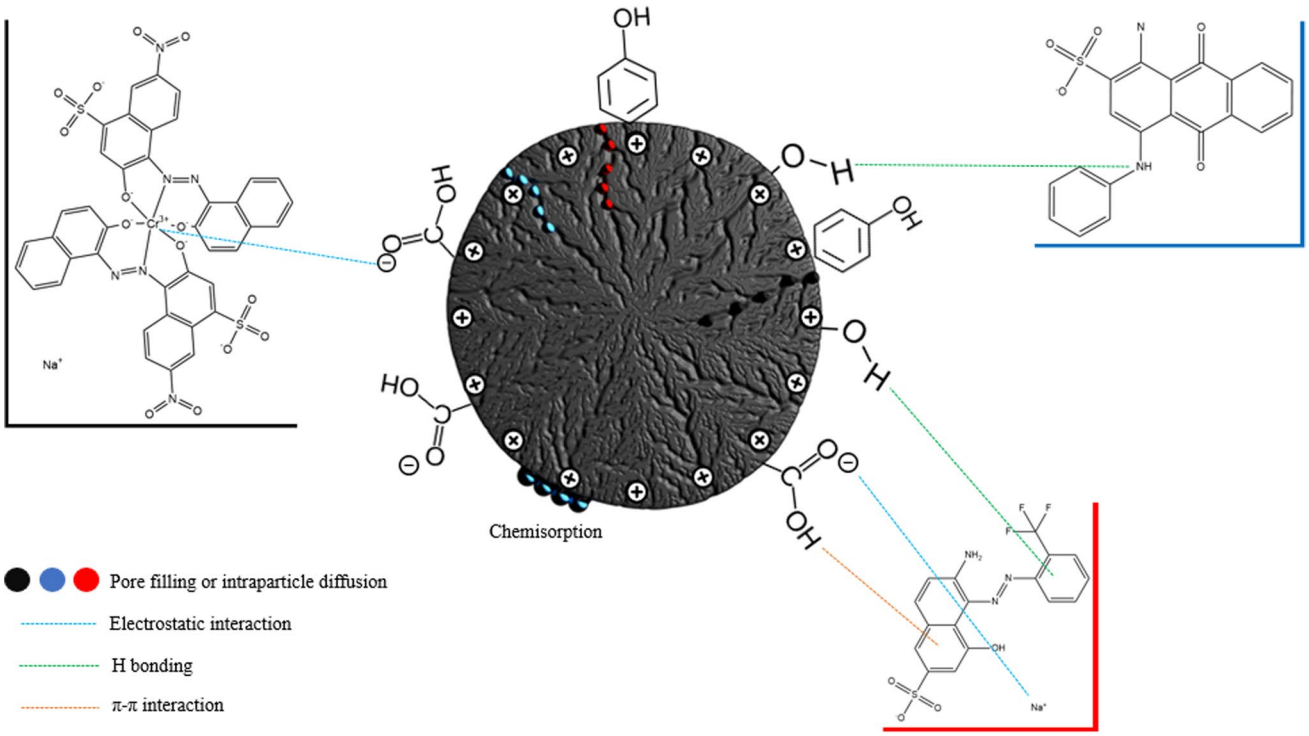

Fig. 12 Proposed adsorption mechanism of blue, red, and black wood dyes on $AC_{ZnCl2\text{-}850}$

The pseudo-second-order kinetic model was the most appropriate model to describe the removal of wood dyes by the activated carbon prepared and it was demonstrated that intraparticle diffusion was also involved in the adsorption mechanism. Equilibrium data was explained by the Freundlich model for the blue and black dyes and by the Langmuir model for the red dye. Furthermore, dye adsorption by the activated carbon is controlled by several mechanisms including electrostatic forces, H-bonding, pore filling, and π-π interactions.

The present work revealed that the activated carbon prepared from pine sawdust ($AC_{ZnCl2\text{-}850}$), an abundant and low-cost organic waste, is a promising adsorbent for the removal of dyes from aqueous solutions. The use of biomass based activated carbons instead of the high-cost commercial ones can contribute to the valorization of low-cost renewable wastes and to environmental sustainability goals, offering a green approach for the removal of wood dyes. Further studies must be performed to explore the effect of coexisting contaminants on dye removal.

Supplementary Information The online version contains supplementary material available at https://doi.org/10.1007/s13399-023-04138-4.

Authors' contribution Catarina H. Pimentel: investigation, validation, visualization, writing — original draft. M. Sonia Freire: conceptualization, methodology, supervision, funding acquisition, writing — review and editing. Diego Gómez-Díaz: conceptualization, methodology, supervision, funding acquisition, writing — review and editing. Julia González-Álvarez: conceptualization, methodology, supervision, funding acquisition, writing — review and editing.

Funding Open Access funding provided thanks to the CRUE-CSIC agreement with Springer Nature. This work was supported by Consellería de Educación, Universidade e Formación Profesional, Xunta de Galicia, grant number ED431B 2020/039.

Data availability All data generated or analyzed during this study are included in this article.

Declarations

Ethical approval Not applicable.

Consent for publication All authors agreed to submit this research work for publication.

Competing interests The authors declare no competing interests.

References

1. Jawad AH, Waheeb AS, Rashid RA, Nawawi WI, Yousif E (2018) Equilibrium isotherms, kinetics, and thermodynamics studies of methylene blue adsorption on pomegranate (*Punica granatum*) peels as a natural low-cost biosorbent. Desalination and Water Treatment 105:322–331. https://doi.org/10.5004/dwt.2018.22021
2. Jawad AH, Kadhum AM, Ngoh YS (2018) Applicability of dragon fruit (*Hylocereus polyrhizus*) peels as low-cost biosorbent for adsorption of methylene blue from aqueous solution: kinetics, equilibrium and thermodynamics studies. Desalination and Water Treatment 109:231–240. https://doi.org/10.5004/dwt.2018.21976
3. Bo L, Gao F, Bian Y, Liu Z, Dai Y (2021) A novel adsorbent *Auricularia Auricular* for the removal of methylene blue from aqueous solution: Isotherm and kinetics studies. Environ Technol Innov 23:101576. https://doi.org/10.1016/j.eti.2021.101576
4. Agarwal S, Tyagi I, Gupta VK, Ghasemi N, Shahivand M, Ghasemi M (2016) Kinetics, equilibrium studies and thermodynamics of methylene blue adsorption on Ephedra strobilacea saw dust and modified using phosphoric acid and zinc chloride. J Mol Liq 218:208–218. https://doi.org/10.1016/j.molliq.2016.02.073
5. Piriya RS, Jayabalakrishnan RM, Maheswari M, Boomiraj K, Oumabady S (2021) Coconut shell derived ZnCl2 activated carbon for malachite green dye removal. Water Sci Technol 83(5):1167–1182. https://doi.org/10.2166/wst.2021.050
6. Chikri R, Elhadiri N, Benchanaa M, El Maguana Y (2020) Efficiency of sawdust as low-cost adsorbent for dyes removal. J Chem 2020:1–17. https://doi.org/10.1155/2020/8813420
7. Yahya MA, Al-Qodah Z, Ngah CWZ (2015) Agricultural bio-waste materials as potential sustainable precursors used for activated carbon production: a review. Renew Sustain Energy Rev 46:218–235. https://doi.org/10.1016/j.rser.2015.02.051
8. Jawad AH, Hum N, Farhan AM, Mastuli MS (2020) Biosorption of methylene blue dye by rice (*Oryza sativa L.*) straw: adsorption and mechanism study. Desalination and Water Treatment 190:322–330. https://doi.org/10.5004/dwt.2020.25644
9. Ahmed MB, Hasan Johir MA, Zhou JL, Ngo HH, Nghiem LD, Richardson C, Moni MA, Bryant MR (2019) Activated carbon preparation from biomass feedstock: clean production and carbon dioxide adsorption. J Clean Prod 225:405–413. https://doi.org/10.1016/j.jclepro.2019.03.342
10. Danish M, Ahmad T (2018) A review on utilization of wood biomass as a sustainable precursor for activated carbon production and application. Renew Sustain Energy Rev 87:1–21. https://doi.org/10.1016/j.rser.2018.02.003
11. Heidarinejad Z, Dehghani MH, Heidari M, Javedan G, Ali I, Sillanpää M (2020) Methods for preparation and activation of activated carbon: a review. Environ Chem Lett 18(2):393–415. https://doi.org/10.1007/s10311-019-00955-0
12. Eleri OE, Azuatalam KU, Minde MW, Trindade AM, Muthuswamy N, Lou F, Yu Z (2020) Towards high-energy-density supercapacitors via less-defects activated carbon from sawdust. Electrochim Acta 362:137152. https://doi.org/10.1016/j.electacta.2020.137152
13. González-García P (2018) Activated carbon from lignocellulosics precursors: a review of the synthesis methods, characterization techniques and applications. Renew Sustain Energy Rev 82:1393–1414. https://doi.org/10.1016/j.rser.2017.04.117
14. Ozdemir I, Şahin M, Orhan R, Erdem M (2014) Preparation and characterization of activated carbon from grape stalk by zinc chloride activation. Fuel Process Technol 125:200–206. https://doi.org/10.1016/j.fuproc.2014.04.002
15. Akçakal Ö, Şahin M, Erdem M (2019) Synthesis and characterization of high-quality activated carbons from hard-shelled agricultural wastes mixture by zinc chloride activation. Chem Eng Commun 206(7):888–897. https://doi.org/10.1080/00986445.2018.1534231
16. Hanafi NAM, Abdulhameed AS, Jawad AH, ALOthman ZA, Yousef TA, Al Duaij OK, Alsaiari NS (2022) Optimized removal process and tailored adsorption mechanism of crystal violet and methylene blue dyes by activated carbon derived from mixed orange peel and watermelon rind using microwave-induced $ZnCl_2$ activation. Biomass Convers Biorefin:1–13. https://doi.org/10.1007/s13399-022-03646-z
17. Suhaimi A, Abdulhameed AS, Jawad AH, Yousef TA, Al Duaij OK, ALOthman ZA, Wilson LD (2022) Production of large surface area activated carbon from a mixture of carrot juice pulp and pomegranate peel using microwave radiation-assisted $ZnCl_2$ activation: an optimized removal process and tailored adsorption mechanism of crystal violet dye. Diam Relat Mater 130:109456. https://doi.org/10.1016/j.diamond.2022.109456
18. Yang Y, Cannon FS (2021) Preparation of activated carbon from pine sawdust with hydrothermal-pressure preconditioning. J Environ Chem Eng 9(6):106391. https://doi.org/10.1016/j.jece.2021.106391
19. Mohanty K, Das D, Biswas MN (2006) Preparation and characterization of activated carbons from *Sterculia alata* nutshell by chemical activation with zinc chloride to remove phenol from wastewater. Adsorption 12(2):119–132. https://doi.org/10.1007/s10450-006-0374-2
20. Wang J, Lei S, Liang L (2020) Preparation of porous activated carbon from semi-coke by high temperature activation with KOH for the high-efficiency adsorption of aqueous tetracycline. Applied Surface Science 530:147187. https://doi.org/10.1016/j.apsusc.2020.147187
21. Kaya N, Yildiz Uzun Z (2020) Investigation of effectiveness of pyrolysis products on removal of alizarin yellow GG from aqueous solution: a comparative study with commercial activated carbon. Water Sci Technol 81(6):1191–1208. https://doi.org/10.2166/wst.2020.213
22. Lopez FA, Centeno TA, Garcia-Diaz I, Alguacil FJ (2013) Textural and fuel characteristics of the chars produced by the pyrolysis of waste wood, and the properties of activated carbons prepared from them. J Anal Appl Pyrolysis 104:551–558. https://doi.org/10.1016/j.jaap.2013.05.014
23. Yumak T (2021) Surface characteristics and electrochemical properties of activated carbon obtained from different parts of Pinus pinaster. Colloids Surf A: Physicochem Eng Asp 625:126982. https://doi.org/10.1016/j.colsurfa.2021.126982
24. Alam S, Khan MS, Bibi W, Zekker I, Burlakovs J, Ghangrekar MM, Bhowmick GD, Kallistova A, Pimenov N, Zahoor M (2021) Preparation of activated carbon from the wood of *Paulownia tomentosa* as an efficient adsorbent for the removal of acid red 4 and methylene blue present in wastewater. Water 13(11):1453. https://doi.org/10.3390/w13111453
25. Cretescu I, Lupascu T, Buciscanu I, Balau-Mindru T, Soreanu G (2017) Low-cost sorbents for the removal of acid dyes from aqueous solutions. Process Saf Environ Prot 108:57–66. https://doi.org/10.1016/j.psep.2016.05.016
26. Heibati B, Rodriguez-Couto S, Al-Ghouti MA, Asif M, Tyagi I, Agarwal S, Gupta VK (2015) Kinetics and thermodynamics of enhanced adsorption of the dye AR 18 using activated carbons prepared from walnut and poplar woods. Journal of Molecular Liquids 208:99–105. https://doi.org/10.1016/j.molliq.2015.03.057
27. Hadi M, Samarghandi MR, McKay G (2010) Equilibrium two-parameter isotherms of acid dyes sorption by activated carbons:

study of residual errors. JChem Eng 160(2):408–416. https://doi.org/10.1016/j.cej.2010.03.016
28. Sarıcı Özdemir Ç (2019) Equilibrium, kinetic, diffusion and thermodynamic applications for dye adsorption with pine cone. Sep Sci Technol 54(18):3046–3054. https://doi.org/10.1080/01496395.2019.1565769
29. Ogana FN, Corral-Rivas S, Gorgoso-Varela JJ (2020) Nonlinear mixed-effect height-diameter model for *Pinus pinaster ait*. and *Pinus radiata d. Don*. Cerne 26:150–161. https://doi.org/10.1590/01047760202026012695
30. Zou W, Bai H, Gao S, Li K (2013) Characterization of modified sawdust, kinetic and equilibrium study about methylene blue adsorption in batch mode. Korean J Chem Eng 30:111–122. https://doi.org/10.1007/s11814-012-0096-y
31. Carabineiro SAC, Thavorn-Amornsri T, Pereira MFR, Serp P, Figueiredo JL (2012) Comparison between activated carbon, carbon xerogel and carbon nanotubes for the adsorption of the antibiotic ciprofloxacin. Catal Today 186(1):29–34. https://doi.org/10.1016/j.cattod.2011.08.020
32. Ho YS, McKay G (1999) Pseudo-second order model for sorption processes. Process Biochem 34:451–465
33. Yakout SM, Hassan MR, El-Zaidy ME, Shair OH, Salih AM (2019) Kinetic study of methyl orange adsorption on activated carbon derived from pine (Pinus strobus) sawdust. BioResources 14(2):4560–4574. https://doi.org/10.15376/biores.14.2.4560-4574
34. Weber WJ Jr, Morris JC (1963) Kinetics of adsorption on carbon from solution. Journal of the Sanitary Engineering Division 89(2):31–59. https://doi.org/10.1061/JSEDAI.0000430
35. Sayğili H, Güzel F (2016) High surface area mesoporous activated carbon from tomato processing solid waste by zinc chloride activation: process optimization, characterization and dyes adsorption. J Clean Prod 113:995–1004. https://doi.org/10.1016/j.jclepro.2015.12.055
36. Üner O, Geçgel Ü, Bayrak Y (2019) Preparation and characterization of mesoporous activated carbons from waste watermelon rind by using the chemical activation method with zinc chloride. Arab J Chem 12(8):3621–3627. https://doi.org/10.1016/j.arabjc.2015.12.004
37. Spagnoli AA, Giannakoudakis DA, Bashkova S (2017) Adsorption of methylene blue on cashew nut shell based carbons activated with zinc chloride: the role of surface and structural parameters. J Mol Liq 229:465–471. https://doi.org/10.1016/j.molliq.2016.12.106
38. Thommes M, Kaneko K, Neimark AV, Olivier JP, Rodriguez-Reinoso F, Rouquerol J, Sing KSW (2015) Physisorption of gases, with special reference to the evaluation of surface area and pore size distribution (IUPAC Technical Report). Pure Appl Chem 87(9-10):1051–1069. https://doi.org/10.1515/pac-2014-1117
39. Sethia G, Sayari A (2015) Comprehensive study of ultra-microporous nitrogen-doped activated carbon for CO2 capture. Carbon 93:68–80. https://doi.org/10.1016/j.carbon.2015.05.017
40. Balsamo M, Silvestre-Albero A, Silvestre-Albero J, Erto A, Rodríguez-Reinoso F, Lancia A (2014) Assessment of CO_2 adsorption capacity on activated carbons by a combination of batch and dynamic tests. Langmuir 30(20):5840–5848. https://doi.org/10.1021/la500780h
41. Açikyildiz M, Gürses A, Karaca S (2014) Preparation and characterization of activated carbon from plant wastes with chemical activation. Microporous and Mesoporous Mater 198:45–49. https://doi.org/10.1016/j.micromeso.2014.07.018
42. Húmpola P, Odetti H, Moreno-Piraján JC, Giraldo L (2016) Activated carbons obtained from agro-industrial waste: textural analysis and adsorption environmental pollutants. Adsorption 22(1):23–31. https://doi.org/10.1007/s10450-015-9728-y
43. Domínguez-Ramos L, Prieto-Estalrich A, Malucelli G, Gómez-Díaz D, Freire MS, Lazzari M, González-Álvarez J (2022) N-and S-doped carbons derived from polyacrylonitrile for gases separation. Sustainability 14(7):3760. https://doi.org/10.3390/su14073760
44. Akmil-Başar C, Önal Y, Kiliçer T, Eren D (2005) Adsorptions of high concentration malachite green by two activated carbons having different porous structures. J Hazard Mater 127(1-3):73–80. https://doi.org/10.1016/j.jhazmat.2005.06.025
45. Ngakou C, Ngomo H, Anagho S (2018) Batch equilibrium and effects of ionic strength on kinetic study of adsorption of phenacetin from aqueous solution using activated carbon derived from a mixture of ayous sawdust and cucurbitaceae peelings. Curr J Appl Sci Technol 26(2):1–24. https://doi.org/10.9734/cjast/2018/37300
46. Hock PE, Zaini MAA (2022) Zinc chloride–activated glycerine pitch distillate for methylene blue removal—isotherm, kinetics and thermodynamics. Biomass Convers Biorefin 12(7):2715–2726. https://doi.org/10.1007/s13399-020-00828-5
47. Kah M, Sigmund G, Xiao F, Hofmann T (2017) Sorption of ionizable and ionic organic compounds to biochar, activated carbon and other carbonaceous materials. Water Res 124:673–692. https://doi.org/10.1016/j.watres.2017.07.070
48. Foroutan R, Peighambardoust SJ, Peighambardoust SH, Pateiro M, Lorenzo JM (2021) Adsorption of crystal violet dye using activated carbon of lemon wood and activated carbon/Fe3O4 magnetic nanocomposite from aqueous solutions: a kinetic, equilibrium and thermodynamic study. Molecules 26(8):2241. https://doi.org/10.3390/molecules26082241
49. Bangash FK, Alam S (2009) Adsorption of acid blue 1 on activated carbon produced from the wood of Ailanthus altissima. Braz J Chem Eng 26:275–285. https://doi.org/10.1590/S0104-66322009000200005
50. Malarvizhi R, Ho YS (2010) The influence of pH and the structure of the dye molecules on adsorption isotherm modeling using activated carbon. Desalination 264(1-2):97–101. https://doi.org/10.1016/j.desal.2010.07.010
51. Shokoohi R, Vatanpoor V, Zarrabi M, Vatani A (2010) Adsorption of Acid Red 18 (AR18) by activated carbon from poplar wood-a kinetic and equilibrium study. J Chem 7(1):65–72. https://doi.org/10.1155/2010/958073
52. Bhadusha N, Ananthabaskaran T (2011) Adsorptive removal of methylene blue onto $ZnCl_2$ activated carbon from wood apple outer shell: kinetics and equilibrium studies. J Chem 8:1696–1707. https://doi.org/10.1155/2011/429831
53. Danish M, Hashim R, Ibrahim MM, Sulaiman O (2013) Characterization of physically activated acacia mangium wood-based carbon for the removal of methyl orange dye. BioResources 8(3):4323–4339
54. Hajati S, Ghaedi M, Yaghoubi S (2015) Local, cheep and non-toxic activated carbon as efficient adsorbent for the simultaneous removal of cadmium ions and malachite green: optimization by surface response methodology. J Ind Eng Chem 21:760–767. https://doi.org/10.1016/j.jiec.2014.04.009
55. Ghaedi M, Nasab AG, Khodadoust S, Rajabi M, Azizian S (2014) Application of activated carbon as adsorbents for efficient removal of methylene blue: kinetics and equilibrium study. J Ind Eng Chem 20(4):2317–2324. https://doi.org/10.1016/j.jiec.2013.10.007
56. Lou K, Rajapaksha AU, Ok YS, Chang SX (2016) Pyrolysis temperature and steam activation effects on sorption of phosphate on pine sawdust biochars in aqueous solutions. Chem Speciat Bioavailab 28(1-4):42–50. https://doi.org/10.1080/09542299.2016.1165080
57. Sun D, Zhang Z, Wang M, Wu Y (2013) Adsorption of reactive dyes on activated carbon developed from Enteromorpha prolifera. Am J Anal Chem 04(07):17–26. https://doi.org/10.4236/ajac.2013.47a003
58. Achour Y, Bahsis L, Ablouh EH, Yazid H, Laamari MR, MEl H (2021) Insight into adsorption mechanism of Congo red dye

onto Bombax Buonopozense bark activated-carbon using central composite design and DFT studies. Surf Interfaces 23:100977. https://doi.org/10.1016/j.surfin.2021.100977

59. Zhao H, Zhong H, Jiang Y, Li H, Tang P, Li D, Feng Y (2022) Porous $ZnCl_2$-activated carbon from shaddock peel: methylene blue adsorption behavior. Materials 15(3):895. https://doi.org/10.3390/ma15030895

Preparation of activated carbon from pine (Pinus radiata) sawdust by chemical activation with zinc chloride for wood dyes adsorption

Supplementary Information (SI)

Catarina H. Pimentel, M. Sonia Freire, Diego Gómez-Díaz, Julia González-Álvarez

Department of Chemical Engineering, School of Engineering, Universidade de Santiago de Compostela, Santiago de Compostela, 15782, Spain

e-mail: julia.gonzalez@usc.es

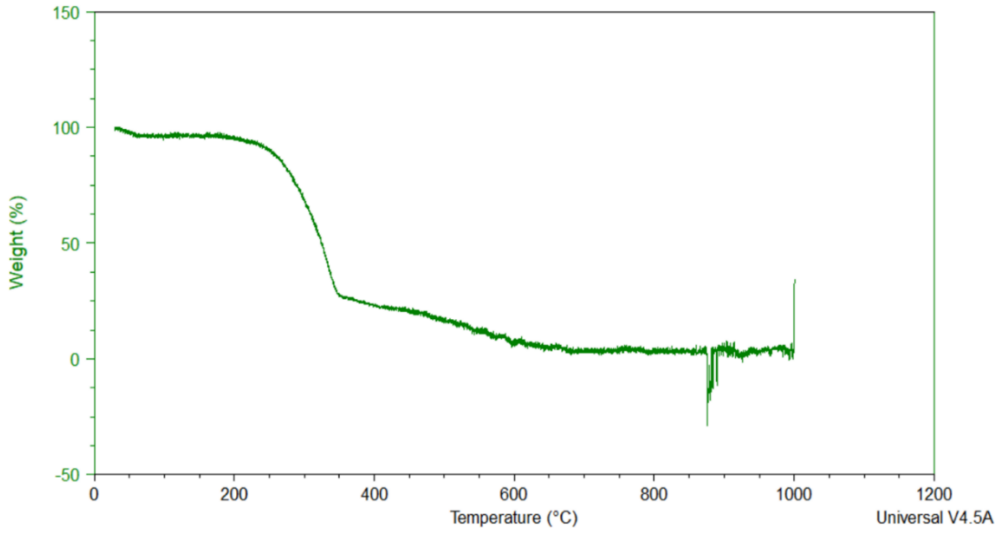

Fig S1. Curve of thermo-gravimetric analysis (TGA) of natural pine sawdust (conditions: Temperature 1000ºC; nitrogen atmosphere at 25 mL min^{-1}).

Journal of Environmental Chemical Engineering 11 (2023) 111378

Contents lists available at ScienceDirect

Journal of Environmental Chemical Engineering

journal homepage: www.elsevier.com/locate/jece

Separation of CO_2 using biochar and KOH and $ZnCl_2$ activated carbons derived from pine sawdust

Catarina Helena Pimentel, Lidia Díaz-Fernández, Diego Gómez-Díaz, María Sonia Freire, Julia González-Álvarez *

Department of Chemical Engineering, School of Engineering, Universidade de Santiago de Compostela, Santiago de Compostela 15782, Spain

ARTICLE INFO

Editor:Dong-Yeun Koh

Keywords:
Activated carbon
Pine sawdust
CO_2 adsorption
Isotherm models
CO_2/N_2 selectivity
Heat of adsorption

ABSTRACT

Due to the CO_2 emissions and greenhouse effect, reducing its harmful impacts on climatic conditions is necessary. CO_2 adsorption in a microporous carbon structure is one of the more effective separation techniques to avoid this type of emissions. In this work, one biochar (BC) and five activated carbons (ACs) were produced from *Pinus radiata* sawdust by chemical activation with potassium hydroxide (KOH) or zinc chloride ($ZnCl_2$). Characterization was performed by scanning and transmission electron microscopy (SEM and TEM), surface area and pore size distribution by volumetric N_2 and CO_2 adsorption experiments using the Brunauer-Emmet-Teller (BET) and Barret-Joyner-Halenda (BJH) methods, respectively, X-ray diffraction (XRD), elemental analysis and X-ray photoelectron spectroscopy (XPS). The performance efficiency of the carbons was analyzed in terms of CO_2 adsorption capacity at an absolute pressure range of 0–760 mmHg and at different temperatures (0, 25 and 50 °C). The apparent and IAST selectivity of CO_2 over N_2 were determined and all carbons showed preferential sorption for CO_2. Langmuir, Freundlich and Toth isotherms were employed to analyze pure CO_2 and N_2 adsorption data and the Toth isotherm gave the best fit. The carbon activated at 600°C with KOH at a ratio of 1:4 w/w achieved the largest CO_2 uptake (5.79 mmol/g at 0 °C and 750 mmHg) due to a combination between high microporosity (89 %) and surface area (2437 m^2/g). This carbon also reached a relatively high selectivity.

1. Introduction

One of the most anthropogenic greenhouse gases (GHG) having a detrimental impact on the environment and associated to climate change is carbon dioxide (CO_2), contributing more than 60 % to global warming. Then, reduction of CO_2 emissions, which in the recent years has been one of the main efforts of the scientific community [1–3], is of great importance. Since the concentration of CO_2 continues to increase it is essential to reduce the carbon footprint in most countries and search for solutions and alternatives for more sustainable forms of energy. Meanwhile, as fossil fuel (coal, natural gas and oil) burning is still the primary energy supply it is crucial to develop carbon capture with low energy penalty and storage technologies (CCS) to deal with the global challenge of CO_2 reduction [4].

Nowadays, the most common technique used in industry for CO_2 capture is chemical absorption with monoethanolamine (MEA) since it is relatively cheap, easily available and a fast reaction occurs with CO_2. However, several disadvantages can be mentioned such as high energy requirements for the regeneration and recycling of the solvent, equipment corrosion and solvent degradation [2,4]. This highlights the importance of using economically viable technologies. Adsorption, as a less expensive technique, ease of handling, presenting a good capturing capacity, high selectivity, extended stability, with lower energy requirements for regeneration and recycling and fast kinetics, represents a promising alternative [5]. Therefore, extensive research has been made to prepare efficient CO_2 adsorbents, such as carbonaceous materials, zeolites, metal organic frameworks (MOFs), clays, alkali-metal based materials, amine loaded materials and nitrogen-rich microporous polymers [1,6]. However, due to economical and/or technical issues some of these materials are still far from large-scale application [2].

The selection of a good adsorbent implies to consider both the type of material (i.e., hydrophobicity, acidity, etc.) and the pore size of the target adsorbent. Particularly, in the case of CO_2 the microporous region (< 2 nm) is the most important one since it is known to be favorable for CO_2 adsorption. Moreover, the importance of the ultra-micropores (< 0.7 nm) for CO_2 adsorption has been emphasized [7]. Additionally, high

* Correspondence to: School of Engineering, Rúa Lope Gómez de Marzoa s/n, 15782 Santiago de Compostela, Spain.
E-mail address: julia.gonzalez@usc.es (J. González-Álvarez).

https://doi.org/10.1016/j.jece.2023.111378
Received 9 June 2023; Received in revised form 11 August 2023; Accepted 29 October 2023
Available online 2 November 2023

adsorption capacity, high CO_2/N_2 selectivity, low affinity to impurities, regeneration ability, mechanical and thermal stability are also essential characteristics [4]. Most notably, porous carbons revealed to be very competitive adsorbents due to their properties such as high specific area, porous structure, favorable surface chemistry, high chemical and thermal stability, reversibility and high recyclability [1].

In the context of circular economy and sustainable development and as commercial activated carbons normally show low CO_2 adsorption capacity, the synthesis of carbons from renewable inexpensive precursors such as agricultural and industrial biomass wastes is highly desirable [4,6]. Various types of biomass have been reported as precursors for activated carbons (AC) production such as garlic peel, corncob, banana peel, rice husk, pine cone, lotus stem, bamboo and nut-shells with CO_2 uptakes in the range of 3–6.5 mmol/g at 1 bar and 0 ºC [8].

AC preparation usually involves two steps: (a) transforming biomass in biochar or hydrochar through carbonization or hydrothermal carbonization, respectively; (b) activation at high temperature, usually between 600 and 900 ºC either physically (by steam, CO_2 or O_2) or chemically (with KOH, K_2CO_3, $ZnCl_2$ or NaOH). Previous studies [9] reported that using a two-step procedure it is possible to obtain AC from biomass with high specific surface area. Usually, if the material is only carbonized a carbon with a low surface area or even non-porous is produced and may not be applicable for CO_2 capture. Among activating agents tested, KOH has been extensively used not only due to its capacity to produce AC with high surface area and a good pore size distribution, but also due to its low environmental pollution, corrosiveness and cost. On the other hand, $ZnCl_2$ has been widely used to produce AC essentially from lignocellulosic and cellulosic precursors. It works as a dampening agent and the movement of volatile substances through $ZnCl_2$ saturated pores is not disrupted and volatile substances can be released from the surface of AC during the activation process. Moreover, chemical activators have dehydrating effect and influence pyrolytic decomposition inhibiting the formation of pore-closing tar [10,11].

Among the existing tree species worldwide, *Pinus radiata* is one of the most widely grown. It is native to the central coast of California, but it has been widely planted around the world, particularly in Spain, New Zealand, Australia, and Chile, and is grown over 4.2 million hectares [12]. Among various materials from industrial or agricultural origin, pine (*Pinus radiata*) sawdust, an abundant and inexpensive industrial bio-waste, can be applied for a lot of applications such as sustainable water remediation, production of activated carbon, oil-water separation and high-performance composites fabrication. Specifically, in previous studies sawdust was revealed as an efficient adsorbent for dyes and heavy metals [10–13]. This residue presents disposal problems and for that reason its recycle and reuse provides a sustainable solution. However, to the best of authors' knowledge, there is a very limited number of studies on CO_2 adsorption applying AC from pine sawdust [14,15] and there are no studies specifically applying the species studied in the present work.

The aim of this study was the synthesis of carbons from pine sawdust to be used as CO_2 adsorbents. A series of ACs were obtained by changing the activation temperature, activating agent and doses of activating agent. The study of the surface and textural characteristics of carbons was performed through different techniques such as scanning and transmission electron microscopy (SEM and TEM), surface area determination by the Brunauer-Emmett-Teller (BET) method, porosity by Barret-Joyner-Halenda (BJH) method and elemental analysis. X-ray diffraction (XRD) was used to analyze the crystalline structure and the surface elemental composition and functional groups by X-ray photoelectron spectroscopy (XPS). The CO_2 adsorption capacity of carbon samples was assessed under different values of gas pressure (0–760 mmHg) at various temperatures 0 ºC, 25 ºC and 50 ºC. Moreover, the experimental equilibrium data for the adsorption under pure CO_2 and N_2 were evaluated by applying the Langmuir, Freundlich and Toth isotherm models. Finally, these data were used for the estimation of the apparent and Ideal Absorbed Solution Theory (IAST) selectivity of CO_2 over N_2.

2. Experimental

2.1. Chemicals

Pine (*Pinus radiata*) sawdust (PS) was provided by a regional sawmill (Lugo, Spain) and received in a bag pre-packed by the supplier. Potassium hydroxide (KOH, 85 %, Probus), zinc chloride ($ZnCl_2$, 98 %, Scharlau), and hydrochloric acid (HCl, 37 %, Sigma Aldrich) were used.

2.2. Carbonization procedure

PS was prepared by air-drying, sieving to a fraction between 0.5 and 1 mm and stored in a plastic container before being used as an organic precursor for the preparation of biochar and activated carbons. Then, to select the optimal carbonization and activation temperatures, the thermal behavior of sawdust was studied by using a thermogravimetric analyzer (TGA Q500, TA Instruments) [16]. One biochar (BC) and five types of activated carbons were synthetized via thermal treatment in a horizontal tubular furnace (Carbolite, Sheffield). PS was carbonized at 600 ºC under inert N_2 atmosphere (10 mL/min) at a heating rate of 5 ºC/min and held for 1 h before cooling to room temperature, and finally was ground in a mortar.

2.3. Activation procedures

The obtained BC was mixed with KOH pellets by a dry procedure at a weight ratio of 1:4 and two different temperatures, 850 ºC and 600 ºC (ACPS850-K-4 and ACPS600-K-4) and at a weight ratio of 1:2 and 850 ºC (ACPS850-K-2). It has been reported that carbon porosity and surface area are affected by the ratio of KOH to biomass and high surface area and porosity were obtained for AC prepared from agricultural biomass using a 1:4 ratio [4]. The samples were placed into the tubular furnace under nitrogen atmosphere (10 mL/min) using a heating rate of 5 ºC/min to reach the selected temperature and, finally, kept for 2 h [17].

Also, another activating agent was employed, $ZnCl_2$, at a weight ratio of 1:4, and the chemical activation was performed both by dry [16] and wet methods at 850 ºC. The $ZnCl_2$ activated carbons were called ACPS850-Z-D and ACPS850-Z-W, respectively. For wet activation, after carbonization a 25 % $ZnCl_2$ solution was mixed with the corresponding biochar mass for 22 h and then dried at 105 ºC for 2 h [18]. For dry activation, the procedure was as previously explained for KOH. In both cases, the activation conditions were as described above.

Finally, after activation, the samples were washed with 100 mL of 0.1 M HCl under stirring for 15 min, then with distilled water under vacuum filtration and dried overnight at 105 ºC [17].

The yield of each carbon was calculated following Eq. (1):

$$Y \quad (\%) = \frac{W_{AC \quad final}}{W_{initial}} \times 100 \tag{1}$$

where Y denotes the yield of biochar or AC obtained after washing, and $W_{initial}$ and $W_{AC\ final}$ correspond to the initial weight of sawdust and final weight of AC on dry basis, respectively.

2.4. Characterization

The morphology of the prepared materials was characterized by scanning electron microscopy on a ZEISS EVO LS 15 microscope and by transmission electron microscopy (TEM). TEM was carried out on a JEOL JEM 2010 transmission electron microscope operated at 200 keV. For TEM measurements, the samples were sonicated in ethanol to form a homogeneous suspension, dropped on a 400 mesh copper TEM grid coated with a thin amorphous carbon film, and then allowed to dry in air.

The specific surface areas were determined by the Brunauer-Emmett-Teller (BET) equation through N_2 adsorption-desorption isotherms at − 196 °C and CO_2 adsorption at 0 °C in a Micromeritics ASAP 2020 sorption analyzer. Prior to measurements, the samples were degassed at 300 °C for 2 h. Total pore volume was determined from the amount of nitrogen adsorbed at a relative pressure (P/P_0) equal to 0.99. To analyze the pore size distribution of carbons the Barret-Joyner-Halenda (BJH) method was applied. The total micropore (< 2 nm) volume was determined by subtracting mesopores (2–50 nm) volume from the total obtained from the adsorption-desorption N_2 isotherm. X-ray diffraction (XRD) was used to analyze the crystalline structure of activated carbons and the measurements were carried out at room temperature in Bragg-Brentano geometry using a BRUKER D8 ADVANCE type X-ray diffractometer (40 kV, 40 mA, theta/theta) equipped with a sealed X-ray tube (CuKα1, λ = 1.5406 Å), and a LYNXEYE XE-T type detector. The diffractograms were obtained in the angular range of $5 < 2\Theta < 60^{o}$ with a step of 0.04° at 4 s per step. The samples were rotated during the measurement to obtain the most optimal peak profile for the analysis, as well as to minimize the effect of the preferred orientation. The BC and activated carbons were analyzed for carbon, nitrogen, hydrogen, sulfur and oxygen (by difference) content using a Flash Smart CHNS Elemental Analyzer (Thermo Scientific). The surface elemental composition and surface functional groups of the materials were determined by X-ray photoelectron spectroscopy (XPS) technique using a Thermo Scientific NEXSA (XPS) instrument equipped with aluminum Kα monochromatized radiation at 1486.6 eV X-ray source. Photoelectrons were collected from a take-off angle of 90° relative to the sample surface. The measurement was done in a Constant Analyser Energy mode (CAE) with a 100 eV pass energy for survey spectra and 20 eV pass energy for high resolution spectra. Charge referencing was done by setting the lower binding energy C1s photo peak at 284.80 eV C1s hydrocarbon peak. Surface elemental composition was determined using the standard Scofield photoemission cross sections.

2.5. CO_2 and N_2 adsorption

The static CO_2 and N_2 adsorption were evaluated using the adsorption isotherms obtained by the volumetric system Micromeritics ASAP 2020 analyzer at the required temperatures (0, 25 and 50 °C) and a pressure range between 0 and 760 mmHg. Prior to experiments, the samples were degassed at 300 °C for 2 h under vacuum to eliminate moisture and impurities. To maintain the targeted temperature, an ice bath in a Dewar was used for experiments at 0 °C and a temperature-controlled vessel using a Selecta Sensoterm sensor for other temperatures.

N_2 and CO_2 adsorption data at different temperatures were fitted to Langmuir (Eq. (2)), Freundlich (Eq. (3)) and Toth (Eq. (4)) models:

Langmuir model:

$$n = \frac{n_{m,L} \cdot K_L \cdot P}{1 + K_L \cdot P} \tag{2}$$

Freundlich model:

$$n = K_F \cdot P^{\frac{1}{n_F}} \tag{3}$$

Toth model:

$$n = \frac{n_{m,T} \cdot K_T \cdot P}{\left\{1 + (K_T \cdot P)^t\right\}^{\frac{1}{t}}} \tag{4}$$

where n (mmol/g) is the loading of adsorbate, P (mmHg) is the pressure and $n_{m,L}$ (mmol/g), $n_{m,T}$ (mmol/g), K_L (1/mmHg), K_F (mmol/g·mmHg$^{1/nF}$), K_T (1/mmHg), n_F and t are the corresponding isotherms' parameters.

The experimental data corresponding to adsorption isotherms of each gas were employed to calculate CO_2 over N_2 apparent and IAST selectivity values. The last one was estimated using GraphIAST software package based on Python module pyIAST [19].

2.6. Statistical analysis

For the activated carbons with $ZnCl_2$, due to the possible similarities, the experiments regarding the specific surface areas were done in quadruplicate and the values averaged. The existence of significant differences among the results for surface areas was analyzed. Thus, the one-way analysis of variance (ANOVA) was used, followed by Brown–Forsythe test according to the significant level. All statistical tests were performed at a 5 % significance level using IBM SPSS Statistics 28 software.

3. Results and discussion

3.1. Effect of experimental parameters on yield

The effect of activating agent, ratio of the carbon to activating agent and activation temperature on the yield was evaluated and the results are presented in Table 1. Carbonization temperature was 600°C for biochar and all activated carbons.

Carbonization essentially involves the pyrolytic decomposition of the precursor and non-carbon species removal [20]. Regarding BC, as expected and observed by the yield percentage, a significant loss of weight was found during the carbonization process as most of the non-carbon elements are released while a carbon skeleton is produced. This result was expected due to a higher mass loss occurred between 200 and 400 °C probably due to cellulose and hemicelluloses decomposition, as well as loss of the leftover adsorbed water. Between 150 and 750 °C lignin decomposition takes place which leads to a less significant decrease on the weight [21,22]. Between 600 and 850 °C there was no mass loss with the increase in the temperature [16]. Similar yields were reported by Tomczyk et al. [23] for biochars produced from wood wastes and sunflower husks.

For the activated carbons, a significant loss in the yield (around 50 %) took place using KOH, while the loss with $ZnCl_2$ was negligible in comparison with BC. This can be due to the fact that during activation with $ZnCl_2$, a polymerization occurs which leads to the creation of a small number of large-ring aromatic compounds. Likewise, $ZnCl_2$ inhibits the volatile matter loss, stabilizing it and eventually increasing the yield in comparison with KOH which typically produces yield losses between 10 % and 40 % [20,24]. However, KOH has been extensively used, as AC with high surface area and porosity is produced due to cavity formation by KOH evaporation from places previously occupied by it. Probably, this fact is due to a mechanism in which the alkali metal interposes in the carbon matrix acting as an electron donor that ignites the reaction during gasification. Also, the presence of oxygen could remove the carbon atoms cross-linking in the crystallites. The release of

Table 1
Effect of experimental parameters on yield of carbon samples.

Type of carbon	Activating agent	Carbon to activating agent ratio	Activation temperature (°C)	Yield (%)
BC	-	-	-	20.1 ± 1.1
ACPS850-K-4	KOH	1:4	850	10.1 ± 1.1
ACPS600-K-4	KOH	1:4	600	14.6 ± 1.2
ACPS850-K-2	KOH	1:2	850	12.4 ± 0.6
ACPS850-Z-D	$ZnCl_2$	1:4	850	19.3 ± 1.3 [16]
ACPS850-Z-W	$ZnCl_2$	1:4	850	17.2 ± 1.5

potassium at elevated temperature interposes and forces a part of the separate lamellae of the crystallite. Moreover, the use of this chemical has advantages such as lower environmental pollution, less corrosiveness and lower cost [20,24].

Additionally, it can be observed that activation temperature strongly influenced yield with KOH activation since when temperature was reduced from 850 to 600 ºC the yield increased. On the other hand, the effect of the biochar/activating agent ratio on yield was less significant. The influence of these variables on the yield of carbons prepared from sawdust was also reported in literature [25]. As a comparison, Table 2 illustrates results obtained in previous investigations for activated carbons prepared from various agricultural and industrial biomass wastes activated with KOH and $ZnCl_2$ with some similar values to the obtained in this work.

3.2. Structural characterization

To have a comprehensive characterization of the structure and qualitatively analyze the morphology of the prepared carbons SEM analysis was performed. Fig. 1 illustrates the SEM images of biochar and activated carbons derived from pine sawdust. SEM revealed that the biochar and activated carbons particles have a honey-comb structure and an arrangement of uniform holes distributed around the surface typically from lignocellulosic materials [32,33].

The carbonized pine sawdust (Fig. 1a) presented few pores in the walls, and this can be ascribed to the decomposition of the pine sawdust natural compounds, such as cellulose, hemicellulose and lignin, during the carbonization process. This initial porosity can facilitate the activating agents access into the carbonized material. After activation with KOH and $ZnCl_2$ the carbonized material maintained the structure, however, the carbon activated with KOH at highest ratio (Figs. 1b and 1c) showed more modifications in the structure which can be due to the strong activation under these conditions. The rupture caused by this agent could explain the obtention of a high specific surface area for these carbons. For carbons with $ZnCl_2$ activation the presence of pores is less evident (Fig. 1e and f) due to the high percentage of microporosity, as will be seen later, that plays a fundamental role in CO_2 adsorption [6].

Furthermore, TEM analysis was implemented to disclose the morphology of the carbons since can provide more information about micropores. The results are illustrated by Fig. 2.

It is possible to observe an abundant disorderly wormhole-like micropore structure on the surface of the materials, which is due to the stacking of graphene layers and indicates a significant amount of microporosity as supported by the textural characterization by N_2 adsorption isotherms. The randomly distributed micropores throughout the carbon skeleton without any pattern indicate the amorphous feature of these adsorbents as inferred by the XRD results (Fig. 3). Besides, the results show that a morphological improvement occurred after the activation process both with KOH or $ZnCl_2$ in agreement with SEM analysis.

Table 2
Comparison of yield of activated carbon prepared from various agricultural wastes and an industrial by-product (Slash pine wood) using $ZnCl_2$ and KOH.

Precursor	Activating agent	Carbon to activating agent ratio (w/w)	Activation temperature (ºC)	Yield (%)	References
Safflower biochar	$ZnCl_2$	1:4	900	26.0	[26]
Waste potato residue	$ZnCl_2$	1:1.5	600	29.2	[27]
Vine shoots	$ZnCl_2$	1:1.3	700	18.2	[28]
Cane pith	KOH	1:5	780	8.2	[29]
Rice straw	KOH	1:4	800	13.5	[30]
Maize stalks	KOH	1:0.75	700	13.1	[31]
Slash pine wood	KOH	1:4	580	24.5[a]	[18]
Slash pine wood	$ZnCl_2$	1:1	580	26.8[a]	[18]

[a] Normalized yield calculated from biochar.

As above mentioned, the crystallographic structure of BC and activated carbons was evaluated from the XRD data, which is shown in Fig. 3. As can be seen, the materials show different degrees of graphitization. The samples activated at higher temperature (850 ºC) with KOH as activated agent show a similar behavior practically without peaks in the diffractograms, while the other ones presented broad diffraction peaks at different ranges (Table 3).

In this way, the weak broad peaks in ACPS850-K-4 and ACPS850-K-2 indicate that these carbons have an amorphous structure with a very low graphitization degree [8]. The other materials show a different degree of amorphous behavior with broad peaks at similar ranges, except for BC. The weak and broad peaks at 2Θ values of around 23º and 43º correspond to the (002) and (100) diffraction of graphite carbon, respectively. Their weak intensities indicate a low crystallinity degree or a partially graphitic crystal structure. The fact that the X-ray diffraction spectrum did not show well-defined peaks, in any case, indicates that no discrete mineral phase was detected. The humps in the 2Θ range (Table 3) are related to the high degree of disorder of carbonaceous materials [34,35]. Thus, ACPS600-K-4 presented the highest graphitization order while the lowest one corresponds to ACPS850-K-4. A possible explanation can be that the activation with KOH at high temperature destroys the atomic arrangement of the samples, as the increase in porosity demonstrates. Concerning the different behavior for the BC, previous studies reported that the microcrystalline structure in biochars can be created due to the superposition of multiple aromatic layers. The diffraction peak at 23.2º characterizes the degree of spatial parallelization and azimuthal orientation of the aromatic layer in the microcrystalline structure. Similar results were reported by Quan et al. [14] for a biochar produced from pine sawdust at 700 ºC. Moreover, the high and narrow peak indicates a better orientation. Additionally, the diffraction peak (100) depicts the size of the aromatic layer. If the peak is high and narrow, this indicates that the diameter of the aromatic layer is large, which means that the degree of aromatic nuclear polymerization is high [14]. As can be observed by Fig. 3 all materials revealed a marked peak at 43º (100), except the carbons activated with KOH at 850 ºC.

Elemental analysis was also performed, and the results are listed in Table 4. The high carbon content determines the highly carbonaceous nature of the adsorbents, that is an important factor to produce high porosity and hence high CO_2 uptake [36]. ACPS850-K-4 is the sample with the highest carbon content (90.3 %), which may enhance the inter-particle force between the CO_2 molecules and the adsorbent [37].

It seems that after KOH activation at higher temperature, independently of KOH ratio used, the hydrogen content decreased since BC goes through dehydrogenation and intermolecular dehydration during activation process. On the contrary, at lower temperature (600 ºC) the hydrogen content increased. The content of hydrogen also decreased after activation with $ZnCl_2$, as expected due to dehydrogenation, but it was less significant [24]. The content of nitrogen was maintained except for the carbon activated with $ZnCl_2$ by the dry method in which it increased, possibly due to a changes in the nitrogen functional groups.

Oxygen content varied from 9.4 % to 46.2 % which can explain a different behavior of carbons on the CO_2 adsorption, although really the effect of oxygen is controversial since some studies reported that the surface oxygen complexes influence CO_2 adsorption, but others showed that oxygen heteroatoms in hydroxyl and carboxyl functional groups may enhance CO_2 uptake [37]. The high oxygen content for ACPS600-K-4 may be attributed to gasification reactions and formation of oxygen groups during activation process at lower temperature in the presence of KOH, which in the present study possibly enhanced CO_2 uptake. At high temperature more decomposition reactions occur which

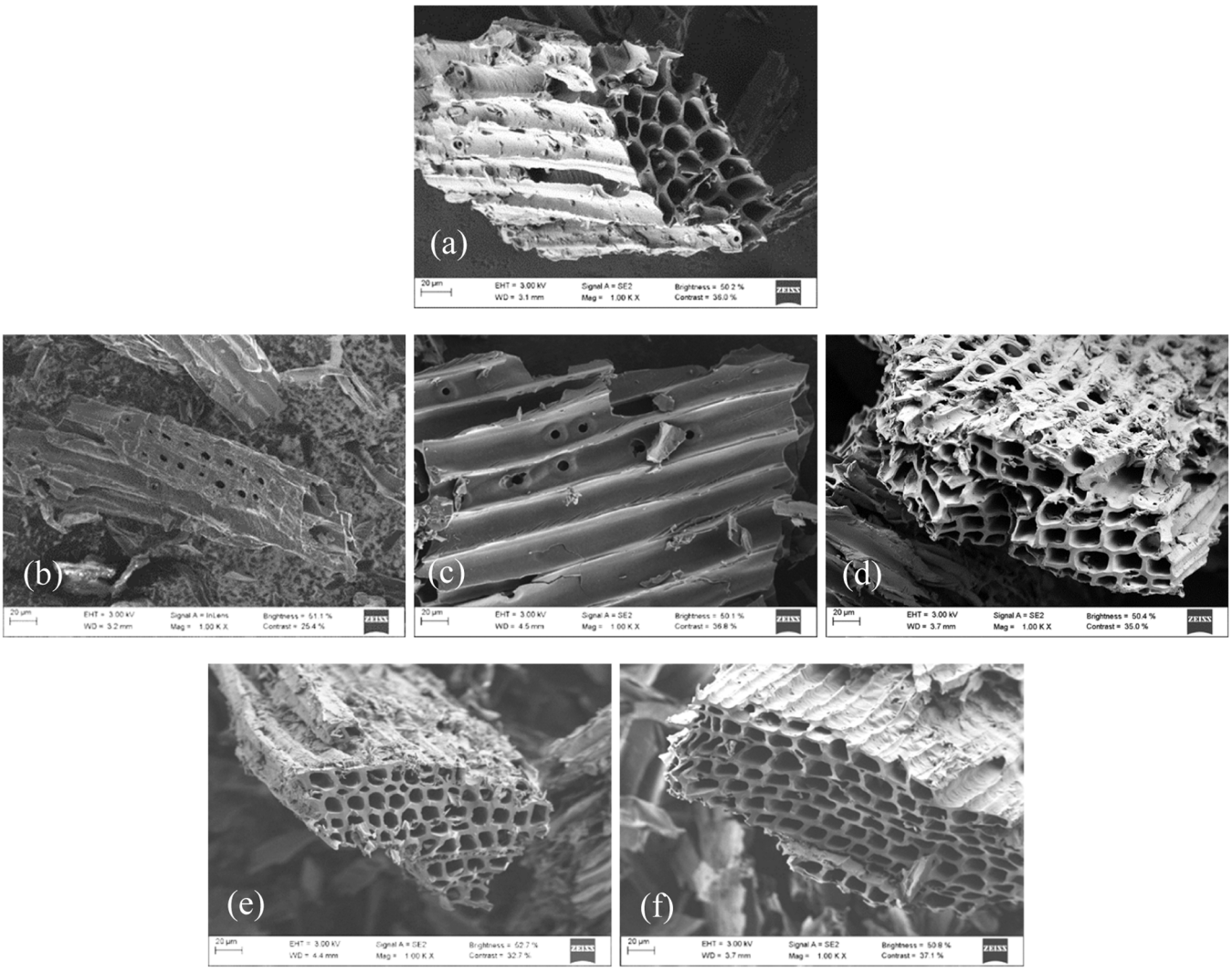

Fig. 1. SEM images of (a) BC, (b) ACPS850-K-4, (c) ACPS600-K-4, (d) ACPS850-K-2, (e) ACPS850-Z-D and (f) ACPS850-Z-W.

can lead to a decrease in oxygen content [38]. The decrease in oxygen content for the carbons activated with $ZnCl_2$ could be due to the catalytic dehydration caused by $ZnCl_2$ [39].

Moreover, as seen in Table 4, for KOH activated carbons, hydrogen and oxygen content decreased with increasing the activation temperature to 850 ºC. Also, an increase in aromaticity for these activated carbons was observed due to the H/C ratio decrease, although for ACPS850-K-4 and ACPS850-K-2 the H/C ratio was very similar. Activation with $ZnCl_2$ produced changes respect to BC reducing the H/C ratio but in less proportion than KOH. On the other hand, the H/C ratio decreased as a result of activation, except for ACPS600-K-4, which showed the highest H/C and O/C ratios indicating a low degree of carbonization and aromaticity and a high polarity [40,41].

In addition, wide XPS spectra analysis has allowed to determine the elemental composition of the carbons' surface and the results are presented in Fig. S1 and Table 5. As seen previously, C and O are the two main components as confirmed by the O1s and C1s peaks (Fig. S1) appearing at 285–287 and 532.5 eV, respectively. A weak feature around 400 eV belongs to N1s photoelectrons, revealing a very low atomic percentage (at%) of nitrogen in almost all samples. These results were consistent with the elemental analysis results (Table 4). Other elements were detected such as silicon, potassium, chlorine, calcium, and sulfur, all in very low concentrations. Traces of inorganic fractions (i.e., Si, Ca…) detected in XPS analysis can come from ashes or from the activated carbon precursors [42].

To obtain further insight on the type of bonding of these elements high resolution spectra for C1s, N1s and O1s were analyzed, and the results are shown in Table 6.

Five peaks were observed in the C1s high resolution spectra and four contributions per carbon. The most abundant contribution was that at 284.8 eV that is usually assigned to C-C, C═C or C-H bonds. In addition, in the C1s spectrum of the sample ACPS600-K-4, the K2p3/2 and K2p1/2 contributions from the spin-orbit splitting of the 2p orbital was clearly observed (Fig. S2) and can be attributed to potassium cations and oxides which means that probably potassium ions bind to remaining oxygen atoms or are intercalated within carbon [43]. On the other hand, the carbons activated with KOH at high temperature had a lower C-C content which can be due to the interaction between KOH and carbon that caused partial degradation of graphite layer destroying the matrix structure [14]. These results are in agreement with XRD results in which ACPS850-K-4 and ACPS850-K-2 presented a very low degree of graphitization. Regarding N1s high resolution spectra, they were fitted with only one component, pyrrolic-N, except for ACPS850-K-4. According to previous studies [44], pyrrole/pyridine-N group can contribute to CO_2 adsorption due to its strong interaction with CO_2 molecules. The O1s high resolution spectra were fitted with two, three or four components depending on the carbon. The binding energy peaks between 532.6 and 533 eV can be assigned to non-carboxyl oxygen (ether structures) in esters and anhydrides and those between 533.1 and 534.0 to oxygen atoms in carboxyl groups (-COOH and –COOR) [45]. The most abundant

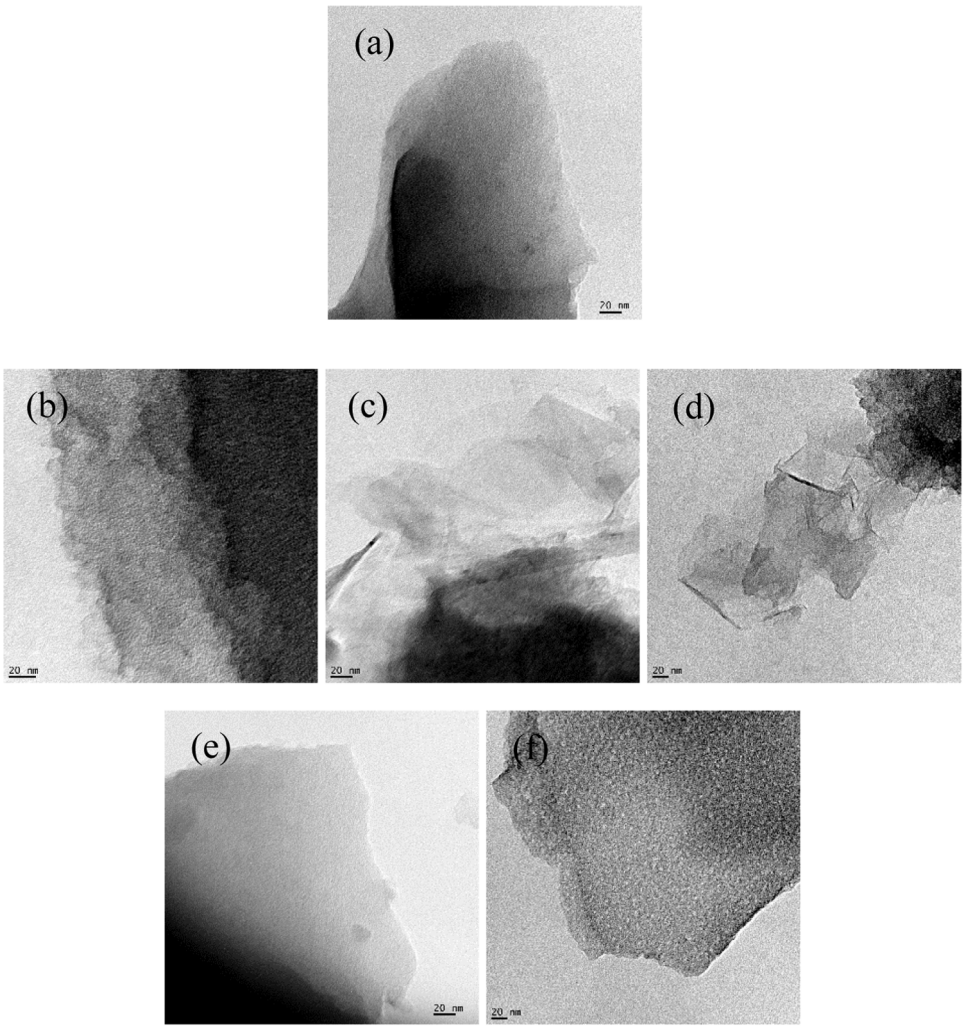

Fig. 2. TEM images of (a) BC, (b) ACPS850-K-4, (c) ACPS600-K-4, (d) ACPS850-K-2, (e) ACPS850-Z-D and (f) ACPS850-Z-W.

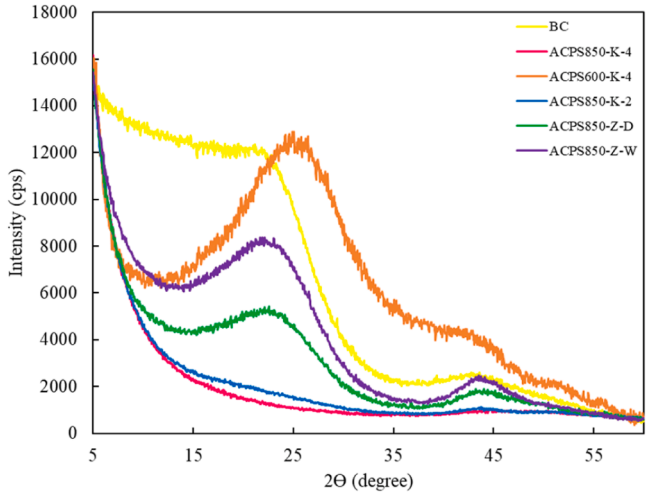

Fig. 3. XRD diffractograms of biochar and activated carbons.

peak was that at 532.6–533 eV for most carbons, but it was not detected for those activated with KOH at the highest ratio. XPS analysis demonstrated the presence of various functional groups in the carbons that suggest that although physical adsorption can be dominant as revealed the CO_2/N_2 selectivity and the isosteric heat of adsorption (see Sections

Table 3
Diffraction peaks of biochar and activated carbons.

Material	2Θ (degree)				
BC	16.8	23.2	42.9	49.5	
ACPS850-K-4	44.2	50.2			
ACPS600-K-4	16.8	25.1	42.3	52.1	55.9
ACPS850-K-2	22.8	43.7	48.8		
ACPS850-Z-D	17.6	23.2	43.7	49.0	
ACPS850-Z-W	18.2	23.4	43.7	49.5	

Table 4
CHNS elemental analysis of BC and activated carbons.

Sample	Elemental analysis (wt%)					
	C	H	N	O*	H/C	O/C
BC	83.71	2.40	0.14	13.75	0.029	0.16
ACPS850-K-4	90.27	0.17	0.081	9.48	0.0022	0.10
ACPS600-K-4	50.61	3.12	0.13	46.14	0.061	0.91
ACPS850-K-2	88.02	0.20	0.14	11.64	0.0022	0.13
ACPS850-Z-D	80.05	1.18	0.38	18.39	0.015	0.23
ACPS850-Z-W	84.05	0.97	0.14	14.84	0.012	0.18

* by difference

Table 5
Elemental composition of the carbons' surface by XPS analysis.

Material	Elemental composition (at%)							
	C	O	N	Si	Ca	K	Cl	S
BC	88.65	9.29	0.47	0.91	0.68	-	-	-
ACPS850-K-4	91.62	6.07	-	1.10	0.48	0.49	0.23	-
ACPS600-K-4	79.99	16.51	1.08	0.94	-	1.20	0.28	-
ACPS850-K-2	88.93	8.44	0.58	1.25	0.80	-	-	-
ACPS850-Z-D	93.10	4.22	1.56	0.57	-	-	0.30	0.25
ACPS850-Z-W	94.86	3.82	0.59	0.59	-	-	0.14	-

3.4.4 and 3.5), chemical adsorption can co-exist in the CO_2 separation process [44].

3.3. Specific surface area and porosity

To assess the surface area and porosity of the synthesized materials this study recorded gas sorption-desorption N_2 isotherms at − 196 °C (Fig. 4) and pore size distribution (Fig. 5).

The N_2 isotherms of all carbons are essentially reversible Type I isotherms, according to the IUPAC classification that agrees with some previous studies using biomass as raw material [9,35]. The sharp uptake at low relative pressure ($P/P_0 < 0.1$) suggests that the synthetized materials are fundamentally microporous with pores highly accessible to the gas molecules and maybe with small mesopores [1]. When the amount adsorbed reaches the limited uptake a monolayer is formed with strong adsorbent-adsorbate interactions in the narrow micropores. Type I isotherms can be subdivided in isotherm type I (a) and type I (b). From Fig. 4 it is possible to conclude that ACPS850-K-4, ACPS850-K-2 and ACPS600-K-4 present type I (b) isotherms which characterize materials with a pore size distribution of wider micropores and narrow mesopores (< 2.5 nm). In this case, a slight curvature is present in Fig. 4 which implies a wide relative pressure range in which the presence of a knee can be observed. This behavior implies that apart from the monolayer formed before reaching the highest value of nitrogen adsorption, a multilayer formation occurs. This is usually observed for large micropores size that allow multilayer formation into the pores. However, the BC and the carbons activated with $ZnCl_2$ (ACPS850-Z-D and ACPS850-Z-W) show type I (a) isotherm corresponding to microporous materials with primarily narrow micropores (< 1 nm) [46]. On the other hand, the amount of adsorbed nitrogen reveals that biochar activated with KOH substantially develops its morphology.

Indeed, Fig. 5 indicates that for all the carbons the amount of pores with size higher than 10 nm is negligible. For those activated with KOH, the volume of available pores in the porous structure increases significantly with small changes in their size, mainly for pore diameters lower than 7 nm. Particularly, for that activated at 850 °C with a KOH ratio of 1:4 (w/w) pores with higher size were detected which is in agreement with its lower microporosity percentage. The behavior is different for the BC and the carbons activated with $ZnCl_2$ in which both pore volume and size were lower. In general, the pore size distribution indicates that the porosity of the materials consists mainly of micropores and a few mesopores.

The textural parameters of the prepared adsorbents calculated from N_2 adsorption isotherms at − 196 °C and CO_2 adsorption isotherms at 0 °C are shown in Table 7.

Previous results confirm the activation process efficiency since BET surface area and pore volume increased significantly for all activated carbons. The activating agent is directly related to the specific surface area of the material, determined with N_2 adsorption, as for the ones activated with KOH the specific surface area is considerably superior to that of those activated with $ZnCl_2$. For instance, ACPS850-K-4 has a surface area 83.5 % and 80.9 % higher than those of ACPS850-Z-D and ACPS850-Z-W, respectively. This evidence confirms the results shown in the SEM images which revealed that activation with KOH caused major

Table 6
Components and relative proportions for C1s, N1s and O1s.

Material	C1s (%)					N1s (%)	O1s (%)			
	C-C, C=C, CH_x (284.8 eV)	C-O-C, C-OH (286.1–286.5 eV)	C=O (288–288.3 eV)	O=C-O (289 eV)	CO_3 (290.3 eV)	Pyrrolic-N (399.9–400.8 eV)	OH groups (531–531.8 eV)	Organic bonds (532.6–533.0 eV)	Organic bonds (533.1–534.0 eV)	$H_2O_{adsorbed}$ (534.3–535.4 eV)
BC	70.60	22.31	4.69	2.39	-	100	22.02	39.94	32.48	5.57
ACPS850-K-4	62.47	19.28	10.25	-	8.01	-	56.44	-	43.56	-
ACPS600-K-4	70.70	15.10	11.04	-	3.17	100	41.26	-	54.34	4.39
ACPS850-K-2	67.01	17.80	10.18	-	5.00	100	37.41	49.13	-	13.46
ACPS850-Z-D	73.90	18.08	4.67	-	3.35	100	12.48	69.77	-	17.74
ACPS850-Z-W	77.94	13.74	5.14	-	3.18	100	20–73	60.63	18.64	-

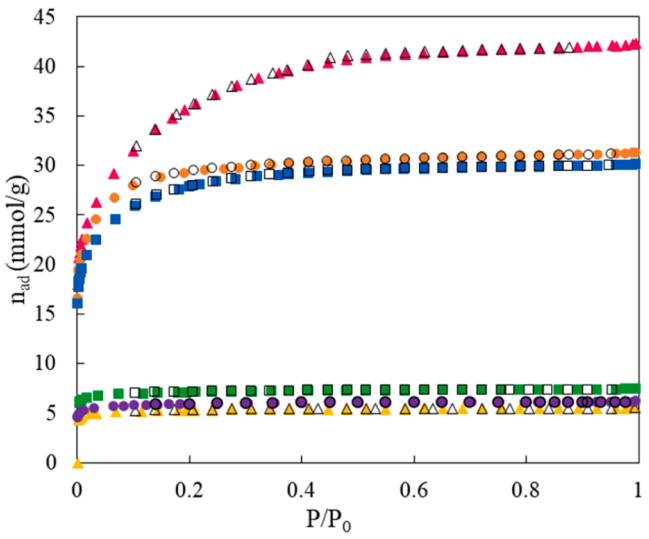

Fig. 4. Nitrogen adsorption/desorption isotherms at − 196ºC. ▲ and Δ: BC; ▲ and Δ: ACPS850-K-4; ● and ○: ACPS600-K-4; ■ and □: ACPS850-K-2; ■ and □: ACPS850-Z-D; ● and ○: ACPS850-Z-W. Full symbols: adsorption. Empty symbols: desorption.

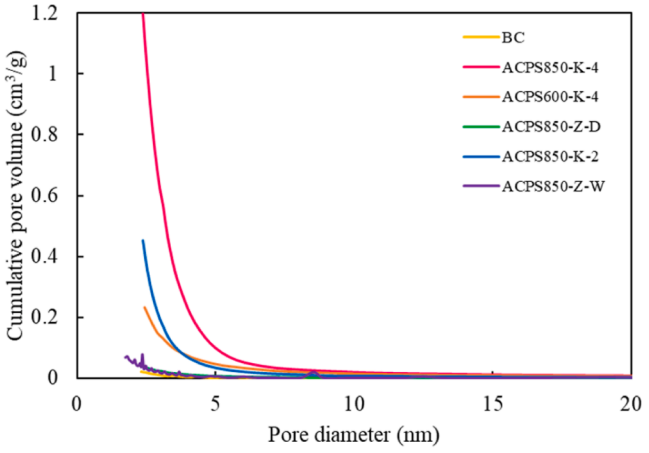

Fig. 5. Pore size distributions for biochar and activated carbons.

changes in the structure and consequently surface area and porosity increased.

Regarding the carbons activated with KOH, it can be observed that an increase in the activation temperature from 600 to 850ºC increased the specific surface area determined with N_2 adsorption by around 17%. On the other hand, the rise in the activating agent mass ratio from 1:2–1:4 (w/w) increased the surface area by around 26%. These results show that both activation temperature and activating agent mass ratio are important process parameters influencing the magnitude of the surface area. On the other hand, in all carbons activated with KOH the surface area calculated with N_2 adsorption was higher than 2000 m^2/g, however, the highest surface area calculated with CO_2 was for ACPS600-K-4 with the highest CO_2 uptake followed by ACPS850-K-4. Nevertheless, ACPS850-K-2 with low surface area showed higher CO_2 uptake, revealing the importance of micropore presence. Therefore, the mild experimental conditions (ACPS600-K-4 and ACPS850-K-2) are better for CO_2 adsorption than extreme conditions. Concerning $ZnCl_2$, the difference for the specific surface area determined with N_2 of the carbons prepared by both activation methods was lower than 7%, therefore the dry method was the one selected for being a more environmentally friendly option.

The total pore volume was higher for the KOH activation, mostly for the one activated with the highest BC/KOH ratio which confirms that a higher ratio favors the formation of pores with higher diameters, which is also in agreement with the surface area values [9]. Another interesting finding is that the use of $ZnCl_2$ (mainly for dry activation) leads to an increase in the N_2 and CO_2 surface areas maintaining the microporosity percentage in comparison with BC, which is very important since several research stand out the importance of small micropores for CO_2 adsorption [2,6,47]. CO_2 uptake is more closely related to the micropore volume rather than to surface area since the minimum uptake occurred for ACPS850-K-4 with the lowest microporosity percentage and the highest surface area.

To obtain a greater insight regarding the porosity of the carbons produced, CO_2 adsorption isotherms at 0 ºC were used to provide a good estimation of surface area provided by the carbon ultra-microporosity (lower than 0.7 nm) [9,48]. Fig. 6 shows the CO_2 adsorption isotherms of the carbon samples prepared. The experimental data show a monotonic increase in the adsorbed amount of gas without reaching a *plateau* due to the low relative pressure values employed in this characterization technique.

Interestingly, the adsorption isotherms indicate that for P/P_0 values above 0.01, BC exhibits the lowest CO_2 uptake and the carbons activated with KOH the highest ones, with distinction for ACPS600-K-4 that presented the highest value reaching 5.8 mmol/g at 0.03. Such differences can be related to their BET surface areas (with N_2 and CO_2) and microporosity. On the other hand, a different behavior is observed for pressure values below 0.01, at which ACPS600-K-4 is still maintaining the highest CO_2 uptake but without considerable differences among all carbons. Furthermore, BC reaches a higher CO_2 uptake than the activated carbons. This can be due to the key role of ultra-micropores in the CO_2 adsorption at low partial pressures as previously stated by Hao et al. [7]. Moreover, at 0 ºC CO_2 adsorption occurs via the pore filling mechanism being critical the pore size [2]. Apart from that, since BC is only carbonized at 600 ºC some functional groups based on lignin fraction that can participate in CO_2 adsorption were better preserved [49].

Table 7
Textural characterization by N_2 adsorption isotherms at − 196ºC and CO_2 adsorption isotherms at 0ºC.

Sample	Adsorption Isotherm N_2 at − 196 ºC					Adsorption Isotherm CO_2 at 0ºC	
	S_{BET} (m^2/g)	Total Pore Volume (cm^3/g)	Mesopore Volume (cm^3/g)	Micropore Volume (cm^3/g)	Microporosity (%)	S_{BET} (m^2/g)	CO_2 uptake[1] (mmol/g)
BC	293.3 ± 7.7	0.19	0.02	0.18	90.7	254.8 ± 1.3	1.17 ± 0.12
ACPS850-K-4	2864.5 ± 0.9	1.46	0.47	0.99	67.8	677.2 ± 0.2	1.03 ± 0.16
ACPS600-K-4	2437.2 ± 5.6	1.09	0.12	0.97	89.0	1354.2 ± 21.8	1.65 ± 0.21
ACPS850-K-2	2270.5 ± 22.5	1.02	0.15	0.87	85.0	588.1 ± 25.9	1.33 ± 0.19
ACPS850-Z-D*	471.4 ± 18.4[a]	0.26	0.02	0.23	90.6	319.5 ± 3.9[a]	1.41 ± 0.15
ACPS850-Z-W	501.1 ± 41.6[a]	0.26	0.03	0.23	88.9	382.1 ± 34.6[a]	1.56 ± 0.15

[1]determined at 105 mmHg; CO_2/N_2 mixture (15 % volume CO_2)
* [16]
[a] different letters indicate significant differences ($p \leq 0.05$) between samples

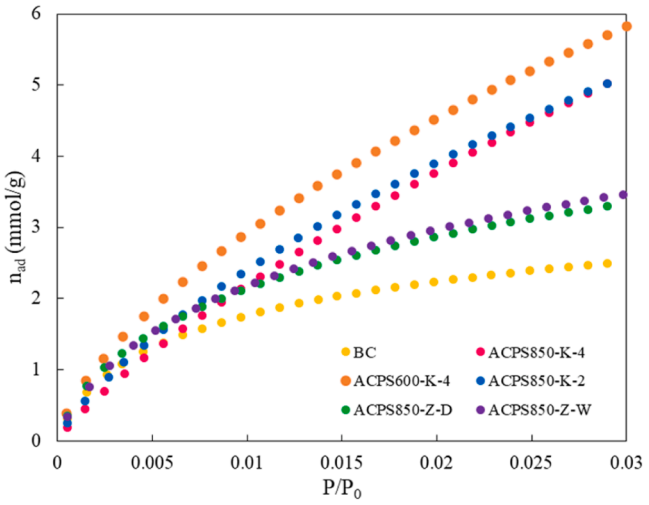

Fig. 6. CO_2 adsorption isotherms at 0ºC for BC and AC prepared.

On the other hand, CO_2 uptake was higher for those AC with higher microporosity percentage (ACPS600-K-4, ACPS850-Z-D and ACPS850-Z-W) as shown in Table 7.

3.4. Adsorption experiments

3.4.1. N_2 and CO_2 adsorption isotherms at 25 ºC

The N_2 and CO_2 adsorption capacities of the carbons prepared from pine sawdust were examined. Fig. 7 presents the N_2 and CO_2 adsorption isotherms of samples at 25 ºC. All carbons presented greater adsorption capacity for CO_2 than for N_2 over the entire pressure range. Besides, CO_2 adsorption isotherms can be classified as Type I which are typical of stronger adsorbate-adsorbent interactions [47].

Regarding N_2 adsorption, there are no substantial differences at low pressures despite differences among surface areas (Table 7). On the contrary, in the range of high pressures, other aspects such as chemical interactions or adsorption kinetics can influence and, thus, some slight differences in N_2 adsorption capacity among carbons were found [9].

Regarding CO_2 adsorption, particularly for the low-pressure region, the BC adsorption capacity is similar to that of the activated carbons due to the preservation of the chemical surface and the importance of the microporosity. On the other hand, for the high-pressure region the smaller CO_2 uptake on BC is due to its low surface area and probably to micropore filling. Although ACPS850-K-4 presented the highest surface area had lower CO_2 uptake than the carbons activated with KOH at lower temperature and BC/KOH ratio. Thus, ACPS600-K-4 showed the largest CO_2 uptake (3.59 mmol/g) which can be related not only to its high CO_2 BET surface area generated by the ultramicroporosity, but also to its high microporosity which largely favors CO_2 capture [1]. These results are also in agreement with elemental analysis and XPS in which the high oxygen content can favor the CO_2 uptake (Table 4). Conversely, in the low-pressure region the trend is not the same, since ACPS600-K-4 showed the best results followed by the carbons activated with $ZnCl_2$. This can be explained considering that at low pressures the presence of ultra-micropores is responsible for most of CO_2 uptake and these carbons presented the higher microporosity percentages (Table 7) [9]. Additionally, as $ZnCl_2$ activation is less aggressive, surface changes are minor which allows a higher affinity between adsorbent and adsorbate. In general, it is possible to infer that a large surface area (mainly due to low-size pores) and high micropore volume are mandatory requirements in CO_2 uptake as stated in previous investigations [8].

Thus, since all carbons presented higher uptake for CO_2 than for N_2 this makes them possible candidates in separation/purification of gaseous streams.

3.4.2. Influence of temperature on CO_2 and N_2 adsorption

CO_2 adsorption isotherms at three different temperatures (0 ºC, 25 ºC and 50 ºC) were also collected to study in detail the dependence of CO_2 adsorption on temperature. Fig. 8 displays the adsorbed amount of CO_2 as a function of both temperature and pressure for all carbons prepared.

It is observed that all materials present the same tendency, thereby the amount of CO_2 adsorbed decreases with increasing temperature which is in agreement with previous studies [6,47]. This behavior indicates that the capture of CO_2 by the carbons is a physisorption process [8].

As previously mentioned, for the low-pressure region the carbons activated with $ZnCl_2$ and ACPS600-K-4 presented higher amounts of CO_2 adsorbed which could be indicative of a higher affinity for the material and evidence the influence of the ultra-microporosity on the CO_2 capture. Also, other authors mentioned that the ultra-micropores responsible for CO_2 adsorption are dependent on the adsorption temperature. For instance, at 75 ºC they found that only the ultra-micropores in the range of 0.33–0.40 nm were effective [6,9] which can explain the worst behavior with increasing temperature in this work.

Regarding N_2 adsorption, the same behavior with respect to the

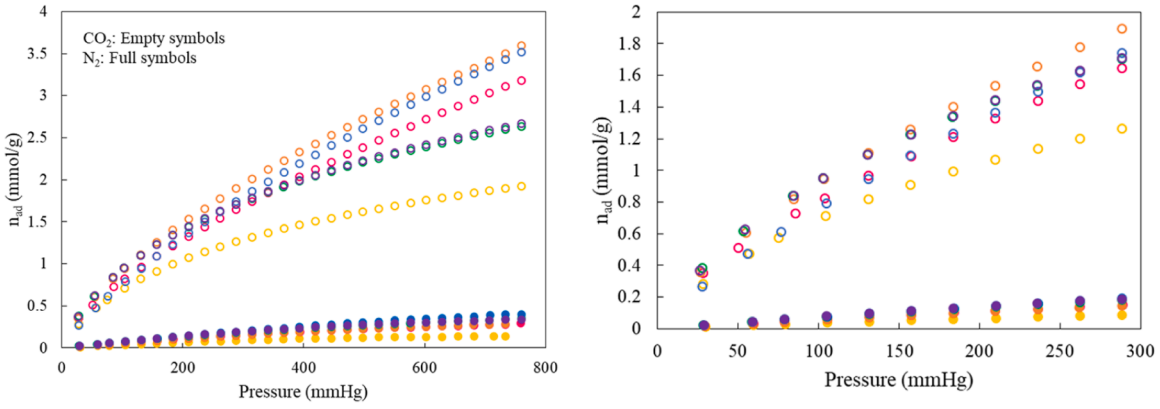

Fig. 7. N_2 and CO_2 adsorption isotherms at 25ºC (right plot is a zoom at the low-pressure range). ● and ○: BC; ● and ○: ACPS850-K-4; ● and ○: ACPS600-K-4; ● and ○: ACPS850-K-2; ● and ○: ACPS850-Z-D; ● and ○: ACPS850-Z-W.

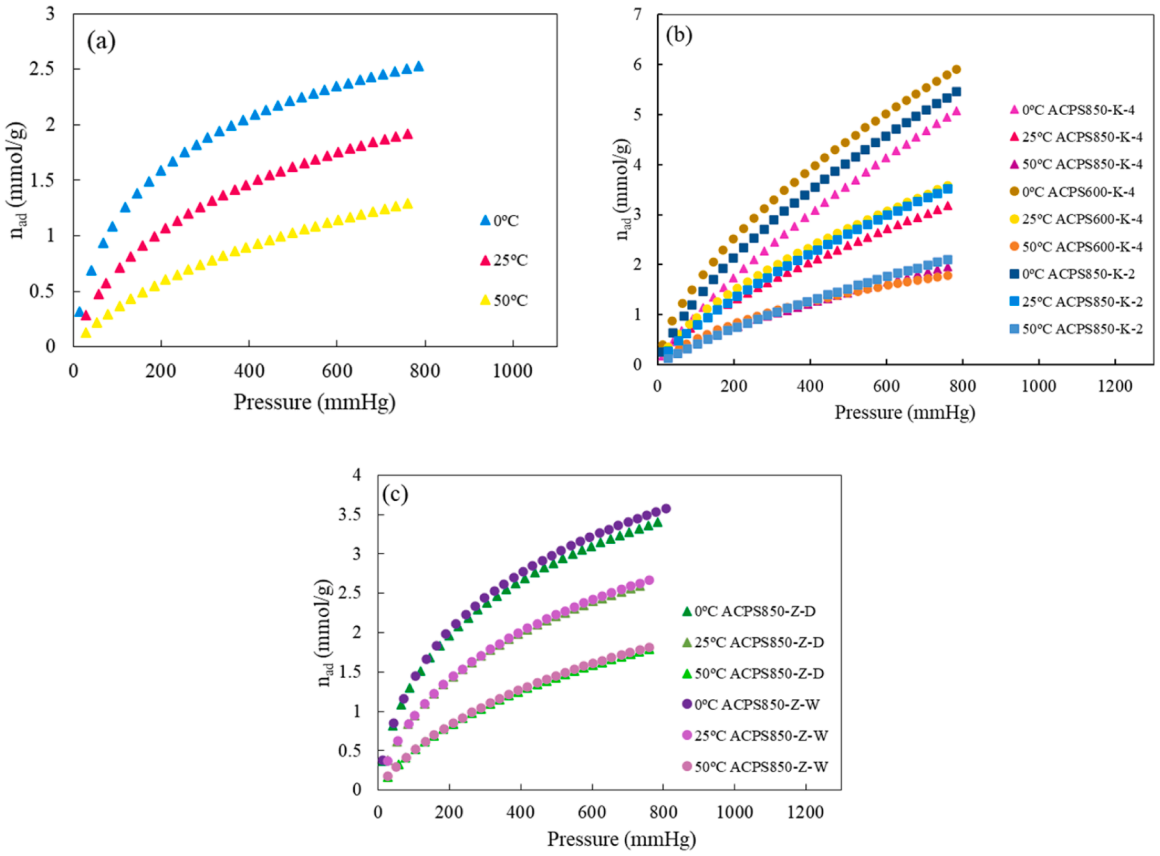

Fig. 8. Adsorption isotherms of CO_2 at different temperature (0 ºC, 25 ºC and 50 ºC) for BC (a) and AC with KOH (b) and $ZnCl_2$ (c).

influence of temperature was observed as for CO_2 adsorption, i.e., a decrease in the amount adsorbed with increasing temperature, being the decrease of N_2 adsorbed more remarkable than for CO_2.

Table 8 lists the CO_2 adsorption capacity of different materials reported in literature. It is noticeable that the pine sawdust derived activated carbon prepared in this study presented a high CO_2 uptake.

Table 8
CO_2 adsorption capacity of different materials reported in literature.

Precursor/ Material	BET Surface area (m^2/g)	Adsorption capacity (mmol/g)	T (ºC)	P (bar)	Reference
Pine nut shell	459–2207	7.7–5.0	0/ 25	1	[6]
Pine nut shell	459–2207	3.3–2.0	0/ 25	0.15	[6]
Pine cone shells	1246–3931	7.6–2.0	0/ 25/ 45	1	[50]
Pine cone shells	1246–3931	2.4–0.6	0/ 25/ 45	0.15	[50]
Water chestnut shell	864–2421	4.5–6.9	25/ 0	1	[51]
Potassium bitartrate	557–1217	3.6–5.2	25/ 0	1	[52]
Petroleum coke	1278	4.2–5.6	25/ 0	1	[53]
Commercial melamine formaldehyde resin	1658	5.0–3.3	0/ 25	1	[54]
Pine sawdust	293–2437	5.8–2.5	0/ 25/ 50	1	This work

Usually, CO_2 adsorption capacity on activated carbons is closely related to their precursors and activating agents. Sawdust is favorable for the preparation of activated carbons since its ordered hollow channels formed after carbonization facilitate the activating agent impregnation and penetration on the pore walls [6].

3.4.3. *N_2 and CO_2 adsorption isotherms at different temperatures*

To better understand and obtain information about the carbon surface properties and their affinity towards both gases, carbon dioxide and nitrogen adsorption experimental data at 0, 25 and 50 ºC were fitted to Langmuir (Eq. (2)), Freundlich (Eq. (3)) and Toth (Eq. (4)) models by means of the Solver tool of Microsoft Excel [55]. Error Sum of Squares (ESS) was employed to assess the performance of the models [1].

Table 9 lists the isotherms parameters for CO_2 adsorption for all carbons at different temperatures and the respective error sum of squares (ESS). Fig. 9 demonstrates, as an example, how the experimental data corresponding to CO_2 adsorption on BC and ACPS850-K-2 fit to Langmuir, Freundlich and Toth models. Toth isotherm best fitted the experimental data for both materials over the entire pressure range for all carbon samples as demonstrate the low ESS values. This model allows to describe the degree of heterogeneity of the multilayer adsorption process.

The t parameter is related to the degree of surface heterogeneity and t values tending to 1 mean that the surface is homogeneous. If t is equal to 1 the Toth model reduces to Langmuir isotherm and if t deviates from 1, the gas-solid system is energetically heterogeneous [9,56]. In this case, t values are between 0.40 and 0.66, therefore, it can be assumed that the surface of all carbons is heterogeneous [1]. In general, an increase in temperature causes a decrease in the adsorption capacity.

Previous investigations suggested that Freundlich model may not be used to describe pure CO_2 adsorption since at high pressures the model cannot explain the sorption behavior [57]. This can be observed in Fig. 9

Table 9
Isotherms parameters for CO_2 adsorption.

	Langmuir			Freundlich			Toth			
T	$n_{m,L}$	K_L	ESS_L	n_F	K_F	ESS_F	$n_{m,T}$	K_T	t	ESS_T
BC										
0	2.99	$6.11{\cdot}10^{-3}$	0.069	2.16	0.127	0.038	4.47	$8.95{\cdot}10^{-3}$	0.53	$1.83{\cdot}10^{-4}$
25	2.56	$3.57{\cdot}10^{-3}$	0.025	1.82	0.053	0.098	4.61	$3.56{\cdot}10^{-3}$	0.53	$1.45{\cdot}10^{-6}$
50	2.09	$2.00{\cdot}10^{-3}$	$7.1{\cdot}10^{-3}$	1.47	0.015	0.035	3.85	$1.40{\cdot}10^{-3}$	0.61	$1.22{\cdot}10^{-4}$
ACPS850-K-4										
0	11.66	$9.17{\cdot}10^{-4}$	0.24	1.23	0.023	0.063	34.69	$3.21{\cdot}10^{-4}$	0.63	0.023
25	5.33	$1.69{\cdot}10^{-3}$	0.22	1.49	0.037	$1.79{\cdot}10^{-3}$	35.27	$4.15{\cdot}10^{-3}$	0.39	0.027
50	3.72	$1.31{\cdot}10^{-3}$	0.062	1.37	0.016	$1.47{\cdot}10^{-4}$	28.53	$2.45{\cdot}10^{-4}$	0.41	$5.97{\cdot}10^{-3}$
ACPS600-K-4										
0	8.86	$2.18{\cdot}10^{-3}$	0.91	1.55	0.082	0.040	20.39	$1.15{\cdot}10^{-3}$	0.57	0.16
25	5.98	$1.74{\cdot}10^{-3}$	0.20	1.47	0.039	0.013	17.34	$7.77{\cdot}10^{-4}$	0.53	0.032
50	4.26	$1.28{\cdot}10^{-3}$	0.057	1.34	0.016	$8.07{\cdot}10^{-3}$	13.63	$4.68{\cdot}10^{-4}$	0.56	$9.11{\cdot}10^{-3}$
ACPS850-K-2										
0	9.64	$1.51{\cdot}10^{-3}$	0.37	1.36	0.042	0.21	42.11	$4.77{\cdot}10^{-4}$	0.46	0.014
25	7.34	$1.13{\cdot}10^{-3}$	0.086	1.30	0.022	0.039	18.27	$5.05{\cdot}10^{-4}$	0.63	0.010
50	5.44	$7.91{\cdot}10^{-4}$	0.019	1.21	0.009	0.011	14.31	$3.17{\cdot}10^{-4}$	0.66	$1.86{\cdot}10^{-3}$
ACPS850-Z-D										
0	4.17	$4.85{\cdot}10^{-3}$	0.183	1.99	0.129	0.42	9.19	$6.81{\cdot}10^{-3}$	0.41	$8.90{\cdot}10^{-5}$
25	3.53	$3.45{\cdot}10^{-3}$	0.062	1.81	0.071	0.14	9.64	$3.37{\cdot}10^{-3}$	0.40	$8.69{\cdot}10^{-4}$
50	2.85	$2.08{\cdot}10^{-3}$	0.016	1.49	0.022	0.064	6.04	$1.38{\cdot}10^{-3}$	0.56	$1.36{\cdot}10^{-4}$
ACPS850-Z-W										
0	4.42	$4.53{\cdot}10^{-3}$	0.174	1.96	0.126	0.42	9.94	$6.28{\cdot}10^{-3}$	0.41	$6.13{\cdot}10^{-4}$
25	3.60	$3.36{\cdot}10^{-3}$	0.051	1.79	0.069	0.14	3.24	$3.11{\cdot}10^{-3}$	0.42	$1.75{\cdot}10^{-4}$
50	2.90	$2.05{\cdot}10^{-3}$	0.018	1.49	0.022	0.064	6.07	$1.36{\cdot}10^{-3}$	0.57	$2.48{\cdot}10^{-4}$

T (°C); $n_{m,L}$ and $n_{m,T}$ (mmol/g); K_L (1/mmHg), K_F (mmol/g·mmHg$^{1/nF}$), K_T (1/mmHg), n_F, t and ESS are dimensionless parameters

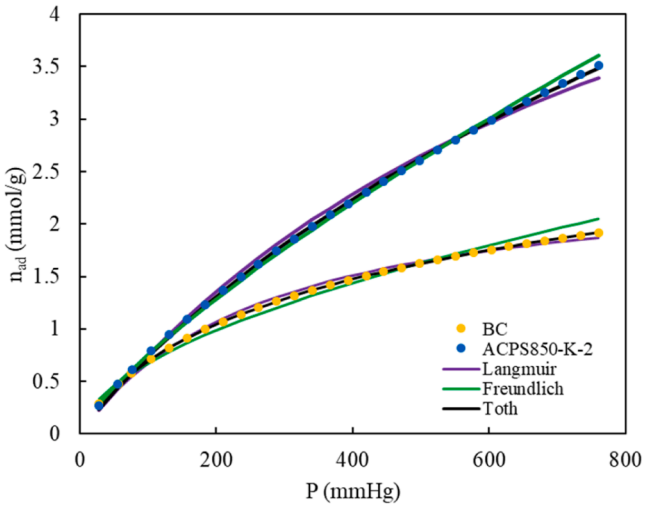

Fig. 9. Experimental CO_2 adsorption data at 25 °C for BC and ACPS850-K-2 and the corresponding fitting curves to Langmuir, Freundlich and Toth models.

especially for BC as above 600 mmHg Freundlich model deviates from the experimental data. However, Freundlich model best fitted ACPS600-K-4 equilibrium data at all temperatures essayed and those for ACPS850-K-4 at 25 and 50 °C.

Similarly, Table 10 shows for all carbons the isotherms parameters for N_2 adsorption at different temperatures and the respective error sum of squares (ESS).

The behavior is similar to that of CO_2 adsorption with a better fit to the Toth isotherm model in most cases, however, as expected the maximum adsorption capacity values are lower for N_2 adsorption due to the less affinity for this gas explained previously.

Regarding t parameter, a high variability among carbons and with changing temperature was found. The good fit to the Toth model shows that in general N_2 molecules were adsorbed in multimolecular layers because of adsorbent surface heterogeneity ($t \neq 1$), also when $t > 1$ lateral interactions between the adsorbed molecules are greater than the adsorptive potential [58]. However, for 0°C the behavior of BC, ACPS600-K-4, ACPS850-Z-D and ACPS850-Z-W carbons changed, t parameter is close to the unity, which means low heterogeneity and may be influenced by the poorer interactions between the N_2 and the surface [56].

3.4.4. CO_2/N_2 selectivity

The great CO_2 uptake ability of carbons previously found promotes the further assessment of their potential application in post combustion CO_2 capture. CO_2/N_2 selectivity is a very important parameter for adsorbent evaluation, and this was determined using single-component gas adsorption isotherms. From the obtained data, interesting information can be extracted regarding the apparent selectivity, or CO_2/N_2 selectivity, which was calculated as follows:

$$S_{CO_2/N_2} = \frac{n_{adCO_2}/P_{CO_2}}{n_{adN_2}/P_{N_2}} \quad (5)$$

where n_{adCO_2} and n_{adN_2} are the uptake capacities (mmol/g) of CO_2 and N_2, respectively, obtained from the isotherm that best fit experimental data at 0 °C. P_{CO_2} and P_{N_2} are the partial pressure of each component at a total pressure of 760 mmHg for a mixture CO_2/N_2 (15 % vol. CO_2).

As mentioned before, a preliminary estimation of the selectivity could be performed using the pure component equilibrium data for CO_2/N_2 separation. Nevertheless, it should be emphasized that the apparent selectivity calculated according to Eq. (5) can lead to conservative estimations since they are determined from the dynamic adsorption of pure components. According to González et al. [59] in a multicomponent system the adsorption of the weak adsorbate, this is nitrogen, could be considerably lower than when it is measured for a pure gas [9].

Table 11 summarizes the results obtained for the CO_2/N_2 selectivity determined by Eq. (5) and adsorption data obtained using the model that best fits the data based on the results shown in Tables 9 and 10, being BC and ACPS600-K-4 the carbons with higher selectivity. Table 12 shows the influence of temperature on selectivity for both materials, showing that selectivity increased with increasing temperature. Both CO_2 and N_2 uptake decreased with increasing temperature, which could be related with a physisorption process, as it was indicated above.

Since the apparent selectivity calculated represents a conservative

Table 10
Isotherms parameters for N_2 adsorption.

	Langmuir			Freundlich			Toth			
T	$n_{m,L}$	K_L	ESS_L	n_F	K_F	ESS_F	$n_{m,T}$	K_T	t	ESS_T
BC										
0	0.82	$7.99{\cdot}10^{-4}$	$1.39{\cdot}10^{-5}$	1.18	$1.19{\cdot}10^{-3}$	$2.12{\cdot}10^{-3}$	0.82	$8.12{\cdot}10^{-4}$	0.99	$9.18{\cdot}10^{-6}$
25	0.27	$1.61{\cdot}10^{-3}$	$2.13{\cdot}10^{-4}$	1.31	$1.07{\cdot}10^{-3}$	$2.18{\cdot}10^{-3}$	0.16	$2.19{\cdot}10^{-3}$	2.07	$1.36{\cdot}10^{-5}$
50	0.08	$4.15{\cdot}10^{-3}$	$3.58{\cdot}10^{-4}$	1.59	$1.12{\cdot}10^{-3}$	$1.35{\cdot}10^{-3}$	0.06	$3.39{\cdot}10^{-3}$	4.56	$7.64{\cdot}10^{-5}$
ACPS850-K-4										
0	2.17	$4.78{\cdot}10^{-4}$	$1.93{\cdot}10^{-5}$	1.11	$1.56{\cdot}10^{-3}$	$3.91{\cdot}10^{-3}$	13.7	$9.21{\cdot}10^{-5}$	0.48	$2.38{\cdot}10^{-4}$
25	0.71	$9.06{\cdot}10^{-4}$	$1.85{\cdot}10^{-4}$	1.19	$1.25{\cdot}10^{-3}$	$3.49{\cdot}10^{-3}$	12.7	$1.06{\cdot}10^{-4}$	0.31	$6.71{\cdot}10^{-4}$
50	0.25	$1.81{\cdot}10^{-3}$	$5.38{\cdot}10^{-4}$	1.35	$1.20{\cdot}10^{-3}$	$3.34{\cdot}10^{-3}$	13.9	$3.79{\cdot}10^{-4}$	0.18	$5.98{\cdot}10^{-5}$
ACPS600-K-4										
0	2.18	$4.7{\cdot}10^{-4}$	$2.02{\cdot}10^{-5}$	1.11	$1.53{\cdot}10^{-3}$	$3.92{\cdot}10^{-3}$	1.70	$5.93{\cdot}10^{-4}$	1.15	$1.10{\cdot}10^{-6}$
25	0.79	$7.91{\cdot}10^{-4}$	$7.41{\cdot}10^{-5}$	1.17	$1.12{\cdot}10^{-3}$	$2.37{\cdot}10^{-3}$	1.18	$5.89{\cdot}10^{-4}$	0.75	$1.20{\cdot}10^{-4}$
50	0.30	$1.48{\cdot}10^{-3}$	$2.80{\cdot}10^{-4}$	1.29	$1.02{\cdot}10^{-3}$	$2.92{\cdot}10^{-3}$	0.96	$8.55{\cdot}10^{-4}$	0.44	$5.73{\cdot}10^{-4}$
ACPS850-K-2										
0	2.84	$4.38{\cdot}10^{-4}$	$1.39{\cdot}10^{-6}$	1.10	$1.81{\cdot}10^{-3}$	$4.69{\cdot}10^{-3}$	8.09	$1.69{\cdot}10^{-4}$	0.63	$1.12{\cdot}10^{-4}$
25	1.27	$6.22{\cdot}10^{-4}$	$9.12{\cdot}10^{-5}$	1.14	$1.30{\cdot}10^{-3}$	$3.57{\cdot}10^{-3}$	1.76	$4.3{\cdot}10^{-4}$	1.22	$1.92{\cdot}10^{-6}$
50	0.54	$1.00{\cdot}10^{-3}$	$2.02{\cdot}10^{-3}$	1.21	$9.86{\cdot}10^{-4}$	$2.02{\cdot}10^{-3}$	1.47	$4.52{\cdot}10^{-4}$	0.55	$2.38{\cdot}10^{-3}$
ACPS850-Z-D										
0	1.45	$9.20{\cdot}10^{-4}$	$1.34{\cdot}10^{-5}$	1.21	$2.67{\cdot}10^{-3}$	$8.33{\cdot}10^{-3}$	1.55	$8.61{\cdot}10^{-4}$	0.96	$1.44{\cdot}10^{-6}$
25	0.83	$9.70{\cdot}10^{-4}$	$1.06{\cdot}10^{-4}$	1.22	$1.63{\cdot}10^{-3}$	$4.43{\cdot}10^{-3}$	0.67	$1.15{\cdot}10^{-3}$	1.17	$6.86{\cdot}10^{-5}$
50	0.38	$1.23{\cdot}10^{-3}$	$2.04{\cdot}10^{-4}$	1.26	$1.03{\cdot}10^{-3}$	$2.51{\cdot}10^{-3}$	0.22	$1.81{\cdot}10^{-3}$	1.92	$1.38{\cdot}10^{-5}$
ACPS850-Z-W										
0	1.43	$1.01{\cdot}10^{-3}$	$7.9{\cdot}10^{-6}$	1.23	$3.08{\cdot}10^{-3}$	$1.09{\cdot}10^{-2}$	1.40	$1.03{\cdot}10^{-3}$	1.02	$6.21{\cdot}10^{-4}$
25	0.73	$1.20{\cdot}10^{-3}$	$3.11{\cdot}10^{-4}$	1.26	$1.94{\cdot}10^{-3}$	$7.03{\cdot}10^{-3}$	0.48	$1.63{\cdot}10^{-3}$	1.57	$2.17{\cdot}10^{-5}$
50	0.31	$1.60{\cdot}10^{-3}$	$4.32{\cdot}10^{-4}$	1.32	$1.25{\cdot}10^{-3}$	$3.54{\cdot}10^{-3}$	0.19	$2.19{\cdot}10^{-3}$	2.35	$3.80{\cdot}10^{-5}$

T (°C); $n_{m,L}$ and $n_{m,T}$ (mmol/g); K_L (1/mmHg), K_F (mmol/g·mmHg$^{1/nF}$), K_T (1/mmHg); n_F, t and ESS are dimensionless parameters

Table 11
Calculated adsorption data of CO_2 and N_2 determined by the isotherm that best fit experimental data at 0°C and the corresponding values of apparent selectivity calculated for all carbons for a CO_2:N_2 (0.15:0.85) mixture.

Sample	n_{ad,CO_2} (mmol/g)	n_{ad,N_2} (mmol/g)	S_{CO_2/N_2}
BC	1.22 (T)	0.28 (T)	24.92
ACPS850-K-4	1.05 (T)	0.51 (L)	11.66
ACPS600-K-4	1.74 (F)	0.51 (T)	19.44
ACPS850-K-2	1.38 (T)	0.63 (L)	12.49
ACPS850-Z-D	1.51 (T)	0.54 (T)	15.87
ACPS850-Z-W	1.50 (T)	0.56 (L)	15.19

F: Freundlich; T: Toth; L: Langmuir.

Table 12
Apparent CO_2/N_2 selectivity, CO_2 and N_2 uptake capacity and IAST selectivity determined by the isotherm that best fit experimental data at 0°C for BC and ACPS600-K-4 carbons for a CO_2:N_2 (0.15:0.85) mixture.

Sample	Temperature (°C)	n_{ad,CO_2} (mmol/g)	n_{ad,N_2} (mmol/g)	S_{CO_2/N_2}	S_{IAST}
BC	0	1.22 (T)	0.28 (T)	24.92	562.03
	25	0.75 (T)	0.13 (T)	32.26	296.50
	50	0.39 (T)	0.06 (T)	36.74	34.46
ACPS600-K-4	0	1.67 (F)	0.51 (T)	19.44	132.87
	25	0.97 (F)	0.37 (L)	20.74	39.73
	50	0.53 (F)	0.14 (L)	26.40	34.65

F: Freundlich; T: Toth; L: Langmuir.

approximation, adsorption selectivity was determined also using the ideal adsorbed solution theory (IAST) and is represented in Fig. 10. IAST is a widely used method for predicting the adsorption equilibrium for components in a mixture using only single component adsorption data at the same temperature and with the same adsorbent. This theory is based on three assumptions: (1) the same surface area is accessible to all adsorbates; (2) the adsorbent is inert; (3) the multicomponent mixture acts as an ideal solution (the strength of interaction is equal between all molecules) at a constant spreading pressure, usually defined as the negative value of the surface tension, and temperature [60,61].

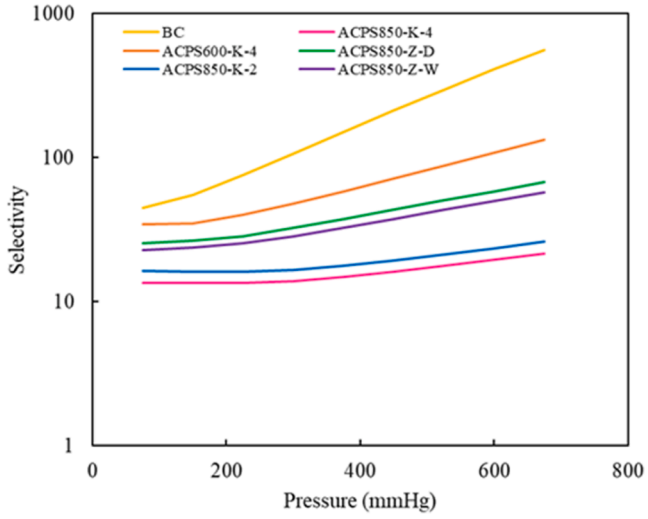

Fig. 10. IAST adsorption selectivity of CO_2 over N_2 calculated at 0 °C for a binary mixture with 15 % CO_2 for all carbons prepared.

From the values of selectivity estimated, it can be confirmed that in all cases CO_2 is preferentially adsorbed over N_2 as reported by Chowdhury & Balasubramanian [56] for other activated carbons derived from biomass, although higher selectivity values were obtained in the present work for carbons based on pine sawdust.

Fig. 10 shows the effect of pressure on CO_2/N_2 selectivity. All materials presented the same trend, however, the effect of pressure on selectivity was more significant for the biochar than for the activated carbons. At higher pressure more CO_2 and N_2 are present, therefore, the competition for adsorption sites intensifies. However, the selectivity significantly raised for the non-activated carbon due to a higher affinity for CO_2 that can be explained by the presence of more functional groups compared to activated carbons, which showed a more homogeneous surface from a chemical point of view, and therefore only a slight increase in selectivity [62].

Moreover, the fundamental role of microporosity on selectivity was

demonstrated as observed in Fig. 11 as an increase in microporosity percentage (%) led to a significant selectivity increase.

Additionally, a considerable decrease in selectivity was observed for those materials with higher surface areas (Fig. 12), which is also related to the previous results. Thus, the activation process with both activated agents, $ZnCl_2$ and KOH, led to an increase in the surface area (and also in the amount of CO_2 adsorbed) but to the loss of surface functional groups and microporosity (mainly in the ultramicroporosity range).

Regarding the selectivity estimated by applying the IAST, an opposite effect of temperature was observed (Table 12) as it decreased with increasing temperature, indicating the importance of competitive adsorption of CO_2/N_2. This finding is in agreement with previous studies employing other types of carbonaceous materials which concluded that CO_2 adsorption is more temperature dependent than N_2 adsorption [63].

3.5. Heat of adsorption

To better understand the behavior of the activated carbons prepared in the separation of carbon dioxide from binary streams, the isosteric heat of CO_2 adsorption (Q_{st}) was determined. The heat of adsorption is a measure of the surface affinity toward CO_2 and indicates the strength of interaction between molecules of the adsorbate and the surface of the adsorbent.

It was calculated using different carbon dioxide loadings which allowed the evaluation of changes in the adsorption mechanisms or in the adsorption sites during the surface coverage process, and the Clausius-Clapeyron equation (Eq. (6)) [1,2]:

$$Q_{st} = R\left[\frac{\partial \ln P}{\partial (1/T)}\right]_{\theta} \quad (6)$$

where Q_{st} (kJ/mol) is the heat of adsorption, R is the ideal gas constant ($8.314 \cdot 10^{-3}$ kJ/mol K), θ is the CO_2 surface coverage at a pressure P (Pa) and temperature T (K). A plot of ln P versus 1/T provides a straight line with a slope of Q_{st}. Also, Toth isotherm parameters were employed (Table 9) since, in general and, as explained previously, this model showed the best fit for the experimental equilibrium data.

Additionally, the results obtained allowed to analyze the influence of the type of material and the amount of gas adsorbed on the CO_2 adsorption isosteric heat as shown in Fig. 13.

It can be observed that, for all materials, the heats of adsorption were low, in the range from 14 to 27 kJ/mol and depended little on the amount of CO_2 adsorbed. Then, it can be concluded that the interactions between the materials and CO_2 correspond to a physical adsorption which implies that these carbons will require a low amount of energy for regeneration which is of great relevance when applying these materials

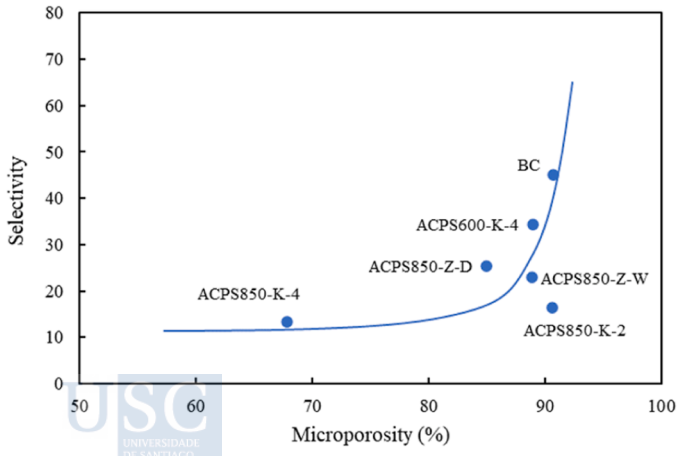

Fig. 11. Influence of the microporosity percentage on the selectivity determined at 0 °C and 75 mmHg.

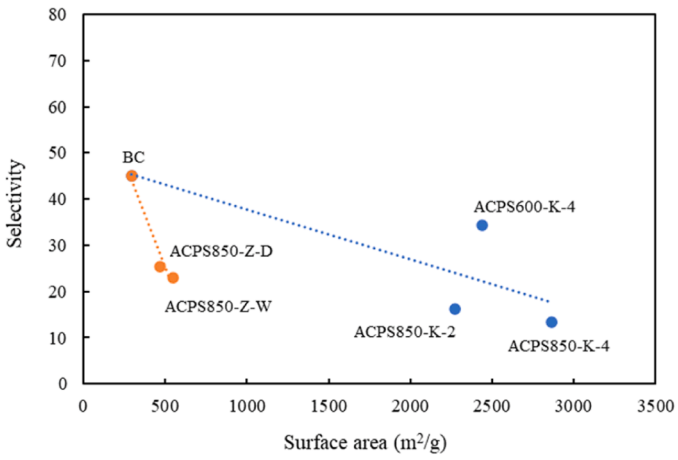

Fig. 12. Influence of the surface area on the selectivity determined at 0 °C and 75 mmHg.

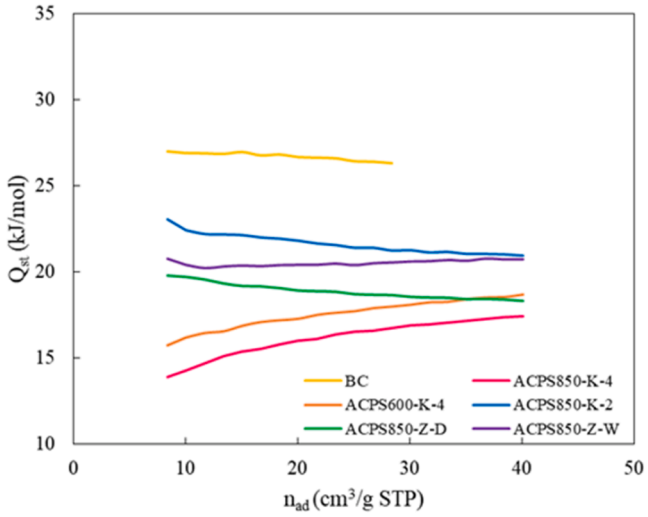

Fig. 13. Influence of amount adsorbed upon isosteric heat of adsorption for CO_2 on the different carbons used.

for the continuous separation of CO_2 from gaseous streams since the costs of the desorption stage will be lower.

On the other hand, the heat of adsorption of the carbons prepared are of the same order than those reported by Manyà et al. [9] for other porous carbons. On the contrary, some previous studies [64,65] showed higher values of the heat of adsorption at low surface coverage related with the presence of active centers on the adsorbent surface that caused a chemical adsorption. However, as mentioned before, for most of the materials, except for the carbons activated with KOH at 1:4 (w/w), there is a low influence of the amount adsorbed upon the heat of adsorption (Fig. 13), which can be related to a low surface heterogeneity.

Among the carbons used, BC presented the highest heat of CO_2 adsorption which is in agreement with the presence of more functional groups on the surface since the activation step did not take place. Regarding the other materials, the carbons activated with the highest amount of KOH, ACPS850-K-4 and ACPS600-K-4, are those that showed the lowest heat of adsorption due to a stronger activation (high temperature and/or BC/KOH ratio) that led to a more homogeneous adsorbent surface.

Besides, different trends of the isosteric heat with the amount of CO_2 adsorbed were observed. For BC, ACPS850-K-2 and ACPS850-Z-D the heat of adsorption decreased with increasing the amount adsorbed, while for ACPS850-K-4 and ACPS600-K-4 increased, and ACPS-850-Z-W

did not show changes. This variation in the trend indicates that small size micropores in carbons are occupied first by CO_2 molecules, which indicates heterogeneous energetic properties of adsorption [8]. On the other hand, the decrease in the isosteric heat can be attributed to the heterogeneous characteristics of the carbon's surface, which implies strong interactions of CO_2 with the carbon surface and negligible intermolecular interaction between CO_2 molecules on the carbon's surface can be assumed [1,66]. Previous studies presented a similar behavior and reported that an increase in isosteric heat could be related to the reinforced intermolecular interaction between the adsorbent and the adsorbate. This behavior implies the multilayer adsorption of CO_2 over the adsorbent.

4. Conclusions

Pine sawdust derived biochar and activated carbons with good CO_2 adsorption properties were successfully prepared through carbonization and activation with KOH or $ZnCl_2$. The experimental results demonstrated that the activating agent had a substantial effect on carbon porosity. All carbons presented an amorphous structure with different degrees of graphitization, C and O as the main components and a branch of functional groups. The microporosity percentage decreased in the next order BC > ACPS850-Z-D > ACPS600-K-4 >ACPS850-Z-W > ACPS850-K-2 >ACPS850-K-4, however, a high microporosity did not imply a high BET surface area. For KOH activation CO_2 uptake improved at moderate conditions (600 ºC). CO_2 uptake can be related with several material characteristics such as micropore geometry and surface chemistry. ACPS600-K-4 displayed the largest CO_2 uptake (5.79 mmol/g at 0 °C and 3.43 mmol/g at 25 °C and 750 mmHg) due to the combination of a high microporosity (89 %) and a high surface area (2437 m^2/g). Moreover, all carbons showed preferential sorption for CO_2 over N_2 and there was a negative effect of temperature on CO_2 adsorption capacity. Toth isotherm model fitted the adsorption experimental data better than Langmuir and Freundlich models in most cases. Furthermore, apparent selectivity and IAST estimated values indicated that BC followed by ACPS600-K-4 showed the best CO_2/N_2 selectivity allowing to reach high purity gas stream. Regarding the heat of CO_2 adsorption, BC presented the highest value which is related with the presence of more functional groups on the surface since the activation step did not take place and in agreement with the high estimated selectivity for BC though this material presents the lowest surface area. On the basis of the results discussed in this work and taking into account various parameters such as the amount of CO_2 adsorbed and the heat of adsorption, ACPS600-K-4 exhibited the best performance since it allowed to reach the highest carbon dioxide uptake, it has the second highest selectivity value combined with the second lowest heat of adsorption. All these findings make this material the most promising option with the appropriate characteristics to be used for CO_2 capture. The results obtained are very promising for the selective separation of CO_2 taking into account that the carbon precursor used is an industrial waste that must be managed.

CRediT authorship contribution statement

Catarina H. Pimentel: Investigation, Data curation, Validation, Visualization, Writing – original draft (catarinahelena.dasilveira@rai.usc.es). **L. Díaz-Fernández**: Investigation, Data curation, Validation, Conducted the experiments and data/evidence collection (lidiadife@gmail.com). **Diego Gómez-Díaz**: Conceptualization, Methodology, Supervision, Verified the accuracy of the results, Funding acquisition, Writing—review & editing (diego.gomez@usc.es). **M. Sonia Freire**: Conceptualization, Methodology, Supervision, Verified the accuracy of the results, Funding acquisition, Writing—review & editing (mariasonia.freire@usc.es). **Julia González-Álvarez**: Conceptualization, Methodology, Supervision, Funding acquisition, Writing—review & editing (julia.gonzalez@usc.es).

Declaration of Competing Interest

The authors declare that they have no known competing financial interests or personal relationships that could have appeared to influence the work reported in this paper.

Data availability

Data will be made available on request.

Acknowledgments

This work was supported by Xunta de Galicia (ED431B 2020/039) and by MCIN/AEI /10.13039/501100011033 / FEDER, UE (PID2021–122923NB-I00). Authors would like to thank the use of RIAIDT-USC analytical facilities.

Appendix A. Supporting information

Supplementary data associated with this article can be found in the online version at doi:10.1016/j.jece.2023.111378.

References

[1] J. Serafin, U. Narkiewicz, A.W. Morawski, R.J. Wróbel, B. Michalkiewicz, Highly microporous activated carbons from biomass for CO_2 capture and effective micropores at different conditions, J. CO_2 Util. 18 (2017) 73–79, https://doi.org/10.1016/j.jcou.2017.01.006.

[2] G. Sethia, A. Sayari, Comprehensive study of ultra-microporous nitrogen-doped activated carbon for CO_2 capture, Carbon 93 (2015) 68–80, https://doi.org/10.1016/j.carbon.2015.05.017.

[3] I.S. Ismail, N.A. Rashidi, S. Yusup, Production and characterization of bamboo-based activated carbon through single-step H3PO4 activation for CO_2 capture, Environ. Sci. Pollut. Res. 29 (2022) 12434–12440, https://doi.org/10.1007/s11356-021-15030-x.

[4] N. Abuelnoor, A. AlHajaj, M. Khaleel, L.F. Vega, M.R.M. Abu-Zahra, Activated carbons from biomass-based sources for CO_2 capture applications, Chemosphere 282 (2021), 131111, https://doi.org/10.1016/j.chemosphere.2021.131111.

[5] A. Sarwar, M. Ali, A. Hussain, A. Nawar, A. Waqas, R. Liaquat, S. Raza, M. Asjid, Synthesis and characterization of biomass-derived surface-modified activated carbon for enhanced CO2 adsorption, J. CO_2 Util. 46 (2021), 101476, https://doi.org/10.1016/j.jcou.2021.101476.

[6] S. Deng, H. Wei, T. Chen, B. Wang, J. Huang, G. Yu, Superior CO_2 adsorption on pine nut shell-derived activated carbons and the effective micropores at different temperatures, Chem. Eng. J. 253 (2014) 46–54, https://doi.org/10.1016/j.cej.2014.04.115.

[7] W. Hao, E. Björkman, M. Lilliestråle, N. Hedin, Activated carbons prepared from hydrothermally carbonized waste biomass used as adsorbents for CO 2, Appl. Energy 112 (2013) 526–532, https://doi.org/10.1016/j.apenergy.2013.02.028.

[8] G. Huang, Y. Liu, X. Wu, J. Cai, Activated carbons prepared by the KOH activation of a hydrochar from garlic peel and their CO 2 adsorption performance, N. Carbon Mater. 34 (2019) 247–257, https://doi.org/10.1016/S1872-5805(19)60014-4.

[9] J.J. Manyà, B. González, M. Azuara, G. Arner, Ultra-microporous adsorbents prepared from vine shoots-derived biochar with high CO_2 uptake and CO_2/N2 selectivity, Chem. Eng. J. 345 (2018) 631–639, https://doi.org/10.1016/j.cej.2018.01.092.

[10] C.I. Orozco, M.S. Freire, D. Gómez-díaz, J. González-álvarez, Removal of copper from aqueous solutions by biosorption onto pine sawdust, 32, 2023. ⟨https://doi.org/10.1016/j.scp.2023.101016⟩.

[11] K.A. Adegoke, O.O. Adesina, O.A. Okon-Akan, O.R. Adegoke, A.B. Olabintan, O. A. Ajala, H. Olagoke, N.W. Maxakato, O.S. Bello, Sawdust-biomass based materials for sequestration of organic and inorganic pollutants and potential for engineering applications, Curr. Res. Green Sustain. Chem. 5 (2022), 100274, https://doi.org/10.1016/j.crgsc.2022.100274.

[12] S. Mallakpour, F. Sirous, C.M. Hussain, Sawdust, a versatile, inexpensive, readily available bio-waste: from mother earth to valuable materials for sustainable remediation technologies, Adv. Colloid Interface Sci. 295 (2021), 102492, https://doi.org/10.1016/j.cis.2021.102492.

[13] S. Velusamy, A. Roy, S. Sundaram, T. Kumar Mallick, A review on heavy metal ions and containing dyes removal through graphene oxide-based adsorption strategies for textile wastewater treatment, Chem. Rec. 21 (2021) 1570–1610, https://doi.org/10.1002/tcr.202000153.

[14] C. Quan, R. Su, N. Gao, Preparation of activated biomass carbon from pine sawdust for supercapacitor and CO_2 capture, Int. J. Energy Res. 44 (2020) 4335–4351, https://doi.org/10.1002/er.5206.

[15] A.D. Igalavithana, S.W. Choi, J. Shang, A. Hanif, P.D. Dissanayake, D.C.W. Tsang, J.H. Kwon, K.B. Lee, Y.S. Ok, Carbon dioxide capture in biochar produced from pine sawdust and paper mill sludge: effect of porous structure and surface

chemistry, Sci. Total Environ. 739 (2020), 139845, https://doi.org/10.1016/j.scitotenv.2020.139845.
[16] C.H. Pimentel, M.S. Freire, D. Gómez-Díaz, J. González-Álvarez, Preparation of activated carbon from pine (Pinus radiata) sawdust by chemical activation with zinc chloride for wood dyes adsorption, Biomass Convers. Biorefin. (2023), https://doi.org/10.1007/s13399-023-04138-4.
[17] O.E. Eleri, K.U. Azuatalam, M.W. Minde, A.M. Trindade, N. Muthuswamy, F. Lou, Z. Yu, Towards high-energy-density supercapacitors via less-defects activated carbon from sawdust, Electrochim. Acta 362 (2020), 137152, https://doi.org/10.1016/j.electacta.2020.137152.
[18] M.B. Ahmed, M.A. Hasan Johir, J.L. Zhou, H.H. Ngo, L.D. Nghiem, C. Richardson, M.A. Moni, M.R. Bryant, Activated carbon preparation from biomass feedstock: clean production and carbon dioxide adsorption, J. Clean. Prod. 225 (2019) 405–413, https://doi.org/10.1016/j.jclepro.2019.03.342.
[19] E. Dautzenberg, S. van Hurne, M.M.J. Smulders, L.C.P.M. de Smet, GraphIAST: a graphical user interface software for ideal adsorption solution theory (IAST) calculations, Comput. Phys. Commun. 280 (2022), 108494, https://doi.org/10.1016/j.cpc.2022.108494.
[20] M.A. Yahya, Z. Al-Qodah, C.W.Z. Ngah, Agricultural bio-waste materials as potential sustainable precursors used for activated carbon production: a review, Renew. Sustain. Energy Rev. 46 (2015) 218–235, https://doi.org/10.1016/j.rser.2015.02.051.
[21] M. Danish, T. Ahmad, A review on utilization of wood biomass as a sustainable precursor for activated carbon production and application, Renew. Sustain. Energy Rev. 87 (2018) 1–21, https://doi.org/10.1016/j.rser.2018.02.003.
[22] Ö. Akçakal, M. Şahin, M. Erdem, Synthesis and characterization of high-quality activated carbons from hard-shelled agricultural wastes mixture by zinc chloride activation, Chem. Eng. Commun. 206 (2019) 888–897, https://doi.org/10.1080/00986445.2018.1534231.
[23] A. Tomczyk, Z. Sokołowska, P. Boguta, Biomass type effect on biochar surface characteristic and adsorption capacity relative to silver and copper, Fuel 278 (2020), https://doi.org/10.1016/j.fuel.2020.118168.
[24] Z. Heidarinejad, M.H. Dehghani, M. Heidari, G. Javedan, I. Ali, M. Sillanpää, Methods for preparation and activation of activated carbon: a review, Environ. Chem. Lett. 18 (2020) 393–415, https://doi.org/10.1007/s10311-019-00955-0.
[25] R. Chikri, N. Elhadiri, M. Benchanaa, Y. El maguana, Efficiency of sawdust as low-cost adsorbent for dyes removal, J. Chem. 2020 (2020) 1–17, https://doi.org/10.1155/2020/8813420.
[26] D. Angin, E. Altintig, T.E. Köse, Influence of process parameters on the surface and chemical properties of activated carbon obtained from biochar by chemical activation, Bioresour. Technol. 148 (2013) 542–549, https://doi.org/10.1016/J.BIORTECH.2013.08.164.
[27] Z. Zhang, X. Luo, Y. Liu, P. Zhou, G. Ma, Z. Lei, L. Lei, A low cost and highly efficient adsorbent (activated carbon) prepared from waste potato residue, J. Taiwan Inst. Chem. Eng. 49 (2015) 206–211, https://doi.org/10.1016/J.JTICE.2014.11.024.
[28] M. Erdem, R. Orhan, M. Şahin, E. Aydın, Preparation and characterization of a novel activated carbon from vine shoots by ZnCl2 activation and investigation of its rifampicine removal capability, Water Air Soil Pollut. 227 (2016) 1–14, https://doi.org/10.1007/S11270-016-2929-5/FIGURES/11.
[29] R.L. Tseng, S.K. Tseng, Characterization and use of high surface area activated carbons prepared from cane pith for liquid-phase adsorption, J. Hazard. Mater. 136 (2006) 671–680, https://doi.org/10.1016/J.JHAZMAT.2005.12.048.
[30] A.H. Basta, V. Fierro, H. El-Saied, A. Celzard, 2-Steps KOH activation of rice straw: an efficient method for preparing high-performance activated carbons, Bioresour. Technol. 100 (2009) 3941–3947, https://doi.org/10.1016/J.BIORTECH.2009.02.028.
[31] A.N.A. El-Hendawy, An insight into the KOH activation mechanism through the production of microporous activated carbon for the removal of Pb2+ cations, Appl. Surf. Sci. 255 (2009) 3723–3730, https://doi.org/10.1016/J.APSUSC.2008.10.034.
[32] M. Jaouadi, Characterization of activated carbon, wood sawdust and their application for boron adsorption from water, Int. Wood Prod. J. 12 (2021) 22–33, https://doi.org/10.1080/20426445.2020.1785605.
[33] S. Álvarez-Torrellas, M. Muñoz, J.A. Zazo, J.A. Casas, J. García, Synthesis of high surface area carbon adsorbents prepared from pine sawdust-Onopordum acanthium L. for nonsteroidal anti-inflammatory drugs adsorption, J. Environ. Manag. 183 (2016) 294–305, https://doi.org/10.1016/j.jenvman.2016.08.077.
[34] E. Köseoğlu, C. Akmil-Başar, Preparation, structural evaluation and adsorptive properties of activated carbon from agricultural waste biomass, Adv. Powder Technol. 26 (2015) 811–818, https://doi.org/10.1016/j.apt.2015.02.006.
[35] Q. Li, S. Liu, W. Peng, W. Zhu, L. Wang, F. Chen, J. Shao, X. Hu, Preparation of biomass-derived porous carbons by a facile method and application to CO_2 adsorption, J. Taiwan Inst. Chem. Eng. 116 (2020) 128–136, https://doi.org/10.1016/j.jtice.2020.11.001.
[36] Q. Pu, J. Zou, J. Wang, S. Lu, P. Ning, L. Huang, Q. Wang, Systematic study of dynamic CO_2 adsorption on activated carbons derived from different biomass, J. Alloy. Compd. 887 (2021), 161406, https://doi.org/10.1016/j.jallcom.2021.161406.
[37] V. Benedetti, E. Cordioli, F. Patuzzi, M. Baratieri, CO_2 Adsorption study on pure and chemically activated chars derived from commercial biomass gasifiers, J. CO_2 Util. 33 (2019) 46–54, https://doi.org/10.1016/j.jcou.2019.05.008.
[38] E. Yagmur, Y. Gokce, S. Tekin, N.I. Semerci, Z. Aktas, Characteristics and comparison of activated carbons prepared from oleaster (Elaeagnus angustifolia L.) fruit using KOH and ZnCl2, Fuel 267 (2020), 117232, https://doi.org/10.1016/j.fuel.2020.117232.
[39] Z. Liu, Y. Huang, Z. Guangjie, Preparation and characterization of activated carbon fibers from liquefied wood by ZnCl2 activation, BioResources 11 (2016) 3178–3190, https://doi.org/10.15376/biores.11.2.3178-3190.
[40] V. Siipola, T. Tamminen, A. Källi, R. Lahti, H. Romar, K. Rasa, R. Keskinen, J. Hyväluoma, M. Hannula, H. Wikberg, Effects of biomass type, carbonization process, and activation method on the properties of bio-based activated carbons, BioResources 13 (2019) 5976–6002, https://doi.org/10.15376/biores.13.3.5976-6002.
[41] S. Marzeddu, M.A. Décima, L. Camilli, M.P. Bracciale, V. Genova, L. Paglia, F. Marra, M. Damizia, M. Stoller, A. Chiavola, M.R. Boni, Physical-chemical characterization of different carbon-based sorbents for environmental applications, Materials 15 (2022) 1–29, https://doi.org/10.3390/ma15207162.
[42] N.A. Rashidi, S. Yusup, Biochar as potential precursors for activated carbon production: parametric analysis and multi-response optimization, Environ. Sci. Pollut. Res. 27 (2020) 27480–27490, https://doi.org/10.1007/s11356-019-07448-1.
[43] Y. Tadjenant, N. Dokhan, A. Barras, A. Addad, R. Jijie, S. Szunerits, R. Boukherroub, Graphene oxide chemically reduced and functionalized with KOH-PEI for efficient Cr(VI) adsorption and reduction in acidic medium, Chemosphere 258 (2020), 127316, https://doi.org/10.1016/j.chemosphere.2020.127316.
[44] S. Shi, Y. Liu, Nitrogen-doped activated carbons derived from microalgae pyrolysis by-products by microwave/KOH activation for CO_2 adsorption, Fuel 306 (2021), 121762, https://doi.org/10.1016/j.fuel.2021.121762.
[45] Y.J. Zhang, Z.J. Xing, Z.K. Duan, M. Li, Y. Wang, Effects of steam activation on the pore structure and surface chemistry of activated carbon derived from bamboo waste, Appl. Surf. Sci. 315 (2014) 279–286, https://doi.org/10.1016/j.apsusc.2014.07.126.
[46] M. Thommes, K. Kaneko, A.V. Neimark, J.P. Olivier, F. Rodriguez-Reinoso, J. Rouquerol, K.S.W. Sing, Physisorption of gases, with special reference to the evaluation of surface area and pore size distribution (IUPAC technical report, Pure Appl. Chem. 87 (2015) 1051–1069, https://doi.org/10.1515/pac-2014-1117.
[47] I. Durán, F. Rubiera, C. Pevida, Separation of CO_2 in a solid waste management incineration facility using activated carbon derived from pine sawdust, Energies 10 (2017), https://doi.org/10.3390/en10060827.
[48] L. Domínguez-Ramos, A. Prieto-Estalrich, G. Malucelli, D. Gómez-Díaz, M.S. Freire, M. Lazzari, J. González-álvarez, N- and S-doped carbons derived from polyacrylonitrile for gases separation, Sustain 14 (2022) 3760, https://doi.org/10.3390/SU14073760.
[49] R. Janu, V. Mrlik, D. Ribitsch, J. Hofman, P. Sedláček, L. Bielská, G. Soja, Biochar surface functional groups as affected by biomass feedstock, biochar composition and pyrolysis temperature, Carbon Resour. Convers. 4 (2021) 36–46, https://doi.org/10.1016/j.crcon.2021.01.003.
[50] K. Li, S. Tian, J. Jiang, J. Wang, X. Chen, F. Yan, Pine cone shell-based activated carbon used for CO_2 adsorption, J. Mater. Chem. A. 4 (2016) 5223–5234, https://doi.org/10.1039/C5TA09908K.
[51] C. Ma, J. Bai, M. Demir, X. Hu, S. Liu, L. Wang, Water chestnut shell-derived N/S-doped porous carbons and their applications in CO_2 adsorption and supercapacitor, Fuel 326 (2022), 125119, https://doi.org/10.1016/j.fuel.2022.125119.
[52] T. Lu, J. Bai, M. Demir, X. Hu, J. Huang, L. Wang, Synthesis of potassium Bitartrate-derived porous carbon via a facile and self-activating strategy for CO_2 adsorption application, Sep. Purif. Technol. 296 (2022), 121368, https://doi.org/10.1016/j.seppur.2022.121368.
[53] J. Bai, J. Huang, Q. Yu, M. Demir, F.H. Gecit, B.N. Altay, L. Wang, X. Hu, One-pot synthesis of self S-doped porous carbon for efficient CO_2 adsorption, Fuel Process. Technol. 244 (2023), 107700, https://doi.org/10.1016/j.fuproc.2023.107700.
[54] Q. Yu, J. Bai, J. Huang, M. Demir, A.A. Farghaly, P. Aghamohammadi, X. Hu, L. Wang, One-pot synthesis of melamine formaldehyde resin-derived N-doped porous carbon for CO_2 capture application, Molecules 28 (2023), https://doi.org/10.3390/molecules28041772.
[55] K.A. Babatunde, B.M. Negash, S.R. Jufar, T.Y. Ahmed, M.R. Mojid, Adsorption of gases on heterogeneous shale surfaces: a review, J. Pet. Sci. Eng. 208 (2022), 109466, https://doi.org/10.1016/J.PETROL.2021.109466.
[56] S. Chowdhury, R. Balasubramanian, Three-dimensional graphene-based porous adsorbents for postcombustion CO_2 capture, Ind. Eng. Chem. Res. 55 (2016) 7906–7916, https://doi.org/10.1021/acs.iecr.5b04052.
[57] M. Mabuza, K. Premlall, M.O. Daramola, Modelling and thermodynamic properties of pure - CO 2 and flue gas sorption data on South African coals using Langmuir, Freundlich, Temkin, and extended Langmuir isotherm models, Int. J. Coal Sci. Technol. (2022), https://doi.org/10.1007/s40789-022-00515-y.
[58] A.P. Terzyk, J. Chatłas, P.A. Gauden, G. Rychlicki, P. Kowalczyk, Developing the solution analogue of the Toth adsorption isotherm equation, J. Colloid Interface Sci. 266 (2003) 473–476, https://doi.org/10.1016/S0021-9797(03)00569-1.
[59] A.S. González, M.G. Plaza, F. Rubiera, C. Pevida, Sustainable biomass-based carbon adsorbents for post-combustion CO_2 capture, Chem. Eng. J. 230 (2013) 456–465, https://doi.org/10.1016/J.CEJ.2013.06.118.
[60] A.L. Myers, J.M. Prausnitz, Thermodynamics of mixed-gas adsorption, AIChE J. 11 (1965) 121–127, https://doi.org/10.1002/AIC.690110125.
[61] N.F. Cessford, N.A. Seaton, T. Dü, Evaluation of ideal adsorbed solution theory as a tool for the design of metal−organic framework, Materials (2012), https://doi.org/10.1021/ie202219w.
[62] W. Lu, W.M. Verdegaal, J. Yu, P.B. Balbuena, H.K. Jeong, H.C. Zhou, Building multiple adsorption sites in porous polymer networks for carbon capture applications, Energy Environ. Sci. 6 (2013) 3559–3564, https://doi.org/10.1039/C3EE42226G.
[63] C. Landaverde-Alvarado, A.J. Morris, S.M. Martin, Gas sorption and kinetics of CO_2 sorption and transport in a polymorphic microporous MOF with open Zn (II)

coordination sites, J. CO_2 Util. 19 (2017) 40–48, https://doi.org/10.1016/J.JCOU.2017.01.029.

[64] L.B. Sun, Y.H. Kang, Y.Q. Shi, Y. Jiang, X.Q. Liu, Highly selective capture of the greenhouse gas CO_2 in polymers, ACS Sustain. Chem. Eng. 3 (2015) 3077–3085, https://doi.org/10.1021/acssuschemeng.5b00544.

[65] C. Xu, Adsorption of CO_2 on a micro-/mesoporous polyimine modified with tris (2-aminoethyl) amine, J. Mater. Chem. A 3 (2015) 16229–16234.

[66] Y. Guo, C. Tan, J. Sun, W. Li, J. Zhang, C. Zhao, Porous activated carbons derived from waste sugarcane bagasse for CO_2 adsorption, Chem. Eng. J. 381 (2020), 122736, https://doi.org/10.1016/j.cej.2019.122736.

Electronic Supplementary Information

Separation of CO_2 using biochar and KOH and $ZnCl_2$ activated carbons derived from pine sawdust

Catarina H. Pimentel, M. Sonia Freire, Diego Gómez-Díaz and Julia González-Álvarez*

Department of Chemical Engineering, School of Engineering, Universidade de Santiago de Compostela, Rúa Lope Gómez de Marzoa s/n, 15782 Santiago de Compostela, Spain.

* corresponding author: julia.gonzalez@usc.es (Tel.: +34 881816761)

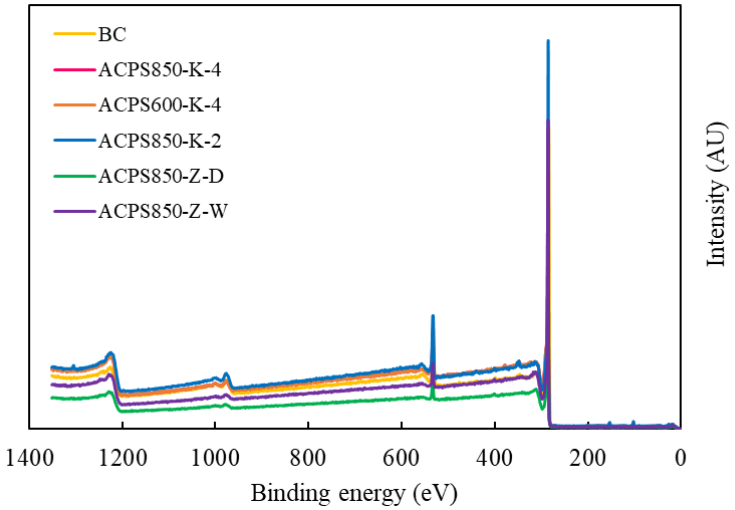

Fig. S1. XPS curve of BC and activated carbons from pine sawdust.

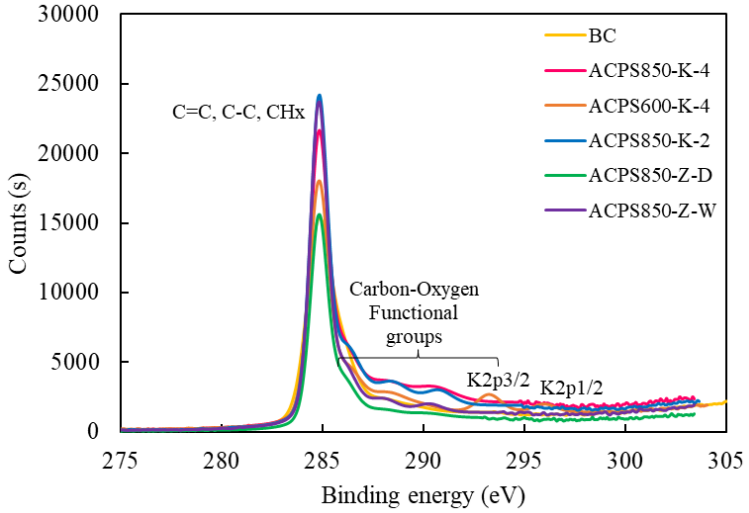

Fig. S2. C1s high resolution XPS spectra of carbons.

5. UNPUBLISHED WORK

Removal of wood dyes from aqueous solutions using KOH chemically activated carbons from pine (*Pinus radiata*) sawdust

Catarina Helena Pimentel, Rubén Castro-Agra, María Sonia Freire, Diego Gómez-Díaz, Julia González-Álvarez*

Department of Chemical Engineering, School of Engineering, Universidade de Santiago de Compostela, Santiago de Compostela, 15782, Spain

Keywords: Pine sawdust, Chemical activation, Activated carbons, Wood dyes, Adsorption, Desorption

Abstract

Chemically activated carbons synthesized from pine sawdust were applied efficiently for the elimination of wood dyes from aqueous solutions. Different proportions (1:2 and 1:4) of activating agent (KOH) and activation temperatures (600 and 850ºC) were used. Carbon surface morphology was characterized. The effect of pH (2-12), initial adsorbate concentration (5-500 mg L^{-1}) and carbon dosage (0.1-0.5 g L^{-1}) on dye adsorption were studied on batch mode. Langmuir model described well the adsorption equilibrium. The maximum found adsorption capacities were 1221.58, 1673.03 and 240.38 mg g^{-1} for blue and red at 500 mg L^{-1} and black at 100 mg L^{-1}, respectively, using activated carbon at 850ºC and 1:4 (ACPS-4-850), at 25ºC, adsorbent dose 0.4 g L^{-1} for blue and black and 0.3 g L^{-1} for red dye and without change the pH for blue and red and at pH = 2 for black dye. The pseudo second order model explained the kinetics of adsorption except for the black dye at 100 mg L^{-1} using ACPS-4-850 for which it was the pseudo first order model. Desorption studies performed with ACPS-4-850 revealed that the adsorption was irreversible by chemical regeneration, whereas for the black dye, regeneration was efficient using H_2O_2 as desorbing agent.

Graphical Abstract

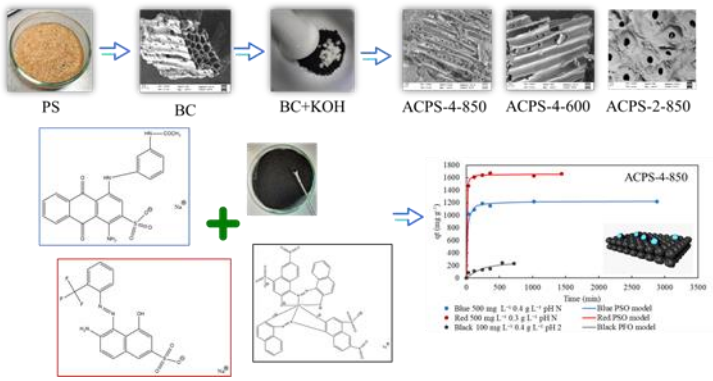

1. Introduction

A huge concern in the past years is the contamination of the aquatic environment. Various industries such as textile, food, wood, paper, etc., are an significant source of this contamination due to the use of great amounts of dyes to color their products that are subsequently directly or indirectly released into the water system [1,2]. The release of synthetic dyes in water streams, if not treated properly, will dramatically affect the ecosystem at long term because wastewaters are not easily biodegradable and due to the stable and complex chemical structure of dyes, beyond what affects aesthetically [3]. It is possible to classify dyes in three groups: anionic (substantive, acidic, and reactive dyes), cationic (alkaline dyes) and non-ionic (granulate dye) [4]. It was estimated that there are more than 100,000 types of dyes available in the world and, the textile industry discharges nearby 280,000 tons of dyes into water streams each year [5]. These

* Corresponding author.
School of Engineering, Rúa Lope Gómez de Marzoa s/n 15782 Santiago de Compostela, Spain. Telephone: +34 881816761; E-mail address: julia.gonzalez@usc.es

dyes are dangerous not only for the aquatic biota but also for the human health because some of them presented toxicity and carcinogenicity. Moreover, they also accumulate in the food chain, and consequently in the human body which demanded their treatment before discharged to the environment [1,6].

Therefore, the treatment of wastewater polluted by dyes is an issue of worldwide interest. Numerous techniques such as coagulation, flocculation, chemical oxidation, membrane process, electrochemical process, filtration, reverse osmosis, ion exchange, advance oxidation, evaporation and magnetic separations, etc. have been used for the elimination of organic pollutants from water system [4,7]. Among them, adsorption was revealed to be one of the most effective ones, due to its characteristics of easy operation, environment-friendly, cost-effective, low health risk, sensitivity towards noxious pollutants, and non-destructive process [8]. Porous materials, which recently have received considerable attention, can be modified to a desired degree of porosity through the use of different activation methods, conditions and raw materials [9]. The term activated carbon (AC) refers to a material rich in carbon and with a well-designed internal pore structure, and it is the most used as adsorbent at large scale. AC is characterized by a high surface area that usually relates to adsorption capacity, well organized porous structure, favorable thermal stability, mechanical strength and a variability of chemical functional groups on the surface [7,9,10]. However, the manufacture of AC using non-renewable materials (like coal, lignite, peat, petroleum) is still expensive and require intensive energy, whereby numerous industrial and agricultural materials have been investigated as promising raw resources to produce AC due to their natural abundance and lack of toxicity [7]. In particular, lignocellulosic precursors arise as promising green precursors in AC preparations since they are renewable, abundantly available, ecologically suitable, and cost effective [9]. In literature, various biomass materials were investigated to produce AC for dye adsorption such as stones of *Ziziphus nummularia*, *Intsia bijuga* sawdust, rubber seed and its shell, and *Cornulaca monacantha* stem [3,4,6,7]. Usually, the synthesis of AC comprises two steps: (1) the carbonization of the precursor and (2) its physical (with CO_2 or water vapor) or chemical (with KOH, H_3PO_4 or $ZnCl_2$) activation leading to an enhanced porous AC [3]. Generally, with chemical treatment the -OH and phenolic groups of lignocellulosic materials can be replaced with negatively charged groups from the activated agents which can increase the adsorption capacity, mainly for cationic dyes [9]. Additionally, the activation can be realized through direct chemical activation (physical mixing) or by impregnation in which the precursor carbonization step is often eliminated. Regarding the porosity, carbonaceous materials can achieve values as low as 1 nm for pore width and the surface area can reach 2500 m^2 g^{-1} [11]. Potassium hydroxide has been broadly used to produce low-cost AC since it is eco-friendly, leads to the increased oxygen functionality develops on carbon surfaces, generates high surface area, taylored pore size distribution, low environmental pollution, and less corrosiveness. Moreover, previous studies presented the effectiveness of KOH-AC for dyes adsorption [12,13].

Since the precursor's characteristics and the conditions of preparation strongly influence the AC characteristics, it is important a careful choice of the precursor which implies to consider the local availability and price of the material [3]. *Pinus radiata* stands out as flexible, quick-growing, medium-density softwood with a wide range of applications. It was assessed that there was more than $4x10^6$ ha of this pine species were planted throughout the world in 2013 and is still one of the species of trees that is widely planted today, mostly in the southern hemisphere. These types of woods are used in pulp and paper industries as well as for furniture and construction and substantial amount of waste are created during the harvesting (twigs, branches, stumps…) and processing (wood chips, sawdust…) activities are produced [14,15]. Mainly in Galicia (northwestern Spain), *Pinus radiata* which is the most frequently employed exotic conifer for reforestation, it is predicted to cover an area of 90,000 ha [16]. Particularly, pine sawdust (PS) from *Pinus radiata* is a low cost and abundantly available residue often discarded as waste or burnt to produce bioenergy, so its re-use to produce activated carbons can be very worthwhile both for waste treatment and pollution reduction. Studies on dyes adsorption by AC derived from pine sawdust are limited [17–20], and there are no studies with wood dyes. Thus, the objective of this investigation work is to produce one biochar and three activated carbons produced from pine sawdust biomass and assess its adsorption capacity to eliminate blue, red and black acid wood dyes. After carbonization, pine sawdust was chemically activated through pyrolysis method and using KOH to improve the surface area and porosity

trying to enhance dye adsorption. The determination of point of zero charge (pH_{PZC}), and scanning electron microscopy together with energy-dispersive X-ray spectrometry (SEM-EDX) and FTIR analyses were employed to have a characterization of the adsorbents. Kinetic and equilibrium studies were conducted in controlled settings to evaluate the adsorption mechanism.

2. Experiments and methods

2.1. Chemicals

Potassium hydroxide (KOH, 85%, Probus), hydrochloric acid (HCl, 37%, Sigma Aldrich) and hydrogen peroxide (H2O2, 33%, Quimipur) were used as received. Acid dyes: blue for wood AGN-270% ($C_{22}H_{16}N_3NaO_6S$), red for wood GRA-200% ($C_{17}H_{11}F_3N_3NaO_4S^+$), and black Hispalan M-RN-140% ($C_{40}H_{20}CrN_6NaO_{14}S_2^{-2}$) were supplied by a wood company in Galicia (Spain). The chemical structure of the wood dyes is shown in Fig. 1. Standard solutions were set at 500 mg L^{-1}, and the solutions with the necessary concentrations were achieved by diluting the most concentrated one using distilled water.

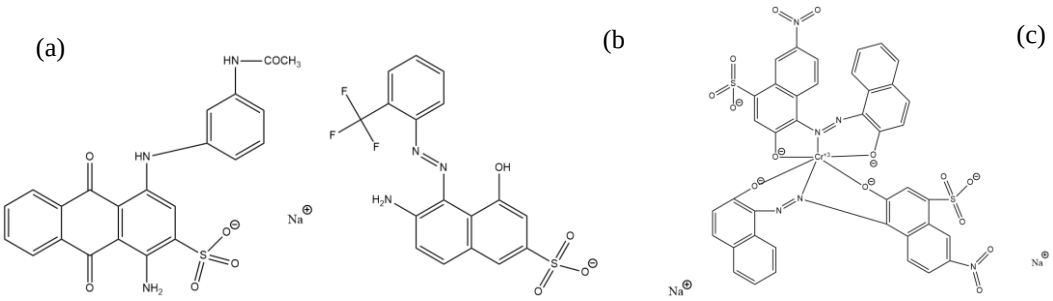

Fig. 1. Structural formula of the dyes: (a) Blue for wood AGN-270%, (b) Red for wood GRA-200% and (c) Black Hispalan M-RN-140%.

2.2. Preparation of biochar and activated carbons

After being dried and sieved (0.5 - 1 mm), pine (*Pinus radiata*) sawdust from a local sawmill in Lugo, Spain, was utilized as an organic precursor for the production of biochar (BC) and ACs.

Carbonization was carried out at 600ºC for 1 h in a N_2 atmosphere (10 mL min^{-1}) in an horizontal tubular furnace (Carbolite, Sheffield) with a ramp of 5ºC min^{-1} up to 600ºC and finally the carbonized sawdust was crushed to obtain a powder and then it was washed with distilled water to remove soluble salts and traces of ashes on the BC surface [21]. Thereafter, the BC produced was mixed with a mortar with the activating agent with the desire weight ratio 1:2 or 1:4 and activated under N_2 atmosphere (10 mL min^{-1}) for 2 h at two different activating temperatures, 600ºC or 850ºC. The acquired material was rinsed with HCl 0.1M under stirring for 15 minutes in a solid/liquid ratio of 1/100 (g/mL) and with distilled water until reach the neutral pH and, finally, dried overnight at 105ºC [22]. The ACs prepared were called ACPS-2-850 (1:2 w/w and 850ºC), ACPS-4-850 (1:4 w/w and 850ºC) and ACPS-4-600 (1:4 w/w and 600ºC).

2.3. Characterization of biochar and activated carbons

The point of zero charge (pH_{PZC}) obtained through the method described by [23] was used to characterize BC and ACs.

Scanning electron microscopy (SEM) was used to examine the structures of BC and ACs. This technique was performed coupled with energy dispersive X-ray analysis (EDX) (ZEISS EVO LS 15 microscope) before and after adsorption, in order to observe changes in its morphology and elemental composition. Furthermore, the carbons were evaluated by Fourier transform infrared spectroscopy (FTIR), using a VARIAN FTIR 670 spectrometer, before and after adsorption [24].

2.4. Batch adsorption experiments

Adsorption experiments in batch mode were performed in a hydro shaking water bath (H20 SOW-LAUDA) at stirring rate of 210 rpm and room temperature. The experiments were conducted by varying the pH (around 2, 6, 7, 9 and 12), initial concentration of dye (5 and 500 mg L^{-1}) and carbon dosage (between 0.5 and 0.1 g L^{-1}) to analyze the elimination of blue, red and black wood dyes using the BC and ACs prepared. After the selected time has elapsed, the suspension was centrifuged (Centronic P Selecta) (4000 rpm, 15 min) and the dye residual concentration was measured at the wavelength that corresponded to the maximum absorbance by UV-Vis spectrophotometry (V-630, Jasco). Thus, the concentrations of blue and black dyes were determined at wavelengths of 602 and 572 nm, respectively, and the concentration of red dye at 506 nm (natural pH), at 499 nm (pH=9) and at 483 nm (pH=12).

The percentage of dye adsorbed was employed for calculating the dye removal efficiency (Eq. (1)). The adsorption capacity of the adsorbent was determined based on the amount adsorbed of dye per mass (Eq. (2)).

$$\%\, Adsorption = (C_0 - C)/C_0 \times 100 \quad (1)$$

$$q\ (mg\ g^{-1}) = (C_0 - C)V/m \quad (2)$$

where C_0 is the initial dye concentration and C corresponds to the residual dye concentration (mg L^{-1}), q is the capacity of adsorption (mg g^{-1}), V corresponds to the volume of the dye dissolution (L) in contact with the material, and m is the dry mass of adsorbent used (g).

2.5. Adsorption kinetics

Pseudo-first order, pseudo-second order and intraparticle diffusion models were employed to assess the kinetic data of dyes adsorption and establish the dynamics of the adsorption processes whichever they are physical or chemical.

The linear pseudo-first order kinetic model, recognized as Lagergren equation, is as indicated in Eq. 3.

$$log\ (q_e - q_t) = log q_e - \frac{k_1 t}{2.303} \quad (3)$$

where k_1 (min^{-1}) is the first-order reaction rate constant, q and q_e (mg g^{-1}) represent the adsorption capacity at time t and equilibrium time, respectively.

One linear form of pseudo-second-order equation is expressed as (Eq. (4)):

$$\frac{t}{q_t} = \frac{1}{k_2 q_e^2} + \frac{1}{q_e} t \quad (4)$$

where k_2 (g mg^{-1} min^{-1}) is the constant rate of the pseudo-second order model [3,25].

Intraparticle diffusion equation (Weber-Morris model) is given by Eq. (5).

$$q_t = k_i \sqrt{t} + C \quad (5)$$

where k_i is the intraparticle diffusion rate constant (mg g^{-1} $min^{-0.5}$) and C is the kinetic constant that gives information about the boundary layer thickness [3,26]. The appropriateness of the models to fit the experimental data was calculated from the determination coefficient (R^2).

2.6. Adsorption equilibrium

In order to improve dyes adsorption, the study of the adsorption equilibrium was performed considering the best operational conditions chosen according to the results of the previous experiments (Table 1).

Table 1. Selected operational conditions for equilibrium studies for the three activated carbons and blue, red and black dyes.

Materials	ACPS-4-850			ACPS-4-600			ACPS-2-850		
	Blue	Red	Black	Blue	Red	Black	Blue	Red	Black
C (mg L^{-1})	500-1900	500-1900	5-100	200-500	25-100	5-25	300-1500	100-700	5-100
Solid-liquid ratio (g L^{-1})	0.4	0.3	0.4	0.5	0.5	0.5	0.5	0.2	0.5
pH*	Natural	Natural	2	Natural	Natural	2	Natural	2	2
Time (h)	24	24	12	48	48	12	48	48	12

*Blue natural pH: ≈ 6; Red Natural pH: ≈ 9.

For equilibrium experiments, the corresponding amount of each AC according to the solid-liquid ratio was added individually to solutions with distinct dye concentrations in Erlenmeyer flasks. The mixes were stirred at 210 rpm and 25ºC in a shaking water bath (H20 SOW-LAWDA) for the selected time. To depict adsorption process, the linearized forms of Langmuir (Eq. (6)), Freundlich (Eq. (7)), Temkin (Eq. (8)) and Dubinin-Radushkevich (Eq. (9)) models were used.

$$q_e = \frac{q_{max} K_L C_e}{1 + K_L C_e} \quad (6)$$

$$q_e = K_F C_e^{1/n} \quad (7)$$

$$q_e = B ln(K_T C_e) \quad (8)$$

$$q_e = q_{m,D} exp(-K_{DR} \varepsilon^2) \quad (9)$$

where C_e is the concentration of dye at equilibrium; q_e is the adsorption capacity at equilibrium (mg g^{-1}); q_{max} and $q_{m,D}$ are the maximum adsorption capacities (mg g^{-1}); K_L corresponds to the Langmuir adsorption constant and denotes the bonding energy (L mg^{-1}); K_F and n are Freundlich model constants; B is equal to (RT)/b_T and is associated to the heat of adsorption (J mol^{-1}); b_T (kJ mol^{-1}) and K_T (L g^{-1}) are Temkin model constants, R is universal constant of gases (J mol^{-1} K^{-1}), T (K) is absolute temperature, ε (kJ mol^{-1}) is Polanyi coefficient and is equal to RTln(1+1/C_e), K_{DR} is activity coefficient (mol^2 J^{-2}) and is associated to the adsorption energy. In the Langmuir model, R_L is an important characteristic and is equal to 1/(1+$K_L C_0$), where Co is the initial dye concentration [27–30].

2.7. Desorption and regeneration

In an attempt to regenerate the activated carbon with the best results for dyes adsorption (ACPS-4-850), H_2O_2 was used as desorbing agent evaluating the removal efficiency (Eq. (1)) in consecutive cycles. The dye saturated activated carbon was put in contact with 0.3% w/v H_2O_2 solution and were left in agitation at 330 rpm for 4 hours at room temperature. Then, the adsorbent was washed with distilled water and dried at 50ºC [31,32]. Then, the adsorbent was put again in contact with dye solution as mentioned before.

Also, to investigate the possibility of the reusability of ACPS-4-850 by thermal regeneration, the saturated material with blue and red dyes was carbonized at 350ºC for 1.5 hours in a pure N_2 (10 mL min^{-1}) atmosphere at 5ºC min^{-1} heating rate, and finally cooled with N_2 flow [33].

2.8. Statistical analysis

For all studies that present statistical analysis, three replications were performed, and the results were averaged. The presence of significant differences relating the adsorption efficiency results of ACPS in relation to all dyes under study was evaluated. According to the significance level, the one-way analysis of variance (ANOVA) was employed, succeeded by the Tukey or T3 Dunnet test. Using the IBM SPSS Statistics 25 program, all statistical analyses were done with a 5% level of significance. Moreover, the

appropriateness of the models to fit the experimental and equilibrium data was calculated from the determination coefficient (R^2).

3. Results and discussion

3.1. Characterization of BC and ACs

The pH_{PZC} stands for the pH level at which the charge on the adsorbent surface is zero, meaning that the electrostatic interactions between the material's positive and negative charges are equal. Adsorbent surface becomes positive (with the existence of a great amount of H+) or negative (with a relevant presence of OH-) charged when the pH is lower and higher than $pH_{PZC,}$ respectively. At pH < pH_{PZC} the positive charge on the surface occurs and could favor the electrostatic attraction of the anionic dyes used in the present work [3,34]. For BC, ACPS-4-850, ACPS-4-600 and ACPS-2-850, pH_{PZC} was found to be 6.7, 7.2, 4.0 and 7.1 respectively (Fig. 2).

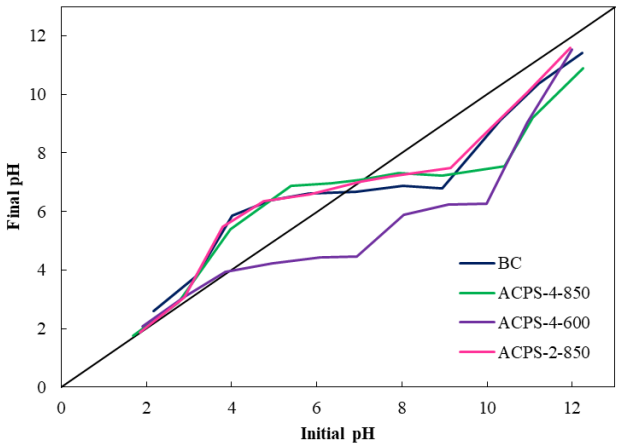

Fig. 2. Point of zero charge of BC and ACs prepared from PS.

SEM was utilized to analyze the micro-morphological structure and surface texture of the biochar and activated carbons. SEM micrographs of the materials are presented in Figure 3(a-d).

All carbon materials showed the same microstructure. An array of uniform porous openings with circular shape distributed around the surface is observed. BC presented a roughness surface, and it is possible to observe that preserved the cell wall structure of the lignocellulosic materials while the activated carbons presented a flat surface. A rougher surface is only observed in ACPS-2-850 (d) possibly due to the lower quantity of KOH used for the activation, which resulted in a less aggressive action [35,36].

Surface morphology of the materials made possible dye removal from aqueous solutions. After adsorption, as it is shown in Fig. 3(e-m) pores were filled with the dye solutions which can cause saturation of the adsorbent binding sites [37].

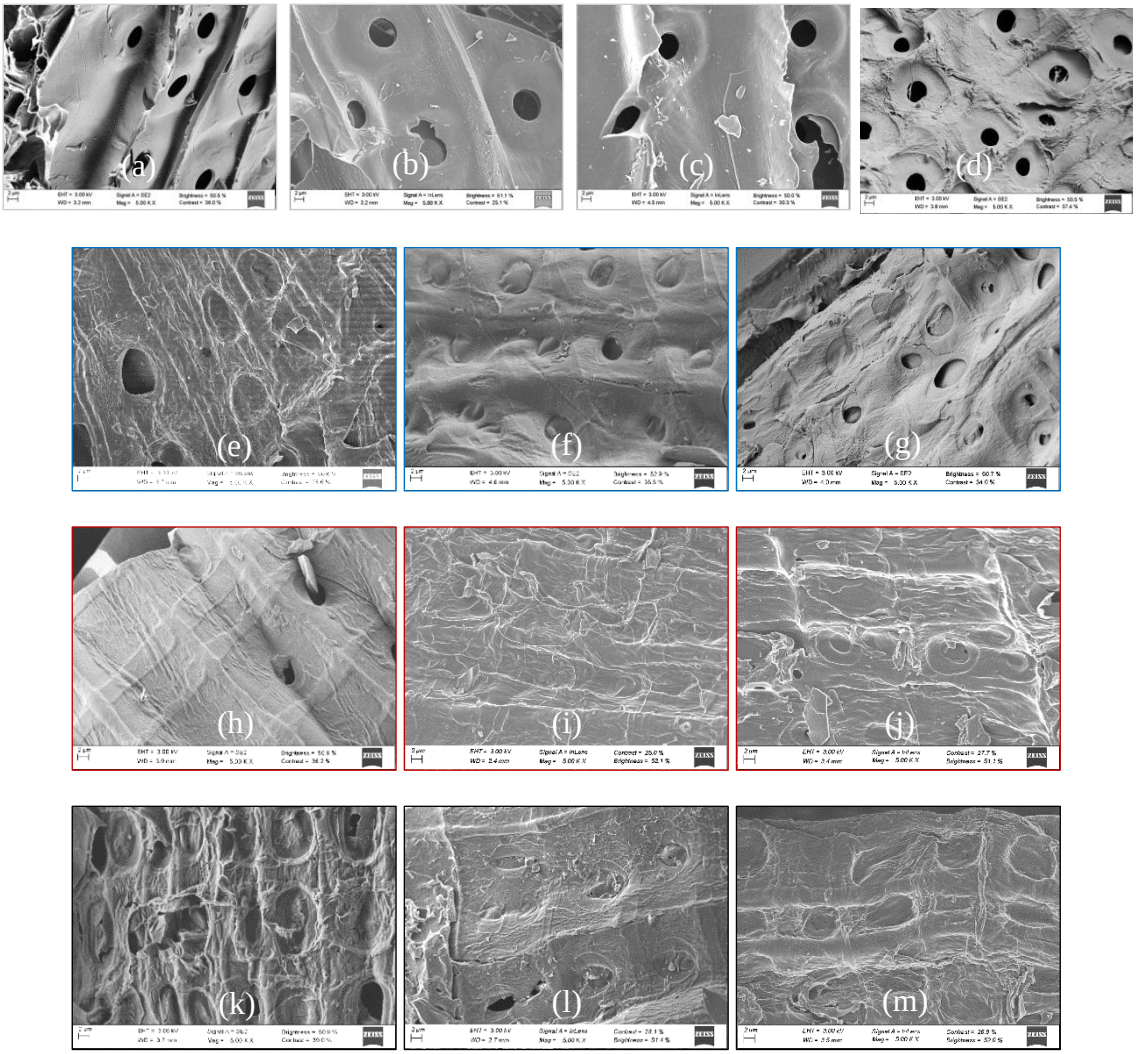

Fig. 3. SEM images of produced biochar and activated carbons (a) BC, (b) ACPS-4-850, (c) ACPS-4-600 and (d) ACPS-2-850 at 5000x magnification before adsorption and after adsorption with blue dye for ACPS-4-850 (e), ACPS-4-600 (f) and ACPS-2-850 (g), with red dye for ACPS-4-850 (h), ACPS-4-600 (i) and ACPS-2-850 (j), and with black dye for ACPS-4-850 (k), ACPS-4-600 (l) and ACPS-2-850 (m) at 5000x magnification.

Surface elemental composition of all the samples determined by EDX analysis before and after adsorption are presented in Table 2. Regarding biochar, the elemental analysis was not performed given the poor dye adsorption [38]. The EDX analysis revealed the existence of elements from the molecular structure of blue, red and black dyes on the surface of ACs (Fig. 1) which confirmed the capability of AC to remove anionic dyes from aqueous solutions.

Table 2. Elemental composition of materials before and after dye adsorption.

	Elemental analysis (%)								
Sample	**C**	**O**	**K**	**Al**	**S**	**N**	**Cr**	**F**	**Na**
BC	91.1	8.0	-	-	-	-	-	-	-
ACPS-4-850	42.6	37.3	14.6	4.5	-	-	-	-	-
ACPS-4-850 + blue	76.6	11.6	1.5	-	5.3	3.0	-	-	-
ACPS-4-850 + red	80.0	11.0	-	-	3.0	-	-	-	1.0
ACPS-4-850 + black	74.7	17.1	-	-	2.2	3.7	1.6	-	-
ACPS-4-600	85.9	12.5	-	-	-	-	-	1.3	-
ACPS-4-600 + blue	75.4	14.2	-	-	4.0	4.1	-	-	1.8
ACPS-4-600 + red	80.5	17.3	-	-	1.9	-	-	-	-
ACPS-4-600 + black	76.6	22.5	-	-	-	-	-	-	-
ACPS-2-850	71.8	8.8	0.8	-	1.7	-	-	-	-
ACPS-2-850 + blue	77.9	18.7	-	-	3.0	-	-	-	-
ACPS-2-850 + red	84.8	13.2	-	-	1.9	-	-	-	-
ACPS-2-850 + black	82.0	15.4	-	-	1.1	-	1.0	-	-

*only presented %weight > 0.5 %.

The FTIR spectra of the materials in the range 400-4000 cm^{-1} were recorded to better understand which functional groups at the surface are responsible for dye adsorption (Fig. 4 and Table 3).

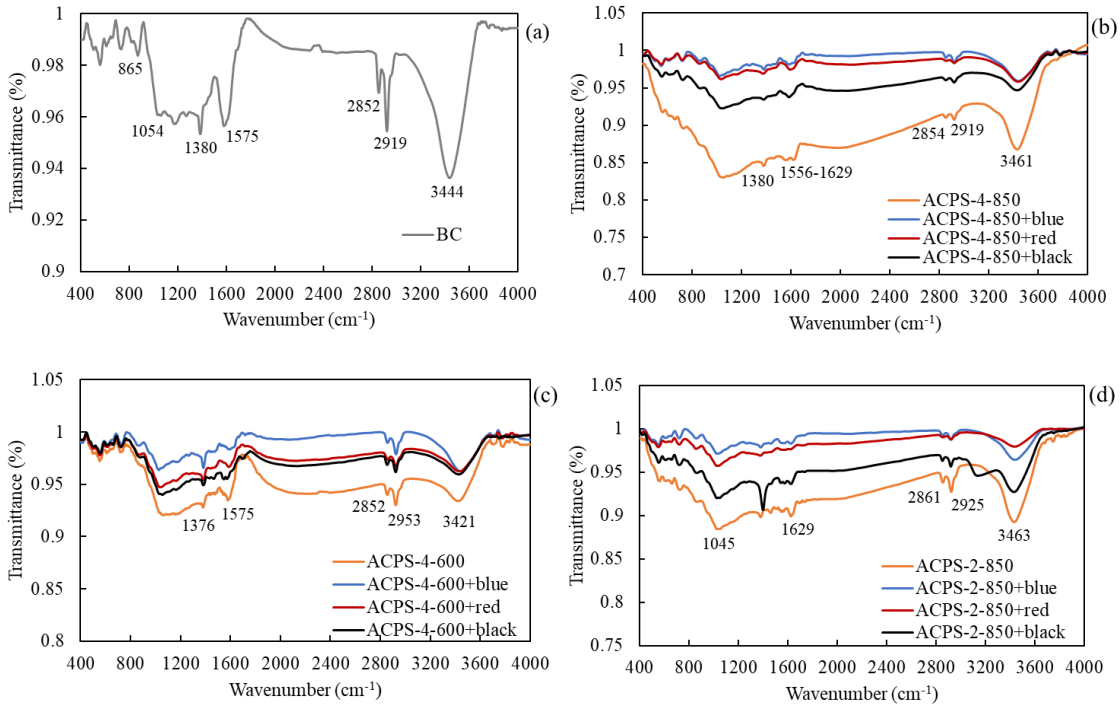

Fig. 4. FTIR graphs of BC (a) before adsorption and ACPS-4-850 (b), ACPS-4-600 (c) and ACPS-2-850 (d) before and after dye adsorption.

Table 3. Identification of the FTIR spectra of the adsorbents.

Adsorbent	Absorption band (cm^{-1})	Functional groups	References
BC	3444	-OH extending vibration characteristic of alcohol, phenols and carboxylic acid	[13]
	2852 and 2919	C-H bond attributed to alkane/alkene groups	[3]
	1575	Stretching vibrations of C=C bond	[5]
	1054-1380	C-O vibrations	[39]
	865	C-O-C or C=O bonds	[27]
ACPS-4-850	3461	-OH extending vibration characteristic of alcohol, phenols and carboxylic acid	[13]
	2854 and 2919	C-H bond attributed to alkane/alkene groups	[3]
	1556-1629	C=C vibrations of aromatic rings and stretch vibrations of C=C bonds in alkene structures	[39]
	1380	C-O vibrations	[39]
ACPS-4-600	3421	-OH extending vibration characteristic of alcohol, phenols and carboxylic acid	[13]
	2852 and 2953	C-H bond attributed to alkane/alkene groups	[3,13]
	1575	Stretching vibrations of C=C bond	[5]
	1376	C-O vibrations	[39]
ACPS-2-850	3463	-OH extending vibration characteristic of alcohol, phenols and carboxylic acid	[13]
	2861 and 2925	C-H bond attributed to alkane/alkene groups	[3]
	1629	C=C bonds in alkene structures	[39]
	1045	C-O bonds of phenols, esters, ethers and alcohols	[9]

Some adsorption bands disappeared after activation process (Fig. 4a, b, c, d), indicating that organic matter vaporization occurred and lead to pore formation [39]. High intensity vibration can be observed at 3400 cm^{-1}, which is due to -OH tensile vibrations. It is possible to notice that that modifications to the functional groups happened after chemical activation, most notably with the decrease of the strength of the bands of 3400, 2919, 2852 and 1575 cm^{-1}. After dye adsorption several peaks' shapes and intensities changed, as a result of the interaction and positioning of the dyes on the adsorbent surface. For instance, the range of -OH vibrations changed for ACPS-4-850 from 3461 cm^{-1} to 3476 cm^{-1} for blue and red and to 3444 cm^{-1} for black, for ACPS-4-600 from 3421 cm^{-1} to 3401 cm^{-1} for blue and red and to 3432 cm^{-1} for black and for ACPS-2-850 from 3463 cm^{-1} to 3450 cm^{-1} for blue and black and to 3436 cm^{-1} for red, which suggests that throughout the adsorption process, hydrogen bonds have been established [27]. Only the ACPS-2-850, after the adsorption with black dye, showed a major peak at around 1400 cm^{-1} due to the skeletal C=C vibrations of aromatic rings.

Regarding BC, the characterization was performed in order to evaluate the efficacy and improvement achieved with the activation of the carbons. Adsorption experiments were not conducted since as seen in a previous study the removal efficiency and adsorption capacity of the dyes used were too low, less than 26% and 3 mg g^{-1} at 5 mg L^{-1}, respectively [38].

3.2. Batch adsorption experiments

3.2.1. Influence of pH and initial dye concentration

The pH of the solution is one of the most important variables that affect dye adsorption once it changes the adsorbent surface and consequently controls how the adsorbent and adsorbate interact electrostatically. The pH of the solution influences both the carbon charge and the ionization degree of the adsorbate. Though, hydrophobic interactions, π-π interactions and hydrogen bonds can also control the adsorption process [6,37]. Figure 5 illustrated how the pH affect the efficiency of the adsorption process of the activated carbons for the blue, red and black dyes.

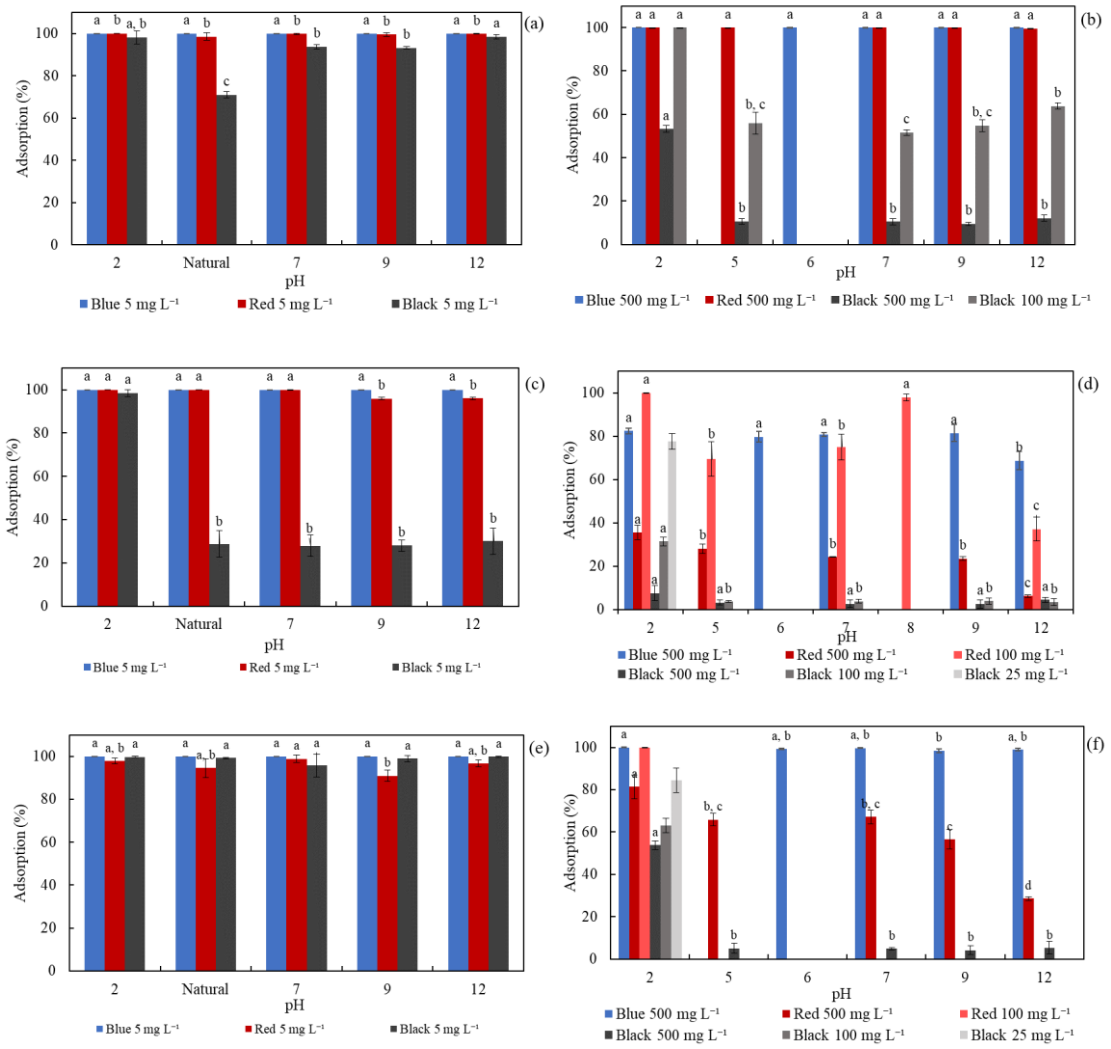

Fig. 5. Influence of the pH and initial dye concentration on the adsorption of blue, red and black dyes onto ACPS-4-850 (a, b), ACPS-4-600 (c, d) and ACPS-2-850 (e, f) (adsorbent dosage 0.5 g L^{-1}, agitation rate 210 rpm, 25ºC, natural pH at 5 mg L^{-1}: 6.0, 5.3 and 5.7 for blue, red and black, respectively, at 25 mg L^{-1}: 4.9 for black dye, at 100 mg L^{-1}: 8.1 and 5.5 for red and black dyes respectively and at 500 mg L^{-1}: 6.2, 9.3 and 5.4 for blue, red and black respectively.

According to the graphs, for 5 mg L^{-1} (Fig. 5 (a, c, e)) the higher removal efficiency was above 95% at natural pH for blue and red dyes for all materials. In the case of black dye, the best adsorption efficiency (> 98%) was obtained at pH 2 for the three activated carbons. Because activated carbon's surface is positively charged at low pH (pH < pH_{PZC}) due to the high concentration of H^+, the better adsorption happens due to the powerful electrostatic interaction between the activated carbon surface and the anionic dyes. Also, the acid dissociation constant (pKa) of blue, red and black dyes needs to be considered. Previous research [40] revealed that the pKa value of blue, red and black dyes was 10.4, 10.6 and 10.3, respectively, which makes that dye molecules exist mostly as anionic salts in solution as they ionize and become negatively charged radicals [41]. As pH increases, the positive sites on the adsorbent surface diminish which impair the electrostatic attraction, which was more evident in the case of ACPS-4-600 (Fig. 5 (c)) where a slight increase in pH causes a large adsorption inhibition. This fact agrees with the low pH_{PZC} value for this material. The higher amount of adsorbed blue, red and black dyes were 9.9, 14.4 and 10.3 mg g^{-1} on ACPS-4-850, 10.9, 10.1 and 9.5 mg g^{-1} on ACPS-4-600 and 8.5, 10.6 and 10.9 mg g^{-1} on ACPS-2-850. As in some cases, mainly for blue and red dyes, the influence of pH was low due to the great adsorption performance

at all pH values, its effect increasing the initial concentration of dye (500, 100 and 25 mg L^{-1}) was also investigated (see figures 5b, 5d and 5f).

A general decrease in dye uptake was seen with the increase in starting dye concentration at 500 mg L^{-1} (which is due to the excessive number of dye molecules relative to the amount of available adsorption sites), except for the ACPS-4-850 for the blue and red dyes and ACPS-2-850 for the blue dye, [6]. At lower concentrations, the molecules of dye fill the available sites without competition and more pollutant can be adsorbed [37]. It was found that the amount of dye adsorbed onto the activated carbons increased significantly with increasing concentration. The highest amount of adsorbed blue, red and black dyes at 500 mg L^{-1} were 1010.9, 1068.7 and 492.2 mg g^{-1} on ACPS-4-850, 849.6, 363.7 and 69.9 mg g^{-1} on ACPS-4-600 and 1007.6, 837.5 and 519.3 mg g^{-1} on ACPS-2-850. Furthermore, the reduction in adsorption effectiveness at high dye concentrations can be due to not only the fact that adsorbent active site being saturated but also to the repulsive electrostatic forces between the dye adsorbed and dye in solution [27]. It is evident that ACPS-4-850 showed the best adsorption performance followed by ACPS-2-850 and ACPS-4-600 which can be explained taking into account that ACPS-4-850 had the highest total pore volume with the lowest percentage of microporosity (67.8%) combined with the largest internal surface area of 2864.5 m^2 g^{-1} (sent to publication). The smaller size of the pores in the ACPS-2-850 and ACPS-4-600 materials means that, on the one hand, there may be a certain size exclusion, and also, exalt the repulsion between molecules of dye that are already adsorbed and the proximity of the walls in the micropores.

To improve the adsorption process, when the removal percentage was lower than 80% the initial dye concentration was reduced to 100 or 25 mg L^{-1}. With ACPS-4-850 for the black dye reducing initial concentration to 100 mg L^{-1} adsorption removal percentage increased to 100%. With ACPS-4-600 and ACPS-2-850 reducing concentration to 100 mg L^{-1} and 25 mg L^{-1} for red and black dyes respectively, the removal percentage increased to 100% for red dye and 77.5% and 84.4% for black dye. These results evidence the significant impact of initial dye concentration on the adsorption performance which depends also on the adsorbent and adsorbate. The higher adsorption capacity of activated carbons in comparison to that of biochar, reported in a previous study [38], can be due to the presence of porous structure which may result in a higher total surface area which grants more functional groups. These findings prove the efficiency of the chemical activation of the biomass to produce activated carbons with improved structural and adsorption capacities.

Thus, on the basis of the experimental results obtained in the present section, pH 2 for black dye or natural pH for blue and red dyes were selected for further investigations.

3.2.2. Effect of adsorbent dose

Adsorbent dose is another factor that may affect the efficiency of the adsorption process and the adsorbent's capacity and also on the overall cost of the process if used in large scale application [9,27]. Changes in dye removal efficiency with varying adsorbent dose are illustrated in Fig. 6.

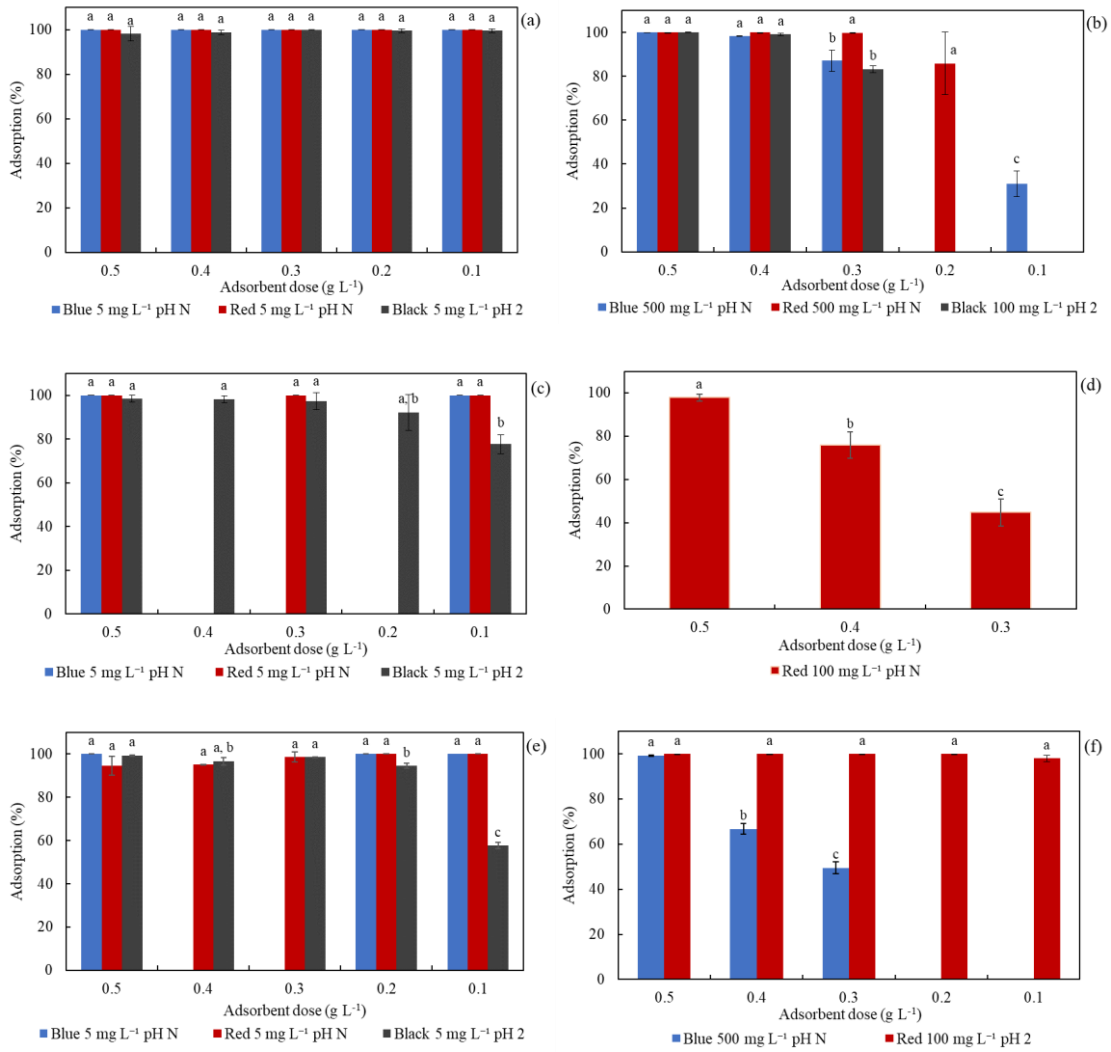

Fig. 6. Influence of the adsorbent dose on dyes removal on (a, b) ACPS-4-850, (c, d) ACPS-4-600 and (e, f) ACPS-2-850 (stirring rate 210 rpm, 25ºC, natural pH (pH N) or pH = 2).

It was observed that at 5 mg L^{-1} the total removal of dyes was achieved in the entire range of adsorbent dose studied (0.5-0.1 g L^{-1}) except for the black dye using ACPS-4-600 and ACPS-2-850 for which at 0.1 g L^{-1} the efficiency decreased from 99% to 78% and from 99% to 58%, respectively. The fact that part of the surface area of the adsorbents is not used in the dye adsorption process may allow the dose to be reduced, avoiding loss in the adsorbed quantity [9]. For blue and red dyes at 5 mg L^{-1}, 0.1 g L^{-1} was the selected adsorbent dose with a removal efficiency of 100% and a maximum adsorption capacity of 53.8 mg g^{-1} and 44.0 mg g^{-1} for ACPS-4-850, 49.0 mg g^{-1} and 52.0 mg g^{-1} for ACPS-4-600 and 54.0 mg g^{-1} and 49.0 mg g^{-1} for ACPS-2-850, respectively. In the case of black dye 0.1 g L^{-1} was the dose chose for ACPS-4-850, 0.2 g L^{-1} for ACPS-4-600 and 0.3 g L^{-1} for ACPS-2-850 with a maximum adsorption capacity of 45.2 mg g^{-1}, 15.3 mg g^{-1} and 17.0 mg g^{-1} respectively. Regarding the initial dye concentration, the study was only performed if the efficiency was 100% at 0.5 g L^{-1}. At higher concentrations it could be noticed that in general, dye removal efficiencies decreased with decreasing the adsorbent dose. For ACPS-4-850 the selected dose was 0.4 g L^{-1} for the blue dye at 500 mg L^{-1} and for the black dye at 100 mg L^{-1} and 0.3 g L^{-1} for the red dye at 500 mg L^{-1} and the maximum adsorption capacity was 1411.0, 1635.0 and 232.1 mg g^{-1}, respectively. Regarding ACPS-4-600 it was not possible to reduce the adsorbent dosage due to the low available surface caused by the high microporosity (89.0%) (sent to publication). Concerning ACPS-2-850 it was only possible to decrease red dye's adsorbent dose at 100 mg L^{-1} and 0.2 g L^{-1} was selected with a maximum adsorption capacity of 480.9 mg g^{-1}. The adsorbent dose was selected taking into account that

the adsorption process' efficiency did not change significatively, which can be due to numerous factors such as the decrease of dye concentration or with the inexistence of contact between the dye and the adsorbent sites due to the collision between adsorbent particles and reduction of the active surface [27]. It should be also pointed out that, generally, the activated carbons' adsorption capacity rose with decreasing the adsorbent dose. This behavior can be accounted for by the observation that as the dose increases, the amount of surface (and mass of carbon) not available for size exclusion adsorption (previously observed) also increases, which leads to a reduce in adsorption capacity [27].

3.2.3. Adsorption kinetics

Adsorption kinetics was investigated to evaluate the adsorption mechanism as well as the rate limiting step. For an efficient process a high adsorption rate, a brief contact time and a substantial adsorption capacity are fundamental factors [42]. Experimental data were fitted to the pseudo-first order (PFO), pseudo-second order (PSO) and intraparticle diffusion models and the experimental and calculated adsorption kinetic curves for the blue, red and black dyes on ACPS-4-850, ACPS-4-600 and ACPS-2-850 are depicted in Fig.7 (a-f).

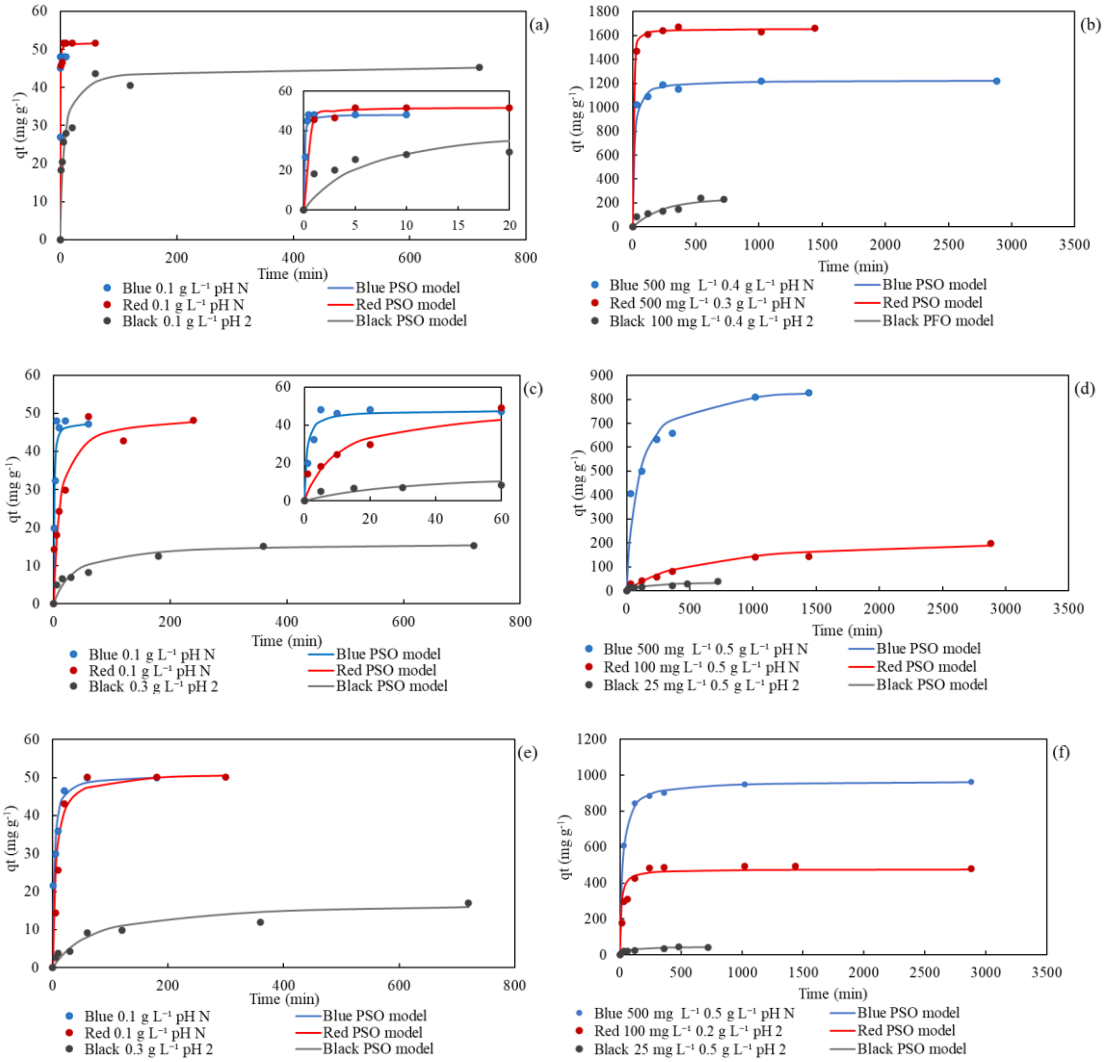

Fig. 7. Kinetic curves for blue, red and black dyes on ACPS-4-850 (a, b), ACPS-4-600 (c, d) and ACPS-2-850 (e, f) (stirring rate 210 rpm, 25ºC, natural pH (pH N) or pH = 2).

As it can be observed, the adsorption of the red dye (the smaller one) is higher for ACPS-4-850 which is the activated carbon with highest macro or mesoporosity and a 68% of microporosity [38]. By the contrary,

when activated carbons with highest microporosity (ACPS-4-600, 89% and ACPS-2-850, 85%) are applied it can be observed that the blue dye adsorption is higher. With highest microporosity percentage (as indicated before) it is possible that the repulsion inside the pore walls or even with other molecules of dye adsorbed could affect the adsorption process.

At 5 mg L^{-1} (Figs. 7 (a), (c) and (e)) the adsorption process occurred fast mainly for ACPS-4-850 that was less than 1h for black dye and less than 5 minutes for blue and red dyes, and in a subsequent step, the rate steadily fell until it reached equilibrium as a result of fewer vacant sites and a decline in the concentration driving force. With the change on the activation conditions, by decreasing the temperature or the ratio of activating agent, the equilibrium time for dye adsorption increased due to a decrease in the pore size that was more evident in the case of black dye. As shown in Fig. 7 (b), (d) and (f) the adsorption capacity increased significantly with the rise in concentration. The highest adsorption capacity at equilibrium corresponded to ACPS-4-850 and it was 1221.58 mg g^{-1} for blue, 1673.03 mg g^{-1} for red and 240.38 mg g^{-1} for black dye, and the equilibrium time was 4h for the blue and red dyes and 9h for the black dye. The calculated kinetic parameters are presented in Table 4.

Pseudo-second-order model was more suited for adsorption data, except for ACPS-4-850 with the black dye at 100 mg L^{-1} that was bet fitted to the pseudo-first-order model (Table 4, Fig. 7) revealing the existence of physical adsorption. Although in some cases the pseudo-first-order kinetic model gave high R^2 values, calculated q_e values are far from the experimental ones, revealing an inaccurate prediction. The appropriateness of the pseudo-second order model demonstrated the possibility of chemical reactions between the activated carbon and dyes contributed to the adsorption process [37]. This suggests that the dyes were adsorbed onto the oxygenated active sites by surface exchange processes until they were completely occupied. In a second phase, the dye molecules diffused into the porous structure and were adsorbed within the inner pores of the activated carbons. The good fit ($R^2 > 0.9$) to the intraparticle diffusion model for the first zone (Table 4) confirmed the proposed mechanism [43].

Thus, the intraparticle diffusion model was used to better understand the various adsorption process stages. When there is only one step and the linear model cross the origin, it is believed that the only mechanism regulating the adsorption process is intraparticle diffusion. Regarding the experiments at high dye concentration there are four occasions where only one step of intraparticle diffusion occurred and with high R^2 (> 0.9), however the linear model did not cross the origin which implies that other adsorption mechanism is occurring. For the other cases, the adsorption process comprises two stages, the initial sharp step corresponds to the quick diffusion on the exterior surface and the second phase is a progressive adsorption under the control of intraparticle diffusion [13]. Besides, it is possible to infer that the adsorption capacity was also influenced by the dye molecular size since the molecular size for blue (1.4 nm) and red (1.3 nm) was lower than that for the black (1.5 nm), which is advantageous for the dye molecular diffusion in the adsorbent through the mesoporous filling mechanism [38,42].

In general, the adsorption capacity of the adsorbents changes with the principal source of the carbons, the specifications of the adsorption process and with the class of pollutant. So, numerous studies have been conducted to find suitable adsorbents with appropriate characteristics and great adsorption capacity. Table 5 shows the results for ACPS-4-850 with the maximum adsorption capacity obtained for 500 mg L^{-1} for blue and red dyes and 100 mg L^{-1} for black dye. compared with that for other activated carbons used in similar dyes adsorption process. It is possible to conclude that all activated carbons developed in this work presented great adsorption capacities, often exceeding those for other adsorbents previously investigated by other researchers. (Table 5).

Table 4. Kinetic parameters for the adsorption of blue, red and black dyes on ACPS-4-850, ACPS-4-600 and ACPS-2-850.

Kinetic Model	Parameter	ACPS-4-850			ACPS-4-600			ACPS-2-850		
		Blue	**Red**	**Black**	**Blue**	**Red**	**Black**	**Blue**	**Red**	**Black**
	(mg L^{-1})	**Low initial dye concentration (5 mg/L)**								
	q_{exp}	48.03	51.61	45.23	48.03	49.11	15.27	50.00	50.10	16.97
Pseudo-first order	R^2	1.000	1.000	0.581	0.631	0.963	0.951	0.978	0.988	0.784
	q_e (mg g^{-1})	148.53	6.62	20.27	12.48	30.55	13.36	35.04	67.08	12.23
	k_1 (min^{-1})	11.70	0.093	0.018	0.047	0.013	0.013	0.11	0.11	0.0028
Pseudo-second order	R^2	1.000	1.000	1.000	0.999	0.995	0.996	1.000	0.999	0.963
	q_e (mg g^{-1})	48.27	51.71	45.54	47.85	49.75	16.00	50.76	51.28	17.39
	k_2 (g mg^{-1} min^{-1})	0.51	0.17	0.0036	0.030	0.020	0.0019	0.0080	0.0039	0.00083
Intraparticle diffusion	R_1^2	0.904	0.760	0.868	0.971	0.913	0.959	1.000	1.000	0.789
	$k_{id,1}$	72.55	4.51	3.33	22.42	7.10	0.55	6.64	12.92	0.43
	C_1	0.96	40.46	15.93	-3.74	2.79	4.01	14.96	-14.77	2.02
	R_2^2	0.00	0.92	0.431	0.077	0.444	0.686	0.608	N/A	0.941
	$k_{id,2}$	48.03	-0.0059	0.15	0.11	2.03	0.19	0.35	-	0.40
	C_2	0.00	51.63	40.85	46.55	24.90	10.49	45.84	-	5.49
		High initial dye concentration								
	(mg L^{-1})	**500**	**500**	**100**	**500**	**100**	**25**	**500**	**100**	**25**
	q_{exp}	1221.58	1673.03	240.38	827.91	199.14	38.87	962.09	492.61	43.12
Pseudo-first order	R^2	0.936	0.604	0.893	0.995	0.958	0.830	0.915	0.205	0.992
	q_e (mg g^{-1})	123.42	93.84	236.38	469.46	168.77	37.96	216.82	67.08	28.51
	k_1 (min^{-1})	0.0018	0.0014	0.0041	0.0032	0.00092	0.0041	0.0030	0.00069	0.0037
Pseudo-second order	R^2	1.000	1.000	0.872	0.998	0.959	0.864	1.000	1.000	0.987
	q_e (mg g^{-1})	1226.99	1655.63	281.45	868.81	225.73	39.37	968.99	476.19	44.64
	k_2 (g mg^{-1} min^{-1})	$7.11 \cdot 10^{-5}$	0.00023	$1.95 \cdot 10^{-5}$	$1.46 \cdot 10^{-5}$	$7.91 \cdot 10^{-6}$	0.00019	$4.97 \cdot 10^{-5}$	0.00021	0.00039
Intraparticle diffusion	R_1^2	0.971	0.918	0.935	0.978	0.987	0.921	0.899	0.921	0.948
	$k_{id,1}$	16.56	17.40	8.41	22.35	3.74	1.14	28.06	30.68	1.24
	C_1	924.74	1389.60	14.31	275.05	4.91	4.31	481.23	58.87	11.53
	R_2^2	0.607	0.242	-	0.953	-	-	0.774	0.363	-
	$k_{id,2}$	1.82	-1.06	-	9.37	-	-	1.61	-0.23	-
	C_2	1134.30	1686.60	-	487.86	-	-	882.16	496.90	-

*1: first stage of ID; 2: second stage of ID

Table 5. Comparison of the q_{max} of various activated carbons derived from biomass precursors used for removal of blue, black and red dyes from aqueous solutions.

Activated carbon precursor	Dye	Dye concentration (mg L^{-1})	q_{max} (mg g^{-1})	References
Rubber seed shells	Methylene blue	20	659.4	[6]
Rubber seeds	Methylene blue	20	769.2	[6]
Sunflower Pith (NaOH)	Methylene blue	1000	958.9	[44]
Sunflower Pith (KOH)	Methylene blue	500-1000	580.6	[44]
Chickpea peel	Methylene blue	500	200.0	[13]
Sugarcane bagasse waste	Methylene blue	250	142.2	[9]
Coconut shell	Maxilon blue dye	10	14.0	[45]
Hazelnut shell	Basic blue 9	-	8.8	[46]
Rubber seed shells	Congo red	40	458.4	[6]
Rubber seeds	Congo red	40	227.3	[6]
Cornulaca monacantha stem	Congo red	20-160	78.2	[7]
Beverage sludge	Allura red	200	287.1	[1]
Ziziphus lotus stones	Basic red 46	250	306.8	[3]
Sesame	Acid red 114	-	102.4	[47]
Leather shaving waste	Acid red 357	750	204.4	[48]
Leather shaving waste	Acid black 210	750	573.9	[48]
Acacia nilotica	Reactive black 5	200	56	[49]
Grape marc	Reactive black 5	-	333	[50]
Pine sawdust	Blue for wood	500	1221.6	This study
Pine sawdust	Red for wood	500	1673.0	This study
Pine sawdust	Black for wood	100	240.4	This study

3.2.4. Equilibrium isotherms

Equilibrium data are of great interest since allow to select the best model which fits to the experimental data, to be then used in other kind of applications like simulation adsorption processes [51]. Thus, adsorption equilibrium data were fitted to the Langmuir, Freundlich, Temkin and Dubinin-Radushkevich isotherm models and the results are shown in Fig. 8 and Table 6.

For all activated carbons, dyes adsorption experimental data were best suited to the Langmuir isotherm model ($R^2 > 0.9$) which suggest that the adsorption occurs in monolayer on a surface with uniform energy sites similarly accessible for interaction. The values of Langmuir isotherm's dimensionless separation factor (R_L) varied from 0 to 1 for all concentrations demonstrating that the adsorption process of dyes onto ACs is favorable [27]. This conclusion is supported by the values of n obtained using the Freundlich isotherm model that showed a favorable adsorption process since in all cases is greater than the unity [11]. Moreover, the average energy value (E) was calculated using D-R model and showed that the adsorption process is not physical because in any case is lower than 8 kJ mol^{-1}. For the black dye E is between 8 and 16 kJ mol^{-1} for all carbons which is related with ion exchange interactions and for the other two dyes and for every ACs is higher than 16 kJ mol^{-1} which implies that during the adsorption process, the molecules of dye undergo through diffusion [52,53].

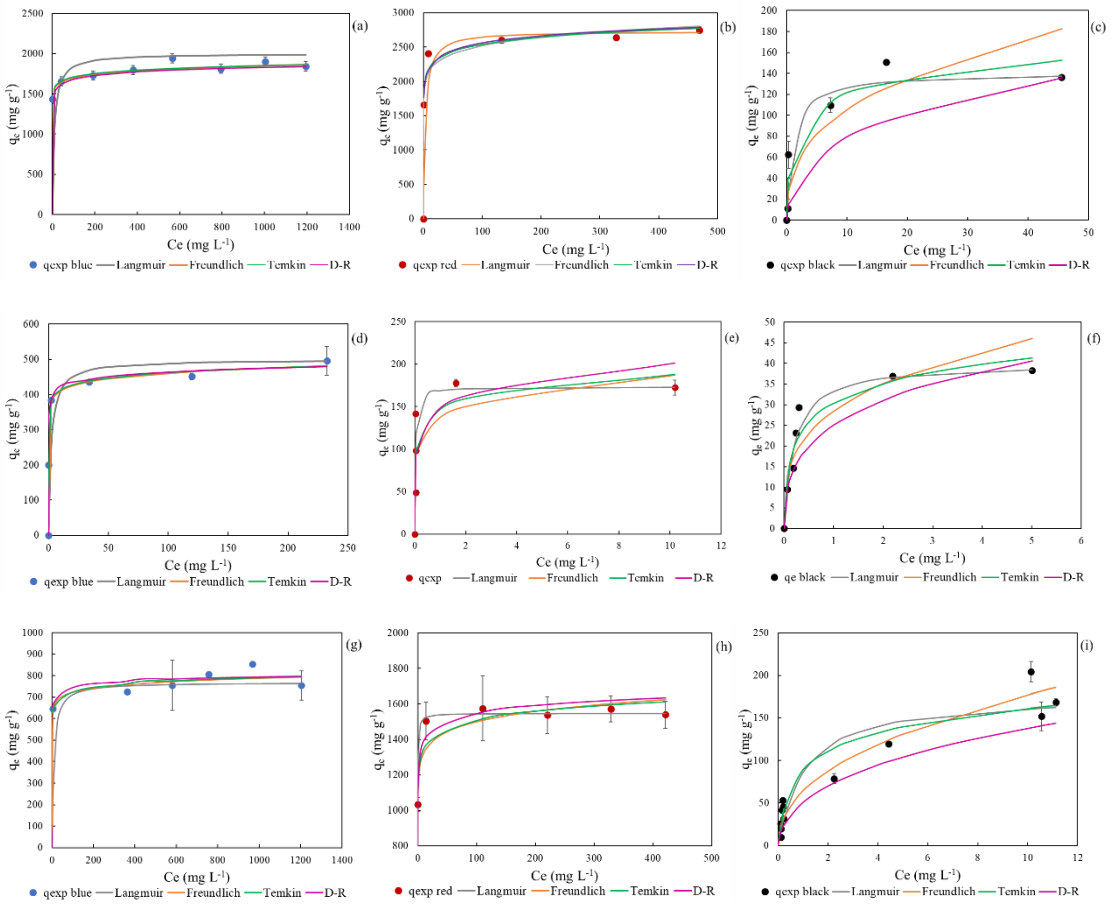

Fig. 8. Adsorption isotherms of blue, red and black dyes for ACPS-4-850 (a, b, c), ACPS-4-600 (d, e, f) and ACPS-2-850 (g, h, i) for selected conditions.

ACPS-4-850 showed higher adsorption capacity for the three dyes than the other carbons which can be explained by its larger surface area and higher mesoporosity (sent to publish). Moreover, in the case of blue and red dyes the isotherms can be categorized as type H2, according to the Giles classification, which indicates elevated affinity between the activated carbon and the dye, as illustrated by the vertical behavior at low initial concentrations. The interaction between the dye and the carbons gets progressively more difficult, as concentration increases, which results in a concave curvature of the isotherms [11,54]. On the other hand, the isotherm for the black dye due to the initial curvature presented with the increase on the concentration, can be classified as L2 which is particular for a strong intermolecular [54].

Table 6. Langmuir, Freundlich, Temkin and Dubinin-Radushkevich parameters and correlation coefficients for adsorption of blue, red and black dyes on ACPS-4-850, ACPS-4-600 and ACPS-2-850 activated carbons.

Activated carbon	**Adsorption isotherm**	**Parameter**	**Dye**		
			Blue	**Red**	**Black**
ACPS-4-850	Langmuir	q_m (mg g^{-1})	2000.00	2732.24	140.85
		K_L (L mg^{-1})	0.11	0.31	0.86
		R_L	0.018-0.0047	0.0065-0.0017	0.19-0.0116
		R^2	0.999	0.999	0.994
	Freundlich	n	27.32	14.33	2.73
		K_F (mg g^{-1} (L $mg^{-1})^{-1/n}$)	1440.15	1827.86	45.11
		R^2	0.903	0.849	0.682
	Temkin	B (J mol^{-1})	59.95	151.21	22.06
		K_T (L mg^{-1})	$2.63 \cdot 10^{10}$	$1.99 \cdot 10^{5}$	22.19
		R^2	0.855	0.879	0.867
	Dubinin-Radushkevich	$q_{m,D}$ (mg g^{-1})	2016.46	3294.80	636.96
		K_{DR} (mol^2 kJ^{-2})	$4.00 \cdot 10^{-10}$	$5.68 \cdot 10^{-10}$	$3.00 \cdot 10^{-9}$
		E (kJ mol^{-1})	35.36	29.21	12.91
		R^2	0.586	0.894	0.699
ACPS-4-600	Langmuir	q_m (mg g^{-1})	500.00	172.98	40.00
		K_L (L mg^{-1})	0.45	37.06	4.90
		R_L	0.011-0.0044	0.0011-0.00027	0.039-0.0081
		R^2	0.998	1.000	0.999
	Freundlich	n	19.84	7.64	3.34
		K_F (mg g^{-1} (L $mg^{-1})^{-1/n}$)	366.10	137.97	28.44
		R^2	0.945	0.401	0.764
	Temkin	B (J mol^{-1})	21.76	17.16	6.73
		K_T (L mg^{-1})	$1.71 \cdot 10^{7}$	5646.40	92.56
		R^2	0.927	0.605	0.860
	Dubinin-Radushkevich	$q_{m,D}$ (mg g^{-1})	551.53	376.91	198.30
		K_{DR} (mol^2 kJ^{-2})	$4.00 \cdot 10^{-10}$	$9.00 \cdot 10^{-10}$	$2.00 \cdot 10^{-9}$
		E (kJ mol^{-1})	35.36	23.57	15.81
		R^2	0.927	0.503	0.792
ACPS-2-850	Langmuir	q_m (mg g^{-1})	769.23	1547.99	177.62
		K_L (L mg^{-1})	0.125	4.65	0.929
		R_L	0.026-0.0053	0.0021-0.00031	0.17-0.011
		R^2	0.989	1.000	0.947
	Freundlich	n	26.74	17.99	2.27
		K_F (mg g^{-1} (L $mg^{-1})^{-1/n}$)	609.42	1161.42	64.44
		R^2	0.717	0.844	0.817
	Temkin	B (J mol^{-1})	27.03	71.27	31.38
		K_T (L mg^{-1})	$4.90 \cdot 10^{9}$	$1.56 \cdot 10^{7}$	16.98
		R^2	0.673	0.851	0.907
	Dubinin-Radushkevich	$q_{m,D}$ (mg g^{-1})	849.20	1838.67	1124.73
		K_{DR} (mol^2 kJ^{-2})	$3.00 \cdot 10^{-10}$	$4.00 \cdot 10^{-10}$	$3.00 \cdot 10^{-9}$
		E (kJ mol^{-1})	40.82	35.36	12.91
		R^2	0.701	0.901	0.834

3.2.5. Desorption and regeneration

Reusing the adsorbent for economic gain is a crucial approach in an advanced adsorption process. The ability of AC to regenerate after numerous cycles of adsorption and desorption determines how cost-effectively dyes can be removed from aqueous solutions using AC. Thus, the recycle of the activated carbon that led to the best results for dyes adsorption, ACPS-4-850, was investigated. Different solvents, namely NaOH (0.1 M; 10M), HCl (0.1 M), ethanol 96%, acetone:water (3:2 v/v), acetone (> 99.5%), acetone 10%, methanol 10% and NaCl 0.1M were used for the desorption of dyes from the activated carbon. Table 7 lists the percentage of desorption of blue, red and black dyes by using these desorption agents.

Table 7. Percentage of desorption of blue, red and black dyes using various desorption agents.

Desorbing agents	Blue (%)	Red (%)	Black (%)
HCl 0.1M	0	0	0.02
NaOH 0.1M	0	0.05	0.06
NaOH 10M	0	-	-
Ethanol 96%	15.42	16.66	5.49
Acetone/water (3:2), 25ºC	17.47	26.83	7.33
Acetone/water (3:2), 50ºC	21.34	-	-
Acetone (> 99.5%)	-	3.21	-
Acetone 10%	-	0.11	-
Methanol 10%	-	0	-
NaCl 0.1M	-	0	-

The results indicate that the amount of dye desorbed in all cases and for the different dyes and conditions was rather low for all desorbing agents, which suggests that anionic dyes adsorption on ACPS-4-850 is generally irreversible by chemical regeneration. This conclusion is supported by the values of the separation factor (R_L) calculated through the Langmuir model since are very close to zero (Table 6) indicating that the adsorption system is irreversible. The same outcomes were reported by Tran et. al [55] for the desorption of cationic dyes from commercial activated-charcoal.

In a further attempt to regenerate the activated carbon, hydrogen peroxide was tried as desorbing agent [31,56] and the removal efficiency in consecutive cycles are presented in Fig. 9.

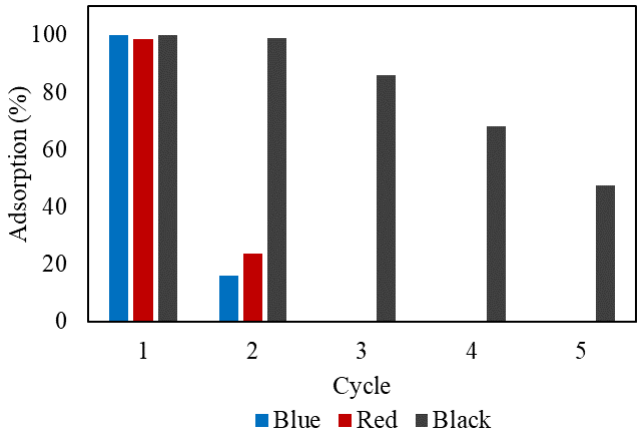

Fig. 9. Reusability of ACPS-4-850 for blue, red and black dye adsorption (H_2O_2 0.3% w/v in water; stirring rate: 330 rpm; time: 4 hours; room temperature).

As demonstrated by Fig. 9, the adsorption efficiencies of blue and red dyes significantly decreased after the second cycle of adsorption from 99.89% and 98.60% to 16.17% and 23.7%, respectively. This demonstrates that for these dyes, the H_2O_2 is also inefficient for the activated carbon regeneration. On the contrary, for the black dye the adsorption efficiency was higher than 80% until the third adsorption cycle and was

reduced to 47.36% after five adsorption cycles. This can be due to the degradation of the activated carbon when used multiple times or possibly due to the saturation of the material surface [39]. For this dye, H_2O_2 considerably increased the effectiveness of the desorption process contrasted to previously essayed solvents (Table 7). This improvement on the efficiency can be attributed to a number of simultaneous mechanisms that are primarily facilitated by the interaction between the oxidizing agent and the activated carbon surface. Nevertheless, for the degradation of highly toxic compounds, although H_2O_2 displays a comparatively significant redox potential (E^0 = 1.77 V), chemical oxidation may not be effective, because it needs a high reaction energy to be activated in order to produce oxidizing species and break the O-O bond (bond energy is 213.8 kJ mol^{-1}) [32]. Also, activated carbon catalyzes the decomposition of H_2O_2 to produce oxidant species •OH the adsorbed dye [31,32]. Usually, the desorption process produces a visible increase on the color intensity of the solution, which was not possible to observe. Possibly, the reducing of the electrostatic interactions between the black dye and the activated carbon structure with the consequent release of dye from the active sites did not occur.

Finally, the carbon with adsorbed blue and red dyes underwent a thermal regeneration as proposed by Ma [33]. For the blue dye the removal efficiency decreased from 99.89% to 28.72% and for red dye from 98.60% to 53.99% which revealed the inefficiency of thermal regeneration, most likely as a result of the thermal treatment-induced collapse of the carbon porous structure. So, for blue and red dyes further studies should be performed to improve the regeneration of the ACPS-4-850.

3.2.6. Adsorption mechanism

Various types of interaction can occur between ACPS and dye molecules, as observed by the kinetic and equilibrium studies, and the suggested mechanism is given in Fig. 10. FTIR before adsorption confirmed the presence of functional groups which could, effectively interaction with the dyes molecules. In addition, SEM analysis showed well developed and distributed pores on the carbons leading to a large surface area that improves the adsorption process.

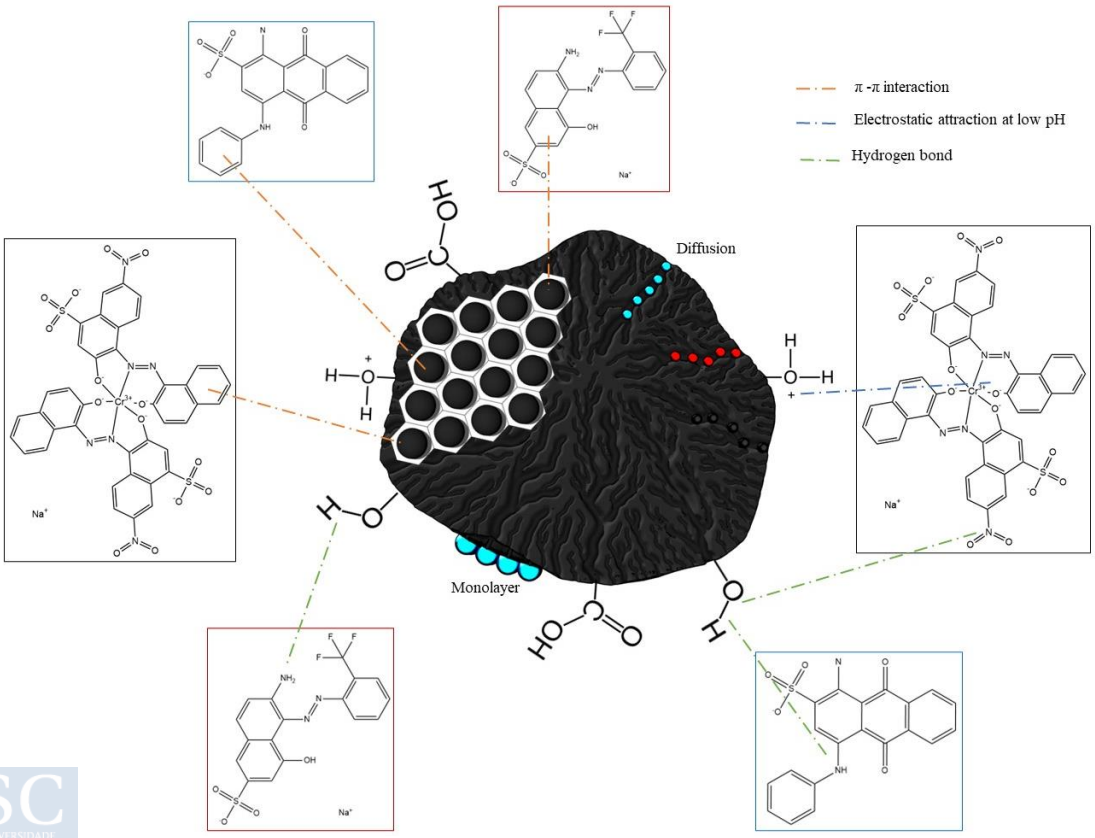

Fig. 10. Illustration of the possible interactions between ACPS surface and blue, red and black dyes.

Moreover, based on pH influence, electrostatic interactions could happen between the anionic dyes and positive charged positions (carbonyl and oxygen-containing functional groups) that are present on the surface of the AC, particularly in neutral and acidic solutions. As seen in the FTIR result following dye uptake, another interaction that can take place between nitrogen in dyes structure and free H of oxygen-containing functional groups on the AC surface is hydrogen bonding. Finally, π-π interaction arises from interaction between dye aromatic rings and the hexagonal skeleton of ACs, as the electron-donating functional groups (-OH) of AC may increase π-donating strength of the aromatic ring [9].

4. Conclusions

High quality activated carbons were prepared from pine sawdust biomass for the elimination of blue, red and black wood dyes from wastewater. SEM results showed a uniform porous surface with ACPS-4-850 having the largest pores. FTIR analysis demonstrated the presence of functional groups (hydroxyl, phenols, alcohols, alkane and carboxyl) in the activated carbons available for dyes adsorption. The carbon activated with KOH 1:4 (w/w) at 850ºC during 2 h showed the best adsorption capacities of 1221.6, 1673.0 and 240.4 for blue, red and black dyes, respectively, at 500 mg L^{-1} for the blue and red dyes and 100 mg L^{-1} for the black dye. The activated carbons with high S_{BET} showed a q_{max} of 15.3 and 1673.0 mg g^{-1}, respectively, which is distinctive among several carbonaceous materials [1,3,48–50,6,7,9,13,44–47]. The operating factors that affected the removal of dyes included pH, initial dye concentration, and ACPS dose. Dyes removal intensified with increasing ACPS dose and reducing with the increase on the initial dye concentration, except for ACPS-4-850 for blue and red that there was no need to decrease the concentration. Generally, the adsorption kinetics were best represented by the pseudo-second order kinetic model, which showed that chemical adsorption was an important factor in the adsorption process. For the three dyes equilibrium data were best suited to the Langmuir model also representative of a monolayer chemical adsorption on the carbon surface. The reusability study showed that ACPS-4-850 can be re-utilized at least up to 5 cycles after black dye adsorption using hydroxide peroxide as desorbing agent but and efficient desorption was not found for the blue and red dyes.

Therefore, results showed that pine sawdust based activated carbon is a novel and capable adsorbent for dyes removal. The results thus point to a unique, promising adsorbent for the removal of wood dyes from water systems that is also safe for the environment. Future research should be conducted on the improvement dyes desorption from the activated carbon, to reuse the adsorbent and become the process even more sustainable.

CRediT authorship contribution statement

Catarina H. Pimentel: Investigation, Data curation, Validation, Visualization, Writing – original draft (catarinahelena.dasilveira@rai.usc.es). **Rubén Castro Agra:** Investigation, Data curation, Validation, Conducted the experiments and data/evidence collection (rubencastroagra@gmail.com). **Diego Gómez-Díaz:** Conceptualization, Methodology, Supervision, Validation, Funding acquisition, Writing—review & editing (diego.gomez@usc.es). **M. Sonia Freire:** Conceptualization, Methodology, Supervision, Validation, Funding acquisition, Writing—review & editing (mariasonia.freire@usc.es). **Julia González-Álvarez:** Conceptualization, Methodology, Supervision, Funding acquisition, Writing—review & editing (julia.gonzalez@usc.es).

Declaration of competing interest

The authors declare that they have no known competing financial interests or personal relationships that could have appeared to influence the work reported in this paper.

Acknowledgments

Authors would like to thank the use of RIAIDT-USC analytical facilities.

Funding

This work was supported by the Ministerio de Ciencia, Innovación y Universidades, grant number PGC2018-101047-B-I00.

References

[1] A.F.M. Streit, L.N. Côrtes, S.P. Druzian, M. Godinho, G.C. Collazzo, D. Perondi, G.L. Dotto, Sci. Total Environ. 660 (2019) 277–87. 10.1016/j.scitotenv.2019.01.027.

[2] Y. Hu, C. Zou, T. Xiong, H. Wang, J. Ind. Eng. Chem. (2023). 10.1016/j.jiec.2023.07.062.

[3] N. Boudechiche, M. Fares, S. Ouyahia, H. Yazid, M. Trari, Z. Sadaoui, Microchem. J. 146(October 2018) (2019) 1010–8. 10.1016/j.microc.2019.02.010.

[4] A. Khasri, M.A. Ahmad, Environ. Sci. Pollut. Res. 25(31) (2018) 31508–19. 10.1007/s11356-018-3046-3.

[5] H. Xue, X. Wang, Q. Xu, F. Dhaouadi, L. Sellaoui, M.K. Seliem, A. Ben Lamine, H. Belmabrouk, A. Bajahzar, A. Bonilla-Petriciolet, Z. Li, Q. Li, Chem. Eng. J. 430(October 2021) (2022). 10.1016/j.cej.2021.132801.

[6] N.U.M. Nizam, M.M. Hanafiah, E. Mahmoudi, A.A. Halim, A.W. Mohammad, Sci. Rep. 11(1) (2021) 1–17. 10.1038/s41598-021-88084-z.

[7] A. Sharma, Z.M. Siddiqui, S. Dhar, P. Mehta, D. Pathania, Sep. Sci. Technol. 54(6) (2019) 916–29. 10.1080/01496395.2018.1524908.

[8] M.S. Reza, C.S. Yun, S. Afroze, N. Radenahmad, M.S.A. Bakar, R. Saidur, J. Taweekun, A.K. Azad, Arab J. Basic Appl. Sci. 27(1) (2020) 208–38. 10.1080/25765299.2020.1766799.

[9] A.H. Jawad, A.S. Abdulhameed, N.N. Bahrudin, N.N.M.F. Hum, S.N. Surip, S.S.A. Syed-Hassan, E. Yousif, S. Sabar, Water Sci. Technol. 84(8) (2021) 1858–72. 10.2166/wst.2021.355.

[10] M. Danish, T. Ahmad, Renew. Sustain. Energy Rev. 87(October 2017) (2018) 1–21. 10.1016/j.rser.2018.02.003.

[11] L. Spessato, K.C. Bedin, A.L. Cazetta, I.P.A.F. Souza, V.A. Duarte, L.H.S. Crespo, M.C. Silva, R.M. Pontes, V.C. Almeida, J. Hazard. Mater. 371(December 2018) (2019) 499–505. 10.1016/j.jhazmat.2019.02.102.

[12] Z. Heidarinejad, M.H. Dehghani, M. Heidari, G. Javedan, I. Ali, M. Sillanpää, Environ. Chem. Lett. 18(2) (2020) 393–415. 10.1007/s10311-019-00955-0.

[13] K. Jahan, V. Singh, N. Mehrotra, K. Rathore, V. Verma, Biomass Convers. Biorefinery (0123456789) (2021). 10.1007/s13399-021-01938-4.

[14] T.M. Santos, V. Rigual, M. Oliet, M.V. Alonso, J.C. Domínguez, F. Rodriguez, J. Chem. Technol. Biotechnol. 94(12) (2019) 3951–9. 10.1002/jctb.6197.

[15] E.G. Brockerhoff, B.A. Gresham, N. Meurisse, H.F. Nahrung, A. Perret-Gentil, A.R. Pugh, S.L. Sopow, R.M. Turner, NeoBiota 84 (2023) 137–67. 10.3897/NEOBIOTA.84.95864.

[16] F. Crecente-Campo, P. Marshall, V. LeMay, U. Diéguez-Aranda, For. Ecol. Manage. 257(12) (2009) 2370–9. 10.1016/j.foreco.2009.03.038.

[17] Y. Yang, F.S. Cannon, Bioresour. Technol. 344(PA) (2022) 126161. 10.1016/j.biortech.2021.126161.

[18] C. Akmil-Başar, Y. Önal, T. Kiliçer, D. Eren, J. Hazard. Mater. 127(1–3) (2005) 73–80. 10.1016/j.jhazmat.2005.06.025.

[19] S.M. Yakout, M.R. Hassan, M.E. El-Zaidy, O.H. Shair, A.M. Salih, BioResources 14(2) (2019) 4560–74. 10.15376/biores.14.2.4560-4574.

[20] G. Zhu, X. Xing, J. Wang, X. Zhang, J. Mater. Sci. 52(13) (2017) 7664–76. 10.1007/s10853-017-1055-0.

[21] K. Lou, A.U. Rajapaksha, Y.S. Ok, S.X. Chang, 2299 (2016). 10.1080/09542299.2016.1165080.

[22] O.E. Eleri, K.U. Azuatalam, M.W. Minde, A.M. Trindade, N. Muthuswamy, F. Lou, Z. Yu, Electrochim. Acta 362 (2020) 137152. 10.1016/j.electacta.2020.137152.

[23] S.A.C. Carabineiro, T. Thavorn-Amornsri, M.F.R. Pereira, P. Serp, J.L. Figueiredo, Catal. Today 186(1) (2012) 29–34. 10.1016/j.cattod.2011.08.020.

[24] L. Domínguez-Ramos, A. Prieto-Estalrich, G. Malucelli, D. Gómez-Díaz, M.S. Freire, M. Lazzari, J. González-álvarez, Sustain. 2022, Vol. 14, Page 3760 14(7) (2022) 3760. 10.3390/SU14073760.

[25] Y.S. Ho, G. Mckay, Process Biochem. 34 (1999) 451–65.

[26] W.J. Weber Jr., J.C. Morris, J. Sanit. Eng. Div. 89(2) (1963) 31–59. https://doi.org/10.1061/JSEDAI.0000430.

[27] R. Foroutan, S.J. Peighambardoust, S.H. Peighambardoust, M. Pateiro, J.M. Lorenzo, Molecules 26(8) (2021) 1–19. 10.3390/molecules26082241.

[28] I. Langmuir, J. Am. Chem. Soc. 40(9) (1918) 1361–403.

[29] H. Freundlich, Zeitschrift Für Phys. Chemie 57(1) (1907) 385–470.

[30] H. Chandarana, S. Suganya, A.K. Madhava, Int. J. Environ. Anal. Chem. (2020). 10.1080/03067319.2020.1798418.

[31] A. Cabrera-Codony, R. Gonzalez-Olmos, M.J. Martín, J. Hazard. Mater. 285 (2015) 501–8. 10.1016/j.jhazmat.2014.11.053.

[32] D.H.S. Santos, J.L.S. Duarte, J. Tonholo, L. Meili, C.L.P.S. Zanta, Sep. Purif. Technol. 250(March) (2020) 117112. 10.1016/j.seppur.2020.117112.

[33] Y. Ma, Waste and Biomass Valorization 8(3) (2017) 549–59. 10.1007/s12649-016-9640-z.

[34] A. Nasrullah, B. Saad, A.H. Bhat, A.S. Khan, M. Danish, M.H. Isa, A. Naeem, J. Clean. Prod. 211 (2019) 1190–200. 10.1016/j.jclepro.2018.11.094.

[35] O. Oginni, K. Singh, G. Oporto, B. Dawson-Andoh, L. McDonald, E. Sabolsky, Bioresour. Technol. Reports 7(June) (2019) 100266. 10.1016/j.biteb.2019.100266.

[36] X. Zhang, L. Zhang, A. Li, J. Environ. Manage. 206 (2018) 989–98. 10.1016/j.jenvman.2017.11.079.

[37] L. Baloo, M.H. Isa, N. Bin Sapari, A.H. Jagaba, L.J. Wei, S. Yavari, R. Razali, R. Vasu, Alexandria Eng. J. 60(6) (2021) 5611–29. 10.1016/j.aej.2021.04.044.

[38] C.H. Pimentel, M.S. Freire, D. Gómez-Díaz, J. González-Álvarez, Biomass Convers. Biorefinery (1) (2023). 10.1007/s13399-023-04138-4.

[39] H.M. El-Bery, M. Saleh, R.A. El-Gendy, M.R. Saleh, S.M. Thabet, Sci. Rep. 12(1) (2022) 1–17. 10.1038/s41598-022-09475-4.

[40] C.H. Pimentel, M.S. Freire, D. Gómez-Díaz, J. González-Álvarez, Proc. 17th Int. Conf. Environ. Sci. Technol. 17(0123456789) (2023). 10.30955/gnc2021.00438.

[41] A.H. Jawad, N.N.A. Malek, T. Khadiran, Z.A. ALOthman, Z.M. Yaseen, Diam. Relat. Mater.

128(July) (2022) 109288. 10.1016/j.diamond.2022.109288.

[42] X. Liu, J. Tian, Y. Li, N. Sun, S. Mi, Y. Xie, Z. Chen, J. Hazard. Mater. 373(March) (2019) 397–407. 10.1016/j.jhazmat.2019.03.103.

[43] S. Álvarez-Torrellas, M. Muñoz, J.A. Zazo, J.A. Casas, J. García, J. Environ. Manage. 183 (2016) 294–305. 10.1016/j.jenvman.2016.08.077.

[44] M. Baysal, K. Bilge, B. Yılmaz, M. Papila, Y. Yürüm, J. Environ. Chem. Eng. 6(2) (2018) 1702–13. 10.1016/j.jece.2018.02.020.

[45] A.M. Aljeboree, A.N. Alshirifi, A.F. Alkaim, Arab. J. Chem. 10 (2017) S3381–93. 10.1016/j.arabjc.2014.01.020.

[46] A. Aygün, S. Yenisoy-Karakaş, I. Duman, Microporous Mesoporous Mater. 66(2–3) (2003) 189–95. 10.1016/j.micromeso.2003.08.028.

[47] P. González-García, Renew. Sustain. Energy Rev. 82(August 2017) (2018) 1393–414. 10.1016/j.rser.2017.04.117.

[48] C. Manera, A.P. Tonello, D. Perondi, M. Godinho, Environ. Technol. (United Kingdom) 40(21) (2019) 2756–68. 10.1080/09593330.2018.1452984.

[49] M.T. Amin, A.A. Alazba, Environ. Earth Sci. 76(16) (2017) 1–13. 10.1007/s12665-017-6927-8.

[50] H. Belayachi, B. Bestani, N. Benderdouche, M. Belhakem, Arab. J. Chem. 12(8) (2019) 3018–27. 10.1016/j.arabjc.2015.06.040.

[51] G. Yin, F. Jameel Ibrahim Alazzawi, S. Mironov, F. Reegu, A.S. El-Shafay, M. Lutfor Rahman, C.H. Su, Y.Z. Lu, H. Chinh Nguyen, Arab. J. Chem. 15(3) (2022). 10.1016/j.arabjc.2021.103612.

[52] A. Bazan-Wozniak, J. Cielecka-Piontek, A. Nosal-Wiercińska, R. Pietrzak, Materials (Basel). 15(16) (2022). 10.3390/ma15165664.

[53] A. Khadir, S.S. Muthu, Polymer Technology in Dye-containing Wastewater, Springer, 2022.

[54] C.H. Giles, T. MacEwan, S. Nakhwa, D. Smith, J. Chem. Soc. 14 (1960) 3973–93.

[55] H.N. Tran, Y.F. Wang, S.J. You, H.P. Chao, Process Saf. Environ. Prot. 107 (2017) 168–80. 10.1016/j.psep.2017.02.010.

[56] D.H. da S. Santos, Y. Xiao, N. Chaukura, J.M. Hill, R. Selvasembian, C.L.P.S. Zanta, L. Meili, Heliyon 8(8) (2022) e10205. 10.1016/j.heliyon.2022.e10205.

Continuous adsorption of acid wood dyes onto an activated carbon prepared from pine sawdust

Catarina Helena Pimentel, María Sonia Freire, Diego Gómez-Díaz, Julia González-Álvarez[2]

Department of Chemical Engineering, School of Engineering, Universidade de Santiago de Compostela, Santiago de Compostela, 15782, Spain

Keywords: Pine sawdust, Wood dyes, Fixed-bed adsorption, Breakthrough curves, Kinetic models, Regeneration

Abstract

In this paper, an activated carbon obtained from *Pinus radiata* sawdust has been applied to remove blue, red, and black wood dyes from aqueous solutions in a fixed-bed column. Flow rate (7.7-30.8 mL min^{-1}), initial dye concentration (25-500 mg L^{-1}), and bed height (2-4 cm) highly influence the breakthrough curves features. The results indicated that the adsorption capacity increased by decreasing the flow rate and increasing the initial dye concentration except for the black dye, and increasing bed height except for the red dye. The activated carbon with a surface area of 2826 m^2 g^{-1} led to a maximum adsorption capacity of 1283.1 mg g^{-1} for the blue dye at an initial concentration of 500 mg L^{-1}, flow rate of 7.7 mL min^{-1} and bed height of 4 cm; 1028.4 mg g^{-1} for the red dye at 500 mg L^{-1}, 7.7 mL min^{-1} and 2 cm; and 153.4 mg g^{-1} for the black dye at 100 mg L^{-1}, 7.7 mL min^{-1} and 4 cm. The Yoon-Nelson and Thomas models were found to be the more suitable ones to describe the adsorption data. The activated carbon saturated with black dye could be used in three successive cycles after regeneration with H_2O_2.

1. Introduction

Industrial effluents frequently contain dyes that are poisonous, carcinogenic, mutagenic, allergic, and/or resistant to biological degradation [1]. Furthermore, the color they give to effluents makes it difficult to disperse sunlight, which also interferes with photosynthesis and limits the ability of aquatic biota to develop and function. Moreover, due to the complexity of the dye's structure molecules, their removal becomes difficult, and dye-laden effluents from industries continue to be the most complicated to treat [1, 2]. Hence, conventional treatment methods have been applied, such as physical, chemical and biological methods, but they are not effective and cannot therefore be used to control the enormous amount of organic contaminants that are discharged in the effluents. Adsorption technique is preferable for industrial processes because it has a straightforward design, and it is simple to use, inexpensive, and feasible at extremely low concentrations and, therefore, an effective method for wastewater treatment [3–5].

Activated carbons are well-known adsorbents used for their outstanding adsorption capacity. However, the cost of production and the difficulty of regeneration make them expensive. Therefore, there is a growing interest in finding readily accessible and affordable options to substitute commercial activated carbons by other materials derived from wastes such as sawdust, orange peel or corn cobs. Particularly, activated carbons derived from biomass wastes usually have several advantages, such as being simple to prepare, affordable, versatile and renewable [2]. Woody materials are considered a good alternative in the manufacture of activated carbon since

[2] Corresponding author. Department of Chemical Engineering, School of Engineering, Universidade de Santiago de Compostela, Rúa Lope Gómez de Marzoa s/n, 15782 Santiago de Compostela, Spain. Tel.: +34 881816761. E-mail address: julia.gonzalez@usc.es.

they have the proper carbon content and a low level of ash. Typically, the lumber industry produces enormous amounts of wood waste in the form of sawdust, which is periodically burned for energy or dumped at disposal sites nearby since they are not fully utilized [3]. Several studies have reported the use of sawdust as a precursor of activated carbons. Thus, Gupta et al. [4] used sawdust from *Acacia nilotica* to produce activated carbon for the removal of Indigo Carmine dye. Kumar et al. [5] investigated the removal of Bismark Brown dye onto activated carbons from rubberwood sawdust and Khasri et al. [3] used *Intsia bijuga* sawdust to remove basic and reactive dyes.

As an established method for comparing adsorbents, batch experiments were commonly chosen to assess their capacity for removing different adsorbates. Although these studies are relevant, the continuous fixed-bed column is the most commonly used for wastewater treatment in industries [6].

Previous studies [7] [sent to publication] in batch mode were performed with several activated carbons from pine sawdust to remove blue, red, and black dyes from aqueous solutions, demonstrating that those carbons, are capable adsorbents for dyes removal since some presented high adsorption capacities at high initial dye concentrations in a short period of time.

As far as the authors know, there are no studies on activated carbon produced from pine sawdust in continuous mode. Therefore, following the previous works about wood dyes adsorption in batch mode [sent to publication] and [7], that carbon activated with KOH at 850ºC and ratio 1:4 (w/w) with the higher adsorption efficiency was selected for studies in column and the influence of inlet dye concentration, flow rate and column bed height on adsorption performance was analyzed.

2. Materials and Methods

2.1. Materials

Pine (*Pinus radiata*) sawdust (PS) was provided by a local sawmill (Lugo, Spain). Acidic wood dyes were utilized: Blue for wood AGN-270% ($C_{22}H_{16}N_3NaO_6S$), Red for wood GRA-200% ($C_{17}H_{11}F_3N_3NaO_4S$) and Black Hispalan M-RN-140% ($C_{40}H_{20}CrN_6NaO_{14}S_2^{-2}$). Potassium hydroxide (KOH, 85%, Probus), hydrochloric acid (HCl, 37%, Sigma Aldrich) and hydrogen peroxide (H_2O_2, 33%, Quimipur) were used.

2.2. Preparation and characterization of the activated carbon

PS was prepared by air-drying, sieving to a fraction between 0.5-1 mm and stored in a plastic container before being employed as precursor for activated carbon production. In an initial step to establish an inert atmosphere in the oven (Nabertherm GmbH-Germany), nitrogen flow (34 L h^{-1}) was kept for 30 minutes. Sawdust carbonization (666.3 g, 60 g per lot) was carried out at 600ºC for 1 hour under a nitrogen atmosphere (34 L h^{-1}) in an oven and using a temperature ramp of 5ºC min^{-1} until reaching the target temperature. After that, the biochar (25.6 g) was mixed with the activating agent (KOH pellets) at a ratio of 1:4 (w/w) by milling. The mixture was activated in the oven at 850ºC for 2 hours with a temperature ramp of 5ºC min^{-1}. The same nitrogen flow (34 L min^{-1}) was applied. After cooling down the activated carbon was put in contact with agitation with HCl (0.1 M) at the ratio of 1g carbon:100 mL HCl for 15 minutes followed by washing with double distilled water until a stable pH was reached. The activated carbon (9.2 g) was then dried overnight at 105ºC, and activated carbon yield was calculated from weight loss.

N_2 and CO_2 adsorption isotherms were obtained as described by Pimentel et. al [7] to determine carbon surface area and pore volume distribution.

2.3. Adsorption in fixed-bed column

Adsorption experiments in fixed-bed column were carried out at ambient temperature (approximately 20ºC) using a cylindrical tube (internal diameter 1.86 cm; height 12.5 cm) made from Pyrex glass as illustrated in Figure 1. Glass-wool was placed at the top and bottom of the column to prevent the movement of the adsorbent. Dye solution at predefined concentration (25-500 mg L^{-1}) was pumped with a peristaltic pump (Heidolph PD5201) at distinct flow rates of 7.7 or 30.8 mL min^{-1} throughout the fixed-bed of PSAC in an up-flow configuration. Bed heights of 2 and 4 cm were also evaluated. In the previous batch study [7] and [sent to publication], it was reported that the greater adsorption percentage was attained at pH = 2 for the black dye and at the natural pH for blue and red dyes, so the experiments were performed at these pH values. For each experiment, samples were collected at the outflow at different times, and dye concentration was measured with a UV/Vis spectrometer (V-630, Jasco) at 602 nm, 506 nm and 572 nm for blue, red and black dye, respectively.

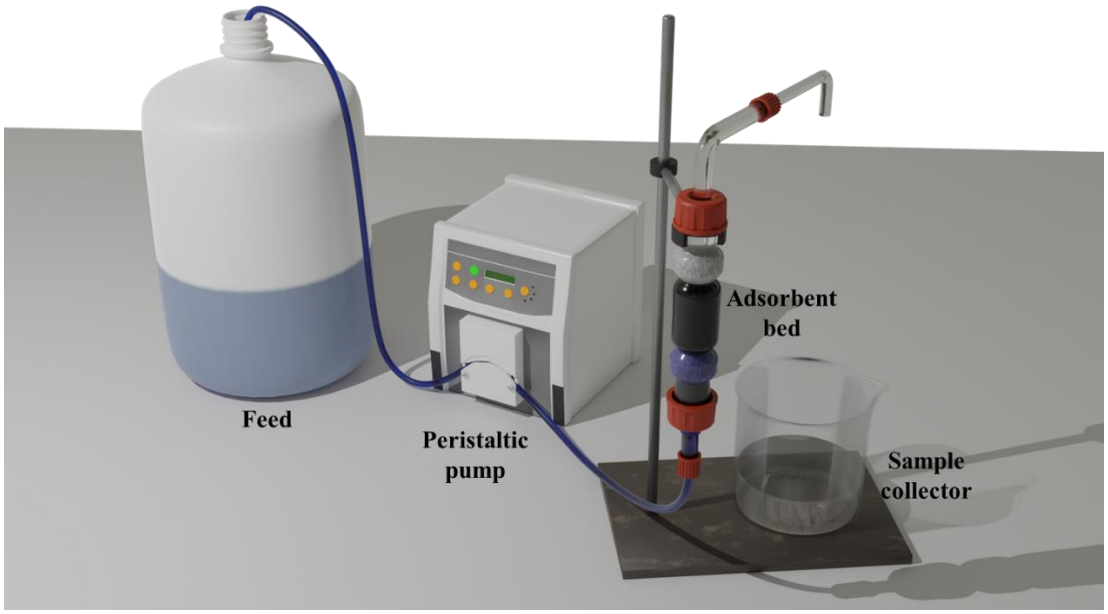

Figure 1. The fixed-bed adsorption setup.

2.4. Analysis of fixed-bed adsorption process

Experimental breakthrough curve (BTC) was used to calculate the breakthrough time (t_b) and the saturation time (t_s) when the concentration of dye at the outlet stays approximately constant (i.e. steady state has been reached). The time of breakthrough was calculated as the time at which the dye concentration at the outlet (C_t) exceeded by 5% the dye concentration at the inlet (C_0) [1]. Usually, the saturation time is the time at which the dye concentration at the outlet reaches that at the inlet (C_t/C_0=1). The adsorption capacity of the PSAC bed (q_{bed}, mg g^{-1}) was determined by numerical integration of the concentration profile (C_t/C_0) of the breakthrough curve according to the trapezoidal rule (Equation (1)):

$$q_{bed} = \int_{t=0}^{t=t_{oper}} \left(\frac{C_0 - C_t}{m_{bed}}\right) Q\ dt \quad (1)$$

where t_{oper} is the total operating time (min), m_{bed} is the amount of activated carbon used in the fixed-bed column (g) and Q is the feed flow (L min^{-1}). Other important parameters of BTC were the total time of the adsorption process (Δt, min), the mass transfer zone (MTZ, cm) which corresponds to the adsorbent bed space in which the greatest exchange between adsorbate and adsorbent molecules take place, and the volume of effluent (V_{ef}, L) [8], [9]. All were determined from the following equations:

$$\Delta t = t_s - t_b \quad (2)$$

$$MTZ = L \times \frac{(t_s - t_b)}{t_s} \quad (3)$$

$$V_{ef} = Q \times t_{oper} \quad (4)$$

where L is the bed height (cm).

The percentage of dye removal is given by equation (5):

$$\%Removal = \frac{q_{total}}{m_{total}} \times 100 \quad (5)$$

where q_{total} (mg) is the total mass of dye adsorbed given by equation (6) and m_{total} (mg) is the amount of adsorbate accumulated in the column provided by equation (7) [3]:

$$q_{total} = \frac{Q}{1000} \int_{t=0}^{t=t_{oper}} (C_0 - C_t)\, dt \quad (6)$$

$$m_{total} = \frac{C_0 Q t_{oper}}{1000} \quad (7)$$

where Q is the feed flow (L min^{-1}), t_{oper} is the total operating time (min) and C_0 and C_t represent the initial dye concentration and the dye concentration (mg L^{-1}) at any time t (min), respectively.

2.5. Modeling dye adsorption in fixed-bed column

Three empirical kinetic models (Thomas, Yoon-Nelson and Bohart-Adams) were used to further study the BTCs, determine the greatest adsorption capacity and the half-time of the column's breakthrough (τ) as well as to evaluate the adsorption's mechanism and effectiveness of the column for dye adsorption. Several researchers [10] have concluded that the use of non-linear regression contributes to better results than linearized equations [11]. For this reason, a non-linear method has been employed in the present work using the Solver tool included in Microsoft Excel that employs the GRG algorithm in order to minimize the sum of squared error (SSE). All the empirical models can be represented by the following non-linear mathematical expression (Eq. (8)), though "a" and "b" parameters are different in each model.

$$\frac{C_t}{C_0} = \frac{1}{1 + e^{(a - bt)}} \quad (8)$$

where C_0 and C_t represent the initial dye concentration and the dye concentration (mg L^{-1}) at any time t (min), respectively.

2.5.1. Thomas model

The Thomas model is based on the premise that the adsorption equilibrium fits the Langmuir model and the kinetic process follows the pseudo-second-order model [12]. According to this model, neither diffusion nor axial dispersion are the rate-limiting steps. It assumes that chemical

reactions and interfacial mass transfer govern the adsorption process. Equation 9 is the nonlinear equation of the Thomas model:

$$\frac{C_t}{C_0} = \frac{1}{1+e^{\left(\frac{K_{Th}q_t m}{Q} - K_{Th}C_0 t\right)}} \quad (9)$$

where K_{Th} is the Thomas rate constant (L mg^{-1} min^{-1}), t is time (min^{-1}), q_t is the amount of dye adsorbed per gram of adsorbent (mg g^{-1}), m is the adsorbent mass (g) and Q is the flow rate (mL min^{-1}).

2.5.2. Yoon-Nelson model

This model assumes that decreasing rate of adsorption is directly proportional to breakthrough and adsorbate adsorption on the adsorbent. It considers the heterogeneous adsorption process in a flow system. The non-linear mathematical form is provided by equation (10) [13], [14]:

$$\frac{C_t}{C_0} = \frac{1}{1+e^{(K_{YN}\tau - K_{YN}t)}} \quad (10)$$

where K_{YN} is the Yoon-Nelson rate coefficient (min^{-1}) and τ is the time needed for retaining 50% of the initial adsorbate (min).

2.5.3. Bohart-Adams model

This model proposes that equilibrium does not happen immediately and that the rate of adsorption is proportional to adsorption capacity that remains on the adsorbent. Equation (11) provides the non-linear form of this model [15]:

$$\frac{C_t}{C_0} = \frac{1}{1+e^{\left(\frac{K_{BA}ZN_0}{F} - K_{BA}C_0 t\right)}} \quad (11)$$

where K_{BA} is the Bohart-Adams coefficient (L mg^{-1} min^{-1}), N_0 is the sorption capacity of adsorbent (mg L^{-1}), Z is the bed height (cm) and F is the superficial velocity (cm min^{-1}) [12], [16].

2.5.4. Error analysis

To evaluate the good fitness of the previously mentioned models with the experimental results to describe the adsorption process an error analysis was performed. The correlation coefficient R^2 alone could not be enough to validate the best model, because it only represents the linear fitness between the isotherms and experimental data. Therefore, in this work, error analysis, through the SSE (equation (12)), together with the assessed determination coefficient (R^2) (equation (13)) from regression analysis were employed to decide the model that best fitted the adsorption experimental data.

$$SSE = \sum_{i=1}^{n}(y_c - y_e)_i^2 \quad (12)$$

$$R^2 = 1 - \frac{SSE}{SST} = 1 - \frac{SSE}{\sum_{i=1}^{n}(y_{e,i} - \overline{y_e})^2} \quad (13)$$

where y_c is the ratio of effluent to influent dye concentrations calculated using the model, y_e is the ratio of effluent to influent dye concentrations using experimental conditions, n is the number of experiments and i is the experiment number [16], [17].

2.6. PSAC regeneration

Adsorbent regeneration was performed based on the results of previous experiments (sent for publication) that demonstrated that it was only effective for the black dye using hydrogen peroxide as desorption agent. Thus, adsorption/desorption cycles were only applied to the black dye. The adsorption stage was carried out, as previously explained, at an initial concentration of 25 mg L^{-1}, a flow rate of 7.7 mL min^{-1} and a bed height of 2 cm or at an initial concentration of 100 mg L^{-1}, a flow rate of 30.8 mL min^{-1} and a bed height of 4 cm. The dye concentration after adsorption was measured as previously mentioned. Once the adsorption experiment was completed, the saturated PSAC was put in contact with 1.2% w/v H_2O_2 by pumping the solution through the packed bed column in an up-flow mode for 4 hours at room temperature at a flow rate of 7.7 mL min^{-1}. Afterwards, the adsorbent was washed with distilled water.

3. Results and discussion

3.1. Physical characterization of PSAC

The N_2 adsorption isotherm of PSAC is shown in Figure 2. Its shape suggests that it belongs to an isotherm Type I, agreeing with the IUPAC classification [18], presenting the same behavior as that produced on a small scale (sent to publication). This type of isotherm is characteristic of a microporous adsorbent which is in agreement with the surface area calculated with CO_2 [19]. Besides, the fact that it presents a very wide knee, which is in agreement with the Type Ib classification, implies an important generation of mesopores and can be more interesting for the adsorption of dyes (large molecules).

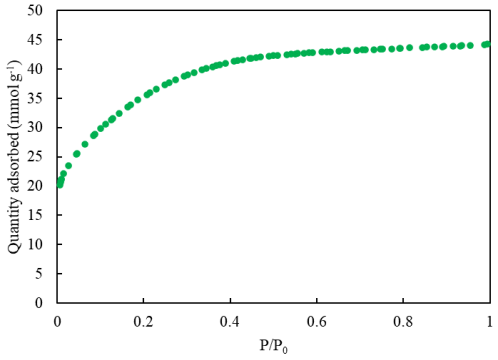

Figure 2. Nitrogen adsorption isotherm at -196ºC of PSAC.

The surface area calculated using adsorption of N_2 and CO_2 at -196ºC and 0ºC, respectively, and other textural properties are presented in Table 1. The high S_{BET} and total pore volume of PSAC tend to facilitate greatly the capacity of dye removal. The average pore diameter determined with N_2 isotherm data is higher than the molecular highest distance between two extreme atoms of the blue, red and black dyes of 1.37 nm, 1.28 nm and 1.53 nm respectively, which could lead to facilitate pore diffusion [7], [20]. However, the pore size distribution determined with N_2 and CO_2 adsorption data simultaneously has shown a lower average pore size (Table 1) which may indicate that part of the porous structure is not available for the adsorption of this type of molecules due to size exclusion and also lead to diffusion limitations. Figure 3 shows the pore size distribution of PSAC with a broad peak between 2 and 5 nm corresponding to the mesoporous region and several peaks in the microporous region (less than 2 nm) which can limit dye diffusion. This could be corroborated by the high CO_2 surface area which reveals the presence of

ultramicropores (< 0.7 nm) (around 30% of the overall volume) which is not available for dye adsorption.

Table 1. Surface characterization of the activated carbon prepared.

Parameters	PSAC
BET surface area N_2 (m^2 g^{-1})	2826 ± 8.97
BET surface area CO_2 (m^2 g^{-1})	910 ± 11.80
Total pore volume (cm^3 g^{-1})	1.54
Mesopore volume (cm^3 g^{-1})	1.07
Micropore volume (cm^3 g^{-1})	0.47
Average pore diameter (nm)	2.18
Average pore diameter N_2/CO_2 (nm)	1.10*

* determined simultaneously with N_2 at -196ºC and CO_2 at 0ºC isotherms.

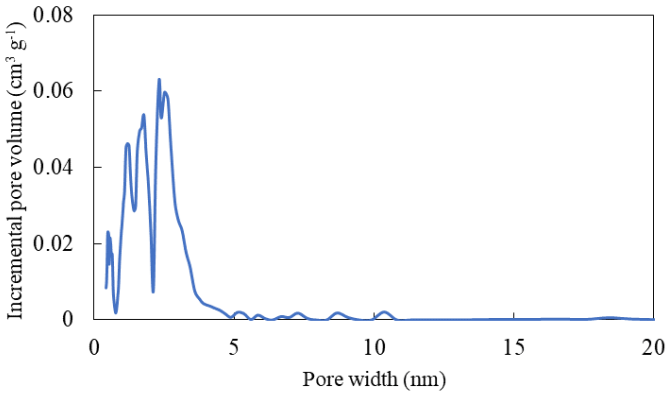

Figure 3. Pore size distribution of PSAC

3.2. Effect of flowrate

In general, a breakthrough curve (BTC) is represented by a graph with $C_{effluent}$ or $C_{effluent}/C_{influent}$ versus the experimental time or the treated volume for a determined bed height. The BTC tendency and time required to reach the breakpoint are important factors for the fixed bed column design and to check the possible application in the industry. The shape of the curve can vary with sorbent characteristics, inlet adsorbate concentration, inlet flowrate, bed height or diameter of the column. Thus, the analysis of BTC is essential for the effective design of the column [16].

Flow rate is a critical variable to determine the efficiency of the adsorbent for application in a large-scale continuous process. The influence of the flow rate on dye adsorption on PSAC was investigated varying the flow rate (7.7 and 30.8 mL min^{-1}) at fixed values of the inlet dye concentration and bed height. The results are shown in Figure 4.

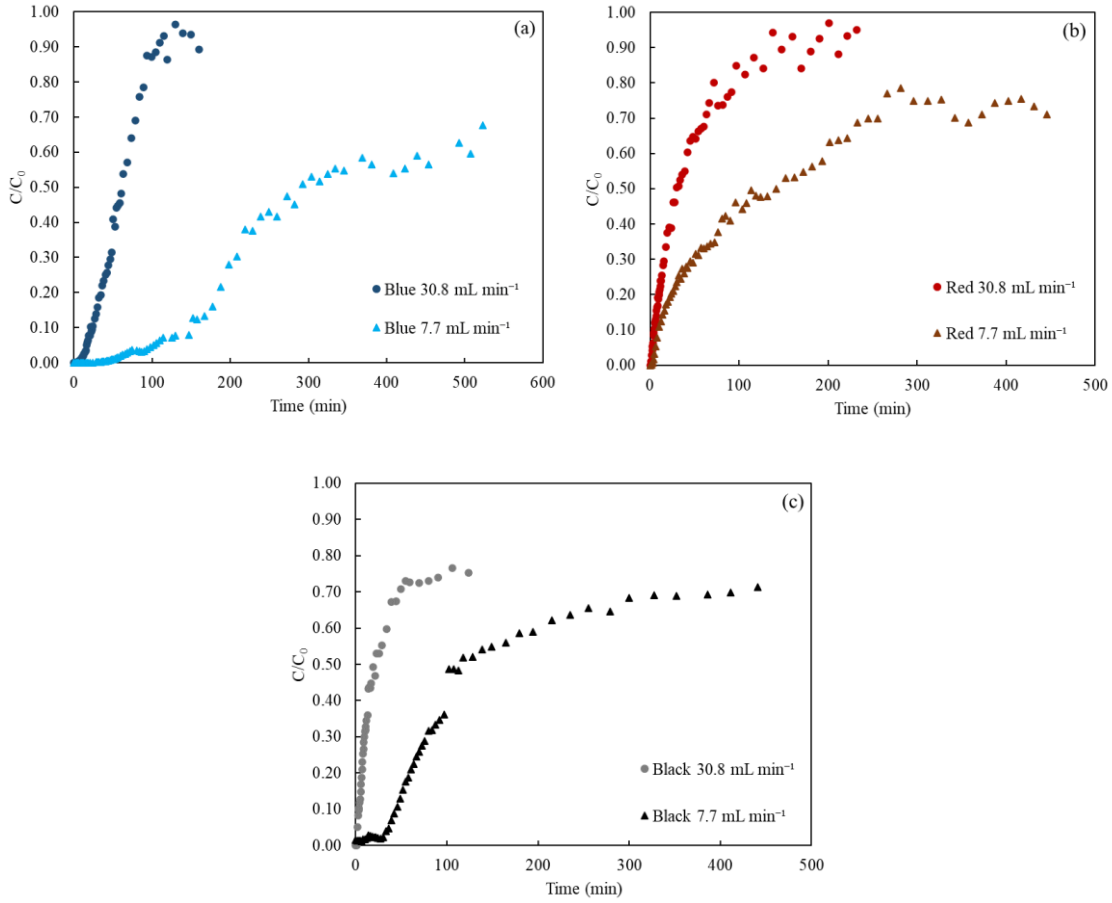

Figure 4. Breakthrough curves for blue (a), red (b) and black (c) dye adsorption onto PSAC at different flow rates (inlet dye concentration: 500 mg L^{-1} for blue and red and 100 mg L^{-1} for black dye; bed height: 4 cm; temperature: 20ºC).

It is observed that increasing the flow rate the breakthrough curve became steeper and the breakthrough time decreased (Table 2), due to the increased mass transfer rate in the adsorption zone. Similar results were obtained by Al-Mahbashi et al. [21] for the removal of dye-contaminated effluent with sewage-sludge-based biochar, Topare and Bokil [22] for the adsorption of textile industry effluent using activated carbon prepared from agro-waste materials and Ali et al. [23] for adsorption of tartrazine anionic dye with synthesized polystyrene/magnetite nanocomposite. Additionally, except for the red dye, the adsorption capacity decreased with increasing the flow rate. This is because at high flow rates, the residence time of the dyes in the column is reduced, which results in less contact time between the dye and the adsorbent, and intraparticle diffusion may be limited [16]. Furthermore, it is observed that by increasing the flow rate fed to the column, higher values of C/C_0 tend to be reached. This fact may be caused by an increase in turbulence generated using greater flow rate and therefore an increase in mass transfer processes.

Table 2. Estimated parameters obtained from the BTCs corresponding to the adsorption of blue, red and black dyes onto PSAC in function of flow rate (bed height: 4 cm; temperature: 20ºC).

Dye	Concentration	Q	t_b	V_{ef}	t_{oper}	m	q_{bed}	%Removal	MTZ
Blue	500	30.8	17	4933	160	1.0	995.2	40.6	3.5
		7.7	42	4029	523	1.0	1283.1	65.0	3.7
Red	500	30.8	3	1789	232	1.0	896.9	24.4	3.9
		7.7	6	3098	446	1.0	705.3	42.2	3.9
Black	100	30.8	2	3818	124	1.0	130.4	36.5	3.9
		7.7	36	3395	441	1.0	153.4	34.1	3.5

Concentration (mg L^{-1}); Q (mL min^{-1}): feed flow; t_b (min): breakthrough time; V_{ef} (mL); volume of effluent; t_{oper} (min): total operating time; m (g): mass of adsorbent; q_{bed} (mg g^{-1}): adsorption capacity of the PSAC bed; MTZ (cm): mass transfer zone.

The variation that can be observed in the slope of the curves and in the adsorption capacity can be explained by limitations on the mass transfer [24].

3.3. Effect of inlet dye concentration

The influence of the inlet dye concentration was investigated at a constant flow rate of 7.7 mL min^{-1}, a bed height of 2 cm and decreasing the initial dye concentration from 500 to 100 mg L^{-1} for blue and red dyes and from 100 to 25 mg L^{-1} for black dye. The results are shown in Figure 5 and Table 3.

It is observed that t_b decreased significantly and sharper BTCs were obtained by increasing the inlet dye concentration. Possibly because a reduced concentration gradient generates a slower transport. These results suggest that the diffusion mechanism depends on the concentration. The mass transfer driving force increases along with the influent concentration and dye loading rate, which results in a reduction in the length of the adsorption zone and enhanced performance [24]. Increasing the initial dye concentration led to an increase in the MTZ because of a fast transport phenomena [16]. Similar results were obtained by Abrouki et al. [25] using agricultural biomass for the adsorption of textile dye, Kashri and Ahmad [3] using Intsia bijuga sawdust-based activated carbon for dyes adsorption and Topare and Bokil [22] using activated carbon prepared from agro-wastes for the adsorption of textile industry effluent.

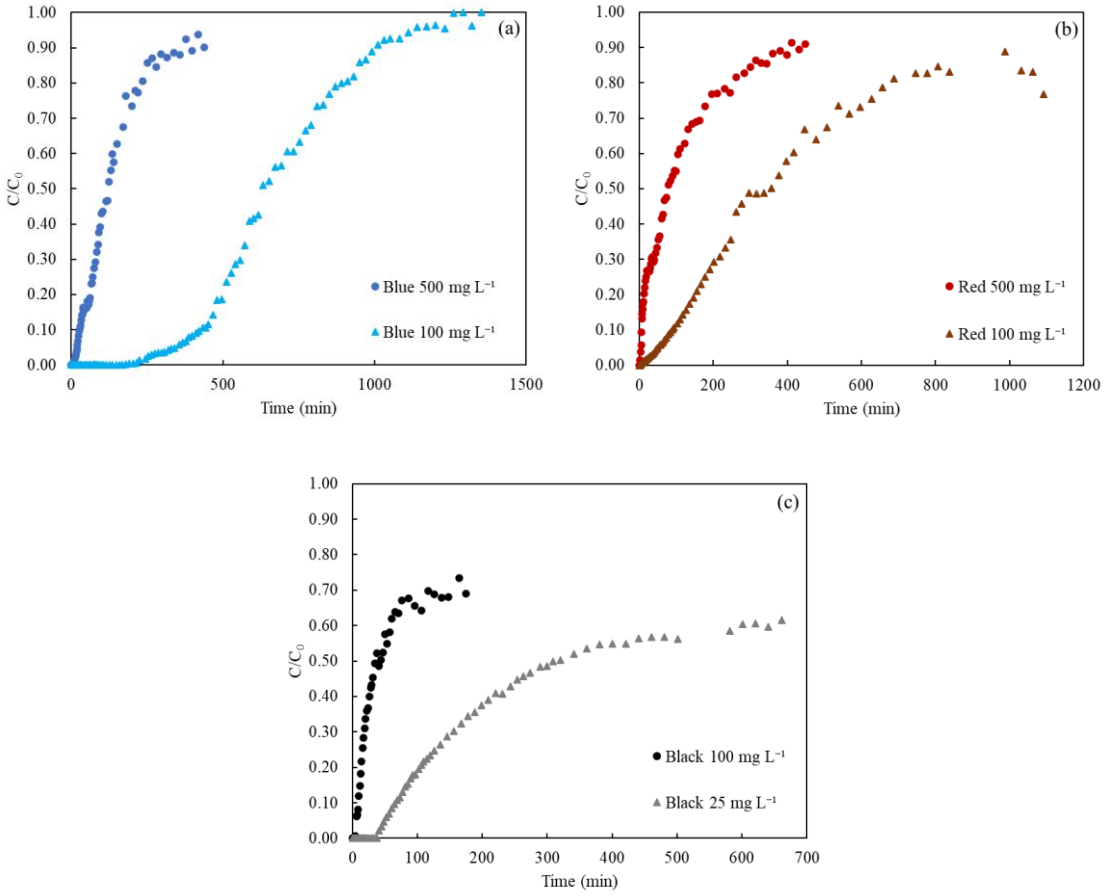

Figure 5. Breakthrough curves for blue (a), red (b) and black (c) dye adsorption onto PSAC at different influent concentrations (Flow rate: 7 mL min^{-1}; bed height: 2 cm; temperature: 20ºC).

Table 3. Estimated parameters obtained from BTCs corresponding to the adsorption of blue, red and black dyes onto PSAC in function of inlet concentrations (Flow rate: 7.7 mL min^{-1}; bed height: 2 cm; temperature: 20ºC).

Dye	Concentration	t_b	V_{ef}	t_{oper}	m	q_{bed}	%Removal	MTZ
Blue	500	20	3370	438	0.5	1165.6	34.7	1.9
	100	341	10407	1352	0.5	1139.3	50.9	1.5
Red	500	5	3445	447	0.5	1028.4	30.0	2.0
	100	50	8409	1092	0.4	863.5	39.7	1.9
Black	100	6	1347	175	0.5	109.3	43.0	1.9
	25	49	5088	661	0.5	146.5	57.2	1.8

Concentration (mg L^{-1}); t_b (min): breakthrough time; V_{ef} (mL); volume of effluent; t_{oper} (min): total operating time; m (g): mass of adsorbent; q_{bed} (mg g^{-1}): adsorption capacity of the PSAC bed; MTZ (cm): mass transfer zone.

3.4. Effect of adsorbent bed height

The experimental BTCs for the adsorption of blue, red and black dye on PSAC at distinct bed lengths of 2 and 4 cm, inlet dye concentration of 500 mg L^{-1} for blue and red dyes and 100 mg L^{-1} for black dye at a flow rate of 7.7 mL min^{-1} are depicted in Figure 6. It is observed that both the breakthrough time and the removal efficiency increased with increasing bed height (Table 4) [16]. On the other hand, the shape of the curves was, in general, steeper for the lower bed height as a

result of the reduced mass transfer zone due to the decrease in adsorbent load which can lead to a reduction in the adsorption capacity and a faster adsorption rate. By increasing the bed height, the number of active sites for adsorption also increases because of the increased surface area [1], [16], [21]. With the increase in the bed height, it was more difficult to reach saturation for the operation time, since C/C_0 values are lower due to the availability of higher adsorption sites.

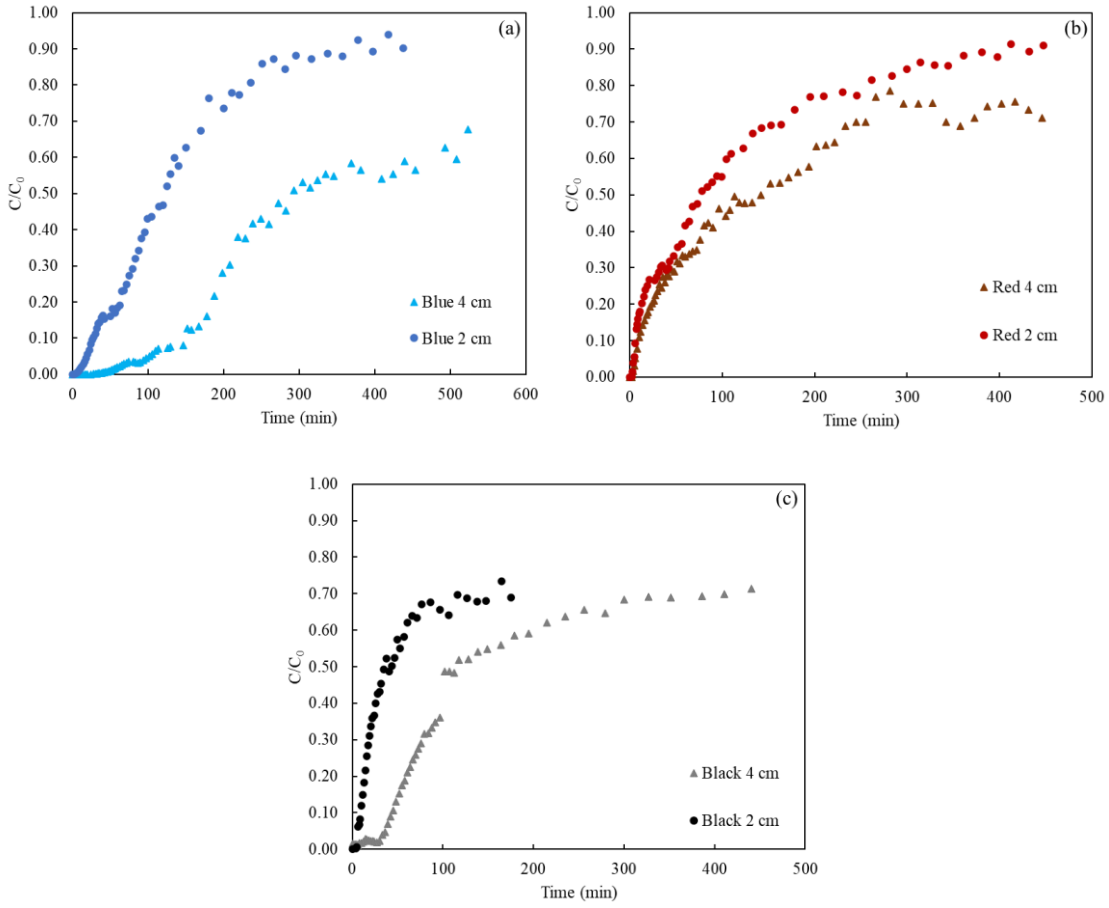

Figure 6. BTCs curves for blue (a), red (b) and black (c) dye adsorption onto PSAC at distinct influent concentrations (initial dye concentration: 500 mg L^{-1} for blue and red and 100 mg L^{-1} for black dye; Flow rate: 7 mL min^{-1}; temperature: 20ºC).

Table 4. Estimated parameters obtained from BTCs corresponding to the adsorption of blue, red and black dyes onto PSAC in function of bed height (500 mg L^{-1} for blue and red and 100 mg L^{-1} for black dye; Flow rate: 7.7 mL min^{-1}; temperature: 20ºC).

Dye	Bed height	t_b	V_{ef}	t_{oper}	m	q_{bed}	%Removal	MTZ
Blue	4	42	4029	523	1.0	1283.1	65.0	3.7
	2	20	3370	438	0.5	1165.6	34.7	1.9
Red	4	6	3098	446	1.0	705.3	42.2	3.9
	2	5	3445	447	0.5	1028.4	30.0	2.0
Black	4	36	3395	441	1.0	153.4	47.3	3.5
	2	6	1347	175	0.5	109.3	43.0	1.9

Bed height (cm); t_b (min): breakthrough time; V_{ef} (mL); volume of effluent; t_{oper} (min): total operating time; m (g): mass of adsorbent; q_{bed} (mg g^{-1}): adsorption capacity of the PSAC bed; MTZ (cm): mass transfer zone.

Additionally, as a comparison, Figure 7 shows in more detail the dye behavior at the same adsorption conditions. It revealed, in agreement with the previous results, that PSAC is more effective in adsorbing the blue dye since the retention time is higher during the experiment. However, for the other two dyes, especially for the black dye, the release of dye occurs in the outlet effluent in a short period of time.

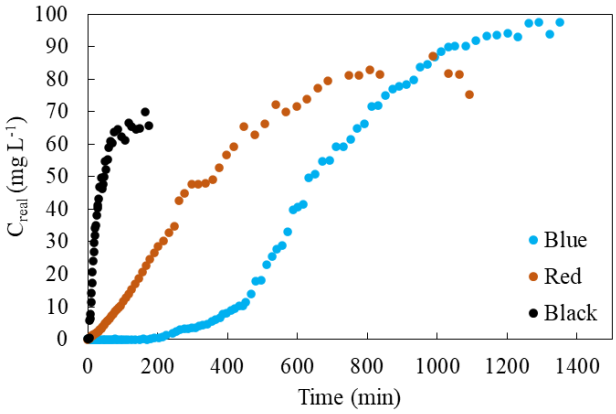

Figure 7. A comparison of fixed-bed column three dyes adsorption onto PSAC in function of time (initial dye concentration: 100 mg L^{-1}; Flow rate: 7 mL min^{-1}; Bed height: 2 cm; temperature: 20ºC).

Comparing the adsorption capacity of PSAC (Table 4) with those of other biomass based activated carbons reported in the literature it can be concluded that PSAC has high capacity for dye adsorption. As an example, the adsorption capacity of *Acacia nilotica* sawdust activated carbon for Indigo Carmine dye was 24.67 mg g^{-1} at bed height, initial dye concentration and flow rate of 30 cm, 100 mg L^{-1} and 250 mL h^{-1}, respectively [4]. Employing sludge-sawdust activated carbon as an adsorbent for malachite green removal, a maximum adsorption capacity of 565 mg g^{-1} was obtained at an inlet dye concentration of 50 mg L^{-1}, flow rate of 20 mL min^{-1} and bed length of 6 cm [26]. An adsorption capacity of 82.35 mg g^{-1} was achieved for the removal of reactive red 195 dye *by Adenanthera paronina* L seed activated carbon at inlet dye concentration, flow rate and bed length of 75 mg L^{-1}, 10 mL min^{-1} and 5 cm respectively [2].

3.5. Dynamic modeling of fixed-bed column

The modeling of the adsorption process in continuous was carried out to predict the dynamics of the process and obtain the corresponding kinetic parameters. For the experimental data that was possible to obtain the fit, the variables determined in each model estimated by non-linear regression analysis are presented in Table 5.

In general, for the cases in which it was not possible to obtain an adjustment, it is probably because, apart from not reaching saturation ($C/C_0 = 1$), the ideal "S" shape profile produced in ideal adsorption systems was not achieved once the dye began to be released at very short times. On the other hand, in cases where an adjustment is only obtained for the first part, the BTC becomes elongated in the second region without reaching saturation, which may be due to mass transfer limitations or non-uniform flow. Moreover, a "S" shape profile is often associated with the adsorption of small and simplest dye molecules, which could be obtained in some cases for the blue dye which is the dye with a less complex chemical structure [7], [27].

Table 5. BTCs model data for dyes adsorption onto PSAC

Dye	Conditions				Thomas			Yoon-Nelson			
	C_0	Q	H	q_t	K_{Th}	R^2	SSR	K_{YN}	τ	R^2	SSR
Blue	500	7.7	2**	824.92	0.059	0.996	0.024	0.030	107.63	0.996	0.024
	100	7.7	2	1115.69	0.077	0.995	0.069	0.0075	673.56	0.995	0.069
	500	30.8	4	945.22	0.11	0.990	0.060	0.055	61.80	0.990	0.060
	500	7.7	4**	982.04	0.037	0.995	0.019	0.0089	347.84	0.884	0.019
Red	100	7.7	2**	586.17	0.11	0.995	0.031	0.011	294.26	0.994	0.031
Black	100	7.7	2**	18.95	1.38	0.991	0.022	0.13	25.75	0.991	0.022
	25	7.7	2**	67.02	0.89	0.990	0.033	0.023	172.95	0.990	0.033
	100	7.7	4**	80.09	0.34	0.989	0.038	0.032	108.82	0.989	0.038

*C_0 (mg L^{-1}); Q (mL min^{-1}); H (cm); q_t (mg g^{-1}); K_{Th} (mL mg^{-1} min^{-1}); K_{YN} (min^{-1}); τ (min). **Fitted to the first stage of the BTC.

The results presented in Table 5 revealed good correlations $R^2 > 0.9$ for both Thomas and Yoon-Nelson models for three dyes and with a low SSR. The Thomas model allows to assume irrelevant radial and axial dispersion and insignificant changes on temperature and pressure inside the column. Apart from that, and in agreement with batch experiments, it suggests that external and intraparticle diffusion do not represent the rate limiting stages but both can have influence on the adsorption process [26] (send to publication). Yoon-Nelson model also represents a good fit, and many times similar to results of the Thomas model. Hui and Zaini 2022 [26], Alardhi et al 2020 [1] and Silva et al 2021 [28] also reported the same observations.

For the blue dye and for the two BTCs that it was possible to adjust all the data, the experimental (q_{exp}) and predicted (q_t) adsorption capacities did not differ significantly.

3.6. PSAC regeneration

Regeneration and reuse of the adsorbent are essential to minimize the cost and maximize the potential of the adsorbent. In this work, regeneration was only performed for the black dye since, in previous work (sent to publication), only promising results were obtained for the black dye using hydrogen peroxide as a desorption agent, but effective desorption was not achieved for the red and blue dyes. Figure 8 and Table 6 show the results obtained for three adsorption/desorption cycles at different inlet dye concentrations. It is observed that both breakthrough time and adsorption capacity decreased with every cycle since active sites are lost due to a progressive degradation of the PSAC surface with the continuous operational conditions and the dye molecules that are irreversible adsorbed [1], [29]. However, it was less significant for the lower inlet dye concentration.

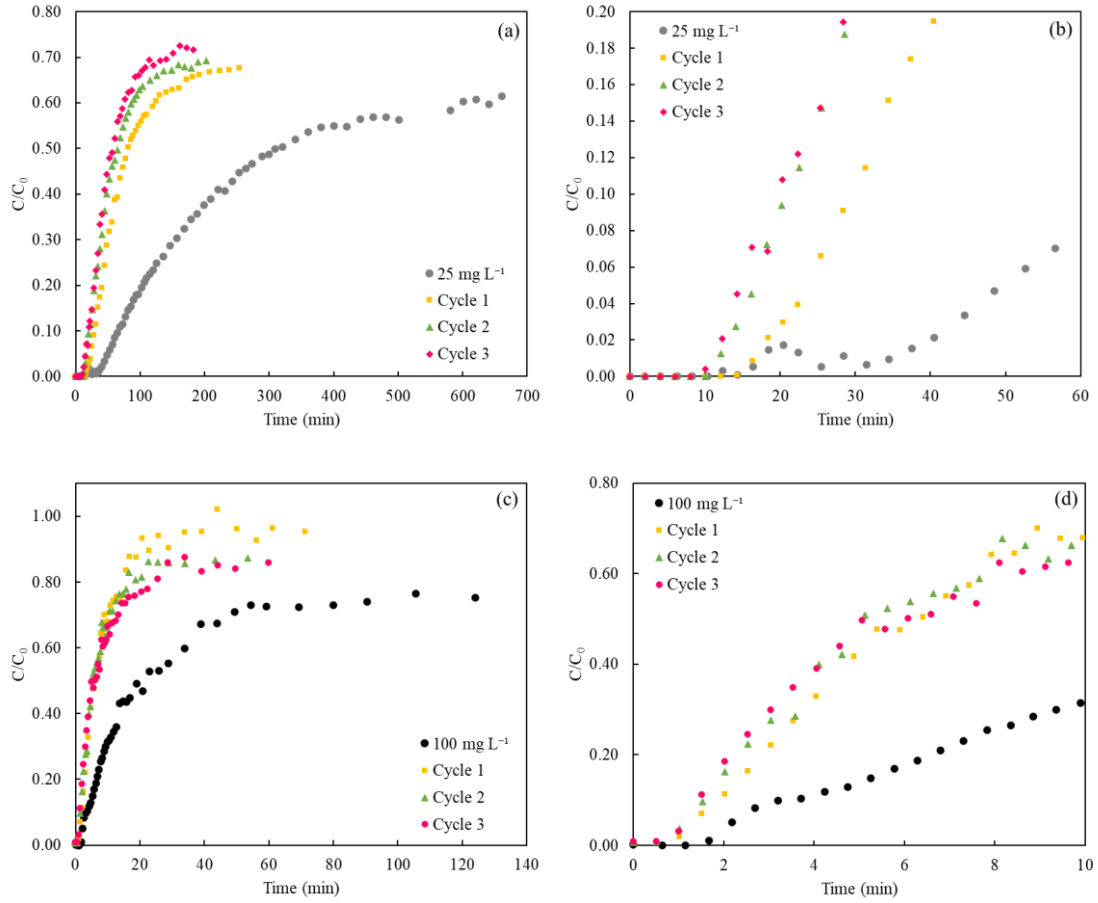

Figure 8. BTCs curves for the adsorption of black dye onto regenerated PSAC beds at different adsorption/desorption cycles (Flow rate: 4.4 mL min^{-1}; bed height: 2 cm (a, b) and 4 cm (c, d); regeneration time: 4 h).

Table 6. Parameters obtained from BTCs analysis for black dye adsorption on regenerated PSAC beds.

BTCs parameters	1st adsorption		Cycle 1		Cycle 2		Cycle 3	
C_0	25	100	25	100	25	100	25	100
q_{bed}	146.5	130.4	45.8	30.9	36.2	37.4	32.0	47.3
% Removal	57.2	36.5	50.4	14.9	48.8	24.1	47.4	25.5
V_{ef}	5087.9	3818.0	1955.1	2195.3	1555.0	1647.4	1402.0	1849.4
t_b	49	2	25	1	16	1	14	1
MTZ	1.8	3.9	1.8	3.9	1.8	3.8	1.8	3.9

C_0 (mg L^{-1}): initial dye concentration; t_b (min): breakthrough time; V_{ef} (mL); volume of effluent; q_{bed} (mg g^{-1}): adsorption capacity of the PSAC bed; MTZ (cm): mass transfer zone.

Moreover, in every cycle, the volume of effluent needed for the experiment was significantly reduced while the MTZ was maintained, which means that the mass transfer is still occurring and the adsorbent is still capable of adsorbing dye molecules. So, mainly at 25 mg L^{-1}, the PSAC possesses a good capability of regeneration since the reduction in adsorption efficiency only corresponds to 17%.

4. Conclusion

An activated carbon from pine sawdust chemically activated with KOH was produced for wood dyes adsorption. The carbon had a high surface area and total pore volume of 2826 $m^2\ g^{-1}$ and of 1.54 $cm^3\ g^{-1}$, respectively. Dyes adsorption onto the activated carbon in a fixed-bed column revealed that the adsorption capacity was affected by the flow rate, inlet dye concentration and bed height. The breakthrough curves became steeper the higher the flow rate and the inlet dye concentration and the lower the bed height. The maximum bed adsorption capacity of 1283.1 mg g^{-1} was obtained at an inlet dye concentration of 500 mg L^{-1}, flow rate of 7.7 mL min^{-1} and bed length of 4 cm. The fixed-bed column behavior was best described by the Thomas and Yoon-Nelson models. Regeneration experiments for ACPS saturated with the black dye using hydrogen peroxide revealed that the carbon can be used for at least three cycles at an inlet concentration of 25 mg L^{-1} with low capacity loss. The results of the present work demonstrated that pine sawdust KOH activated carbon can be an alternative to commercial activated carbons for treating industrial wastewater containing dyes.

Acknowledgments

This work was financial supported by Xunta de Galicia (ED431B 2020/039).

Author contribution

Catarina H. Pimentel: Investigation, Validation, Visualization, Writing – original draft (catarinahelenada.silveiramirandaguedes@usc.es). **M. Sonia Freire:** Conceptualization, Methodology, Supervision, Funding acquisition, Writing—review & editing (mariasonia.freire@usc.es). **Diego Gómez-Díaz:** Conceptualization, Methodology, Supervision, Funding acquisition, Writing—review & editing (diego.gomez@usc.es). **Julia González-Álvarez:** Conceptualization, Methodology, Supervision, Funding acquisition, Writing—review & editing (julia.gonzalez@usc.es).

Availability of data and materials All data generated or analyzed during this study are included in this article.

Declarations

Ethics approval Not applicable.

Consent to participate Not applicable.

Consent to publish Not applicable.

Competing interests The authors declare no competing interests.

References

[1] S. M. Alardhi, T. M. Albayati, and J. M. Alrubaye, "Adsorption of the methyl green dye pollutant from aqueous solution using mesoporous materials MCM-41 in a fixed-bed column," *Heliyon*, vol. 6, no. 1, p. e03253, 2020, doi: 10.1016/j.heliyon.2020.e03253.

[2] P. Ashokan, M. Asaithambi, V. Sivakumar, and P. Sivakumar, "Batch and column mode adsorption studies of reactive red 195 dye using Adenanthera paronina L seed activated carbon," *Groundw. Sustain. Dev.*, vol. 15, no. March, p. 100671, 2021, doi:

10.1016/j.gsd.2021.100671.

[3] A. Khasri and M. A. Ahmad, "Adsorption of basic and reactive dyes from aqueous solution onto Intsia bijuga sawdust-based activated carbon: batch and column study," *Environ. Sci. Pollut. Res.*, vol. 25, no. 31, pp. 31508–31519, 2018, doi: 10.1007/s11356-018-3046-3.

[4] T. Gupta *et al.*, "Adsorption of Indigo Carmine Dye by Acacia nilotica sawdust activated carbon in fixed bed column," *Sci. Rep.*, vol. 12, no. 1, pp. 1–14, 2022, doi: 10.1038/s41598-022-19595-6.

[5] B. G. P. Kumar, L. R. Miranda, and M. Velan, "Adsorption of Bismark Brown dye on activated carbons prepared from rubberwood sawdust (Hevea brasiliensis) using different activation methods," *J. Hazard. Mater.*, vol. 126, no. 1–3, pp. 63–70, 2005, doi: 10.1016/j.jhazmat.2005.05.043.

[6] H. Patel, "Fixed-bed column adsorption study: a comprehensive review," *Appl. Water Sci.*, vol. 9, no. 3, pp. 1–17, 2019, doi: 10.1007/s13201-019-0927-7.

[7] C. H. Pimentel, M. S. Freire, D. Gómez-Díaz, and J. González-Álvarez, "Preparation of activated carbon from pine (Pinus radiata) sawdust by chemical activation with zinc chloride for wood dyes adsorption," *Biomass Convers. Biorefinery*, no. 1, 2023, doi: 10.1007/s13399-023-04138-4.

[8] H. E. Reynel-Avila, D. I. Mendoza-Castillo, and A. Bonilla-Petriciolet, "Relevance of anionic dye properties on water decolorization performance using bone char: Adsorption kinetics, isotherms and breakthrough curves," *J. Mol. Liq.*, vol. 219, pp. 425–434, 2016, doi: 10.1016/j.molliq.2016.03.051.

[9] K. J. Fernández-Andrade *et al.*, "Evaluation of mass transfer in packed column for competitive adsorption of Tartrazine and brilliant blue FCF: A statistical analysis," *Results Eng.*, vol. 14, 2022, doi: 10.1016/j.rineng.2022.100449.

[10] K. V. Kumar and S. Sivanesan, "Selection of optimum sorption kinetics: Comparison of linear and non-linear method," *J. Hazard. Mater.*, vol. 134, no. 1–3, pp. 277–279, 2006, doi: 10.1016/j.jhazmat.2005.11.003.

[11] J. L. Diaz de Tuesta, A. M. T. Silva, J. L. Faria, and H. T. Gomes, "Adsorption of Sudan-IV contained in oily wastewater on lipophilic activated carbons: kinetic and isotherm modelling," *Environ. Sci. Pollut. Res.*, vol. 27, no. 17, pp. 20770–20785, 2020, doi: 10.1007/s11356-020-08473-1.

[12] S. K. Mani and R. Bhandari, "Efficient Fluoride Removal by a Fixed-Bed Column of Self-Assembled Zr(IV)-, Fe(III)-, Cu(II)-Complexed Polyvinyl Alcohol Hydrogel Beads," *ACS Omega*, vol. 7, no. 17, pp. 15048–15063, 2022, doi: 10.1021/acsomega.2c00834.

[13] J. T. Nwabanne, O. C. Iheanacho, C. C. Obi, and C. E. Onu, "Linear and nonlinear kinetics analysis and adsorption characteristics of packed bed column for phenol removal using rice husk-activated carbon," *Appl. Water Sci.*, vol. 12, no. 5, pp. 1–16, 2022, doi: 10.1007/s13201-022-01635-1.

[14] T. G. Myers, A. Valverde, and A. Cabrera-Codony, "On the Development of a Consistent Mathematical Model for Adsorption in a Packed Column (and Why Standard Models Fail)," *SSRN Electron. J.*, 2022, doi: 10.2139/ssrn.4100971.

[15] B. Kiran and A. Kaushik, "Cyanobacterial biosorption of Cr(VI): Application of two parameter and Bohart Adams models for batch and column studies," *Chem. Eng. J.*, vol. 144, no. 3, pp. 391–399, 2008, doi: 10.1016/j.cej.2008.02.003.

[16] S. Charola, R. Yadav, P. Das, and S. Maiti, "Fixed-bed adsorption of Reactive Orange 84 dye onto activated carbon prepared from empty cotton flower agro-waste," *Sustain.*

Environ. Res., vol. 28, no. 6, pp. 298–308, 2018, doi: 10.1016/j.serj.2018.09.003.

[17] M. B. Fard, D. Hamidi, K. Yetilmezsoy, J. Alavi, and F. Hosseinpour, "Utilization of Alyssum mucilage as a natural coagulant in oily-saline wastewater treatment," *J. Water Process Eng.*, vol. 40, no. November 2020, p. 101763, 2021, doi: 10.1016/j.jwpe.2020.101763.

[18] M. Thommes *et al.*, "Physisorption of gases, with special reference to the evaluation of surface area and pore size distribution (IUPAC Technical Report)," *Pure Appl. Chem.*, vol. 87, no. 9–10, pp. 1051–1069, 2015, doi: 10.1515/pac-2014-1117.

[19] A. H. Jawad *et al.*, "Microporous activated carbon developed from KOH activated biomass waste: surface mechanistic study of methylene blue dye adsorption," *Water Sci. Technol.*, vol. 84, no. 8, pp. 1858–1872, 2021, doi: 10.2166/wst.2021.355.

[20] S. Wang, M. Soudi, L. Li, and Z. H. Zhu, "Coal ash conversion into effective adsorbents for removal of heavy metals and dyes from wastewater," *J. Hazard. Mater.*, vol. 133, no. 1–3, 2006, doi: 10.1016/j.jhazmat.2005.10.034.

[21] N. M. Y. Al-Mahbashi *et al.*, "Bench-Scale Fixed-Bed Column Study for the Removal of Dye-Contaminated Effluent Using Sewage-Sludge-Based Biochar," *Sustain.*, vol. 14, no. 11, 2022, doi: 10.3390/su14116484.

[22] N. S. Topare and S. A. Bokil, "Adsorption of textile industry effluent in a fixed bed column using activated carbon prepared from agro-waste materials," *Mater. Today Proc.*, vol. 43, pp. 530–534, 2020, doi: 10.1016/j.matpr.2020.12.029.

[23] M. A. Ali, M. F. Mubarak, M. Keshawy, M. A. Zayed, and M. Ataalla, "Adsorption of Tartrazine anionic dye by novel fixed bed Core-Shell- polystyrene Divinylbenzene/Magnetite nanocomposite," *Alexandria Eng. J.*, vol. 61, no. 2, pp. 1335–1352, 2022, doi: 10.1016/j.aej.2021.06.016.

[24] A. A. Ahmad and B. H. Hameed, "Fixed-bed adsorption of reactive azo dye onto granular activated carbon prepared from waste," *J. Hazard. Mater.*, vol. 175, no. 1–3, pp. 298–303, 2010, doi: 10.1016/j.jhazmat.2009.10.003.

[25] Y. Abrouki *et al.*, "Optimization and modeling of a fixed-bed biosorption of textile dye using agricultural biomass from the moroccan sahara," *Desalin. Water Treat.*, vol. 240, no. 2021, pp. 144–151, 2021, doi: 10.5004/dwt.2021.27704.

[26] T. S. Hui and M. A. A. Zaini, "Textile sludge–sawdust chemically produced activated carbon: equilibrium and dynamics studies of malachite green adsorption," *Biomass Convers. Biorefinery*, vol. 12, no. 7, pp. 2847–2859, 2022, doi: 10.1007/s13399-020-00955-z.

[27] J. López-Cervantes, D. I. Sánchez-Machado, R. G. Sánchez-Duarte, and M. A. Correa-Murrieta, "Study of a fixed-bed column in the adsorption of an azo dye from an aqueous medium using a chitosan–glutaraldehyde biosorbent," *Adsorpt. Sci. Technol.*, vol. 36, no. 1–2, pp. 215–232, 2018, doi: 10.1177/0263617416688021.

[28] M. C. Silva *et al.*, "H3PO4–activated carbon fibers of high surface area from banana tree pseudo-stem fibers: Adsorption studies of methylene blue dye in batch and fixed bed systems," *J. Mol. Liq.*, vol. 324, 2021, doi: 10.1016/j.molliq.2020.114771.

[29] P. Zheng, B. Bai, W. Guan, H. Wang, and Y. Suo, "Fixed-bed column studies for the removal of anionic dye from aqueous solution using TiO2@glucose carbon composites and bed regeneration study," *J. Mater. Sci. Mater. Electron.*, vol. 27, no. 1, pp. 867–877, 2016, doi: 10.1007/s10854-015-3828-z.

6. GENERAL DISCUSSION

For many years, the linear economy's production route has resulted in significant changes to the environment, the economy, and the ecosystem. Large amounts of waste are produced by linear economies, which end up in the atmosphere and water bodies. In order to successfully have a circular economy instead of a linear one, the European Union bioeconomy should place environmentally friendly practices and circularity at the centre of its industrial structure. International energy authorities predicted that the necessity for bioenergy will increase by 2060, indicating the importance of making a switch to renewable energy and materials for the generation of chemical products, fuels and electrical power, such as lignocellulosic biomass [42].

Thus, the management of biomass residues is fundamental and for instance, pine sawdust is a lignocellulosic material that comes from nature and for that reason is widely available. Besides, this material is also a waste from industrial or agricultural activities which present disposal problems if not reused. So, different potential applications were reported such as the compost production, building materials, as a source of fuel in thermal processes and in remediation and management of pollution as a raw material or activated carbon precursor [37,38]. Among the applications mentioned, pine sawdust and derived carbons have been widely investigated for wastewater treatment.

A first attempt to introduce sawdust as a valuable biowaste was by using it without any pretreatment as a biosorbent for wood dye removal from aqueous solutions, as explained in the first paper published within the present Thesis entitled *Removal of wood dyes from aqueous solutions by sorption on untreated pine (Pinus radiata) sawdust* (Chapter 3). The use of adsorbents such as pine sawdust (PS), in its raw form, is a great advantage in terms of operational costs and is an alternative for solving the problem of wastewater contamination. However, previous investigations indicate that the material can be greatly improved through its modification, which can lead to an increase in the level of effectiveness, stability and reusability [7]. Currently, the most commonly employed adsorbents are activated carbons. However, one of the biggest disadvantages of commercial activated carbons is their high price (about US$ 2.0-2.2/kg) [17], so the production of alternative carbons is a challenge. In this regard, sawdust can be used to produce activated carbons since its carbon content is high. Thus, part of this Thesis focuses on the production of one biochar and five activated carbons from pine sawdust as alternative adsorbents for dye removal. Activated carbons were prepared by chemical activation with KOH and $ZnCl_2$ (the last one using both dry and wet method). $ZnCl_2$ was essentially chosen as it is known for its ability to produce activated carbon with a high surface area and for increasing the development of pores in the activated carbon structure and the yield of the material obtained [17]. KOH has been extensively used and was chosen due to its capacity to produce activated carbon with a high surface area, distribution of fine pore size under repeated conditions, low environmental pollution, low corrosiveness and low cost [40].

Several factors can affect the activated carbon production and its characteristics such as the activating agent, carbonization or activation temperature and time, and the composition of the precursor or the activation procedure that can be by dry mixing or by impregnation [43]. The effect of activation temperature (600 and 850 °C), type of activation method (dry mixing or wet), type of

activating agent and carbon/activating agent ratio (1:2 and 1:4 w/w) on the carbon structure and its chemical and morphological properties, which influence on the carbon adsorption performance, were studied. The results of these investigations are collected in two publications of these Thesis *Preparation of activated carbon from pine (Pinus radiata) sawdust by chemical activation with zinc chloride for wood dye adsorption* (Chapter 3) and *Removal of wood dyes from aqueous solutions using KOH chemically activated carbons from pine (Pinus radiata) sawdust* (submitted for publication, Chapter 4). Subsequently, with the activated carbon that led to the best adsorption results in batch mode, the material was produced on a large scale for application in continuous mode to approximate the process to an industrial scale. The results are presented in the paper entitled *Continuous adsorption of acid wood dyes onto an activated carbon prepared from pine sawdust* (in preparation, Chapter 4).

Furthermore, an additional application was proposed for pine sawdust and the prepared activated carbons, their use for the CO_2 adsorption. One of the most appealing strategies to reduce CO_2 emissions is carbon sequestration, which involves the capture and storage of CO_2 in the microporous assembly present in activated carbon matrix. Therefore, the study of the CO_2 adsorption capacity of the biochar and activated carbons was evaluated under different conditions of gas pressure (0-760 mmHg) and temperatures (0-50 °C), and the corresponding modelling was performed to comprehend the adsorption process and involved mechanisms. The results of these investigations are shown in the paper *Separation of CO_2 using biochar and KOH and $ZnCl_2$ activated carbons derived from pine sawdust* (Chapter 3).

To summarize, Figure 4 illustrates the different investigations carried out in this Thesis. Briefly, in a first stage pine sawdust was characterized by several methods that include the determination of BET surface area and pore volume from N_2 and CO_2 adsorption isotherms, scanning electron microscopy coupled with energy dispersive X-ray spectroscopy and point of zero charge determination and used without any pretreatment for wood dye adsorption (blue, red and black dyes). Then, it was used as a precursor for the production of activated carbons using $ZnCl_2$ and KOH as activating agents. The materials were characterized and applied for dye removal and CO_2 adsorption. Finally, the carbon that provided the best results was selected and experiments in a large-scale were performed in order to evaluate system performance in dynamic mode.

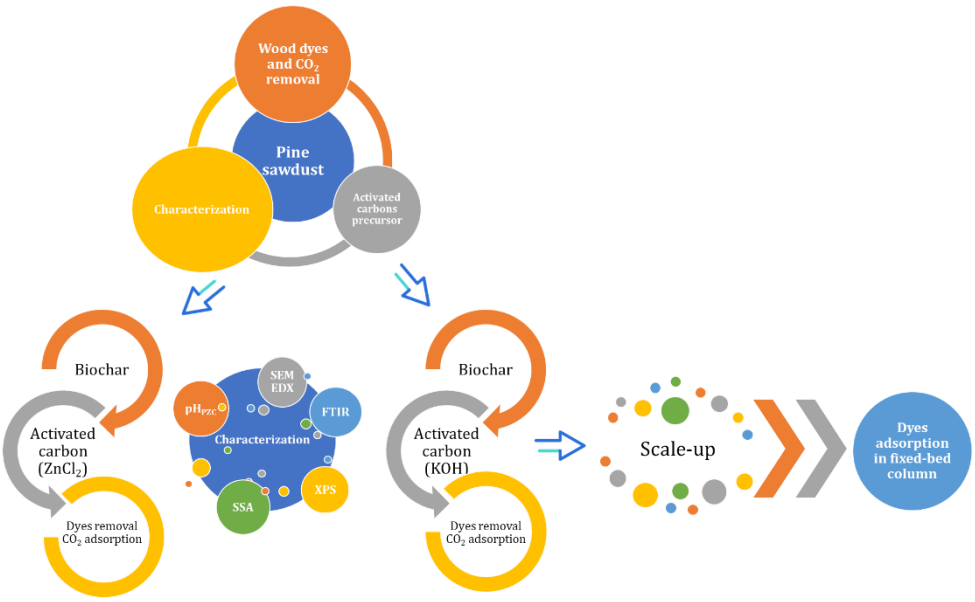

Figure 4. Diagram of different investigations performed on the present Thesis.

6.1 Dye adsorption onto pine *(Pinus radiata)* sawdust

In the present Thesis, acid wood dyes (blue, red and black dyes) were used and characterized. The acid dissociation constant (pK_a) was determined, and it was 10.6 for red, 10.4 for blue and 10.3 for black showing no significant differences and representing weak acids. The dye's stability was also investigated at different pH and for an initial dye concentration of 25 mg L^{-1}. The blue and red dyes showed no changes in their stability over 4 days, while black dye at acidic pH was instable. Therefore, for the black dye, the experiments only took up to 12 hours. The main differences between them are: (1) the molecular distance between two extreme atoms that was calculated with ChemDraw software and it was 1.37 nm for blue, 1.28 nm for red and 1.53 nm for black; (2) its functional groups by containing azo groups (-N=N-) linked to a benzene ring for red and black dyes, sulfonic acid groups ($-SO_3H$) more presented for black dye or acetyl group ($-COCH_3$) attached as for the blue dye; and (3) in its elemental composition since red dye contains fluor and the black one has chromium. These differences could explain the different behavior found in the adsorption process.

As indicated previously, in this first part of the Thesis, *Pinus radiata* sawdust was evaluated as a biosorbent for the removal of the blue, red, and black wood dyes from aqueous solutions, so it is important to comprehend the physicochemical and structural characteristics of this material to more accurately describe the adsorption process. In this case, the analysis of N_2 and CO_2 adsorption isotherms (Figure 5) evidenced that pine sawdust is a macroporous material with heterogeneous surface [10]. The presence of a hysteresis cycle revealed that the material also presents micro and mesoporosity, being the calculated values of surface area, total pore volume, and average diameter for N_2 1.55 $m^2\ g^{-1}$, 1.94 × 10^{-3} $cm^3\ g^{-1}$ and 5.15 nm (mesoporous material), respectively. Moreover, the CO_2 surface area was greater than the obtained from N_2 isotherm (17.83 $m^2\ g^{-1}$) which confirmed the existence of microporosity. The presence of a tubular structure with the existence of pores of different sizes accessible to dyes was also verified through SEM analysis. The point of zero charge

(pH_{PZC}) was also determined and it was 4.8. As the dyes used in the present work are anionic dyes, when the surface is positively charged it will favour the adsorption process, which is why it would be interesting to work at a pH lower than pH_{PZC}.

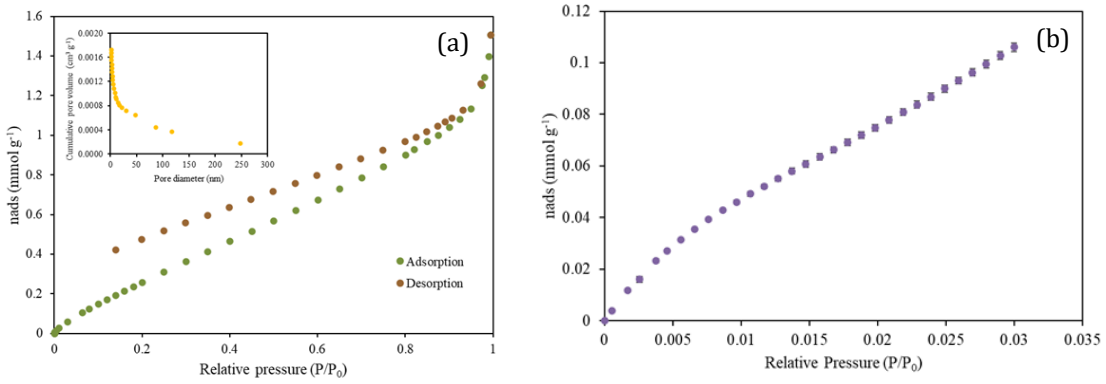

Figure 5. N_2 adsorption-desorption at −196 °C on PS and BJH pore size distribution (a) and CO_2 adsorption isotherm at 0 °C (b).

In order to analyze the adsorption performance of pine sawdust, in a first stage adsorption experiments were performed at natural pH, and the effect of adsorbent dose (5 and 10 g L^{-1}) and agitation rate (100 and 210 rpm) on dye removal efficiency at initial dye concentration of 5 mg L^{-1} was studied. The adsorption occurred in two stages, since at the beginning there were more available sites in the pine sawdust surface which favoured a faster dye adsorption. Afterwards, the surface began to become saturated and finally equilibrium was reached. Under the conditions essayed the time needed to reach equilibrium was between 48 and 96 hours. The adsorption efficiency was better for the blue dye which can be related to its lower natural pH of 5.1 compared to the black (6.0) and red (6.2) dyes. As mentioned above, at pH higher than pH_{PZC} electrostatic repulsion due to the presence of negative charges may occur causing a decrease in the adsorption efficiency. Also, the adsorption efficiency increased by increasing the adsorbent dose since more available active sites are present and hence an enhanced surface area which improves the adsorption process. Regarding the agitation rate, its increase favored the first adsorption stage and for this reason, the subsequent experiments were performed at the highest rate essayed (210 rpm).

As adsorption efficiency could improve by decreasing the pH, adsorption experiments were performed at distinct pH values (2-9), in order to evaluate the pH influence. The maximum dye adsorption efficiency increased from 67.7% to 100%, 29.9% to 95.1% and 34.5% to 85.5% for the blue, red and black dyes, respectively, with decreasing the pH from the natural to 2. This confirms that at pH lower than pH_{PZC}, as the surface is positively charged, the adsorption of anionic dyes through electrostatic interactions is favoured.

Taking the previous results into account, at the best pH (pH = 2) the adsorbent dose (2-10 g L^{-1}) and contact time (up to 96 h) were investigated in order to optimize the process and the adsorbent dose could be reduced to 6 g L^{-1} maintaining removal efficiency for all dyes. This enhancement could be related to the effect of ionic interactions at low pH [17,44]. In the next stage, the effect of the initial dye concentration was studied, increasing it to 300 mg L^{-1} using 10 g L^{-1}. Removal efficiency

decreased with increasing initial concentration, which was expected since high concentrations lead to a saturation of the adsorbent and also the repulsion between the adsorbed and non-adsorbed dye molecules could possibly occur [45,46]. Furthermore, as previously observed, the exact distance measured of the dye molecules was larger than 0.7 nm, which implies that ultra-micropores surface area is not available for adsorption. Despite the reduction in the adsorption efficiency, there is an increase in the maximum adsorption capacity with increasing concentration, which may be due to the increase in the driving force generated by the concentration gradient [47]. The adsorption of dyes to the surface of pine sawdust was also confirmed by SEM images after adsorption, which demonstrated surface coverage and pore blockage. This, together with EDX results which demonstrated the presence of elements of the dye composition on the adsorbent surface proving dye adsorption.

Regarding the adsorption process kinetics, to assess the mechanisms that explain it, experimental data were fitted to pseudo-first, pseudo-second and intraparticle diffusion models. The pseudo-second order kinetic model was the one that best fit the experimental data ($R^2 > 0.98$). Furthermore, the values of the predicted capacity were very close to the experimental ones. Also, regarding the intraparticle diffusion model, where the process was separated into two linear regions, high correlation coefficients ($R^2 > 0.82$) were obtained for the first region. This demonstrates that along with the second-order model that suggests a chemical adsorption process, the diffusion of the adsorbate also occurs in the pores of the adsorbent [47,48].

Adsorption equilibrium was investigated by fitting the experimental data to the Langmuir, Freundlich, Temkin and Dubidin-Radushkevich (D-R) isotherms. In all cases, Freundlich and D-R were the models that best fit the experimental data. Both models assume that a saturation condition is not reached and a heterogeneous adsorbate surface is present [47,49]. While Freundlich is related to a favorable adsorption in a heterogeneous surface, D-R represents the occurrence of a pore filling mechanism with subsequent adsorption in agreement with the kinetic results. Also, the mean adsorption energy provided by D-R model is in the range for chemical adsorption. This agrees with the macroporosity and heterogeneity revealed by the N_2 and CO_2 adsorption isotherms and the existence of great porosity also revealed by SEM.

After carrying out and optimizing the dye adsorption conditions with pine sawdust, the desorption process was evaluated to analyze the possibility of recycling the adsorbent and thus improving the economy of the process. Sodium hydroxide was selected as desorbent agent and desorption efficiencies of 16.3%, 90.9% and 24.8% were achieved for the blue, red and black dyes, respectively, at the first desorption stage. When several adsorption/desorption cycles were carried out the adsorption efficiency was improved over the 4 cycles for the red dye, since NaOH often serves to improve the surface properties of the materials [47,50]. The fact that NaOH presents better desorption results may be related to the fact that it provides alkalinity to the adsorbents' surface leading to electrostatic repulsion of the molecules. Regarding the blue and black dyes, the efficiency shows a slight reduction over the four cycles. These differences could be related since the red dye is the smallest one and can be easier removed from the surface. Furthermore, it contains less functional

groups than black dye which is the most difficult to desorb, possibly, due to the strong interaction with the surface of the material. In a future perspective to improve results, the concentration of desorbing agent can be increased, although this can also lead to the degradation of active centers [51]. The application of other eluents such as acetone or ethanol could also be tested [52].

Finally, since the adsorption capacity obtained from the CO_2 isotherm was quite low (0.1 mmol g^{-1}) pine sawdust was not considered as an adsorbent for CO_2 removal.

6.2 Preparation and characterization of biochar and activated carbons

Part of the study of this Thesis aimed to transform pine sawdust into high-efficiency biochar and activated carbons for the removal of dyes from aqueous solutions as well as for CO_2 capture from post combustion gas streams.

Table 3 shows all the produced materials with the respective conditions used for their preparation and the yield obtained.

Table 3. Conditions for the prepared biochar and activated carbons and their respective yield.

Type of carbon	Activating agent	Carbon to activating agent ratio	Carbonization temperature (°C)	Activation temperature (°C)	Yield (%)
BC	-	-	600	-	20.1±1.1
ACPS850-K-4	KOH	1:4		850	10.1±1.1
ACPS600-K-4	KOH	1:4		600	14.6±1.2
ACPS850-K-2	KOH	1:2		850	12.4±0.6
ACPS850-Z-D	$ZnCl_2$	1:4		850	19.3±1.3
ACPS850-Z-W	$ZnCl_2$	1:4		850	17.2±1.5

Selection of the carbonization and activation temperatures was based on literature [12,33,41] and on the results of a thermogravimetric analysis (TGA) of pine sawdust that demonstrated that a mass loss did not occur between 600 and 850 °C. Chemical activation can be performed by using different activating agents such as alkali compounds (KOH or NaOH), acid compounds (H_3PO_4 or H_2SO_4) and salts ($AlCl_3$ or $ZnCl_2$). Apart from being the most commonly used agents, KOH and $ZnCl_2$ were chosen since the chemical activation can produce carbons with higher surface areas. Also, KOH can lead to a good micropore size distribution whereas $ZnCl_2$ can promote the development of small mesopores [53,54]. Besides, there are also two distinct methods that can be applied, dry (by mixing of carbon and activation agent) and wet (by impregnation of carbon) activation, and both were used for the carbons activated with $ZnCl_2$ analyzing its influence on the materials' characteristics. Since the carbon elemental composition, specific surface area and morphological structures did not present significant differences, activated carbon by the dry method was selected for dye adsorption since no liquid wastes are produced thus being more environmentally friendly.

A significant weight loss occurred during pine sawdust pyrolysis to produce biochar (BC), a carbon-rich product, due to the loss of volatiles and non-carbon components that led to a low yield as shown

in Table 3. Regarding the activated carbons, the yield loss was more significant for carbons activated with KOH than for those activated with $ZnCl_2$. The high temperature applied in the biochar activation together with the use of activating agents that act as dehydrating materials removing volatile compounds through the decomposition of aliphatic and aromatic bonds, were mainly responsible for this loss [3].

The values of pH_{PZC} of the different materials produced is shown in Figure 6. For all carbons, except for the one activated at low temperature (ACPS600-K-4), the pH_{PZC} is basic (pH ≥ 7), which indicates that basic functional groups predominate in the carbon surface. In the case of ACPS600-K-4, the acid functional groups are dominant. In the case of anionic dyes that are negatively charged adsorption efficiency will improve at a pH lower than pH_{PZC}.

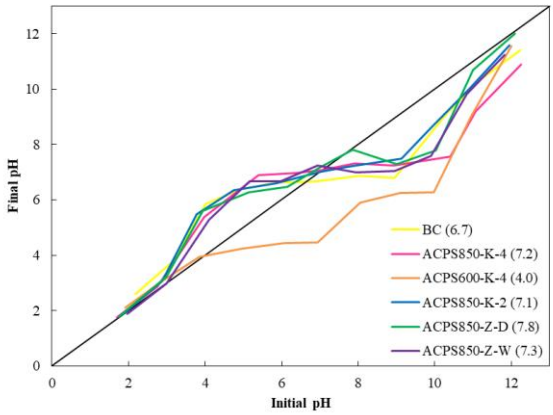

Figure 6. pH_{PZC} for biochar and activated carbons prepared.

Specific surface area and porosity of each carbon were determined by means of the sorption-desorption N_2 isotherms at -196 °C and the pore size distribution. The isotherms were essentially type I according to the IUPAC classification [55,56]. In particular, BC and $ZnCl_2$ activated carbons showed type I (a) isotherms corresponding to microporous materials with primarily narrow micropores [57]. The other carbons presented type I (b) isotherms which characterize materials with a pore size distribution of wider micropores and narrow mesopores. Hence, pores with size higher than 10 nm were negligible for all carbons. For BC and $ZnCl_2$ activated carbons both total pore volume and size were lower than 0.3 $cm^3\ g^{-1}$ and 1 nm, respectively. Concerning the KOH activated ones, the total volume of available pores was greater (up to 1.5 $cm^3\ g^{-1}$ for ACPS850-K-4), but with small changes in their average pore diameter (between 1.8 and 2.0 nm). The results confirmed the activation process efficiency since N_2 and CO_2 BET surface areas and total pore volume increased significantly for all activated carbons. Anyway, KOH activated carbons had higher N_2 and CO_2 surface area than those for activated with $ZnCl_2$. The highest surface area determined with N_2 at -196 °C (2865 $m^2\ g^{-1}$) corresponded to ACPS850-K-4 while ACPS600-K-4 showed the highest surface area determined with CO_2 at 0 °C (1354 $m^2\ g^{-1}$).

In order to better understand the structural morphology and porosity of the carbons' surface, SEM and TEM analysis were performed and are shown in Figure 7.

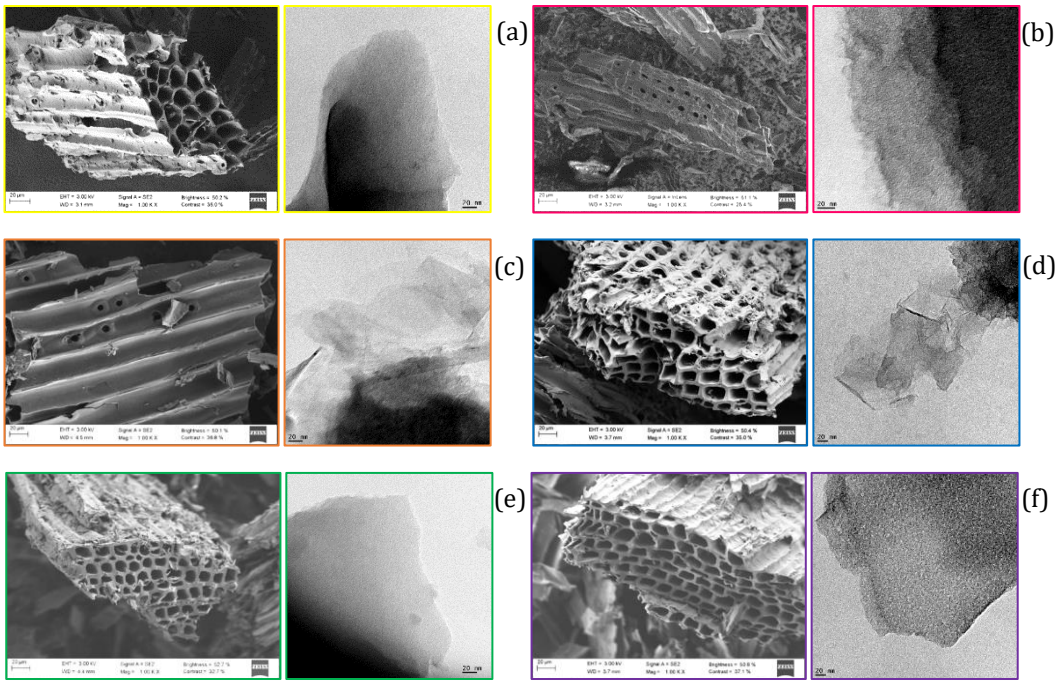

Figure 7. SEM and TEM images of BC (a), ACPS850-K-4 (b), ACPS600-K-4 (c), ACPS850-K-2 (d), ACPS850-Z-D (e) and ACPS850-Z-W (f).

The presence of porosity in the carbonized sawdust could be detected (Fig. 7 (a)), due to the loss of the previously mentioned components during carbonization, which could facilitate the activation of the material. In relation to KOH activated carbons (Fig. 7 (b-d)), they showed more structural damage but also the presence of more porosity, which was proven by the existence of a high surface area. Regarding the carbons activated with $ZnCl_2$ (Fig. 7 (e), (f)), the structure was maintained and there was less porosity on the material surface. The common structure of a honeycomb is characteristic of the cell wall of the raw lignocellulosic materials [41,58]. TEM analysis was also used to have more details about the microporosity, and the images showed, in general, a disorganized wormhole-like micropore structure (Fig. 7), which is due to the stacking of graphene layers indicating the presence of an important amount of micropores. Besides, the arbitrary distribution of the micropores suggested an amorphous structure of the carbons.

To have a greater insight into the carbons' structure, the crystallographic structure of the materials was evaluated through XRD analysis, verifying that the materials presented different degrees of graphitization. Thus, ACPS850-K-4 and ACPS850-K-2 presented an amorphous structure with a low graphitization degree [59]. ACPS600-K-4 presented the highest graphitization degree while the lowest one corresponded to ACPS850-K-4. On the contrary, BC presented a different behaviour with a microcrystalline structure due to the superposition of aromatic layers with a high degree of aromatic nuclear polymerization [60]. The presence of graphitization degree and amorphous structure were also demonstrated previously by TEM analysis.

Furthermore, carbons composition was assessed by EDX, XPS and CHNS elemental analysis. Elemental analysis revealed that, with the exception of ACPS600-K-4, all carbons presented high carbon content (higher than 80%). The hydrogen content only increased for the one activated with

KOH at the lowest temperature (600 °C) and this carbon also presented the highest oxygen content maybe due to gasification reactions and formation of oxygen-containing groups during activation process at low temperature in the presence of KOH. For the carbons activated with KOH at 850 °C an increase in the aromaticity was observed due to H/C ratio decreased. ACPS600-K-4 showed the highest H/C and O/C ratios indicating a low degree of carbonization and aromaticity and high polarity [61,62]. XPS and EDX analysis confirmed the results of elemental composition. Furthermore, XPS showed a further insight on the type of bonding of the elements through high resolution spectra for C1s, N1s and O1s. Functional groups such as carbon groups (C-C, C=C, CH_x), hydroxyl groups or ether linkages (C-O-C, C-OH, OH) and carboxyl group (C=O) were present in all activated carbons. Particularly, the biochar showed an additional group corresponding to ester group (O=C-O) which disappears after the activation process. FTIR analysis also showed the presence of various functional groups in the carbon's surfaces such as alcohols, phenols, carboxylic acid, alkane groups, C=C bond and C-O vibrations. Also, referring to the FTIR analysis, the BC revealed the presence of an additional peak at 865 cm^{-1}, again revealing the presence of more functional groups.

On the other hand, the activated carbon (ACPS850-K-4) was selected to carry out fixed-bed adsorption experiments because of the best results for dyes adsorption, as will be explained later. This carbon was produced at large scale (the amount produced increased from 1 to 26 g) and was also characterized to verify that its characteristics match with those of the carbon produced on a smaller scale. As demonstrated, the N_2 surface areas were quite similar, 2865 and 2826 $m^2\ g^{-1}$ for small and large scale, respectively, however, the CO_2 surface area increased from 677 to 910 $m^2\ g^{-1}$, the average pore diameter slightly increased from 2.0 to 2.2 nm, and the microporosity percentage diminished from 68 to 30%, which could be due to modifications in the preparation procedure as the change of the oven.

6.3 Dye adsorption onto carbons

Despite pine sawdust biomass presented good results as a dye adsorbent and could be more suitable as a sustainable and low-cost material, the biochar and activated carbons were produced in an attempt to obtain materials with an elevated surface area and porous structure, which could improve the effectiveness for adsorbing the wood dyes and carbon dioxide. In this way, dye adsorption on biochar and activated carbons was studied evaluating the influence of several parameters that can influence their adsorption capacity.

6.3.1 Effect of pH and initial dye concentration

As mentioned, the adsorptive performance of BC in function of pH was studied for blue, red and black dyes and the results are presented in Figure 8.

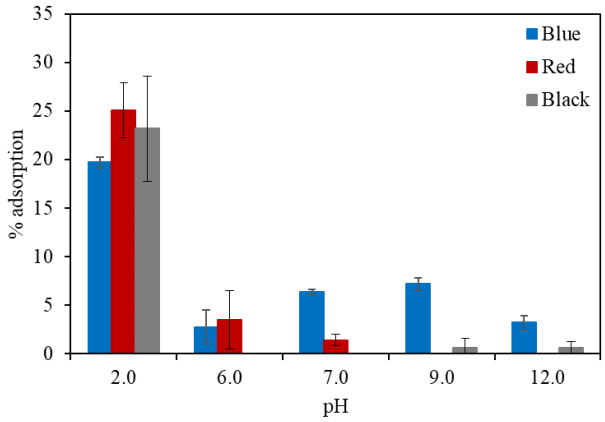

Figure 8. Adsorption efficiency of biochar for blue, red and black dyes (Conditions: adsorbent dose 0.5 g L^{-1}; initial dye concentration 5 mg L^{-1}; time 48 h; temperature 25 °C).

As observed adsorption efficiency was quite low, and the best results were obtained at pH = 2, well below the pH_{PZC} value (6.7), which represents favorable conditions for the adsorption of anionic dyes since the surface is positively charged. Moreover, adsorption was limited, probably due to the small surface area (293 m^2 g^{-1}) and high percentage of microporosity (90.7%), which could lead to mass transfer limitations. Furthermore, the preferential adsorption of the red dye can be explained by its lower molecular size compared to the blue and black ones.

The influence of the pH was also evaluated for KOH and $ZnCl_2$ activated carbons. Initially, the effect of pH was studied at the same conditions than BC, an initial dye concentration of 5 mg L^{-1}, an adsorbent dose of 0.5 g L^{-1} and a contact time of 48 h at 25 °C to assure the equilibrium, except for the black dye that was 12 h due to stability issues. Regarding the ACPS850-Z-D adsorption efficiencies close to 100% were attained for the blue and red dyes, but only a 56% for the black one. For all the carbons activated with KOH a high efficiency (around 100%) was also obtained for the blue and red dyes at all pH range, while for the black dye decreased in general with increasing pH mainly for the ACPS600-K-4. The limitations regarding the adsorption of the black dye, with the largest molecular size, can be related both to the carbon surface area or to the presence of microporosity and ultramicroporosity that was evidenced for ACPS850-Z-D with the lowest S_{BET} calculated with N_2 adsorption isotherm data (471 m^2 g^{-1}) and a S_{BET} calculated with the CO_2 isotherm data of 320 m^2 g^{-1} and with the highest microporosity percentage (91%) between the activated carbons. Although for all KOH activated carbons the N_2 surface area was greater than 2000 m^2 g^{-1}, for ACPS600-K-4 a high percentage of microporosity (89%) was found as the S_{BET} calculated with CO_2 was 1354 m^2 g^{-1}.

As, in some cases, the influence of pH was not clearly observed at low dye concentrations due to high adsorption yields, the effect of the initial concentration (25-500 mg L^{-1}) was also evaluated at the same pH range (Figure 9).

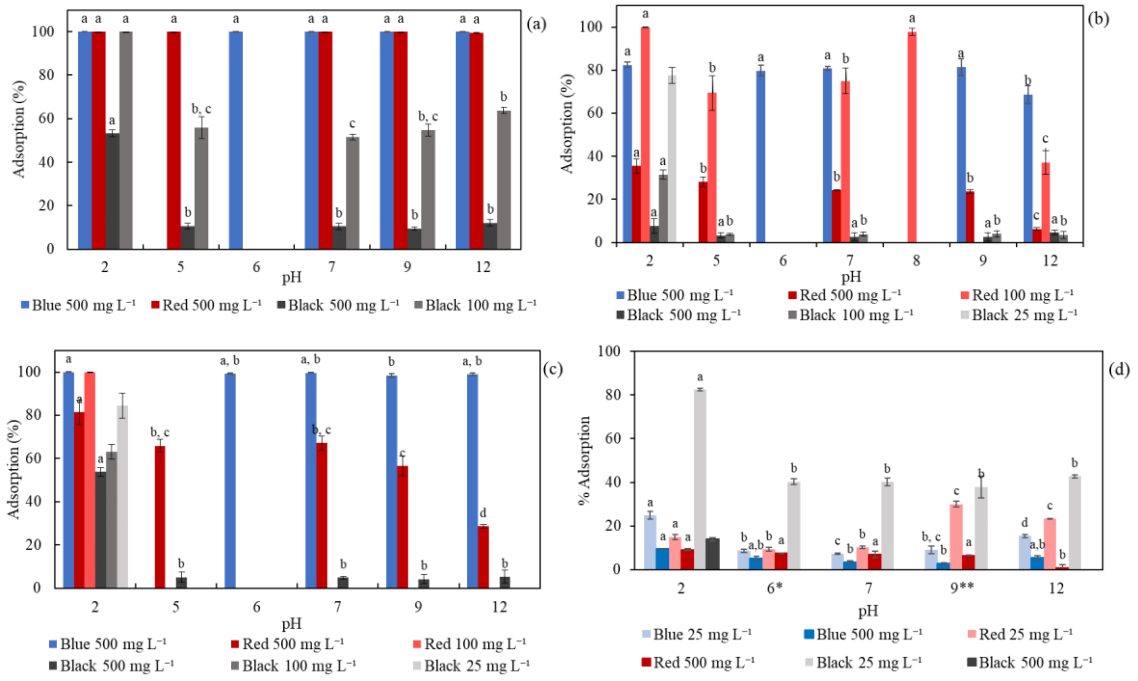

Figure 9. Influence of pH and initial dye concentration on the adsorption of blue, red and black dyes onto (a) ACPS850-K-4, (b) ACPS600-K-4, (c) ACPS850-K-2 and (d) ACPS850-Z-D (adsorbent dose: 0.5 g L^{-1} except for the black dye using ACPS850-Z-D that was 1 g L^{-1}; temperature 25 °C; agitation speed 210 rpm; contact time 48 h for blue and red dyes and 12 h for black). For each dye, distinct letters indicate significant differences ($p \leq 0.05$) between samples.

In the case of the carbons with high microporosity (Fig. 9 (b), (c), (d)) adsorption efficiency was lower than for the ACPS850-K-4 (Fig. 9 (a)) and the best results were achieved at pH = 2. These difficulties in the adsorption performance can be explained by the fact that the increase in the initial concentration leads to a saturation of the active sites. In the case of more macroporous activated carbons, high adsorption efficiencies were attained for the blue and red dyes, even at high concentrations (500 mg L^{-1}), being ACPS850-K-4 the one that showed the best results (100% for blue and red dyes at 500 mg L^{-1} and all pH values and 100% for black dye at 100 mg L^{-1} and pH = 2). The better efficiency presented by ACPS850-K-4 may be due to its high surface area (2865 m^2 g^{-1}) and low microporosity (68%). Moreover, the blue and red dyes were better adsorbed than black dye since this is the one with the largest molecular size. Furthermore, dye adsorption was negatively influenced by carbon microporosity (ACPS600-K-4 and ACPS850-K-2) and particularly the red dye, despite having the lowest molecule size, presented less adsorption efficiency than the blue dye. This can be due to the interaction between the functional groups and dye molecules, since as evaluated by XPS, ACPS850-K-4 is the only one that does not have pyrrolic-N group and with the highest decrease on the percentage of C-C, C=C and CH_x compared to the other carbons and the functional groups can highly influence the adsorption capacity [63]. Regarding ACPS850-Z-D the high microporosity combined with a low surface area and total pore volume adversely affected dye adsorption and led to the worst results. Moreover, in all cases, it is evident that the increase in surface area and pore size of the activated carbons compared to biochar favoured significantly dye adsorption.

6.3.2 Effect of adsorbent dose

For ACPS850-Z-D, which showed low adsorption efficiencies even at low dye concentrations, the adsorbent dose was increased. By increasing the adsorbent dose at an initial dye concentration of 25 mg L^{-1} from 0.5 to 4 g L^{-1} for blue and red dyes and to 2 g L^{-1} for the black, complete dye removal was achieved. This improvement can be explained by the increase in available active sites with increasing the adsorbent dose. For KOH activated carbons, the adsorbent dose was reduced between 0.5 and 0.1 g L^{-1} to determine how far the adsorbent dose can be reduced without reducing efficiency. For an initial dye concentration of 5 mg L^{-1}, for ACPS850-K-4 the dose could be reduced to 0.1 g L^{-1} for all dyes; for ACPS600-K-4 the dose could be reduced to 0.1 g L^{-1} for blue and red and to 0.2 g L^{-1} for black; regarding ACPS850-K-2 the adsorbent dose was reduced to 0.1 g L^{-1} for blue and red and to 0.3 g L^{-1} for black dye. At high initial concentrations, the best adsorbent dose for ACPS850-K-4 at 500 mg L^{-1} was 0.4 g L^{-1} and 0.3 g L^{-1} for the blue and red dyes, respectively, and it was 0.4 g L^{-1} for the black dye at 100 mg L^{-1} (Figure 10). For ACPS600-K-4 it was not possible to reduce the adsorbent dose and concerning ACPS850-K-2, adsorbent dose could only be decreased for the red dye up to 0.2 g L^{-1} at 100 mg L^{-1}.

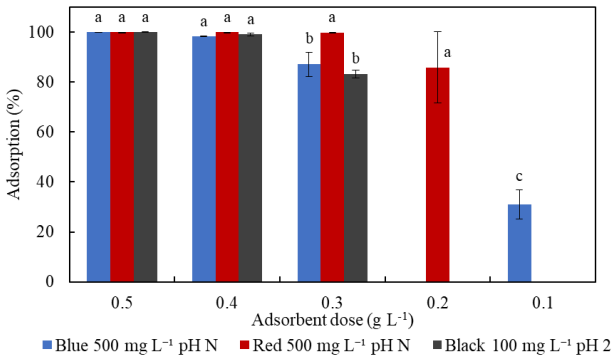

Figure 10. Influence of adsorbent dose on dyes removal on ACPS850-K-4 (stirring rate 210 rpm; temperature 25 °C; natural pH (pH N) or pH = 2).

Thus, kinetic studies were carried out using the best conditions obtained for each material.

6.3.3 Adsorption kinetics

Adsorption kinetic data for biochar and activated carbons were fitted to the pseudo-second order, pseudo-first order and intraparticle diffusion to better understand the adsorption mechanism. Except for ACPS850-K-4 with the black dye at high concentration (100 mg L^{-1}) kinetic data were best fitted to the pseudo-second order model associated to a chemisorption mechanism. Data for the adsorption of the black dye at 100 mg L^{-1} on ACPS850-K-4 were best fitted to the pseudo-first order model related to a physical adsorption mechanism. As an example, Figure 11 shows the kinetic curves for blue, red and black dyes on ACPS850-K-4, where the highest adsorption capacity was 1222 mg g^{-1}, 1673 mg g^{-1} and 240 mg g^{-1} for blue, red and black dyes at the best conditions previously evaluated.

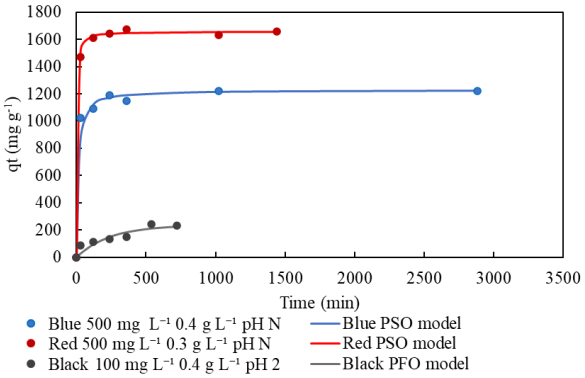

Figure 11. Kinetic curves for blue, red and black dye on ACPS850-K-4 (stirring rate 210 rpm; temperature 25 °C, natural pH (pH N) or pH = 2).

Regarding the plots corresponding to fit the data to the intraparticle diffusion model it showed multilinearity, which revealed the existence of two adsorption process stages, and the good fit in the first zone suggests that diffusion through the carbon pores occurred.

In general, KOH activated carbons showed an outstanding adsorption capacity which makes them potential adsorbents for dye removal.

6.3.4 Adsorption equilibrium

Langmuir isotherm model was best fitted to equilibrium experimental data for all KOH-activated carbons and for ACPS850-Z-D with the red dye. This model suggests an adsorption process in monolayer and an energetically homogeneous surface for the dye-carbon interaction. Additionally, the values for the theoretical separation factor of Langmuir's model (R_L) varied between 0 and 1 demonstrated that the adsorption process onto activated carbons is favorable. However, for ACPS850-Z-D with the blue and black dyes the Freundlich isotherm was the model that best fitted experimental data. Unlike Langmuir model, this suggests that the adsorption process occurs in multilayer over a heterogeneous surface. Besides, for the KOH activated carbons Dubinin-Radushkevich model also fitted the equilibrium data in some cases. The average energy value predicted (> 8 kJ mol^{-1}) is an indication of a chemical adsorption process, in some cases related with the existence of ionic interactions (between 8 and 16 kJ mol^{-1}) and in other cases with intraparticle diffusion (higher than 16 kJ mol^{-1}). This demonstrates that operational factors such as pH, contact time and adsorbent dose have a significant influence on the adsorption mechanism, but also other factors such as size-dependent separation and chemical interactions through functional groups, which depend on the structure of the dye and the carbon properties, also have an impact [64].

6.3.5 Activated carbon characterization after adsorption

SEM-EDX and FTIR techniques were applied after dye adsorption to confirm the adsorption process. The SEM images revealed that the surface and pores of the adsorbent were covered by dyes. Furthermore, EDX analysis showed that elements present in the dyes' structures were also on the surface of the materials, demonstrating the adsorption of the dye molecules. FTIR spectra showed

some changes in the peaks in terms of intensity and shape, demonstrating the interaction of the dye with the functional groups on the surface of the carbons.

6.3.6 Desorption and regeneration of the activated carbon

Dyes' desorption was analysed for the carbon that led to the best results in batch experiments (i.e., ACPS850-K-4), in order to evaluate the possibility of reusing the carbon in successive cycles improving the economy of the process. Different desorbing agents, namely NaOH (0.1 M; 10M), HCl (0.1 M), ethanol 96%, acetone:water (3:2 v/v), acetone (> 99.5%), acetone 10%, methanol 10% and NaCl 0.1M were used for the desorption of dyes from the activated carbon. It was found that the amount of dye desorbed was rather low in all cases (< 26.8%), which suggests that anionic dyes adsorption onto ACPS850-K-4 is generally irreversible by chemical regeneration. This conclusion is supported by the parameter R_L of the Langmuir model, since is very close to zero indicating the irreversibility of the process. Given the poor results, in a further attempt to achieve dye desorption, H_2O_2 was also tried as desorbing agent and successive adsorption/desorption cycles were performed. While for blue and red dyes was ineffective, for the black dye the adsorption efficiency was higher than 80% until the third adsorption cycle and was reduced to 47.4% after five adsorption cycles. One of the factors that could contribute to the efficiency of the process could be the oxidation of the adsorbed black dye promoted by the reaction with OH^- groups produced by the decomposition of H_2O_2 catalysed by the activated carbon [65,66]. Finally, for blue and red dyes, ACPS850-K-4 underwent thermal regeneration, which was also inefficient.

6.3.7 Fixed-bed adsorption and desorption experiments

As mentioned before, for ACPS850-K-4, which presented the best results for dye adsorption in batch mode, experiments were performed through continuous fixed-bed adsorption. The effect of fundamental variables such as flow rate (7.7 and 30.8 mL min^{-1}), initial dye concentration (25-500 mg L^{-1}) and bed height (2 and 4 cm) on the continuous dye adsorption process was studied at natural pH for blue and red dyes and pH = 2 for the black one. As an example, Figure 12 shows the influence of the flow rate, initial dye concentration and bed height on blue wood dye adsorption onto ACPS850-K-4.

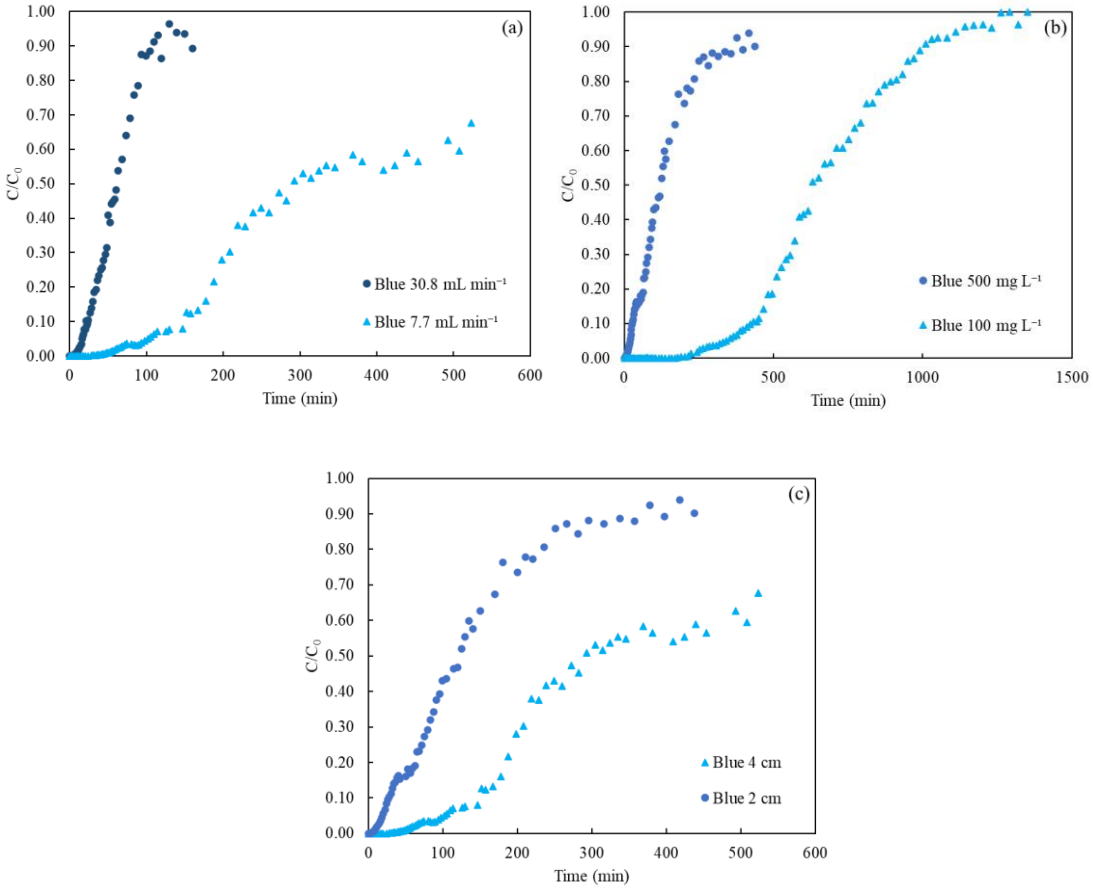

Figure 12. Breakthrough curves for blue wood dye adsorption onto ACPS850-K-4 in function of (a) influent flow rate, (b) initial dye concentration and (c) bed height (temperature 25 °C; pH natural (a) initial dye concentration: 500 mg L^{-1}; bed height: 4 cm; (b) Flowrate: 7.7 mL min^{-1}; bed height: 2 cm; (c) initial dye concentration: 500 mg L^{-1}; Flowrate: 7.7 mL min^{-1}).

In general, results demonstrated that the breakthrough time diminished with increasing the flow rate and the initial concentration and with decreasing the bed height. A greater flow rate decreases the contact time between the dye and the carbon, which limits intraparticular diffusion and the adsorption process [67]. Regarding the initial dye concentration, its increase led to a decrease on the breakthrough time since the mass transfer driving force increases as in the batch experiments and the adsorbate became saturated faster. Finally, the increase on the bed height results in an increase on the breakthrough time due to the increase on the number of active sites available, similarly to the adsorbent dose effect on batch experiments. Afterwards, dynamic modeling of the fixed-bed column was performed by applying non-linear regression analysis using Thomas, Yoon-Nelson and Bohart-Adams models. In general, Thomas and Yoon-Nelson best fitted the experimental data with high correlation coefficient (R^2) and low sum of square error. Thomas model suggests that there is no axial and radial dispersion and negligible variations on the pressure and temperature inside the column. Besides, according to this model, external and intraparticle diffusion do not represent the rate limiting steps, but both can have influence on the adsorption process [68].

The highest adsorption capacity at the operational time was obtained for the blue dye (1283 mg g^{-1}) at an initial dye concentration of 500 mg L^{-1}, flow rate of 7.7 mL min^{-1} and bed height of 4 cm. In batch

experiments, blue and red dyes showed the same behavior (both with 100% of adsorption yield) except when the adsorbent dose was reduced that favored red dye adsorption. In continuous mode the difference between these dyes increased and the blue dye showed a better performance. The differences between batch and continuous can be explained taking into account that in batch experiments the adsorption process occurs in the solid-liquid phase and the solid is continuously mixed with the liquid, while in fixed-bed adsorption the adsorbate is in continuous flow through the adsorbent, the concentration profiles change over space and time, preferential ways can be formed and the adsorption becomes non-uniform [69]. Also, as previously mentioned, the differences can be related to the interaction between the functional groups and as the breakthrough time was slower for the red dye than for the blue, the residence time was not enough to achieve adsorption results as good as those of batch experiments. A comparison with results shown in literature [70–77] revealed that this activated carbon presented an elevated adsorption capacity, and it is a promising material for dye adsorption from aqueous solutions.

As for batch experiments, dye desorption was only achieved for the black dye using H_2O_2 as desorbing agent and the results demonstrated that both the breakthrough time (t_b) and the adsorption capacity decreased over the three cycles applied. From the first to the third cycle, at 25 mg L^{-1}, flow rate of 4.4 mL min^{-1}, bed height of 2 cm and regeneration time of 4 h, the adsorption capacity decreased from 147 mg g^{-1} to 32 mg g^{-1} with a t_b of 49 and 14 min, respectively. For 100 mg L^{-1}, at the same conditions previously described but with a bed heigh of 4 cm it was reduced from 130 to 47 mg g^{-1} with a t_b of 2 and 1 min, respectively. This is due not only to the saturation of the active sites with the irreversibly adsorbed molecules, but also to the possible degradation of the adsorbent after several uses [78,79].

6.4 CO_2 gas adsorption onto carbons

In this last stage of the Thesis' work, the performance of biochar and activated carbons in CO_2 adsorption was evaluated and adsorption isotherms at various temperatures were obtained. Regarding the adsorption isotherms at 0 °C, ACPS600-K-4 stated the highest CO_2 uptake achieving 5.8 mmol g^{-1} at a relative pressure of 0.03. However, at lower pressures a distinct behaviour was observed as ACPS600-K-4 was still the best activated carbon, with no substantial differences, but BC reached higher CO_2 adsorption than activated carbons which can be due to the role of ultra microporosity at low partial pressures [80]. Furthermore, this is possibly due to the mechanism that controls CO_2 adsorption at 0 °C that is the pore filling, and for this reason, pore size is critical since this isotherm gives an estimation of the surface area governed by ultra-micropores (lower than 0.7 nm) [81].

Besides, since BC was only carbonized more functional groups to interact with CO_2 could be maintained, as observed by FTIR results. Comparing N_2 and CO_2 adsorption isotherms at 25 °C all carbons displayed a larger CO_2 adsorption capacity than N_2. Moreover, type I isotherms, which are characteristics of compelling adsorbate-adsorbent interactions, represent the CO_2 adsorption isotherms [82]. Considering N_2 adsorption there were no considerable differences in the amount adsorbed at low pressures. Regarding CO_2 adsorption in the high-pressure region the lowest CO_2

uptake was for BC and largest for ACPS600-K-4 (3.6 mmol g^{-1}) followed by ACPS850-K-4. In the low-pressure region ACPS600-K-4 also presented the best results followed by the $ZnCl_2$ activated ones. Then, the influence of temperature on N_2 and CO_2 adsorption was evaluated from 0 to 50 °C. All carbons revealed the same trend, with the temperature increases, the amount of CO_2 adsorbed decreased, which indicated that CO_2 adsorption is a physisorption process [6] and the same behaviour was observed for N_2.

The equilibrium experimental data were fitted to Langmuir, Freundlich and Toth models. Toth isotherm presented a good fit for all carbon samples describing a multilayer adsorption process and indicating that the carbons surface is heterogeneous (t≠1) [83]. On the other hand, for ACPS600-K-4 the model that best fit equilibrium data at all temperatures was the Freundlich model, as where those for ACPS850-K-4 at 25 and 50 °C. Similarly to the results for CO_2 adsorption, which were better adjusted to the Toth model, N_2 presented the same behaviour in most cases. However, due to the lower affinity between this gas and the materials, the N_2 adsorption capacity values were lower.

A critical parameter to evaluate the adsorbent is the CO_2/N_2 selectivity, which was calculated using single-component gas adsorption isotherms, representing an estimation of the selectivity (apparent selectivity). BC showed the highest selectivity followed by ACPS600-K-4. Furthermore, selectivity increased with increasing temperature. Adsorption selectivity was also calculated employing the ideal adsorbed solution theory (IAST), as the apparent selectivity determined presented a conservative approximation, and in all cases CO_2 is preferentially adsorbed over N_2. Regarding the effect of the pressure on selectivity, increasing the pressure also leads to an increase in selectivity, however, for BC the increase in selectivity was more significant. The competition for adsorption sites will intensify at high pressure due to the high amount of CO_2 and N_2. The increase for BC can be due to the existence of more functional groups and a more homogeneous surface from a chemical point of view [84]. Also, an increase in the microporosity led to an increased selectivity, being the BC and ACPS850-K-4 the carbons with highest and lowest selectivity, respectively. Furthermore, for the materials with high surface area, a substantial decrease occurs in the selectivity. Thus, after the activation process, there was an increase in surface area but, on the other hand, a loss in functional groups and a decrease in microporosity, mainly ultramicroporosity. Unlike the apparent selectivity, the selectivity calculated by IAST decreased with increasing temperature, which highlights the importance of competitive adsorption of CO_2/N_2.

Finally, the heat of adsorption was studied to assess the surface affinity towards CO_2 and evaluate the strength of the interaction between the adsorbent and the adsorbate. All the materials presented a low heat of adsorption, from 14 to 27 kJ mol^{-1}, and slightly dependent on the amount of CO_2 adsorbed. So, the interaction between the carbons and CO_2, as previously mentioned, is a physical adsorption which suggests that the energy needed to regenerate these carbons will be minimal, which is crucial for enhancing process economy. BC exhibited the highest heat of adsorption which can be related to the existence of more functional groups. However, the lowest heat of adsorption was observed for the activated carbons with the highest KOH dosage, most likely as a result of the stronger activation that produced a more homogeneous adsorbent surface. Besides, a distinct

tendency of the isosteric heat with the amount of CO_2 adsorbed was perceived. The isosteric heat of adsorption increased with the increase on CO_2 adsorbed amount (BC, ACPS850-K-2 and ACPS850-Z-D) when ultramicropores are occupied first by the CO_2 molecules whereas it decreased with the increase on the amount adsorbed due to the strong interaction with the carbon surface and negligible intermolecular interaction [59,85,86].

Finally, activated carbon prepared from pine sawdust revealed an outstanding CO_2 adsorption capacity when compared with other materials from literature [87–92].

7. CONCLUSIONS

Conclusions

In the present Thesis, pine (*Pinus radiata*) sawdust was exploited in a first stage as an adsorbent for both the elimination of acid wood dyes for wastewater treatment and CO_2 capture. Then, it was employed as a precursor for the production of biochar and activated carbons for the removal of the mentioned pollutants. Through a careful analysis of the morphological and structural characteristics of the materials, the activated carbons stood out for their properties. Furthermore, the results obtained at laboratory scale revealed the great capacity of these materials to be used as promising adsorbents and as an alternative to the commercial ones. Activated carbons production was carried out under different activation conditions and the evaluation of the adsorption performance has shown the potential of these carbons to remove dyes from aqueous solutions and capture CO_2 from gas streams of post-combustion processes. From the work performed in the present Thesis, a few particular findings can be attained.

From the use of pine sawdust as an adsorbent for the elimination of acid wood dyes (blue, red and black) from aqueous solutions, it could be concluded that some factors such as pH, adsorbent dose or initial dye concentration influence the adsorption process. For all dyes, the highest removal percentage was attained at acid pH (pH = 2) and increased with increasing the contact time and adsorbent dose, while decreased with increasing the initial dye concentration. At this pH and for 5 mg L^{-1} at an adsorbent dose of 6 g L^{-1} the highest adsorption efficiencies attained were: 100.0%, 99.7%, and 92.4% for the blue, black and red dyes, respectively. Increasing the concentration to 300 mg L^{-1} the adsorption percentage decreased to 85.6% for the blue, 57.0% for the black, and 63.8% for the red. Adsorption kinetics was better described by the pseudo-second order kinetic model which represents a chemisorption process. However, intraparticle diffusion had an important contribution to the global process, and mainly for the first adsorption stage which implies the dye transfer into the pores. The equilibrium data was best fitted by the Freundlich and Dubinin-Radushkevich isotherm models, which represent a multilayer adsorption process and the heterogeneity of the surface. Desorption studies were performed, and sodium hydroxide with the highest desorption efficiency was selected as desorption agent. A slight decrease in the adsorption efficiency was observed after various adsorption/desorption cycles, except for the red dye for which the adsorption efficiency onto sawdust was improved.

Regarding the activated carbons prepared form pine sawdust using $ZnCl_2$ and KOH as activated agents, both the structural characteristics (such as surface area and pore volume) and adsorption capacity improved, mainly for those activated with KOH. The adsorption efficiency usually decreased with increasing pH and initial dye concentration. On the other hand, the dye removal efficiency increased with increasing the adsorbent dose, mainly for the carbons activated with $ZnCl_2$. In general, the pseudo-second order kinetic model fitted better the kinetic data. Equilibrium data for KOH activated carbons were best fitted to the Langmuir model for all dyes whereas for $ZnCl_2$ activated carbons equilibrium data were better explained by the Freundlich model for the blue and black dyes and by the Langmuir model for the red dye (typical of monolayer chemical adsorption in the carbon surface). Based on the results obtained, the carbon activated with KOH at 850 °C and a ratio of 1:4 (ACPS850-K-4) was selected. It showed the highest surface area determined with the N_2 adsorption

isotherm of 2865 $m^2 g^{-1}$ and the highest adsorption capacities of 1221.58, 1673.03 and 240.38 mg g^{-1} for blue and red at 500 mg L^{-1} and black at 100 mg L^{-1}, respectively, at an adsorbent dose of 0.4 g L^{-1} for blue and black and 0.3 g L^{-1} for red dye and at the natural pH for blue and red and at pH = 2 for black dye. Desorption was studied for this activated carbon, but it was only effective for the black dye using hydroxide peroxide as desorption agent. Adsorption in continuous mode was carried out with the selected activated carbon and factors such as flow rate, initial dye concentration and bed height were found to influence the adsorption efficiency. Specifically, the breakthrough curves became steeper with increasing the flow rate and the initial dye concentration and with decreasing the bed height. The highest adsorption capacity was 1283.1 mg g^{-1} for the blue dye at an initial dye concentration of 500 mg L^{-1}, flow rate of 7.7 mL min^{-1} and bed height of 4 cm. Thomas and Yoon-Nelson models best fitted the experimental data. Desorption experiments conducted with hydroxide peroxide for the black dye at 25 mg L^{-1} revealed that it could be reused several cycles.

Finally, biochar and activated carbons were also applied for gases separation. The largest CO_2 uptake, 5.79 mmol g^{-1} at 0 °C and 750 mmHg was attained for the KOH activated carbon at moderate conditions (600 °C and ratio 1:4) due to a combination of high microporosity (89%) and elevated specific surface area (2437 $m^2 g^{-1}$). Furthermore, all the materials showed preferential adsorption by CO_2 over N_2. Toth isotherm best fitted the adsorption equilibrium data in most cases. Regarding adsorption selectivity, biochar followed by the activated one with KOH (600 °C and ratio 1:4) showed the highest CO_2/N_2 selectivity.

The advantageous characteristics of the activated carbons fabricated from pine sawdust make them promising materials to replace commercial activated carbons for CO_2 capture and storage as well as for the elimination of dyes from wastewater. Further studies must be performed to explore the effect of coexisting contaminants on dye removal and in real wastewater treatment, to improve dye desorption from activated carbon and to analyze the reusability of carbons through CO_2 adsorption/desorption cycles.

List of Tables

List of Figures

References

[1] Y. Dai, Q. Sun, W. Wang, L. Lu, M. Liu, J. Li, S. Yang, Y. Sun, K. Zhang, J. Xu, W. Zheng, Z. Hu, Y. Yang, Y. Gao, Y. Chen, X. Zhang, F. Gao, Y. Zhang, Utilizations of agricultural waste as adsorbent for the removal of contaminants: A review, Chemosphere. 211 (2018) 235–253. https://doi.org/10.1016/j.chemosphere.2018.06.179.

[2] J. Li, C. Shi, A. Bao, Design of boron-doped mesoporous carbon materials for multifunctional applications: Dye adsorption and CO2capture, J. Environ. Chem. Eng. 9 (2021). https://doi.org/10.1016/j.jece.2021.105250.

[3] S.M. Yakout, M.R. Hassan, M.E. El-Zaidy, O.H. Shair, A.M. Salih, Kinetic study of methyl orange adsorption on activated carbon derived from pine (Pinus strobus) sawdust, BioResources. 14 (2019) 4560–4574. https://doi.org/10.15376/biores.14.2.4560-4574.

[4] A. Koli, A.K. Battu, R.K. Motkuri, S. Sabale, Hierarchical porous activated carbon derived from agro-waste for potential CO2 capture and efficient dye removal applications, Biomass Convers. Biorefinery. (2022). https://doi.org/10.1007/s13399-022-03067-y.

[5] S. Wang, T. Zhang, J. Li, Y. Hua, J. Dou, X. Chen, S. Li, Potassium citrate-derived porous carbon with high CO2 capture and Congo red adsorption performance, Environ. Sci. Eur. 35 (2023). https://doi.org/10.1186/s12302-023-00712-9.

[6] S. Roy, B. Dasgupta Ghosh, K.L. Goh, J. Kim, H.J. Ahn, Y.W. Chang, Pores on Pores: A novel approach to fabricate super adsorbents from used face masks for large CO2 capture and dye removal, Carbon N. Y. 206 (2023) 422–433. https://doi.org/10.1016/j.carbon.2023.02.040.

[7] P. Boakye, G. Ohemeng-boahen, L. Darkwah, Y.A. Sokama-neuyam, E. Appiaf-Effah, S. Oduro-Kwarteng, B.A. OseiPrince Junior Asilevi, S. Han Woo, Waste biomass and biomaterials adsorbents for wastewater treatment, (2022) 1–25. https://doi.org/10.5772/GEET.05.

[8] M.S. Reza, C.S. Yun, S. Afroze, N. Radenahmad, M.S.A. Bakar, R. Saidur, J. Taweekun, A.K. Azad, Preparation of activated carbon from biomass and its' applications in water and gas purification, a review, Arab J. Basic Appl. Sci. 27 (2020) 208–238. https://doi.org/10.1080/25765299.2020.1766799.

[9] S. Jha, R. Gaur, S. Shahabuddin, I. Tyagi, Biochar as Sustainable Alternative and Green Adsorbent for the Remediation of Noxious Pollutants: A Comprehensive Review, Toxics. 11 (2023) 1–23. https://doi.org/10.3390/toxics11020117.

[10] N. Jagadeesh, B. Sundaram, Adsorption of Pollutants from Wastewater by Biochar: A Review, J. Hazard. Mater. Adv. 9 (2023) 100226. https://doi.org/10.1016/j.hazadv.2022.100226.

[11] Y. Zhou, J. Lu, Y. Zhou, Y. Liu, Recent advances for dyes removal using novel adsorbents: A review, Environ. Pollut. 252 (2019) 352–365. https://doi.org/10.1016/j.envpol.2019.05.072.

[12] R. Chikri, N. Elhadiri, M. Benchanaa, Y. El maguana, Efficiency of sawdust as low-cost adsorbent for dyes removal, J. Chem. 2020 (2020). https://doi.org/10.1155/2020/8813420.

[13] L. Xing, F. Yang, X. Zhong, Y. Liu, H. Lu, Z. Guo, G. Lv, Ultra-microporous cotton fiber-derived activated carbon by a facile one-step chemical activation strategy for efficient CO 2 adsorption, Sep. Purif. Technol. 324 (2023) 124470. https://doi.org/10.1016/j.seppur.2023.124470.

[14] C.V. Reddy, K.R. Reddy, V.V.N. Harish, J. Shim, M. V. Shankar, N.P. Shetti, T.M. Aminabhavi, Metal-organic frameworks (MOFs)-based efficient heterogeneous photocatalysts: Synthesis, properties and its applications in photocatalytic hydrogen generation, CO2 reduction and photodegradation of organic dyes, Int. J. Hydrogen Energy. 45 (2020) 7656–7679. https://doi.org/10.1016/j.ijhydene.2019.02.144.

[15] S. Jellali, M. Labaki, A.A. Azzaz, H. Akrout, L. Limousy, M. Jeguirim, Biomass-derived chars used as adsorbents for liquid and gaseous effluents treatment, Elsevier Inc., 2019. https://doi.org/10.1016/B978-0-12-814893-8.00007-9.

[16] V. Katheresan, J. Kansedo, S.Y. Lau, Efficiency of various recent wastewater dye removal methods: A review, J. Environ. Chem. Eng. 6 (2018) 4676–4697. https://doi.org/10.1016/j.jece.2018.06.060.

[17] R. Chikri, N. Elhadiri, M. Benchanaa, Y. El maguana, Efficiency of Sawdust as Low-Cost Adsorbent for Dyes Removal, J. Chem. 2020 (2020) 1–17. https://doi.org/10.1155/2020/8813420.

[18] P. Madejski, K. Chmiel, N. Subramanian, T. Kus, Methods and Techniques for CO 2 Capture : Review of Potential, Energies. 15 (2022) 887.

[19] C.H. Yu, C.H. Huang, C.S. Tan, A review of CO2 capture by absorption and adsorption, Aerosol Air Qual. Res. 12 (2012) 745–769. https://doi.org/10.4209/aaqr.2012.05.0132.

[20] A. Gautam, M.K. Mondal, Review of recent trends and various techniques for CO2 capture: Special emphasis on biphasic amine solvents, Fuel. 334 (2023) 126616. https://doi.org/10.1016/j.fuel.2022.126616.

[21] T.A. Jimoh, F.O. Omoarukhe, E.I. Epelle, P.U. Okoye, E. Oke Olusola, A. Mukherjee, J.A. Okolie, Introduction to Carbon Capture by Solvent-based Technologies, in: Ref. Modul. Earth Syst. Environ. Sci., 2023. https://doi.org/10.1016/b978-0-323-93940-9.00003-7.

[22] M.T. Yagub, T.K. Sen, S. Afroze, H.M. Ang, Dye and its removal from aqueous solution by adsorption: A review, Adv. Colloid Interface Sci. 209 (2014) 172–184. https://doi.org/10.1016/j.cis.2014.04.002.

[23] C. Tien, Introduction to adsorption: Basics, analysis, and applications., Elsevier, 2018.

[24] S. Dutta, R.K. Sharma, Sustainable Magnetically Retrievable Nanoadsorbents for Selective Removal of Heavy Metal Ions From Different Charged Wastewaters, in: Sep. Sci. Technol. (New York), 2019. https://doi.org/10.1016/B978-0-12-815730-5.00015-6.

[25] J. Rouquerol, F. Rouquerol, P. Llewellyn, G. Maurin, K.S.W. Sing, Adsorption by Powders and Porous Solids: Principles, Methodology and Applications, in: Adsorpt. by Powders Porous Solids Princ. Methodol. Appl., 2nd ed., Academic Press, London, UK, 2014: pp. 1–22. https://doi.org/10.1016/C2010-0-66232-8.

[26] S. Afroze, T.K. Sen, A Review on Heavy Metal Ions and Dye Adsorption, Water, Air, Soil Pollut. 229 (2018) 1–50. https://doi.org/10.1007/s11270-018-3869-z.

[27] Y. Shi, Q. Chang, T. Zhang, G. Song, Y. Sun, G. Ding, A review on selective dye adsorption by different mechanisms, J. Environ. Chem. Eng. 10 (2022) 108639. https://doi.org/10.1016/j.jece.2022.108639.

[28] Y. Hu, T. Guo, X. Ye, Q. Li, M. Guo, H. Liu, Z. Wu, Dye adsorption by resins: Effect of ionic strength on hydrophobic and electrostatic interactions, Chem. Eng. J. 228 (2013) 392–397. https://doi.org/10.1016/j.cej.2013.04.116.

[29] M.X. Zhu, L. Lee, H.H. Wang, Z. Wang, Removal of an anionic dye by adsorption/precipitation processes using alkaline white mud, J. Hazard. Mater. 149 (2007) 735–741. https://doi.org/10.1016/j.jhazmat.2007.04.037.

[30] Y. Gao, S.Q. Deng, X. Jin, S.L. Cai, S.R. Zheng, W.G. Zhang, The construction of amorphous metal-organic cage-based solid for rapid dye adsorption and time-dependent dye separation from water, Chem. Eng. J. 357 (2019) 129–139. https://doi.org/10.1016/j.cej.2018.09.124.

[31] B. Petrovic, M. Gorbounov, S. Masoudi Soltani, Influence of surface modification on selective CO2 adsorption: A technical review on mechanisms and methods, Microporous Mesoporous

Mater. 312 (2021) 110751. https://doi.org/10.1016/j.micromeso.2020.110751.

[32] O.H.P. Gunawardene, C.A. Gunathilake, K. Vikrant, S.M. Amaraweera, Carbon Dioxide Capture through Physical and Chemical Adsorption Using Porous Carbon Materials: A Review, 2022. https://doi.org/10.3390/atmos13030397.

[33] Z. Heidarinejad, M.H. Dehghani, M. Heidari, G. Javedan, I. Ali, M. Sillanpää, Methods for preparation and activation of activated carbon: a review, Environ. Chem. Lett. 18 (2020) 393–415. https://doi.org/10.1007/s10311-019-00955-0.

[34] J.Y. Lai, L.H. Ngu, S.S. Hashim, A review of CO2 adsorbents performance for different carbon capture technology processes conditions, Greenh. Gases Sci. Technol. 11 (2021) 1076–1117. https://doi.org/10.1002/ghg.2112.

[35] Z. Velkova, G. Kirova, M. Stoytcheva, S. Kostadinova, K. Todorova, V. Gochev, Immobilized microbial biosorbents for heavy metals removal, Eng. Life Sci. 18 (2018). https://doi.org/10.1002/elsc.201800017.

[36] A. Bhatnagar, A.K. Jain, A comparative adsorption study with different industrial wastes as adsorbents for the removal of cationic dyes from water, J. Colloid Interface Sci. 281 (2005) 49–55. https://doi.org/10.1016/j.jcis.2004.08.076.

[37] S. Mallakpour, F. Sirous, C.M. Hussain, Sawdust, a versatile, inexpensive, readily available bio-waste: From mother earth to valuable materials for sustainable remediation technologies, Adv. Colloid Interface Sci. 295 (2021) 102492. https://doi.org/10.1016/j.cis.2021.102492.

[38] K.A. Adegoke, O.O. Adesina, O.A. Okon-Akan, O.R. Adegoke, A.B. Olabintan, O.A. Ajala, H. Olagoke, N.W. Maxakato, O.S. Bello, Sawdust-biomass based materials for sequestration of organic and inorganic pollutants and potential for engineering applications, Curr. Res. Green Sustain. Chem. 5 (2022) 100274. https://doi.org/10.1016/j.crgsc.2022.100274.

[39] M.A. Yahya, Z. Al-Qodah, C.W.Z. Ngah, Agricultural bio-waste materials as potential sustainable precursors used for activated carbon production: A review, Renew. Sustain. Energy Rev. 46 (2015) 218–235. https://doi.org/10.1016/j.rser.2015.02.051.

[40] Z. Heidarinejad, M.H. Dehghani, M. Heidari, G. Javedan, I. Ali, M. Sillanpää, Methods for preparation and activation of activated carbon: a review, Environ. Chem. Lett. 18 (2020) 393–415. https://doi.org/10.1007/s10311-019-00955-0.

[41] O.E. Eleri, K.U. Azuatalam, M.W. Minde, A.M. Trindade, N. Muthuswamy, F. Lou, Z. Yu, Towards high-energy-density supercapacitors via less-defects activated carbon from sawdust, Electrochim. Acta. 362 (2020) 137152. https://doi.org/10.1016/j.electacta.2020.137152.

[42] M. Mergbi, M.G. Galloni, D. Aboagye, E. Elimian, P. Su, B.M. Ikram, W. Nabgan, J. Bedia, H. Ben Amor, S. Contreras, F. Medina, R. Djellabi, Valorization of lignocellulosic biomass into sustainable materials for adsorption and photocatalytic applications in water and air remediation, Environ. Sci. Pollut. Res. 30 (2023) 74544–74574. https://doi.org/10.1007/s11356-023-27484-2.

[43] M. Gayathiri, T. Pulingam, K.T. Lee, K. Sudesh, Activated carbon from biomass waste precursors: Factors affecting production and adsorption mechanism, Chemosphere. 294 (2022) 133764. https://doi.org/10.1016/j.chemosphere.2022.133764.

[44] M. Özacar, I.A. Şengil, Adsorption of metal complex dyes from aqueous solutions by pine sawdust, Bioresour. Technol. 96 (2005) 791–795. https://doi.org/10.1016/j.biortech.2004.07.011.

[45] J. Bortoluz, F. Ferrarini, L.R. Bonetto, J. da Silva Crespo, M. Giovanela, Use of low-cost natural waste from the furniture industry for the removal of methylene blue by adsorption: isotherms, kinetics and thermodynamics, Cellulose. 27 (2020) 6445–6466. https://doi.org/10.1007/s10570-020-03254-y.

[46] H. Esmaeili, R. Foroutan, Adsorptive Behavior of Methylene Blue onto Sawdust of Sour Lemon, Date Palm, and Eucalyptus as Agricultural Wastes, J. Dispers. Sci. Technol. 40 (2019) 990–999. https://doi.org/10.1080/01932691.2018.1489828.

[47] I. Şentürk, M.R. Yıldız, Highly efficient removal from aqueous solution by adsorption of Maxilon Red GRL dye using activated pine sawdust, Korean J. Chem. Eng. 37 (2020) 985–999. https://doi.org/10.1007/s11814-020-0526-1.

[48] L. Semerjian, Removal of heavy metals (Cu, Pb) from aqueous solutions using pine (Pinus halepensis) sawdust: Equilibrium, kinetic, and thermodynamic studies, Environ. Technol. Innov. 12 (2018) 91–103. https://doi.org/10.1016/j.eti.2018.08.005.

[49] F. Deniz, F. Dogan, Effective cleaning of a hazardous synthetic triarylmethane-type dye from aquatic environment with a multifunctional waste biomass–based biosorbent, Biomass Convers. Biorefinery. (2022). https://doi.org/10.1007/s13399-021-01995-9.

[50] A.A. Azzaz, S. Jellali, Chemical treatment of orange tree sawdust for a cationic dye enhancement removal from aqueous solutions : kinetic , equilibrium and thermodynamic studies, (2015). https://doi.org/10.1080/19443994.2015.1103313.

[51] M. Maqbool, S. Sadaf, H.N. Bhatti, S. Rehmat, A. Kausar, S.A. Alissa, M. Iqbal, Sodium alginate and polypyrrole composites with algal dead biomass for the adsorption of Congo red dye: Kinetics, thermodynamics and desorption studies, Surfaces and Interfaces. 25 (2021) 101183. https://doi.org/10.1016/j.surfin.2021.101183.

[52] E. Rapo, S. Tonk, Factors Affecting Synthetic Dye Adsorption; Desorption Studies: A Review of Results from the Last Five Years (2017-2021), Molecules. 26 (2021) 5419–5450. https://doi.org/10.3390/molecules26175419.

[53] Suhdi, S.C. Wang, Fine activated carbon from rubber fruit shell prepared by using ZnCl2 and KOH activation, Appl. Sci. 11 (2021). https://doi.org/10.3390/app11093994.

[54] F. Cesano, S. Cravanzola, V. Brunella, D. Scarano, Porous carbon spheres from poly(4-ethylstyrene-co-divinylbenzene: role of ZnCl2 and KOH agents in affecting porosity, surface area and mechanical properties, Microporous Mesoporous Mater. 288 (2019) 109605. https://doi.org/10.1016/j.micromeso.2019.109605.

[55] J.J. Manyà, B. González, M. Azuara, G. Arner, Ultra-microporous adsorbents prepared from vine shoots-derived biochar with high CO2 uptake and CO2/N2 selectivity, Chem. Eng. J. 345 (2018) 631–639. https://doi.org/10.1016/j.cej.2018.01.092.

[56] Q. Li, S. Liu, W. Peng, W. Zhu, L. Wang, F. Chen, J. Shao, X. Hu, Preparation of biomass-derived porous carbons by a facile method and application to CO2 adsorption, J. Taiwan Inst. Chem. Eng. 116 (2020) 128–136. https://doi.org/10.1016/j.jtice.2020.11.001.

[57] M. Thommes, K. Kaneko, A. V. Neimark, J.P. Olivier, F. Rodriguez-Reinoso, J. Rouquerol, K.S.W. Sing, Physisorption of gases, with special reference to the evaluation of surface area and pore size distribution (IUPAC Technical Report), Pure Appl. Chem. 87 (2015) 1051–1069. https://doi.org/10.1515/pac-2014-1117.

[58] R.S. Piriya, R.M. Jayabalakrishnan, M. Maheswari, K. Boomiraj, S. Oumabady, Coconut shell derived ZnCl2activated carbon for malachite green dye removal, Water Sci. Technol. 83 (2021) 1167–1182. https://doi.org/10.2166/wst.2021.050.

[59] G. Huang, Y. Liu, X. Wu, J. Cai, Activated carbons prepared by the KOH activation of a hydrochar from garlic peel and their CO 2 adsorption performance, New Carbon Mater. 34 (2019) 247–257. https://doi.org/10.1016/S1872-5805(19)60014-4.

[60] C. Quan, R. Su, N. Gao, Preparation of activated biomass carbon from pine sawdust for supercapacitor and CO2 capture, Int. J. Energy Res. 44 (2020) 4335–4351. https://doi.org/10.1002/er.5206.

[61] V. Siipola, T. Tamminen, A. Källi, R. Lahti, H. Romar, K. Rasa, R. Keskinen, J. Hyväluoma, M. Hannula, H. Wikberg, Effects of biomass type, carbonization process, and activation method on the properties of bio-based activated carbons, BioResources. 13 (2019) 5976–6002. https://doi.org/10.15376/biores.13.3.5976-6002.

[62] S. Marzeddu, M.A. Décima, L. Camilli, M.P. Bracciale, V. Genova, L. Paglia, F. Marra, M. Damizia, M. Stoller, A. Chiavola, M.R. Boni, Physical-Chemical Characterization of Different Carbon-Based Sorbents for Environmental Applications, Materials (Basel). 15 (2022) 1–29. https://doi.org/10.3390/ma15207162.

[63] T. Maneerung, J. Liew, Y. Dai, S. Kawi, C. Chong, C.H. Wang, Activated carbon derived from carbon residue from biomass gasification and its application for dye adsorption: Kinetics, isotherms and thermodynamic studies, Bioresour. Technol. 200 (2016) 350–359. https://doi.org/10.1016/j.biortech.2015.10.047.

[64] B. Qiu, Q. Shao, J. Shi, C. Yang, H. Chu, Application of biochar for the adsorption of organic pollutants from wastewater: Modification strategies, mechanisms and challenges, Sep. Purif. Technol. 300 (2022) 121925. https://doi.org/10.1016/j.seppur.2022.121925.

[65] D.H. da S. Santos, Y. Xiao, N. Chaukura, J.M. Hill, R. Selvasembian, C.L.P.S. Zanta, L. Meili, Regeneration of dye-saturated activated carbon through advanced oxidative processes: A review, Heliyon. 8 (2022) e10205. https://doi.org/10.1016/j.heliyon.2022.e10205.

[66] A. Cabrera-Codony, R. Gonzalez-Olmos, M.J. Martín, Regeneration of siloxane-exhausted activated carbon by advanced oxidation processes, J. Hazard. Mater. 285 (2015) 501–508. https://doi.org/10.1016/j.jhazmat.2014.11.053.

[67] A.A. Ahmad, B.H. Hameed, Fixed-bed adsorption of reactive azo dye onto granular activated carbon prepared from waste, J. Hazard. Mater. 175 (2010) 298–303. https://doi.org/10.1016/j.jhazmat.2009.10.003.

[68] H. Patel, Fixed-bed column adsorption study: a comprehensive review, Appl. Water Sci. 9 (2019) 1–17. https://doi.org/10.1007/s13201-019-0927-7.

[69] A. Negrea, M. Mihailescu, G. Mosoarca, M. Ciopec, N. Duteanu, P. Negrea, V. Minzatu, Estimation on fixed-bed column parameters of breakthrough behaviors for gold recovery by adsorption onto modified/functionalized amberlite XAD7, Int. J. Environ. Res. Public Health. 17 (2020) 1–14. https://doi.org/10.3390/ijerph17186868.

[70] A.F.M. Streit, L.N. Côrtes, S.P. Druzian, M. Godinho, G.C. Collazzo, D. Perondi, G.L. Dotto, Development of high quality activated carbon from biological sludge and its application for dyes removal from aqueous solutions, Sci. Total Environ. 660 (2019) 277–287. https://doi.org/10.1016/j.scitotenv.2019.01.027.

[71] N. Boudechiche, M. Fares, S. Ouyahia, H. Yazid, M. Trari, Z. Sadaoui, Comparative study on removal of two basic dyes in aqueous medium by adsorption using activated carbon from Ziziphus lotus stones, Microchem. J. 146 (2019) 1010–1018. https://doi.org/10.1016/j.microc.2019.02.010.

[72] N.U.M. Nizam, M.M. Hanafiah, E. Mahmoudi, A.A. Halim, A.W. Mohammad, The removal of anionic and cationic dyes from an aqueous solution using biomass-based activated carbon, Sci. Rep. 11 (2021) 1–17. https://doi.org/10.1038/s41598-021-88084-z.

[73] A. Sharma, Z.M. Siddiqui, S. Dhar, P. Mehta, D. Pathania, Adsorptive removal of congo red dye (CR) from aqueous solution by Cornulaca monacantha stem and biomass-based activated carbon: isotherm, kinetics and thermodynamics, Sep. Sci. Technol. 54 (2019) 916–929. https://doi.org/10.1080/01496395.2018.1524908.

[74] A.H. Jawad, A.S. Abdulhameed, N.N. Bahrudin, N.N.M.F. Hum, S.N. Surip, S.S.A. Syed-Hassan, E. Yousif, S. Sabar, Microporous activated carbon developed from KOH activated biomass waste: surface mechanistic study of methylene blue dye adsorption, Water Sci. Technol. 84 (2021)

1858–1872. https://doi.org/10.2166/wst.2021.355.

[75] K. Jahan, V. Singh, N. Mehrotra, K. Rathore, V. Verma, Development of activated carbon from KOH activation of pre-carbonized chickpea peel residue and its performance for removal of synthetic dye from drinking water, Biomass Convers. Biorefinery. (2021). https://doi.org/10.1007/s13399-021-01938-4.

[76] M. Baysal, K. Bilge, B. Yılmaz, M. Papila, Y. Yürüm, Preparation of high surface area activated carbon from waste-biomass of sunflower piths: Kinetics and equilibrium studies on the dye removal, J. Environ. Chem. Eng. 6 (2018) 1702–1713. https://doi.org/10.1016/j.jece.2018.02.020.

[77] A.M. Aljeboree, A.N. Alshirifi, A.F. Alkaim, Kinetics and equilibrium study for the adsorption of textile dyes on coconut shell activated carbon, Arab. J. Chem. 10 (2017) S3381–S3393. https://doi.org/10.1016/j.arabjc.2014.01.020.

[78] S.M. Alardhi, T.M. Albayati, J.M. Alrubaye, Adsorption of the methyl green dye pollutant from aqueous solution using mesoporous materials MCM-41 in a fixed-bed column, Heliyon. 6 (2020) e03253. https://doi.org/10.1016/j.heliyon.2020.e03253.

[79] P. Zheng, B. Bai, W. Guan, H. Wang, Y. Suo, Fixed-bed column studies for the removal of anionic dye from aqueous solution using TiO2@glucose carbon composites and bed regeneration study, J. Mater. Sci. Mater. Electron. 27 (2016) 867–877. https://doi.org/10.1007/s10854-015-3828-z.

[80] W. Hao, E. Björkman, M. Lilliestråle, N. Hedin, Activated carbons prepared from hydrothermally carbonized waste biomass used as adsorbents for CO 2, Appl. Energy. 112 (2013) 526–532. https://doi.org/10.1016/j.apenergy.2013.02.028.

[81] G. Sethia, A. Sayari, Comprehensive study of ultra-microporous nitrogen-doped activated carbon for CO2 capture, Carbon N. Y. 93 (2015) 68–80. https://doi.org/10.1016/j.carbon.2015.05.017.

[82] I. Durán, F. Rubiera, C. Pevida, Separation of CO2 in a solid waste management incineration facility using activated carbon derived from pine sawdust, Energies. 10 (2017). https://doi.org/10.3390/en10060827.

[83] S. Chowdhury, R. Balasubramanian, Three-Dimensional Graphene-Based Porous Adsorbents for Postcombustion CO2 Capture, Ind. Eng. Chem. Res. 55 (2016) 7906–7916. https://doi.org/https://doi.org/10.1021/acs.iecr.5b04052.

[84] W. Lu, W.M. Verdegaal, J. Yu, P.B. Balbuena, H.K. Jeong, H.C. Zhou, Building multiple adsorption sites in porous polymer networks for carbon capture applications, Energy Environ. Sci. 6 (2013) 3559–3564. https://doi.org/10.1039/C3EE42226G.

[85] J. Serafin, U. Narkiewicz, A.W. Morawski, R.J. Wróbel, B. Michalkiewicz, Highly microporous activated carbons from biomass for CO2 capture and effective micropores at different conditions, J. CO2 Util. 18 (2017) 73–79. https://doi.org/10.1016/j.jcou.2017.01.006.

[86] Y. Guo, C. Tan, J. Sun, W. Li, J. Zhang, C. Zhao, Porous activated carbons derived from waste sugarcane bagasse for CO2 adsorption, Chem. Eng. J. 381 (2020) 122736. https://doi.org/10.1016/j.cej.2019.122736.

[87] S. Deng, H. Wei, T. Chen, B. Wang, J. Huang, G. Yu, Superior CO2 adsorption on pine nut shell-derived activated carbons and the effective micropores at different temperatures, Chem. Eng. J. 253 (2014) 46–54. https://doi.org/10.1016/j.cej.2014.04.115.

[88] K. Li, S. Tian, J. Jiang, J. Wang, X. Chen, F. Yan, Pine cone shell-based activated carbon used for CO2 adsorption, J. Mater. Chem. A. 4 (2016) 5223–5234. https://doi.org/10.1039/C5TA09908K.

[89] C. Ma, J. Bai, M. Demir, X. Hu, S. Liu, L. Wang, Water chestnut shell-derived N/S-doped porous carbons and their applications in CO2 adsorption and supercapacitor, Fuel. 326 (2022) 125119. https://doi.org/10.1016/j.fuel.2022.125119.

[90] T. Lu, J. Bai, M. Demir, X. Hu, J. Huang, L. Wang, Synthesis of potassium Bitartrate-derived porous carbon via a facile and Self-Activating strategy for CO2 adsorption application, Sep. Purif. Technol. 296 (2022) 121368. https://doi.org/10.1016/j.seppur.2022.121368.

[91] J. Bai, J. Huang, Q. Yu, M. Demir, F.H. Gecit, B.N. Altay, L. Wang, X. Hu, One-pot synthesis of self S-doped porous carbon for efficient CO2 adsorption, Fuel Process. Technol. 244 (2023) 107700. https://doi.org/10.1016/j.fuproc.2023.107700.

[92] Q. Yu, J. Bai, J. Huang, M. Demir, A.A. Farghaly, P. Aghamohammadi, X. Hu, L. Wang, One-Pot Synthesis of Melamine Formaldehyde Resin-Derived N-Doped Porous Carbon for CO2 Capture Application, Molecules. 28 (2023). https://doi.org/10.3390/molecules28041772.

Appendix A: Papers in which this Thesis is based

Removal of wood dyes from aqueous solutions by sorption on untreated pine (*Pinus radiata*) sawdust

Catarina H. Pimentel, M. Sonia Freire, Diego Gómez-Díaz & Julia González-Álvarez

Department of Chemical Engineering, School of Engineering, Universidade de Santiago de Compostela, Rúa Lope Gómez de Marzoa s/n, 15782, Santiago de Compostela, Spain

Journal: Cellulose (2023), ed. Springer Nature B.V. (ISSN: 0969-0239), 30: 4587–4608.

DOI: https://doi.org/10.1007/s10570-023-05145-4

Impact factor = 5.7 (2022), ranking it 1/21 in Paper and Wood Materials Science (Q1) and 2/26 in Textiles Materials Science (Q1).

Author contribution (CRediT taxonomy): Investigation, Validation, Visualization, Writing–original draft.

Chapters reproducing the article content: Chapter 3.

Preparation of activated carbon from pine (*Pinus radiata*) sawdust by chemical activation with zinc chloride for wood dye adsorption

Catarina H. Pimentel, M. Sonia Freire, Diego Gómez-Díaz & Julia González-Álvarez

Department of Chemical Engineering, School of Engineering, Universidade de Santiago de Compostela, Rúa Lope Gómez de Marzoa s/n, 15782, Santiago de Compostela, Spain

Journal: Biomass Conversion and Biorefinery (2023), ed. Springer Nature B.V. (ISSN: 2190-6815), 1-19.

DOI: https://doi.org/10.1007/s13399-023-04138-4

Impact factor = 4.0 (2022), ranking it 52/142 in Chemical Engineering (Q2) and 67/119 in Energy and Fuels (Q3).

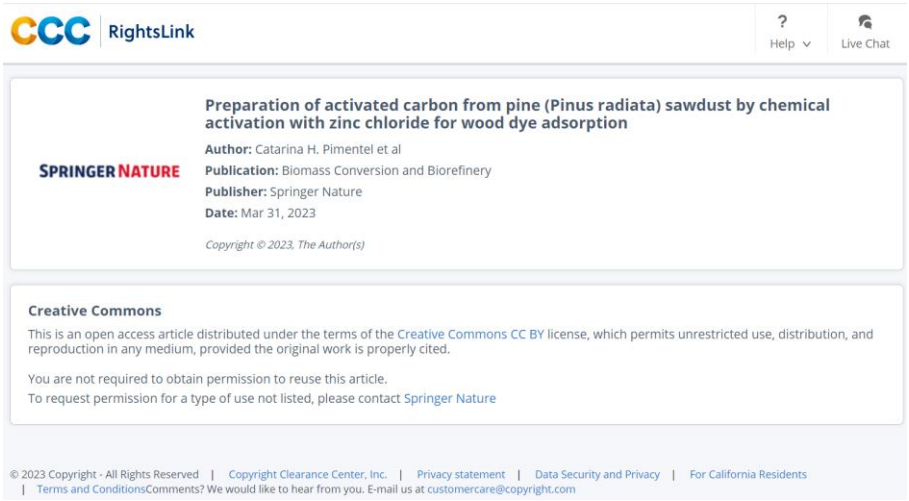

Author contribution (CRediT taxonomy): investigation, validation, visualization, writing — original draft.

Chapters reproducing the article content: Chapter 3

Separation of CO_2 using biochar and KOH and $ZnCl_2$ activated carbons derived from pine sawdust

Catarina Helena Pimentel, Lidia Díaz-Fernández, Diego Gómez-Díaz, María Sonia Freire, Julia González-Álvarez

Department of Chemical Engineering, School of Engineering, Universidade de Santiago de Compostela, Rúa Lope Gómez de Marzoa s/n, 15782, Santiago de Compostela, Spain

Journal: Journal of Environmental Chemical Engineering (2023), ed. Elsevier B.V (ISSN: 2213-2929), 1-16.

DOI: https://doi.org/10.1016/j.jece.2023.111378

Impact factor = 7.7 (2022), ranking it 16/142 in Chemical Engineering (Q1) and 12/55 in Environmental Engineering (Q1).

Author contribution (CRediT taxonomy): Investigation, Data curation, Validation, Visualization, Writing – original draft.

Chapters reproducing the article content: Chapter 3

Appendix B: “Resumo” (Summary, in Galician)

A contaminación ambiental da auga e da atmosfera, como resultado da rápida expansión industrial e da sobre explotación dos recursos naturais, é responsable do efecto invernadoiro e de considerables problemas para a saúde dos ecosistemas, e especialmente, para a saúde humana. Por unha banda, un dos gases de efecto invernadoiro (GEI) máis antropoxénicos, que ten un impacto prexudicial sobre o medio ambiente e que está asociado ao cambio climático é o dióxido de carbono, que contribúe máis do 60% ao quecemento global na Terra. Dado que a concentración de CO_2 segue aumentando é fundamental reducir a pegada de carbono na maioría dos países e buscar solucións e alternativas para formas de enerxía máis sostibles. Mentres tanto, como a queima de combustibles fósiles (carbón, gas natural e petróleo) segue sendo o principal abastecemento de enerxía é fundamental desenvolver técnicas de captura e almacenamento de carbono para facer fronte ao reto global da redución de CO_2. Hoxe en día, a técnica máis utilizada na industria para a captura de CO_2 é a absorción química con monoetanolamina, non obstante, presenta varias desvantaxes debido aos altos requisitos enerxéticos para a rexeneración e reciclaxe do disolvente, a corrosión dos equipos e a degradación do disolvente. Por outra banda, outro factor importante que produce preocupación a nivel mundial é a contaminación da auga e dos hábitats debidos á vertedura ás augas residuais de distintos contaminantes como colorantes. Estes compostos son moi utilizados en diversas industrias como téxtiles, cosméticas e da madeira, estimándose que hai máis de 100.000 colorantes comerciais e unhas 350.000 toneladas son vertidas cada ano. A descarga directa destes colorantes en augas residuais é moi preocupante xa que reducen a transmisión da luz na auga impedindo a fotosíntese, e comprometendo o bo funcionamento da cadea alimentaria. Ademais, os colorantes poden causar trastornos funcionais no corpo humano por tratarse moitas veces de produtos tóxicos e canceríxenos. Debido á súa estrutura estable e complexa, tenden a resistir a degradación por axentes oxidantes ou luz, entre outros.

Polo tanto, para resolver todos estes problemas ambientais existe un crecente interese no campo da investigación para desenvolver técnicas baseadas en métodos físicos, químicos e biolóxicos para a eliminación dos colorantes e para a captura de CO_2. A adsorción destaca como unha das técnicas máis prometedoras con moitas vantaxes sobre outros métodos. Trátase dunha técnica rendible que require de equipos cun deseño e funcionamento sinxelos, revelándose como un dos procesos máis eficaces para a separación de contaminantes. Así, en distintas aplicacións, unha ampla gama de adsorbentes son utilizados como sólidos para reter as moléculas de colorante ou de CO_2. En concreto, os carbóns activados, materiais ricos en carbono, son os máis aplicados, principalmente pola súa gran área superficial e elevada porosidade, estabilidade térmica favorable, resistencia mecánica e unha variabilidade de grupos funcionais químicos na superficie. Non obstante, o seu alto custo e a súa dificultade de rexeneración favoreceron a investigación doutros adsorbentes máis accesibles.

Con máis de 24.25 millóns de m^3 anuais producidos en todo o mundo, a serradura de piñeiro é un material natural e lignocelulósico dispoñible e económico. Xeralmente, provén de residuos de actividades tanto agrícolas como industriais e, polo tanto, está amplamente distribuído, xerando moitas veces problemas para a súa eliminación. Por iso, recentemente, hai moito interese na súa xestión, polo que estanse a realizar estudos de investigación para usar a serradura sen tratamento

ou convertela en outros materiais con diferentes aplicacións como a de adsorbente. Algunhas das propiedades máis salientables deste material inclúen a súa superficie rugosa, porosidade elevada, contido elevado de carbono, boa estabilidade mecánica e facilidade de degradación biolóxica e de modificación. Non obstante, para mellorar a súa capacidade de adsorción, normalmente relacionada cunha elevada área superficial e presenza dunha estrutura porosa ben organizada no material, pódese converter en carbón activado mediante activación física (na que se pode usar vapor de auga, nitróxeno ou dióxido de carbono) ou química (na cal emprégase un axente químico deshidrátante) en un ou dous pasos. Normalmente o carbón activado preparado por activación química presenta maior área superficial, menor tamaño de poro e ten un amplo uso en moitas aplicacións. Dos axentes químicos máis utilizados pódense mencionar o $ZnCl_2$, KOH, H_3PO_4 e K_2CO_3, que presentan un efecto mellorado sobre a área superficial e a porosidade do carbón. Dado que as características do precursor e as condicións de preparación inflúen fortemente nas características do carbón activado, é importante unha escolla coidadosa do precursor, o que implica ter en conta a dispoñibilidade local e o prezo do material.

Por iso, polas vantaxes sinaladas anteriormente para as serraduras de piñeiro e, en concreto, a procedente da especie *Pinus radiata* cunha grande importancia forestal en Galicia que destaca por ser flexible, de crecemento rápido e baixos turnos de tala e cunha ampla gama de aplicacións, nesta tese proponse utilizala como un material sostible que poida contribuír ao tratamento de efluentes de augas residuais e tamén captar o CO_2 da atmosfera.

Así, o obxectivo xeral desta Tese foi o emprego da serradura de piñeiro (*Pinus radiata*), un residuo abundante e de baixo coste procedente dunha industria local, como adsorbente para a eliminación de tres colorantes usados na tinguidura da madeira (azul, vermello e negro) de disolucións acuosas, e de CO_2 de correntes gasosas. A serradura utilízase sen tratamento previo e, posteriormente, como precursor de carbóns activados obtidos despois da súa carbonización e activación química. Nunha primeira etapa avalíase a capacidade da serradura para a adsorción en descontinuo dos colorantes en disolución acuosas empregando o material sen tratar e analizando a influencia de diferentes variables (dose de adsorbente, pH, concentración inicial de colorante, velocidade de axitación e tempo de contacto). Tamén se avalía a súa capacidade para adsorber CO_2. Para coñecer a súa morfoloxía e estrutura, a serradura de piñeiro, antes e despois dos experimentos de adsorción, caracterízase mediante o uso de diferentes técnicas (a determinación da superficie específica BET e a distribución de tamaño de poros a partir das isotermas de adsorción de N_2 a -196 °C e de CO_2 a 0 °C, a análise da superficie e da composición elemental por microscopia electrónica de varrido acoplada con análise de enerxía de dispersión de raios X (SEM-EDX) e a determinación do punto de carga cero).

Posteriormente, para investigar se a eficacia de adsorción dos colorantes e do CO_2 podía mellorar, utilízase a serradura de piñeiro como precursor de carbón e de carbóns activados mediante o uso de dous axentes químicos, KOH ou $ZnCl_2$, amplamente usados para a activación química de carbóns. Os carbóns preparados son caracterizados coas técnicas empregadas para a serradura e con outras

como microscopia eletrónica de transmisión (TEM), difracción de raios X (XRD), análise elemental CHNS, espectroscopia fotoelectrónica de raios X (XPS) e infravermella con transformada de Fourier (FTIR) para analizar a influencia das condicións de preparación dos carbóns (temperaturas de carbonización e de activación, tipo e concentración de axente e o método de activación empregado) sobre as características dos materiais e o seu comportamento na adsorción. Ao mesmo tempo, realízanse experimentos, tamén en descontinuo, para analizar o efecto das variables estudadas de maneira previa para a serradura sen tratar sobre a adsorción dos colorantes. Para a separación de CO_2 de correntes gasosas pos combustión (N_2/CO_2), analízase o efecto da temperatura e da presión sobre a eficacia de separación e a selectividade para o CO_2.

Ademais, tanto para a serradura de piñeiro como para todos os carbóns preparados, e para investigar os mecanismos responsables da adsorción, estúdanse a cinética da adsorción dos colorantes e o equilibrio de adsorción dos colorantes e do CO_2 e N_2, utilizando diferentes modelos cinéticos e isotermas de adsorción coñecidos, respectivamente. Para ambos os dous casos, estúdase a rexeneración dos adsorbentes para seleccionar as mellores condicións de operación e o axente de desorción mais adecuado.

Finalmente, avalíase a capacidade de adsorción dos colorantes operando en continuo cunha columna de leito fixo e co carbón activado que presenta os mellores resultados en descontinuo, para estudar o efecto de diferentes variables como o caudal de entrada de efluente, a concentración inicial de colorante e a altura de leito, e empregando modelos dinámicos amplamente estudados analízanse as características do proceso de adsorción. Ao mesmo tempo, e para avaliar a posible aplicación industrial do carbón escollido, faise a rexeneración do carbón en ciclos de adsorción-desorción con axentes adecuados.

En primeiro lugar, os colorantes empregados (azul, vermello e negro) foron caracterizados como ácidos débiles polos seus valores da constante de disociación ou pK_a. Tamén foi investigada a súa estabilidade química co pH e co tempo para unha concentración inicial de 25 mg L^{-1}, o que puxo de manifesto que mentres os colorantes vermello e azul eran estables durante catro días, o colorante negro era inestable para certos valores do pH, polo que os experimentos de adsorción, neste caso, tiveron que limitarse a 12 h. A presenza de diferentes grupos funcionais e da distancia molecular entre dous dos seus átomos extremos puideron explicar o seu comportamento diferente no proceso de adsorción. Seguidamente, como se indica enriba, utilizouse a serradura de piñeiro sen tratar para avaliar a capacidade de adsorción dos tres colorantes a partir de disolucións acuosas e de CO_2 de correntes gasosas. A caracterización do material mediante a análise das isotermas de adsorción de N_2 e CO_2 indicaron que o material é macroporoso cunha superficie heteroxénea, aínda que tamén presenta meso e microporosidade. Ademais, resultou ter un valor do punto de carga cero de 4.8, polo que ao tratar con colorantes aniónicos, as condicións de operación nas que a carga da súa superficie sexa positiva pode favorecer a adsorción dos colorantes.

Por outra banda e, en concreto, da determinación da área superficial BET con CO_2 a 0 °C inferiuse que se producía unha moi baixa adsorción do gas, polo que non se realizaron máis estudos de separación de CO_2 con este material sen tratar. En relación co estudo de adsorción de colorantes, avaliouse o efecto de varios parámetros sobre a eficacia de adsorción e os resultados demostraron que a maior eficiencia de eliminación producíase a pH ácido favorecida pola interacción electroestática e, especialmente para o colorante azul, e que esta aumentaba co aumento do tempo de contacto ata alcanzar o equilibrio, e co aumento da dose de serradura. Por outra banda, a eficacia de eliminación diminuíu co aumento da concentración inicial de colorante, aínda que a maior capacidade de adsorción correspondeu á concentración máis alta utilizada. A análise SEM-EDX demostrou que a adsorción ocorreu. Os datos cinéticos axustáronse satisfactoriamente ao modelo cinético de pseudo-segunda orde, indicativo dun proceso de adsorción química. Ademais, a presenza de máis de dúas rexións no axuste dos datos ao modelo de difusión intraparticular indica que hai difusión das moléculas de colorante a través dos poros do material . Os resultados do equilibrio revelaron que os modelos que mellor describen o proceso de adsorción foron os de Freundlich e Dubinin-Radushkevich, que indican a existencia dunha superficie heteroxénea e un proceso de adsorción en multicapa. Nos experimentos de desorción, o hidróxido de sodio foi o que mostrou mellor eficiencia para a eliminación dos tres colorantes da serradura, posiblemente ao proporcionar alcalinidade á superficie da serradura e, polo tanto, foi seleccionado como axente desorbente para a realización dos ciclos de adsorción/desorción. No caso do colorante vermello, a serradura mostrou unha alta eficiencia de adsorción despois de catro ciclos. En relación co colorante azul e o negro, a pesar dos baixos resultados de desorción, non houbo unha diminución significativa da porcentaxe de adsorción ao longo dos ciclos polo que, combinado con outras técnicas de post-tratamento, podería ser igualmente aplicado como axente de desorción. Os resultados demostraron que a serradura de piñeiro é un adsorbente eficiente para a eliminación de colorantes de disolucións acuosas e que factores como pH, tempo de contacto, dose de adsorbente e concentración inicial de colorante inflúen no proceso de adsorción.

Non obstante, a pesar de que a serradura de piñeiro presenta bos resultados como adsorbente dos colorantes e podería ser máis axeitado como material sostible e de baixo custo, como se indicou anteriormente, para tentar obter unha área superficial máis elevada e unha estrutura porosa ben desenvolvida que mellorase a eficacia de adsorción, producíronse un material só carbonizado a 600 °C e cinco carbóns activados (a 600 ou 850 °C). Na táboa seguinte móstranse as condicións de preparación dos carbóns.

Táboa 1. Condicións de preparación dos carbóns.

Tipo de carbón	Axente de activación	Dose de carbón/axente de activación	Temperatura de carbonización (°C)	Temperatura de activación (°C)
BC	-	-	600	-
ACPS850-K-4	KOH	1:4		850
ACPS600-K-4	KOH	1:4		600
ACPS850-K-2	KOH	1:2		850
ACPS850-Z-D	$ZnCl_2$	1:4		850
ACPS850-Z-W	$ZnCl_2$	1:4		850

As temperaturas foron seleccionadas tendo en conta os resultados dunha análise termogravimétrica da serradura de piñeiro que demostrou que non había perda de peso nese intervalo de temperaturas. Todos os materiais foron caracterizados e utilizáronse para a adsorción dos colorantes e de CO_2, avaliando a influencia de varios parámetros sobre a capacidade de adsorción dos carbóns. O proceso de activación realizouse tras seleccionar KOH e $ZnCl_2$ como axentes de activación, xa que poderían dar lugar a materiais con altos valores de superficie e porosidade. Alén de estudar a variación das condicións de activación como a temperatura e a dose de axente, no caso do $ZnCl_2$, tamén se probaron dous métodos de activación, por impregnación do carbón cunha disolución do cloruro de zinc (activación húmida) ou mestura directa de carbón e $ZnCl_2$. Non obstante, como non se observaron diferenzas estruturais e morfolóxicas significativas dos carbóns, só se aplicou o producido por mestura directa xa que non xera a produción de residuos líquidos.

Os resultados obtidos de área superficial e porosidade revelaron a efectividade do proceso de carbonización e activación, xa que aumentaron de forma significativa, aínda que hai unha perda de rendemento despois da pirólise da serradura e especialmente despois da súa activación e, en concreto, con KOH. As isotermas de adsorción de nitróxeno de tipo I segundo a clasificación da IUPAC, revelaron que o material carbonizado e os carbóns activados con $ZnCl_2$ eran materiais microporosos (Tipo Ia), mentres que os outros carbóns (Tipo Ib) tiñan microporos de maior tamaño e mesoporos. Os carbóns activados con KOH mostraron valores de área superficial superiores aos activados con $ZnCl_2$, sendo o valor máis alto determinado con N_2 a -196°C de 2865 $m^2\ g^{-1}$ correspondente ao carbón activado a 850°C cunha proporción de carbón/KOH 1:4 (p/p) e con CO_2 a 0°C de 1354 $m^2\ g^{-1}$ correspondente ao carbón activado a 600°C cunha proporción de carbón/KOH 1:4 (p/p). Polo tanto, os resultados da caracterización revelaron que o axente de activación tiña un efecto substancial sobre a porosidade dos materiais. Todos os carbóns presentaron unha estrutura amorfa con diferentes graos de grafitización, sendo o carbono e o osíxeno os compoñentes maioritarios e presentando varios grupos funcionais, sendo a serradura só carbonizada a que presentou máis grupos funcionais. A porcentaxe de microporosidade foi maior para o material só carbonizado e menor para o material activado con KOH a 850 °C cunha proporción 1:4 (p/p).

Tendo en conta os experimentos de adsorción de colorantes, avaliouse primeiro a influencia do pH e da concentración inicial de colorante na eficacia da adsorción. Os resultados de adsorción para o material carbonizado foron bastante limitados, posiblemente debido á súa escasa área superficial e á alta porcentaxe de microporos. A concentracións baixas (5 mg L^{-1}) e pH = 2 para todos os carbóns activados obtivéronse porcentaxes próximas ao 100%, agás para o colorante negro co carbón activado con $ZnCl_2$ que foi do 56%, quizais por ser o colorante de maior tamaño molecular e este carbón activado ter unha área superficial máis pequena e unha microporosidade elevada. Co aumento da concentración inicial de colorante, e nos materiais con maior microporosidade, a eficiencia de adsorción foi menor. O carbón activado a 850 °C nunha proporción de carbón/KOH 1:4 (p/p) foi para o que se obtiveron os mellores resultados, ata a concentracións elevadas (500 mg L^{-1} para os colorantes azul e vermello e 100 mg L^{-1} para o negro) o que poido deberse á elevada área superficial e á baixa microporosidade. A interacción cos grupos funcionais tamén influíu na adsorción de colorantes. A altas concentracións, o carbón activado con $ZnCl_2$ mostrou os resultados máis baixos. O aumento da dose de adsorbente levou a resultados de eficiencia de adsorción mellorados debido ao aumento do número de sitios activos dispoñibles. Non obstante, para os materiais que mostraron unha alta eficiencia de adsorción, por razóns económicas, propúxose reducir a dose de adsorbente e nos que mostraron peores resultados ($ZnCl_2$) aumentouse a dose.

As imaxes microscópicas SEM revelaron que a superficie e os poros estaban cubertos por unha capa de colorante. Tamén, a análise elemental revelou a presenza de elementos da composición dos colorantes presentes na superficie e os espectros FTIR realizados en mostras despois da adsorción demostraron o cambio nalgúns picos e nas súas respectivas intensidades. Todo isto corroborou a adsorción dos colorantes.

En canto aos resultados da cinética de adsorción, agás para o carbón activado a 850 °C con KOH en proporción 1:4 (p/p) co colorante negro a altas concentracións, todos os datos experimentais se axustaron mellor ao modelo cinético de pseudo-segunda orde asociado cun mecanismo de adsorción química. No caso do colorante negro a 100 mg L^{-1} o axuste foi mellor ao modelo cinético de pseudo-primeira orde que revela un mecanismo de adsorción físico. No modelo de difusión intraparticular obtívose multilinealidade, revelando a existencia de dúas zonas de adsorción, e o bo axuste lineal obtido para a primeira zona revela a difusión dos colorantes nos poros. Considerando os resultados das isotermas de equilibrio, o modelo de Langmuir foi o que mellor axustou os datos experimentais para os carbóns activados con KOH e para o activado con $ZnCl_2$ co colorante vermello. Isto suxire un proceso de adsorción en monocapa cunha superficie dos carbóns enerxéticamente homoxénea para a interacción. O valor medio da enerxía determinado polo modelo de Dubinin-Radushkevich (D-R) (> 8 kJ mol^{-1}) corroborou a existencia dun proceso de adsorción química. Para o carbón activado con $ZnCl_2$ cos colorantes azul e negro, o mellor axuste foi ó modelo de Freundlich, que suxire un proceso de adsorción en multicapa e unha superficie heteroxénea.

Tendo en conta os resultados obtidos ponse de manifesto o papel que a estrutura dos colorantes e as propiedades do adsorbente teñen na adsorción dos colorantes.

Analizouse tamén a desorción dos tres colorantes co carbón que deu os mellores resultados nos experimentos en descontinuo, o activado con KOH a 850 °C na proporción 1:4 (p/p), co fin de avaliar a posibilidade de reutilizar o carbón en ciclos sucesivos e mellorar así a economía do proceso. Probáronse varios axentes de desorción, pero cun resultado de desorción moi baixo (< 27%), o que suxeriu que a adsorción de colorantes polo carbón é xeralmente irreversible por rexeneración química. Para tentar mellorar este resultado, realizouse a desorción con peróxido de hidróxeno que só produciu resultados satisfactorios para o colorante negro.

Ademais, seleccionouse este mesmo carbón activado para realizar os experimentos de adsorción en continuo, producíndoo a maior escala. Para comprobar a eficiencia do proceso de produción tamén se caracterizou pola súa área superficial e distribución de tamaño de poros. A superficie e o diámetro medio dos poros determinados para a adsorción de N_2 a -196 °C foron moi similares aos do carbón obtido en pequena escala, agora ben a área BET determinada para a isoterma de adsorción de CO_2 aumentou en torno a 200 $m^2\ g^{-1}$, como consecuencia de que a porcentaxe de microporosidade diminuíu.

Os resultados dos experimentos en continuo demostraron que o tempo de ruptura diminuíu ao aumentar o caudal de efluente de entrada a columna e a concentración inicial e ao diminuír a altura do leito. Os datos experimentais axustáronse posteriormente a modelos dinámicos amplamente estudiados mediante regresión non lineal. En xeral, os modelos de Thomas e Yoon-Nelson foron os que mellor se axustaron aos datos experimentais. De modo similar ao proceso en descontinuo, realizáronse experimentos de desorción en varios ciclos de adsorción-desorción con peróxido de hidróxeno para o carbón saturado co colorante negro con base nos resultados en descontinuo que para os colorantes azul e vermello non foron favorables. Os resultados demostraron que tanto o tempo de ruptura como a capacidade de adsorción diminuíron en xeral coa aplicación dos ciclos.

Finalmente, aplicáronse os carbóns para a separación de CO_2 das correntes post-combustión (mestura de N_2/CO_2 85/15%). En relación aos carbóns activados con KOH, a capacidade de adsorción de CO_2 é maior en condicións de activación moderadas (600 °C) o que pode estar relacionado con as características dos materiais como a estrutura microporosa e a composición química da superficie. Así, o carbón activado con KOH a 600°C en proporción 1:4 (p/p) foi o que presentou maior capacidade de adsorción de CO_2 debido à combinación dunha elevada porcentaxe de microporosidade e elevada área superficial determinada con CO_2. Ademais, todos os materiais mostraron preferencia na adsorción de CO_2 en relación ao N_2 e o aumento da temperatura influíu negativamente no proceso de adsorción. En xeral, o modelo de Toth axustou mellor os datos experimentais que o de Langmuir e Freundlich. A selectividade aparente e a IAST indicaron que a serradura carbonizada seguida do carbón activado con KOH a 600 °C na proporción 1:4 (p/p) foron os que mostraron a mellor selectividade CO_2/N_2, permitindo a obtención dun alto grao de pureza de CO_2. En canto a calor de adsorción, a serradura de piñeiro só carbonizada presentou o valor máis alto, que está relacionado coa presenza de máis grupos funcionais na superficie do material, xa que non se produciu o proceso de activación e que está de acordo cos altos valores de selectividade, a pesar

de ter unha escasa área superficial. Segundo os resultados o carbón activado con KOH a 600°C na proporción 1:4 (p/p) foi o que presentou un mellor desempeño xa que permitiu alcanzar altos valores de adsorción de CO_2, sendo o segundo que presentou maior selectividade combinada co segundo valor máis baixo de calor de adsorción.

O presente traballo revelou que o desenvolvemento de novos materiais, como os carbóns activados producidos a partir de serradura de piñeiro de *Pinus radiata*, como adsorbentes rendibles e eficientes de CO_2 e colorantes aniónicos, podería ser unha alternativa viable e atractiva para o control da contaminación da auga e do aire. Non obstante, máis investigacións para a implantación do proceso de adsorción usando os carbóns activados derivados da serradura da madeira a escala industrial deberán de levarse a cabo. De calquera xeito, o máis salientable desta Tese é a súa importante contribución para proporcionar unha substitución potencialmente máis económica dos carbóns activados comerciais existentes, dándolle ademais un valor engadido a estes residuos da madeira axudando, ao mesmo tempo, a solucionar o problema da súa xestión como residuos.

Os obxectivos desta Tese foron acadados dando como resultado os seguintes traballos:

- Pimentel, C.H., Freire, M.S., Gómez-Díaz, D., González-Álvarez, J. Removal of wood dyes from aqueous solutions by sorption on untreated pine (*Pinus radiata*) sawdust. Cellulose 30, 4587–4608 (2023). https://doi.org/10.1007/s10570-023-05145-4
- Pimentel, C.H., Freire, M.S., Gómez-Díaz, D., González-Álvarez, J. Preparation of activated carbon from pine (*Pinus radiata*) sawdust by chemical activation with zinc chloride for wood dye adsorption. Biomass Conv. Bioref. (2023). https://doi.org/10.1007/s13399-023-04138-4
- Pimentel, C.H., Castro-Agra, R., Freire, M.S., Gómez-Díaz, D., González-Álvarez, J. Removal of wood dyes from aqueous solutions using KOH chemically activated carbons from pine (*Pinus radiata*) sawdust, submitted for publication.
- Pimentel, C.H., Freire, M.S., Gómez-Díaz, D., González-Álvarez, J. Continuous adsorption of acid wood dyes onto an activated carbon prepared from pine sawdust, in preparation.
- Pimentel, C.H., Díaz-Fernández, Lidia, Freire, M.S., Gómez-Díaz, D., González-Álvarez, J. Separation of CO_2 using biochar and KOH and $ZnCl_2$ activated carbons derived from pine sawdust, Journal of Environmental Chemical Engineering (2023). https://doi.org/10.1016/j.jece.2023.111378

Carbon dioxide accumulation in the atmosphere and the presence of dyes in water resources are severe environmental issues to be solved. Consequently, in this work, adsorption is proposed as an efficient technique for both CO_2 capture from post-combustion process streams and dye removal from aqueous solutions. Pine sawdust, an eco-friendly and abundant residue from the wood industry, was used as adsorbent directly and after its conversion in biochar and activated carbons. The materials produced were thoroughly characterized and applied for CO_2 capture and for acid wood dye removal in batch and continuous mode analyzing the effect of various operational conditions. The results obtained demonstrated that pine sawdust-based carbons are promising alternatives to commercial activated carbons for the applications proposed.